MOLECULAR LEVEL MODELING OF NATURAL AND COMPACTED EXPANSIVE CLAYS

BY

HABIB-UR-REHMAN AHMED

A Dissertation Presented to the

FACULTY OF THE COLLEGE OF GRADUATE STUDIES

KING FAHD UNIVERSITY OF PETROLEUM & MINERALS

DHAHRAN, SAUDI ARABIA

In Partial Fulfillment of the
Requirements for the Degree of

DOCTOR OF PHILOSOPHY

In

CIVIL & ENVIRONMENTAL ENGINEERING

JANUARY 2015

KING FAHD UNIVERSITY OF PETROLEUM & MINERALS

DHAHRAN- 31261, SAUDI ARABIA

DEANSHIP OF GRADUATE STUDIES

This thesis, written by **Habib-ur-Rehman Ahmed** under the direction of his thesis advisor and approved by his thesis committee, has been presented and accepted by the Dean of Graduate Studies, in partial fulfillment of the requirements for the degree of **DOCTOR OF PHILOSOPHY IN CIVIL ENGINEERING.**

Dr. Sahel N. Abduljauwad
(Advisor)

Dr. Nedal T. Ratrout 01 JAN 2015
Department Chairman

Dr. Ahmet U. Dogan
(Co-Advisor)

Dr. Salam A. Zummo
Dean of Graduate Studies

Dr. Ibnelwaleed A. Hussein
(Member)

6/1/15
Date

Dr. Mohammed H. Baluch
(Member)

Dr. Hamad I. Abdul Wahhab
(Member)

Dedicated to my **Mother** to whom I owe all of my academic achievements

ACKNOWLEDGMENTS

All praise and thanks be to ALLAH, the Almighty, whose blessings and help are all the time with me, and He is the only one Who helps and His help is best of all, and peace and blessings of ALLAH be upon the messenger of ALLAH.

I wish to express my sincere gratitude and special thanks to my thesis advisor Dr. Sahel N. Abduljauwad and co-advisor Dr. Ahmet U. Dogan for their valuable guidance, support, and encouragement throughout this research. I would also like to extend special thanks to my other committee members, Dr. Ibnelwaleed A. Hussein, Dr. Mohammed H. Baluch, and Dr. Hamad I. Abdul Wahhab, for their valuable suggestions and support throughout the course of this work.

Acknowledgement is also due to King Fahd University of Petroleum & Minerals for extending all the testing facilities and support for my PhD program. In this regard, special thanks are extended to Dr. Zain Hassan Yamani, Director, Center of Excellence in Nano Technology and Dr. Sulaiman S. Al-Khattaf, Director, Center of Research Excellence in Refining & Petrochemicals at Research Institute (RI) of KFUPM. I would also like to highly acknowledge R&D center at Saudi Aramco Dhahran and Mr. Mansour A. Shafei for the conductance of some specialized tests for my research.

I am also highly grateful to Dr. Fadlo T. Touma, owner and Director of Riyadh Geotechnique & Foundations (RGF) for permitting and facilitating me to pursue PhD degree as part-time student.

Last, but not the least, I extend my thanks to my wife and kids for their sacrifice, patience, moral support, encouragement, and prayers throughout my studies.

TABLE OF CONTENTS

LIST OF TABLES

LIST OF FIGURES

LIST OF ABBREVIATIONS

CEC	**:**	**Cation Exchange Capacity**
CED	**:**	**Cohesive Energy Density**
CT	**:**	**Computed Tomography**
EDS	**:**	**Energy Dispersive Spectroscopy**
ESEM	**:**	**Environmental Scanning Electron Microscope**
FTIR	**:**	**Fourier Transform Infrared Spectroscopy**
LJ	**:**	**Lennard Jones**
LL	**:**	**Liquid Limit**
MC	**:**	**Monte Carlo**
MD	**:**	**Molecular Dynamics**
MM	**:**	**Molecular Mechanics**
NPT	**:**	**Constant Number of Particles, Pressure, and Temperature Ensemble**
PI	**:**	**Plasticity Index**
PL	**:**	**Plastic Limit**
OMC	**:**	**Optimum Moisture Content**
XRD	**:**	**X-Ray Diffraction**

ABSTRACT

Full Name : [Habib-ur-Rehman Ahmed]

Thesis Title : [Molecular Level Modeling of Natural and Compacted Expansive Clays]

Major Field : [Civil Engineering]

Date of Degree : [January 2015]

Expansive clays are widely prevalent as one of the most challenging subjects in geotechnical, geoenvironmental, petroleum engineering, agriculture, and pharmaceutical fields. These clays/soils undergo significant volume change with a change in the moisture regime, thereby posing problems to the stability of the structures founded on such strata. Expansive clays are also commonly present in Saudi Arabia and concentrate mostly in the populated cities. Empirical and experimental based solutions and formulae to predict the expansive potential of these clays/soils have not been able to provide a comprehensive understanding for possible variations in the fabric and structure of the natural and compacted environments. Nano or molecular level processes, considered to play a central role in the volume change behavior of the expansive clays, is only partially considered in the current behavior models and even this partial consideration lacks the incorporation of natural clay fabrics with multiple clay minerals, silt and sand inclusions, micro fissures, cementation, over-consolidation, induration, and other such features. This research constituted four major levels of activities to encompass such challenges; (i) macro level testing, (ii) micro level imaging and analysis, (iii) molecular level simulations, and (iv) constitutive modeling. Molecular scale modeling of the swelling behavior was carried out using the concepts of molecular mechanics (MM), molecular dynamics (MD), and Monte

Carlo (MC) simulation techniques. The results of the molecular level simulations pertaining to different CECs, moisture, density, exchangeable cations, and cementation effects were compiled to form a nano model to determine the swelling potential of expansive clays. Swell potential, final dry densities, and final moisture contents predictions using the nano model have been found very close for the results from laboratory control samples. Therefore, the developed constitutive surfaces and equations can be comprehensively used for the expansive soils with both clay and non-clay minerals and all possible combinations of CEC, water content, density, total cations, and exchangeable cations. These models can also be applied to the clay/soil behavior in other fields including geoenvironmental, pharmaceutical, agriculture, geology, and petroleum engineering.

ملخص الرسالة

الاسم الكامل: حبيب الرحمن أحمد

عنوان الرسالة: النمذجة الجزيئية للتربة الطينية الطبيعية والمدموكة القابلة للانتفاخ

التخصص: الهندسة المدنية

تاريخ الدرجة العلمية: يناير 2015م

تعتبر التربة الطينية القابلة للانتفاخ والسائدة على نطاق واسع كأحد المواضيع الاكثر تحديا في الجيوتقنية، الجيوبيئية ، هندسة البترول، والزراعة، والمجالات الدوائية. هذه الطين او التربة تتعرض لتغير في الحجم نتيجة تغيير في الرطوبة، مما يؤدي الى مشاكل استقرار الهياكل التي تأسست على مثل هذه الطبقات. هذا الطين القابل للانتفاخ يتوجد بشكل كبير في المملكة العربية السعودية ويتركز معظمها في المدن السكنية. وتتعتبر الحلول والصيغ التجريبية والاختبارية القائمة والمستخدمة للتنبؤ باحتمالية الانتفاخ لهذا النوع من الطين او التربة غير قادرة على توفير الفهم الشامل للتغيرات المحتملة في نسيج وهيكل التربة الطبيعي والمدموك. تلعب عمليات النانو أو الجزيئات دورا محوريا في تغيير السلوك الحجمي للطين المنتفخ، والذي يكون فقط في السلوك الحالي للنموذج و يفتقر إلى دمج النسيج الطبيعي للطين مع المعادن الطينية المتعددة، والطمي و شوائب الرمل، الصدوع صغيرة، والاسمنتية، وعالية التصلب، والميزات الأخرى. يتكون هذا البحث من أربعة مستويات رئيسية للتغلب على هذه التحديات؛ (أ) اختبار المستوى الكلي، (ب) التصوير والتحليل علي المستوى الجزئي، (ج) المحاكاة الجزيئية، و (د) النموذج الاساسي. ان النمذجة الجزيئية للسلوك الانتفاخي تم عملة باستخدام مفاهيم الميكانيكا الجزيئية (MM)، والديناميك الجزيئية (MD)، و تقنية محاكاة مونت كارلو (MC). وجمعت نتائج المحاكاة الجزيئية المتعلقة ب CECs المختلفة، الرطوبة ،الكثافة ،الكاتيونات القابلة للاستبدال، تاثير المواد الاسمنتية لتشكيل نموذج النانو وذلك لتحديد إمكانية انتفاخ التربة الطينة القابلة للانتفاخ. تم العثور على ان استخدام نموذج النانو للتنبؤ على إمكانية الانتفاخ، والكثافة الجافة النهائية، ومحتويات الرطوبة النهائية قريبة جدا للنتائج الحاصل عليها للعينات التي تم اختبرها في المعمل. ولذلك، فإن السطوح والمعادلات التأسيسية المستنتجة يمكن استخدامها بشكل شامل للترب الانتفاخية مع

كل من الطين وغير الطين المعدني و احتمالية المزيج الممكن من CEC، ومحتوى الماء، والكثافة، ومجموع الكاتيونات، والكاتيونات القابلة للاستبدال. هذا النموذج يمكن تطبيقه لسلوك الطين او التربة في المجالات الاخرى بما في ذلك الجيوبيئية ، والمستحضرات الدوائية، والزراعة، والجيولوجيا، وهندسة البترول.

CHAPTER 1

INTRODUCTION

Expansive clays are widely prevalent all over the world as one of the most problematic and challenging soils. These soils undergo significant volume change with the change in the moisture regime, thereby posing problems to the stability of the structures founded on such strata. The expansive clays become highly erratic in behavior especially when present in unsaturated / partially saturated state having fluctuations of the saturation levels. More challenging is the fact that foundations of the most of the civil engineering structures are generally placed in the partially saturated soil zones with a continuously varying degree of saturation with the environmental and weather conditions. The American Society of Civil Engineers (ASCE, 2013) estimates that 25% of all the homes in the United States suffer some extent of damage by expansive soils and an estimate shows that in a typical year in the United States these soils cause a financial loss to property owners greater than other natural disasters such as earthquakes, floods, hurricanes and tornadoes combined. Expansive soils are also commonly present in the Kingdom of Saudi Arabia and concentrate mostly in the populated cities (Figure 1-1). These expansive soil deposits present in most parts of the Kingdom contain high percentages of expansive clay minerals (Table 1-1). Presence of high percentages of the expansive clay minerals result in high to very high swell potential of these soil deposits (Table 1-2). Consequently, structural and

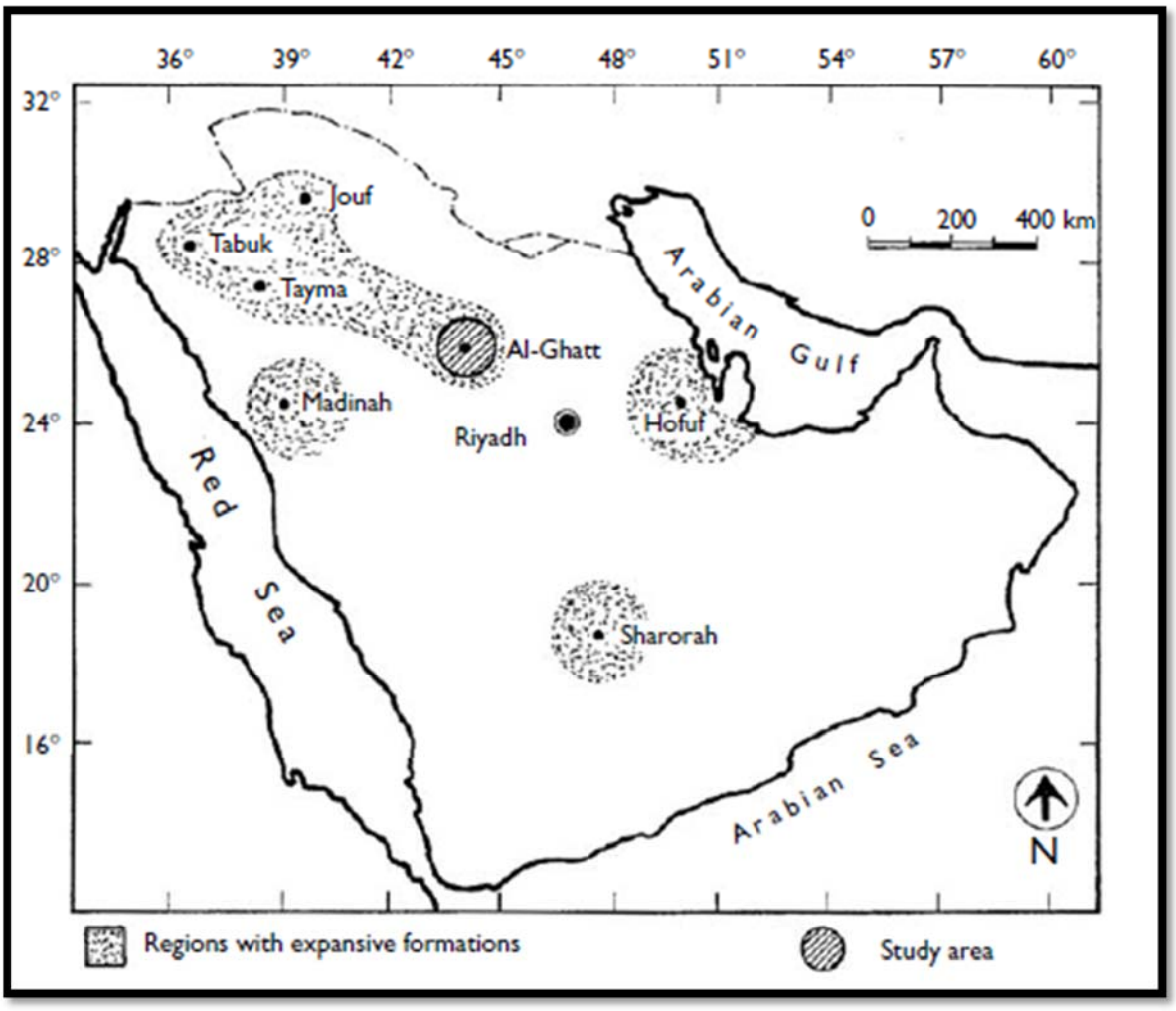

Figure 1-1 Prevalence of expansive clay deposits in Kingdom of Saudi Arabia (Abduljauwad et al., 1998).

functional damage to the structures of the entire housing complexes by the expansive clays is quite common in several areas of KSA (Figure 1-2). Empirical and experimental based solutions and formulae to predict the expansive potential of these soils have not been able to provide a comprehensive understanding for the various possible variations in the fabric and structure of the natural and compacted expansive clay soils. This chapter covers a brief overview of the limitations in the existing research, objectives of this research, and the corresponding outline of the proposed research plan.

Table 1-1 Mineralogical analysis of expansive clay deposits in the Kingdom of Saudi Arabia (Hameed, 1991).

Sample No.	Location	BH / TP No.	Depth (m)	Mineral type (% composition)
1	Al-Khars, Al-Hasa	BH-9	2.5-2.7	C(50), Q(10), P(8), K(5), I(9), S(7)
2	Mahasen-Aramco, Al-Hasa	BH-13	2.0-2.25	C(34), Q(16), P(8), K(3), I(31), S(4), St(4)
3	Al-Hamadiya	BH-11	1.0-1.3	C(35), Q(10), P(8), K(3), I(30), S(8), St(5)
4	Al-Salehiya	BH-12	2.4-2.7	C(19), Q(19), P(4), K(4), I(47), D(1), S(8)
5	Al-Khars, Al-Hasa	TP-7	1.1	C(39), Q(11), P(10), K(11), I(19), S(6), St(4)
6	Al-Naathel, Al-Hasa	TP-11	2.0-2.2	C(61), Q(24), P(6), K(3), S(6)
7	Mahasen-Aramco, Al-Hasa	TP-11	2.0-2.2	C(27), Q(19), P(10), K(5), I(32), S(4), St(3)
8	Housing Area	BH-1	3.8	Q(9), P(9), S(30), St(12), T, I(40)
9	Housing Area	BH-3	1.8-2.1	Q(7), K(<1), S(25), St(10), D(32), I
10	Umm Al-Sahek	BH-6	0.45-0.6	Q(4), K(<1), P(2), S(13), G(11), D(48), I(22)
11	Umm Al-Hammam	BH-8	5.6-5.75	C(<1), Q(10), P(11), D(<1), S(39), I(39)

C = Calcite
Q = Quartz
P = Palygorskite
St = Sepiolite
S = Smectite
K = Kaolinite
I = Illite
D = Dolomite
G = Gypsum
T = Talc

1.1 Background

The study of the interaction of clay minerals with the pore fluids and their contributions to the fabric, structure, and macroscale behavior and properties are critical not only in the fields of geotechnical engineering but also in geoenvironmental engineering, material sciences, pharmaceutical sciences etc. (Katti et al., 2011). Since the emergence of the

Table 1-2 Geotechnical properties of the expansive clay deposits in Qatif area, Kingdom of Saudi Arabia (Dafalla and Shamrani, 2012).

Brown calcareous green and brown clay, symbol (USCS): CH and MH	Property range for Al Qatif soils	
	Avg. min.	Avg. max.
Dry unit weight, gd, kN/m^3	10	14
Water contet, wn, %	15	40
Liquid limit, LL, %	120	160
Plastic limit, PL, %	30	60
Plasticity index, PI, %	90	100
Shrinkage limit, SL, %	9	15
Percent sand, %	0	5
Percent silt, %	15	50
Percent clay, %	50	90
Specific gravity, Gs	2.5	2.6
Selling pressure, kN/m^3	200	1000
Swell percent	2	20

unsaturated geotechnical engineering, performance of numerical modeling of the realistic volume change behavior of the expansive clays is a challenge for the geotechnical engineers. Consequently, several efforts have been made to develop constitutive models for the behavior of the expansive soils by performing parametric study mostly at the macro behavior level and to quite lesser extent at molecular level. All the developed constitutive models do not comprehensibly incorporate the coupling of the behavior at the macro, micro, and nano / molecular levels. Moreover, most of the developed constitutive models pertain to the standard expansive clay minerals compacted under controlled conditions; models covering the natural and real soil fabric do not exist.

Lack of proper understanding and knowledge of the nano / molecular level interactions of the clay minerals with the pore fluids and the other non-swelling constituents have limited

the development of specific constitutive models encompassing the accurate behavior under several possible combinations of clay, fluid and other non-swelling particles. This behavior becomes further complex for the swelling clays when the interaction between clay, fluid, and the non-swelling clay particles become predominant.

The swelling behavior of expansive soils is intrinsically controlled by their natural fabric and structure. Although the fabric of expansive soils is quite complex, Mitchell (2005) attempted to discretize soil fabric to be consisting of three general regimes of elementary particle arrangements as single form of particle interaction at the level of individual clay, silt, or sand particles, particle assemblage as units of particle organization having definable physical boundaries and pore spaces as fluid and/or gas filled voids within the soil fabric. Mitchell (2005) divided the fabric of a soil into three levels of scale as microfabric, minifabric, and macrofabric. Microfabric is defined as regular aggregations of particles and the very small pores between them; typical fabric units are up to a few tens of micrometers across. The minifabric consists of the aggregations of the microfabric and the interassemblage pores between them; minifabric being a few hundred micrometers in size. Finally, macrofabric may contain cracks, root holes, laminations, and the like that correspond to the transassemblage pores. Abduljauwad and Al-Sulaimani (1993) carriedout detailed research on the swelling potential of the clay soils in Qatif area of Saudi Arabia. As a result of these studies, they found substantial differences in the swelling potential assessed from the laboratory conventional Oedometer tests, laboratory tests on large scale block samples, and field tests on the subsurface strata (Table 1-3). They attributed these differences to the contribution of several macro to nano level structural features that might have been masked in the small scale laboratory tests. Moreover,

Figure 1-2 Views of the typical structural damages due to expansive clays in Kingdom of Saudi Arabia (Dafalla and Shamrani, 2012).

Table 1-3 Comparison of swelling potential based on the results from the laboratory and field tests (Abduljauwad and Al-Sulaimani, 1993).

Method	Percentage of Swell, %	Swelling Pressure, kPa	Heave, mm
Oedometer			
Improved simple oedometer	36	3100	63.9
Constant volume	--	800	47.5
Reverse curve	8.8	2000	58.6
Suction	--	--	36.8
Triaxial	14.3	420	39.6
Simulation swelling test	15.0	--	37.4
Field	15.4	180	38.4

El Sohby and Rabba (1981) also showed that swell percentage and pressure does not have a linear relationship with the various percentages of sand and silt content (Figure 1-3).

Based on the premise by Mitchell (2005) and the conclusions of Abduljauwad et al. (1993) and El Sohby and Rabba (1981), it seems essential that in addition to macro to nano level behavior, macro to nano level features should also be considered in the constitutive modeling of expansive clays. Gens and Alonso (1992) are considered as the pioneers in presenting a mathematical model for the expansive clays. Lumped fabric consisting of micro and nano level pores and idealization of a single mineral fabric attained under controlled compaction conditions by Gens and Alonso (1992) and their followers might not have led to the formulation of a complete representative behavior model.

1.2 Research objectives

Based on the deliberations in the narrated background, it could be inferred that nano or molecular level processes play a central role in the understanding of the volume change

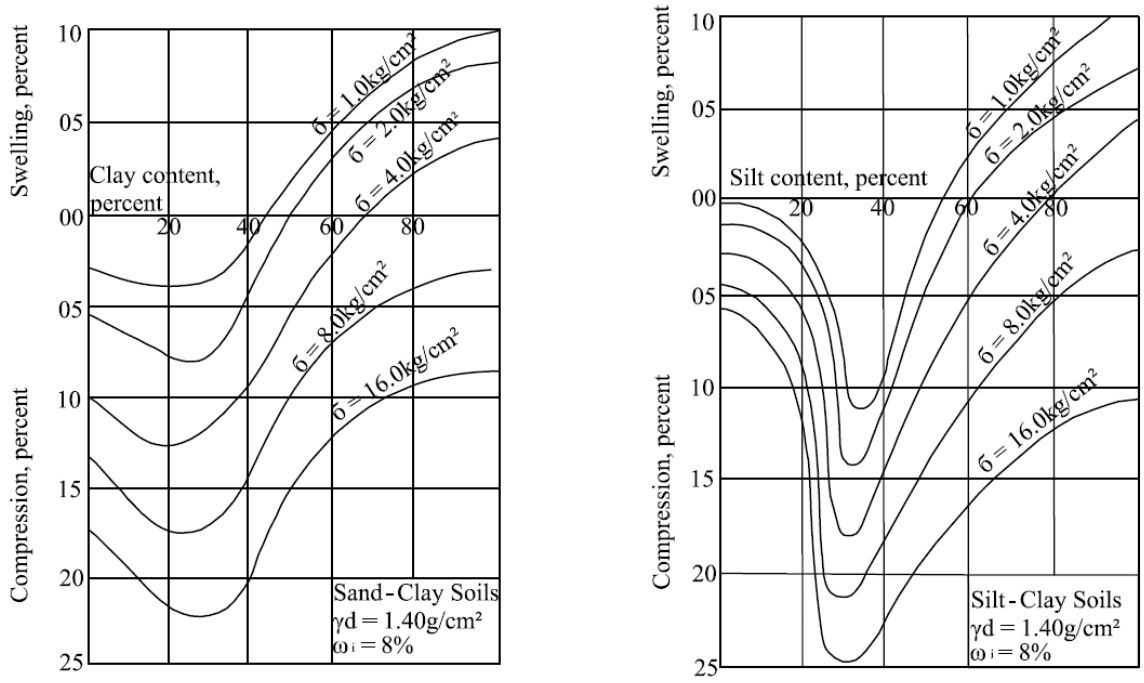

Figure 1-3 Comparison of swelling behavior of Sand-Clay and Silt-Clay mixtures (El Sohbi and Rabba, 1981).

behavior of the expansive clays. Although some studies have been conducted to simulate the swelling and / or water absorption behavior of the single or isolated expansive clay minerals, but modelling of the real / natural expansive soil fabric and its interaction with pore fluids at molecular level is still lacking. Moreover, no efforts have been directed even to couple the macro and micro scale material behavior based on the findings of these molecular simulations. As molecular level modeling studies could lead to the real insights into soil behavior, it would result in the validation and / or modifications of several macroscopic (continuum) constitutive behaviors. Recent advances in the numerical computational methods, high performance hardware, molecular modeling software, and the experimental techniques could be used to provide the real insight into the real behavior at the molecular level. This research aims at simulating the behavior of the natural expansive soils at micro and nano level using the molecular simulation techniques. Fabric and structure of the natural and compacted soil samples, required as an input in the simulations, would be evaluated using micro imaging and analysis through the specified laboratory imaging techniques. Based on the background described in the previous section, objectives of the proposed research could be summarized as follows:

- Mapping and analysis of the fabric and structure of the laboratory compacted and natural undisturbed expansive clays specimens using several nano / micro level imaging laboratory techniques at the pre and post swell states.
- Molecular scale modeling of the swelling behavior of the above mentioned natural and compacted fabric and structure using Molecular Mechanics (MM), Molecular Dynamics (MD), and Monte Carlo (MC) techniques.

- Formulation of constitutive relationships between swell potential and the various forms and types of fabrics and structures of the expansive soils.

1.3 Research Plan

The proposed research plan consists of preparation of laboratory compacted specimens, undisturbed sample collection of natural expansive clay deposits, conducting laboratory tests to acquire the parameters related with fabric and structure of natural and compacted specimens, swell potential tests, and finally conductance of molecular level modeling. The proposed activities are briefly narrated as under:

- Study and selection of the laboratory based investigation techniques for the clayey soils' fabric and structure, case studies on molecular level modeling of the swelling clays, and the software being used for the molecular level modeling purposes.
- Acquisition of undisturbed expansive clayey soil samples from several sources of expansive clay deposits in Qatif and Hofuf areas of the Kingdom of Saudi Arabia.
- Acquisition of individual clay and non-clay minerals from known / standard sources and preparation of the control specimens with known proportions of clay and non-clay minerals / particles and compacted at various known densities and moisture contents. Samples consisting of various proportions of Na-montmorillonite, Ca-montmorillonite, bentonite, kaolinite, sand, calcium carbonate, and gypsum would be prepared using static and dynamic compaction techniques.
- All the natural samples acquired from the field and the laboratory prepared specimens would be subjected to a series of free swell potential tests in general agreement with ASTM D 5890.

- Study and evaluation of the fabric, structure, and molecular level mapping of the natural expansive clay and control specimens would be carried out through the micro / nano level imaging techniques on the pre and post swell test specimens. This laboratory study would provide the real insight of the crystal level orientation and interaction among swelling and non-swelling soil particles with variations in the moisture and the density. All the field and laboratory prepared specimens would be sampled before and after the swell tests and would be evaluated using the following laboratory testing techniques:
    - X-ray powder diffraction (XRD)
    - Fourier Transform Infrared Spectroscopy (FTIR)
    - Environmental Scanning Electron Microscopy (ESEM)
    - Computerized X-ray Tomography (micro CT)

  These tests were performed at R&D Center of Saudi Aramco, Nanotechnology and Petroleum Refining Research Centers of the Research Institute (RI) of KFUPM, and Geotechnical Testing Laboratory of Riyadh Geotechnique & Foundations (RGF), Al-Khobar.

- The results of both the macro and micro level studies would be used to delineate the parameters required as an input in the molecular level modeling of the natural and compacted fabrics. Molecular mechanics (MM), molecular dynamics (MD), and Monte Carlo (MC) simulation techniques would be used to study the interactions between clay, hydrated cations, and the non-swelling soil particles under various fabric and structure conditions. Ensembles would be prepared to replicate the density and fabric of different type, nature, and orientation of the soil

particles on the wet and dry side of optimum moisture content. The simulations would be performed using Forcite and Sorption modules of Materials Studio software (2013) using the High Performance Computing (HPC) facility at KFUPM and NESER supercomputer at King Abdullah University of Sciences and Technology (KAUST), KSA.

- Compilation of all the results to formulate relationships between volume change and various parameters related with fabric and structure of the expansive clays such as Cation Exchange Capacity (CEC), type and concentration of exchangeable cations, anions, cementation effects, density, and moisture content.

CHAPTER 2

LITERATURE REVIEW

Although behavior modeling of expansive clays, as one of the most problematic soils, has always been a challenge for the geotechnical engineers, the study of the interaction of clay minerals with the pore fluids and their contributions to the fabric, structure, and macroscale behavior and properties are also central in geoenvironmental engineering, material sciences, agriculture, and pharmaceutical sciences. Although lot of research work has been done in this regard, empirical and experimental based solutions and formulae to predict the expansive potential of these soils have not been able to provide a comprehensive understanding for the various possible variations in the fabric and structure of the natural and compacted expansive clayey soils. Since the emergence of the unsaturated geotechnical engineering, performance of numerical modeling of the realistic volume change behavior of the expansive clays is a challenge for the geotechnical engineers. Consequently, several efforts have been made to develop constitutive models for the behavior of the expansive soils by performing parametric study mostly at the macro behavior level and to quite lesser extent at molecular level. All the developed constitutive models do not comprehensibly incorporate the coupling of the behavior at the macro, micro, and nano levels. Moreover, most of the developed constitutive models pertain to the standard expansive clay minerals compacted under controlled conditions; models covering the natural and real soil fabric do not exist.

Lack of proper understanding and knowledge of the molecular and nano level interactions of the clay minerals with the pore fluids and the other non-swelling constituents have limited the development of specific constitutive models encompassing the accurate behavior under several possible combinations of clay, fluid and other non-swelling particles. This behavior becomes further complex for the swelling clays when the interaction between clay, fluid, and the non-swelling clay particles become predominant.

This chapter covers the general comprehension of the fabric and structure of the swelling clays, swelling mechanism, and the corresponding level of efforts in the constitutive and molecular level modeling of expansive clayey soils. All these pertinent issues related to expansive clays are discussed in detail in the subsequent sections.

2.1 Fabric and structure of unsaturated expansive clays

Excessive volume change tendency of expansive clays is mainly attributed to the presence of expansive clay minerals in the soil fabric. These expansive clay minerals have got high affinity to the water and dissolved ions due to the net unbalanced electrical charges present on their surfaces. Volume change of the clay structure occurs once these expansive minerals absorb water and move from one partially saturated state to another. The volume change behavior is invariably controlled by many factors including type of clay minerals, current degree of saturation, past wetting-drying cycles, fabric and structure created during the compaction / natural deposition, presence of non-expansive minerals, their sizes, percentages and distribution in the matrix. A comprehensive constitutive model should encompass all these factors and their relative contribution to the physico-chemical-mechanical interactions at various scale levels. In order to integrate all these factors in a

constitutive model, understanding the behavior of the fabric at micro and nano level and its association with the macro behavior is required.

Most of the expansive clay minerals belong to the Smectite group and their typical expandable structure consisting of alternate silicate and alumina sheets is shown in Figure 2-1 (Mitchell, 2005). Each clay particle could be conceptualized as a flake / sheet like structure having dimensions of an order of nanometer with a length or width to thickness ratio of about 2000:1 (Sharma, 1998). The clay particles are also referred to as particles (Quirk and Murray, 1991), lamellae (Oades and Waters, 1991) or micelles at these finest levels. Isomorphous substitution, broken edges, and eccentric positive and negative charge centers result in net unbalanced charges on these particles. As a result of these unbalanced charges, these clay particles or sheets combine to form platelets of each about ten sheets (100:1) (Oades and Water, 1991). These have also been called grains, crystals or quasi-crystals (Quirk and Murray, 1991). Various bonding forces ranging from hydrogen bonds in kaolinite to van der Waals and cation bonding in montmorillonite exist in the individual clay particles or sheets. The group of platelets are present as micro-aggregates (Oades and Water, 1991) and clusters at the microscopic level and peds (Thomasson, 1978), macro-aggregates (Oades and Waters, 1991) or prisms (Cabidoche and Ruy, 2001) at macro level.

Most of the above explained terminologies and concepts related to the clay fabric pertain to the soils dealt by soil scientists. From geotechnical point of view, the first conceptual framework for the clay fabric was presented by Lambe (1958). Although his work was mainly related to the compacted clays only, he was able to provide a conceptual picture of

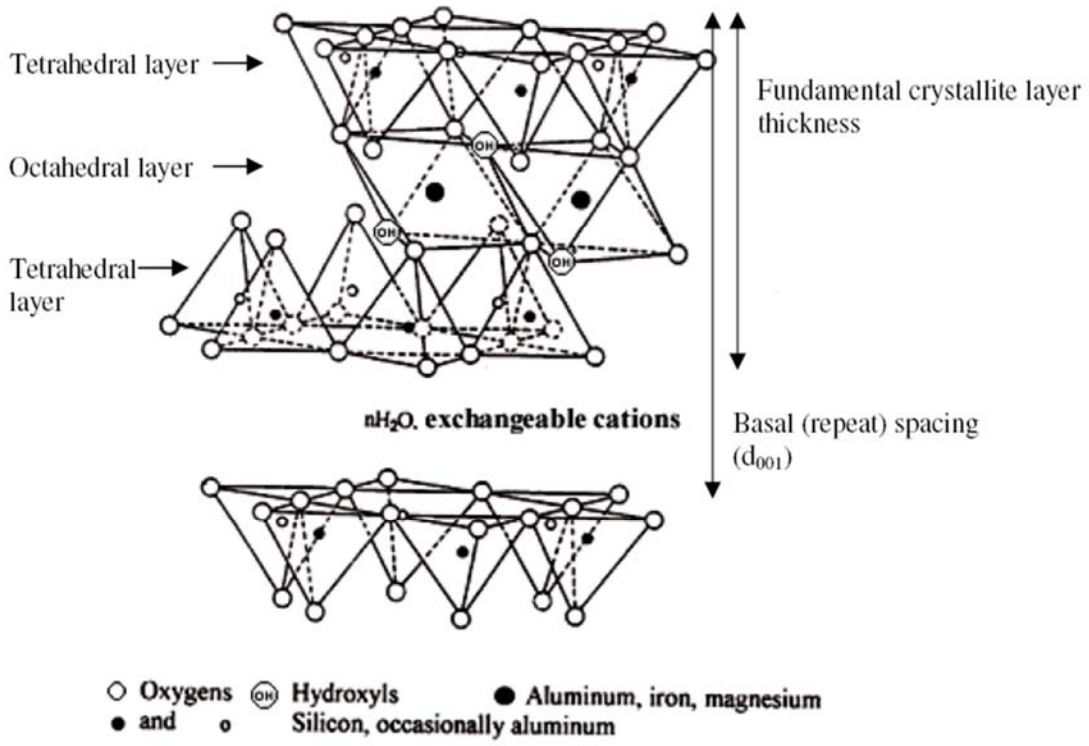

Figure 2-1 Schematics of smectite clay mineral group (Mitchell, 2005).

the clay fabric. He defined the bimodal fabric on dry side and massive and unimodal fabric on wet side of the optimum with the microvoids in between platelets and macrovoids in group of platelets. In his models, he identified three levels of fabric corresponding to three levels of void / fluid filled spaces, intra-platelet spaces between individual unit layers, small voids (microvoids) between individual clay platelets between larger flocs of packets of soils, and macrovoids between larger flocs and packets.

Gens and Alonso (1992), considered as pioneers in formulating the first constitutive model framework for the expansive soils, envisaged an expansive clay fabric (Figures 2-2a and 2-2b). They conceptualized the structural arrangement consisting of three basic microfabric features: elementary particle arrangements or quasi-crystals, particle assemblages, and pore spaces. Gens and Alonso (1992) described the particle assemblages formed by arrays of elementary particle arrangements as matrices. In their model, pore spaces in the matrices are made up of intramatrix pores existing between elementary particle arrangements. Elementary particle arrangements join together to make aggregates resulting in a three-dimensional structure of a granular type. Both inter and intra-aggregate pore spaces exist in the aggregated structure. A further level of void space also exists in the intraelement pores separating the clay platelets in the elementary particle arrangements. They related both the expansive and collapse type of phenomena to these forms of fabric. Clay structure conceptualized by Gens and Alonso (1992) was further supported by SEM micrographs of clay samples at optimum and dry and wet sides of optimum by Delage and Graham (1996). Conceptual clay structure in Figures 2-2a and 2-2b, respectively, represent the fabric on wet and dry side of optimum. However, one of major limitation in Gens and

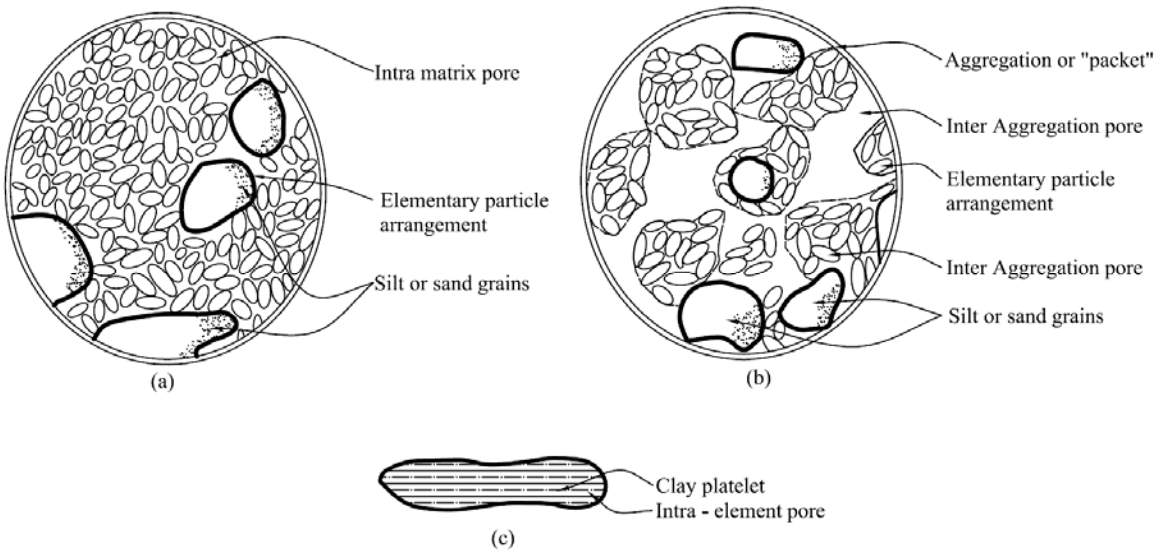

Figure 2-2 a) Micro b) Macro and c) Platelet level clay fabric (Gens and Alonso, 1992).

Alonso (1992) model is the consideration of the two micro level voids as one. This leads to the presence of two global levels only (intraplatelet spaces and microvoids between platelets) and contradicting the fact that microvoids and intervoid space between platelets may also be present in an unsaturated state. Therefore, their model may only be considered applicable to heavily compacted clays such as ones being used for the nuclear and other types of waste containment. Likos and Lu (2006) were the first to consider a more realistic fabric consisting of inter-aggregate, intra-aggregate (or inter-particle) and interlayer space levels. Their model is shown in Figure 2-3.

The clay fabric was also further elaborated by Sharma (1998), defining the micro and macro structure as assemblage of particles with three levels of voids as micro, macro and intra platelet voids. His conceptual model is shown schematically in Figure 2-4. Sanchez et al. (2005) also adopted the model of Gens and Alonso (1992) considering the two general levels of structures (Figure 2-5) and the assumption that microstructure is being considered as saturated at all the field conditions. Pinyol et al. (2007) studied and modeled the weathering of the soft clayey rocks and also considered a model similar to the Gens and Alonso (1992) with the addition of cementation at the platelet contacts. They also modeled the degradation of the cementation upon cyclic loading and weathering conditions. The conceptual model prepared by them for the cyclic load simulation is shown in Figure 2-6. This model could be considered a promising attempt to incorporate natural soil behavior but may be applicable to the homogenous type of clay rocks only and not to the soils consisting of multiple minerals. Moreover, Pinyol et al. (2007) did not consider the effects

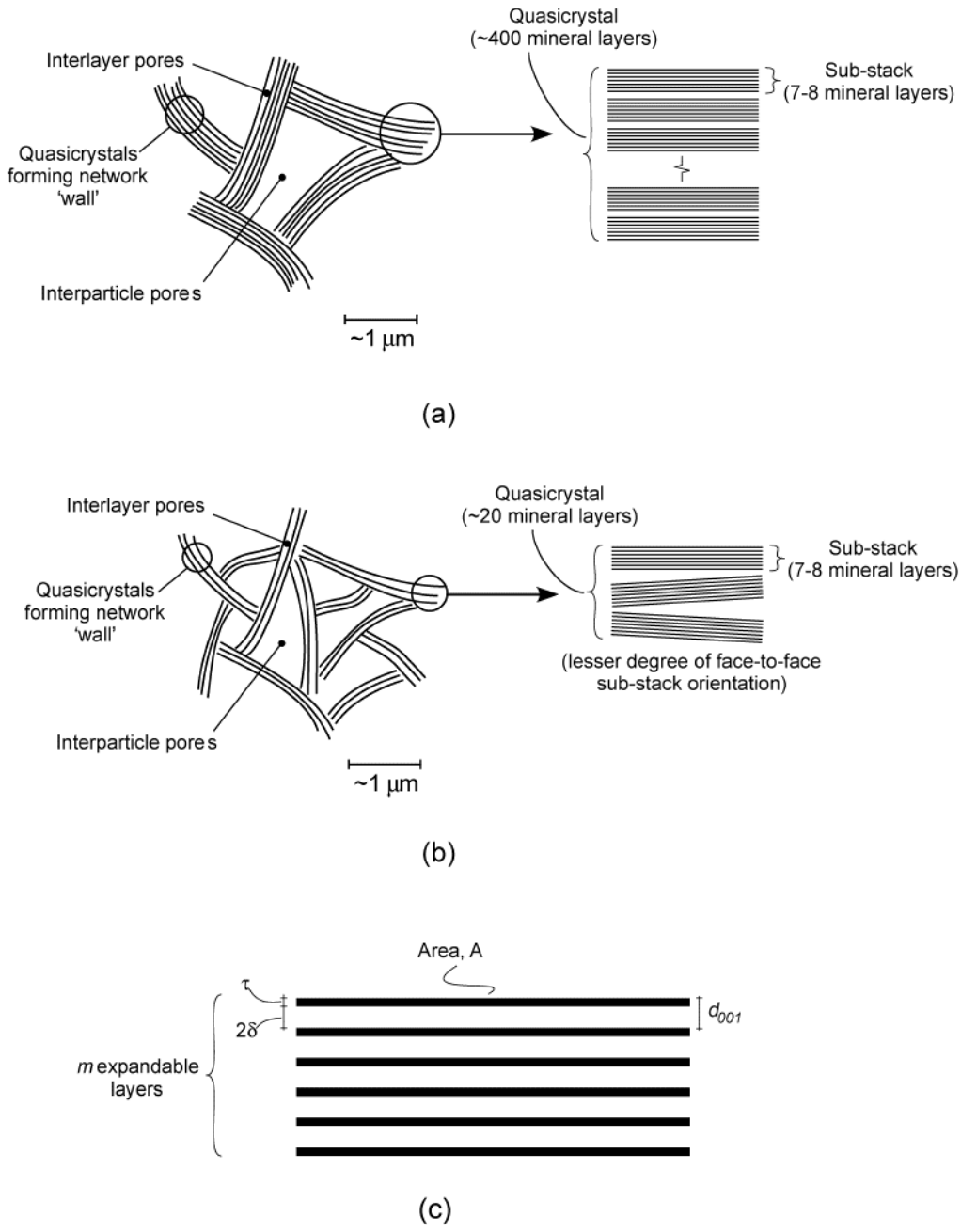

Figure 2-3 Conceptual microstructures for a) Ca^{2+} - smectite b) Na^{+} - smectite c) Features of an individual quasicrystal for the quantitative microstructural model (Likos and Lu, 2006).

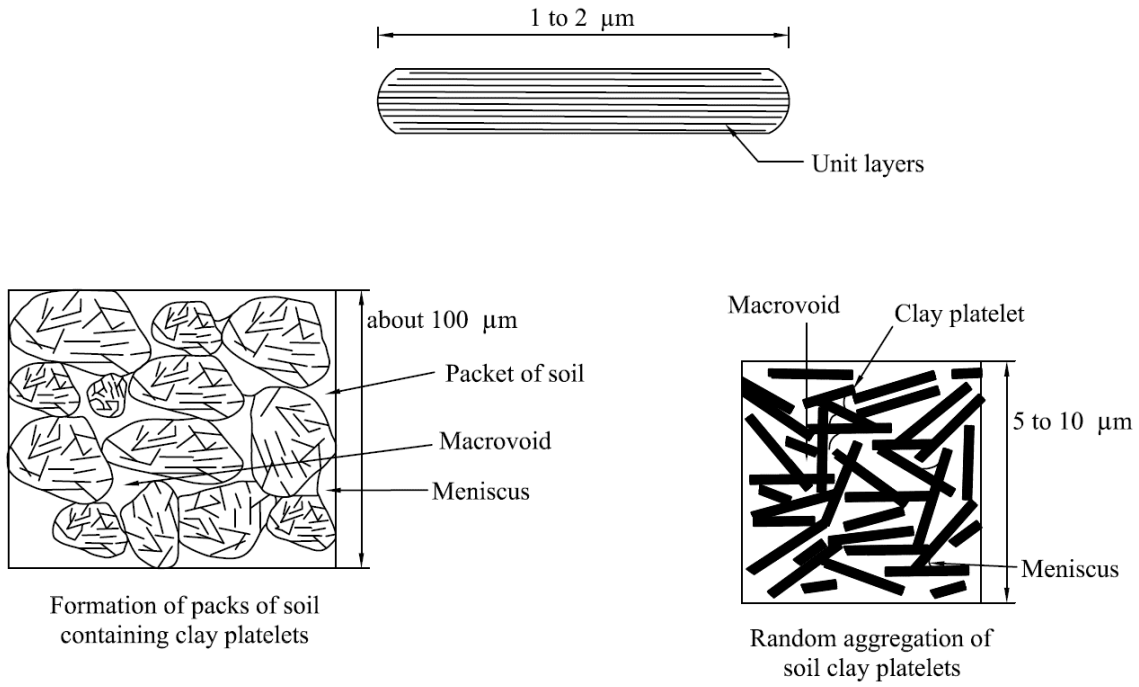

Figure 2-4 Conceptual fabric of clayey soils (Sharma, 1998).

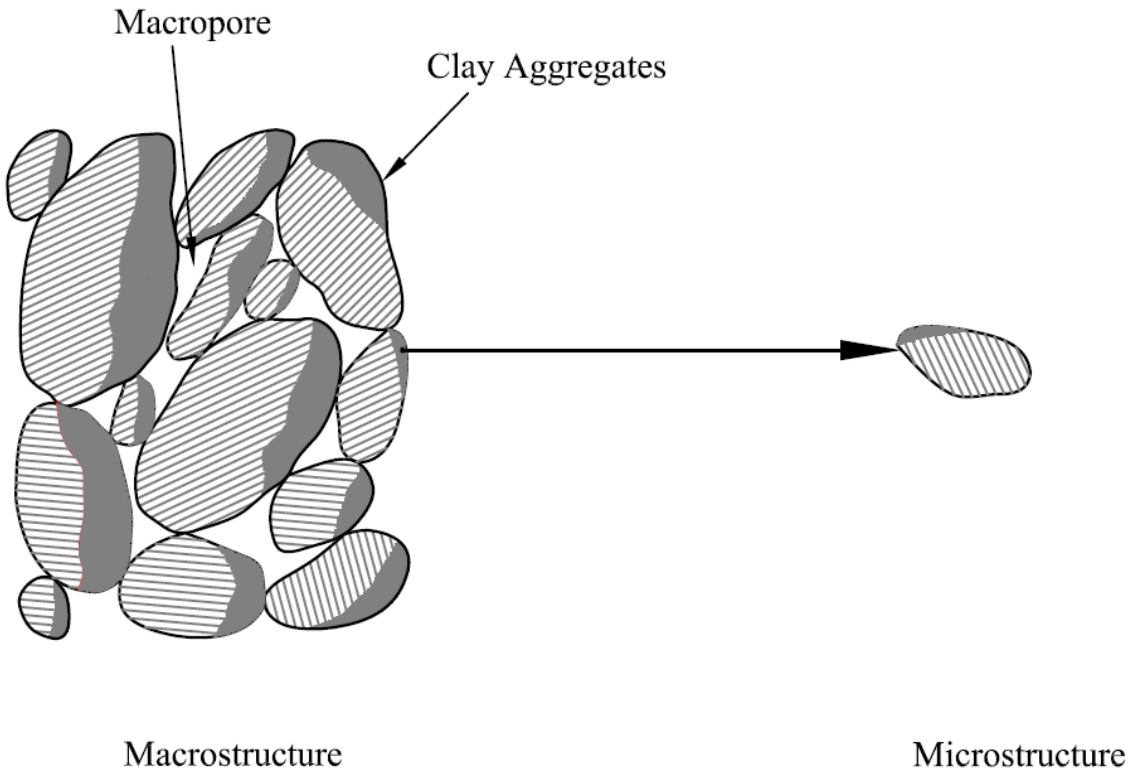

Figure 2-5 Micro and macro level clay structure concept (Sanchez et al., 2005).

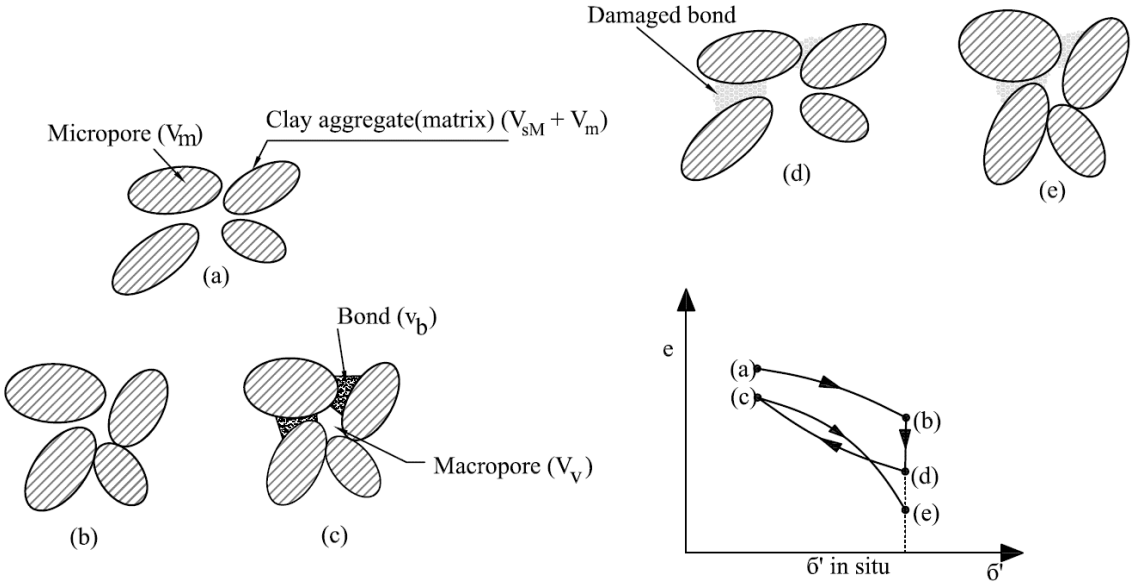

Figure 2-6 Interpretation of diagenesis process and structural effects of loading (a, b, and d), unloading (d and c) and reloading (c and e) cycle on a clayey rock (Pinyol et al., 2007).

of presence of fissures and cracks present in the natural clay fabric. These fissures and cracks should be considered inherent part of the natural deposits and contribute significantly towards the digenesis and weathering processes.

Fityus and Buzzi (2008) discussed and reviewed the effects of the clay microfabric on the volume change of the macrofabric in the existing models. They conceptualized clay structure as a group of aggregates and clusters into single structural element group called peds. A ped is a naturally occurring, structured soil element within a ripened (Pons and Van der Molen, 1977) heavy clay soil; that is bounded by discontinuities (typically cracks) that separate it from the adjacent elements of similar form. The ped could therefore be considered as basic unit of natural heavy clay soil at the macro scale. Particle size of montmorillonite particle size being in the order of 50 to 1600 nm (Robertson et al., 1968), it becomes difficult to characterize the structure and the pore spaces even using the most advanced and sophisticated Environmental Scanning Electron Microscope (ESEM) and X-ray Computed Tomography (CT) scanning or mercury porosimetry techniques (Fityus and Buzzi, 2008). In both naturally occurring and soils created from the consolidation of slurries have a very small pore size of an order of 3-10 nm and air entry value of 80-100 MPa as reported by Alymore and Quirk (1962), Oades and Water (1991), Quirk and Murray (1991), Villar (2000), and Meunier (2006). Based on this fact, saturation of the peds pass through drying and shrinkage cycles without any water loss and complete saturation is ensured at all the field suction values. However, Terzaghi's saturation and effective stress concepts could not be considered applicable to the saturated peds (Lambe and Whitman, 1959: Sridharan and Venkatappa, 1973: Heuckel, 1992). The structure envisioned as saturated soil peds separated by air-filled macroscopic desiccation cracks

(Figure 2-7) confirms that it cannot be modeled either as continuum or as unsaturated soils due to non-existence of surface films and water bridges.

Likos and Wayllace (2010) studied the porosity evolution of free and confined bentonite during the phase of the interlayer hydration. They came up with a bimodal porosity model developed for Wyoming bentonite using SEM image of the compacted bentonite. The schematic sketch of the model at several levels is shown in Figure 2-8. Hueckel (1992), while presenting his mixture theory approach for water-mineral interaction in clays under environmental loads provided in a schematic sketch various forms of water in high density clayey soil. His concept of various forms of water and the corresponding pores in a natural soil deposit are shown in Figure 2-9.

In addition to the fabric visualization of the expansive clayey soils, another important input required in any molecular level modeling / simulation is the size of the fundamental / smallest clay mineral crystallites. Several researchers have come up with a fundamental size ranging from as small as 100 Å (Longuet-Escard et al., 1960) to much greater than 1000 Å. Most probable reason for such wide range of clay mineral crystallite is the method used for the determination of the size. It has been observed that at most of the times, the imaging or mapping methods involve use of dry specimens. In dry form, the crystallites most probably get fused at the edges and ends and grow into larger crystallites. Moreover, flocculated fabric may also be responsible for such discrepancy. Therefore, the techniques involving the wet specimens such as ESEM and in the dispersed fabric form could provide the real fundamental crystallite size for clay minerals.

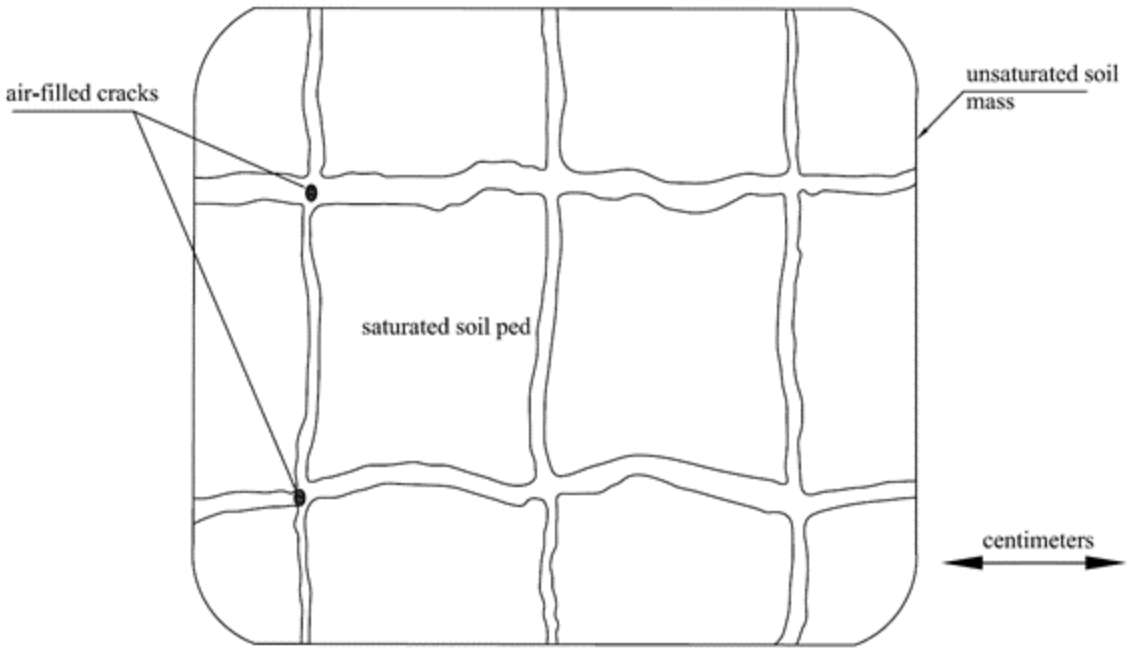

Figure 2-7 Schematic representation of a desiccated clay soil showing the differentiation between the unsaturated soil mass and the saturated soil elements (Fityus and Buzzy, 2009).

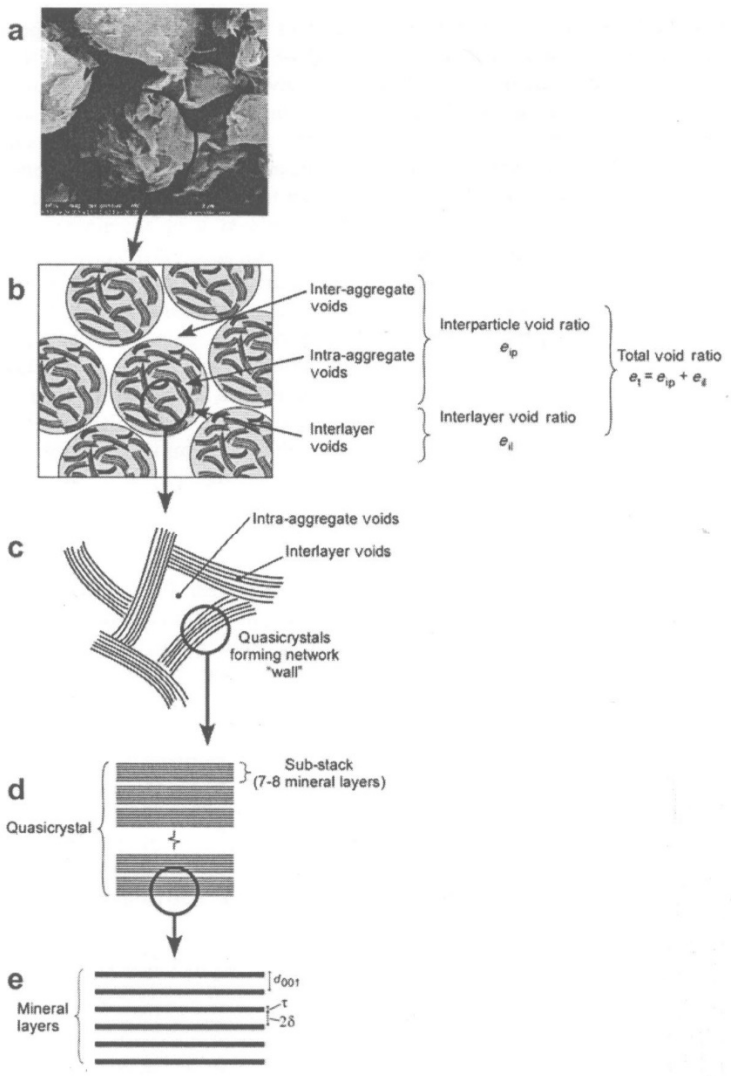

Figure 2-8 SEM Image (a) of compacted Wyoming bentonite showing bimodal porosity (image obtained parallel to compacted direction). Parts b-e are conceptual diagrams of pore spaces on the (b) inter-aggregate scale, (c) intra-aggregate scale, (d) quasicrystal scale, and (e) interlayer scale (Likos and Wayllace, 2010).

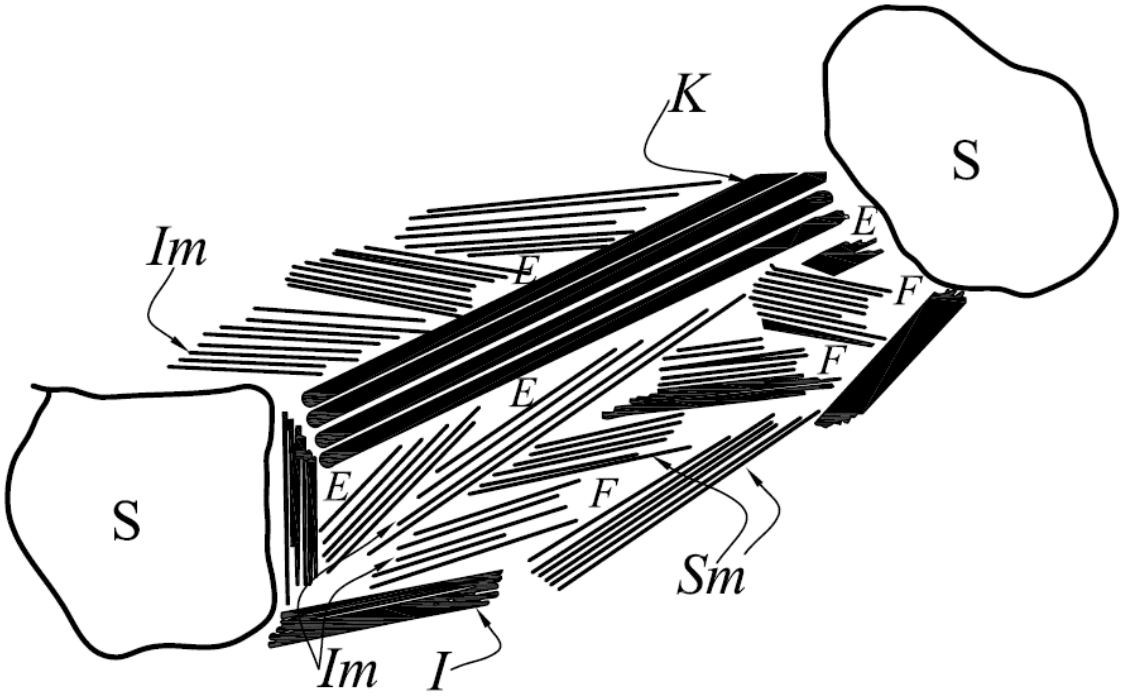

Figure 2-9 Forms of water in high-density clay soil. F, Free or bilk water; E, external or inter-cluster water; Im, inter-lamellar or intra-clsuter water; S, Silt; K, Kaolinite; I, Illite; Sm, Smectite (Hueckel, 1992).

The above discussions on the fabric of clays being conceptualized in the existing constitutive models reveal that there are several underlying simplified assumptions that obscure the real behavioral contribution from several levels. This fact is particularly true for the molecular / nano level contributions to macro level behavior. All the existing models ignore the molecular level considerations in their assumed clay fabric and hence its fundamental role in the overall behavior of expansive clays.

2.2 Swelling mechanism

Highly charged clay particles / platelets make bonds with water and the dissolved ions to satisfy their charges and consequently an expansion of their structures occurs. These expanded structures have a tendency to collapse / compress / shrink upon loss of water. Clay particle-water interaction theories date back to early 20th century when Guoy (1910) and Chapman (1913) came up with their diffuse double layer (DDL) theory. This theory was later on further refined by Stern (1923). In order to satisfy charges, DDL develops for individual clay units and platelets and is schematically shown in Figure 2-10. DDL can successively model the effects of cation valence, dielectric constant, electrolyte concentration, and temperature. However, there are certain limitations associated with DDL such as cations are being considered as point charges, DDL may not develop in highly compacted soils and there is less likelihood of presence of parallel clay particles in real clay fabric. Recently, Wayllace (2008) developed a general understanding of the structure of the swelling clay minerals, short and long-term water adsorption mechanisms, and influences of particle and pore fabric on swelling behavior using the porosity evolution

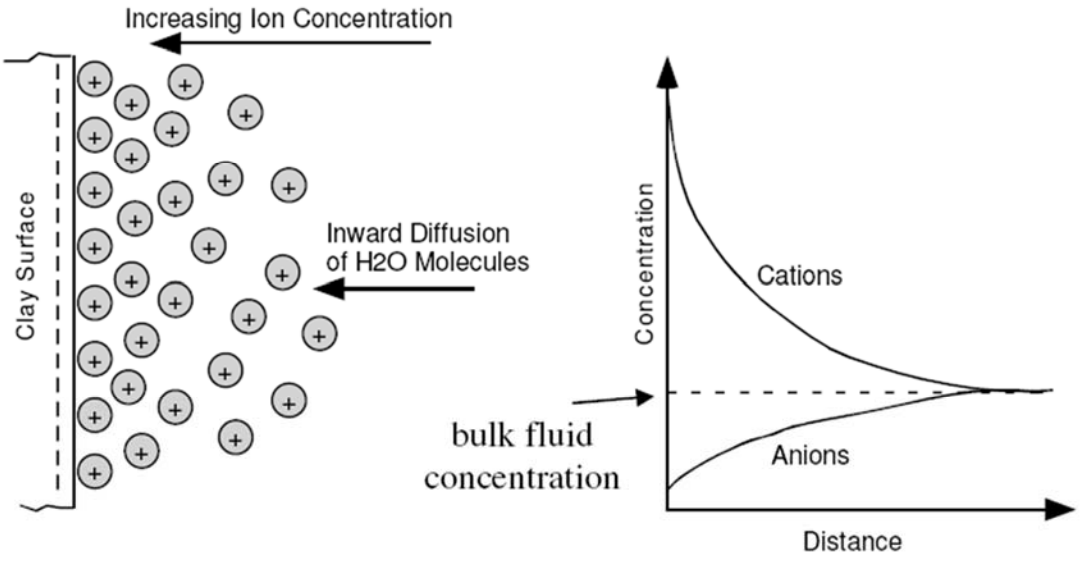

Figure 2-10 Diffuse Double Layer (DDL) concept (Guoy, 1910 and Chapman, 1913).

model developed by Likos and Lu (2006); the model is conceptually shown in Figure 2-11.

Wayllace (2008) divided the water adsorption phenomenon of the clay minerals into three micro-scale mechanisms as hydration, capillarity, and osmosis. Hydration and osmosis play a central role in two main clay swelling processes i.e. crystalline and osmotic swelling (Marshall, 1949; Van Olphen, 1977; Madsen and Muller-Vonmoos, 1989). Capillary mechanism is responsible only for the provision of the water for other major and short-ranged water adsorption mechanisms (Snethen et al., 1977; Miller, 1996). Wallayce (2008) emphasized the importance of the crystalline or type-I swelling as the key mechanism leading to a better understanding of the swelling behavior. Crystalline swelling is a process whereby expandable 2:1 phyllosilicates sequentially intercalate one, two, three or four discrete layers of H_2O molecules between the mineral interlayer (Norrish, 1954) shown schematically in Figure 2-12. Type-II swelling mechanism involves the hydration of the cations dissolved in the water layers. For example, Van Olphen (1963) calculated that for Ca-montmorillonite, the pressure associated with removing the water from the fourth, third, second, and first hydration states were 20,000 kPa, 125,000 kPa, 250,000 kPa, and 600,000 kPa, respectively.

Osmotic theory has also been used to explain the swelling characteristics of the clay particles (Bolt, 1956). An equilibrium analysis is carried out between the unit layers, clay platelets, and water by balancing the external and internal forces in order to achieve the maximum number of layers in a platelet. In order to maintain equilibrium, water flows from low concentration (bulk water) to higher concentration of ions (DDL water) and

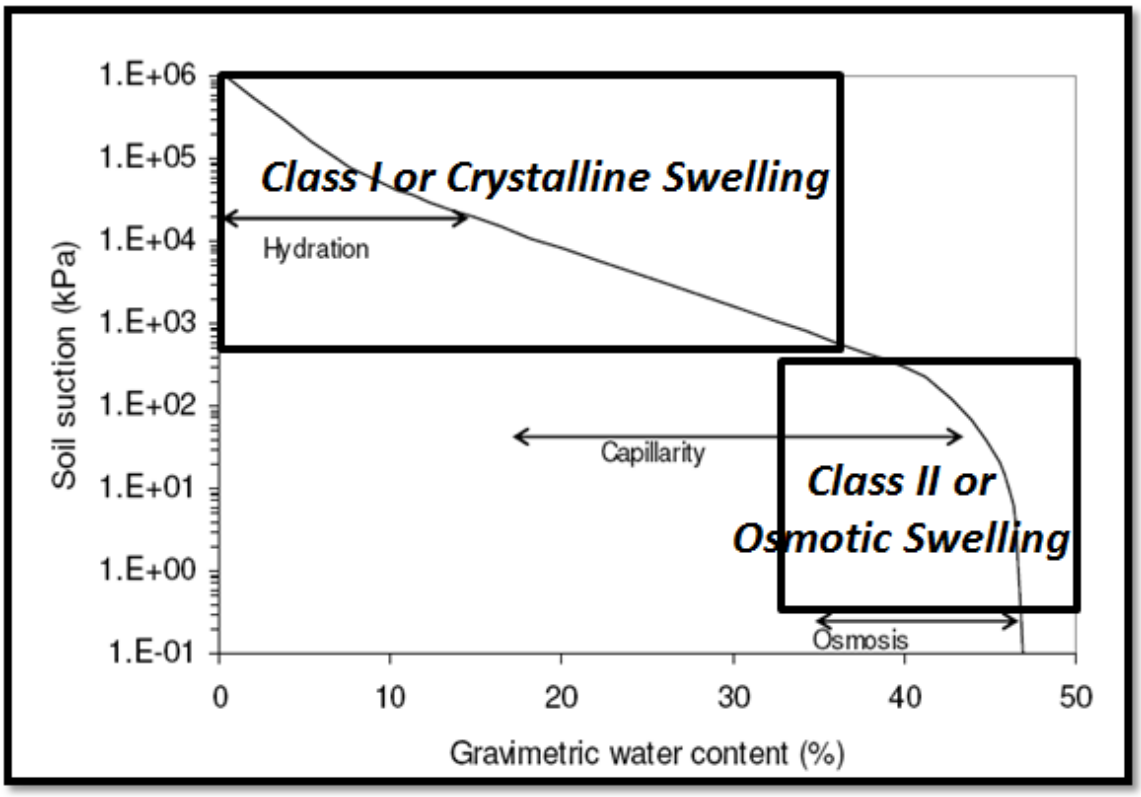

Figure 2-11 Regimes of crystalline and osmotic swelling (Wayllace, 2008)

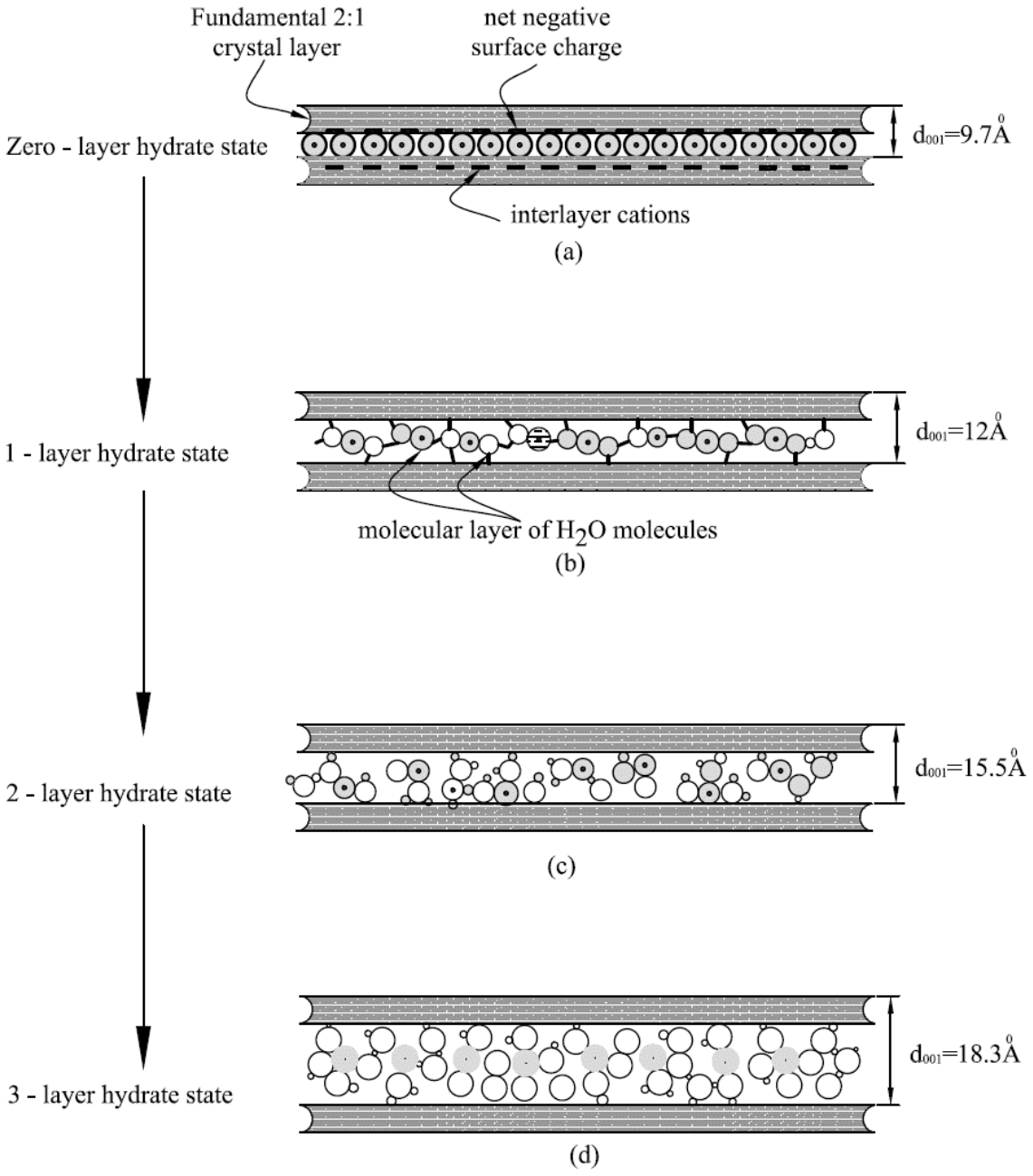

Figure 2-12 Hydration process of the clay particle layers (Wallayce, 2008)

increases the pressure in the DDL. This high pressure in turn causes the tendency to have a reverse flow till a balance is reached.

Few efforts have also been made at nano level to model the swelling mechanism of the swelling clays. The results of these studies are in some cases in contradiction of our general understanding of the swelling clays as per the above described models. This fact provides motivations and emphasizes the need for nano level modelling and consequently refinement and augmentation of the existing micro and macro scale models. Some of the nano scale simulation studies related to the swelling clays have been discussed under Nano Scale Modeling section.

2.3 Expansive clay modeling studies

Swell potential modeling of expansive clays have been carried out by several researchers with an objective of formulating the representative constitutive models. In this regards, efforts have been made at macro, micro, and nano / molecular levels to constitute behavior models for the expansive clays. As most of the constitutive modeling studies are carried out at macro / micro levels and the simulations have been performed at nano / molecular level, corresponding literature review has been divided into macro / micro and nano / molecular level studies and are detailed in the next sections.

2.3.1 Macro and micro level modeling

Constitutive model of expansive clays could be considered as a special case of the general constitutive models for the unsaturated soils. Therefore, chronology of models for

unsaturated soils are briefly discussed before a detailed review of the ones for expansive clays is presented.

In the realm of unsaturated soils, Matyas and Radhakrishna (1968) could be considered as the pioneers to create the concept of state (constitutive) surfaces relating the void ratio and degree of saturation with the state parameters net stress, p and suction, s. These surfaces are characterized by one of the very basic observation of the wetting induced swelling at low mean net stress while wetting induced collapse / compression at high mean net stress. The idea of state surfaces was, later on, extended and developed by Fredlund and Morgenstern (1977) and Fredlund (1979) and was called State Surface Approach (SSA). The equations suggested by the authors represent the planar surfaces and are limited by the fact that these do not account for the wetting induced collapse and swelling. Moreover these are valid only for monotonic loading and not for wetting and drying cycles. In addition, as stated above, no distinction can be made between elastic and plastic strains as these are only representative of the elastic zones. However, Fredlund (1979) suggested that these relations could be representative of the elasto-plastic strains if constants are functions of stress state. Later on, Lloret and Alonso (1985) proposed state surfaces relating void ratio and degree of saturation. Although these relations represent surfaces that can simulate the wetting induced compression and swelling behavior but these were again valid only over a limited stress interval.

Alonso et al. (1987) were the first ones to present an integrated volumetric and shear strength elasto-plastic framework of the unsaturated soils. The qualitative framework was further developed into its mathematical form by Alonso et al. (1990) in their landmark paper and was named Barcelona Basic Model (BBM). It would be quite correct to state

that all the recent models for unsaturated expansive and non-expansive soils are based on the same core of the BBM. Alonso et al. (1990) provided a complete mathematical formulation of the critical state based model for non-expansive or slightly expansive unsaturated soils. Four state variables i.e., mean net stress, suction, deviator stress, and the specific volume were used to formulate the model. The projection of the yield surface on p-s space (isotropic stress space) is a curved line known as Load-Collapse (LC) curve and shown in Figures 2-13 and 2-14. Plastic compression at high stress level upon wetting is modeled in a similar way as the plastic compression after crossing the yield point and change of specific volume upon plastic yielding. Volumetric decrease as a result of the increase in suction is delimited by the yield surface or limiting line of Suction Increase (SI) shown in Figure 2-14. Both SI and LC together mark the area characterized as elastic zone. They used the modified cam clay model as the interface with the saturated counterpart. Therefore, yield surface is an ellipse in anisotropic states in q:p plane at all suctions (Figure 2-15). Although non-linearity of the shear strength is well established but for the sake of the simplicity for the initial model, it has been taken as linear. Their proposed shear strength equation collapses to the one proposed by Fredlund (1979) when $c'=0$. They proposed non-associated flow rule model to match well with the K_o conditions of saturated sand. Ten soil constants are required for the development of the model while current soil state is defined as p, q, s and v or p, q, s and p(0). The model developed by Alonso et al. (1990) is volumetric in nature only and no consideration of mechanical behavior is taken in the model. Simplifying assumptions adopted in the model are the use of straight lines for the e – ln p relationships (implying a continuous increase of the collapse strains upon wetting) and the linear increase of apparent cohesion with suction. Moreover, no hydraulic

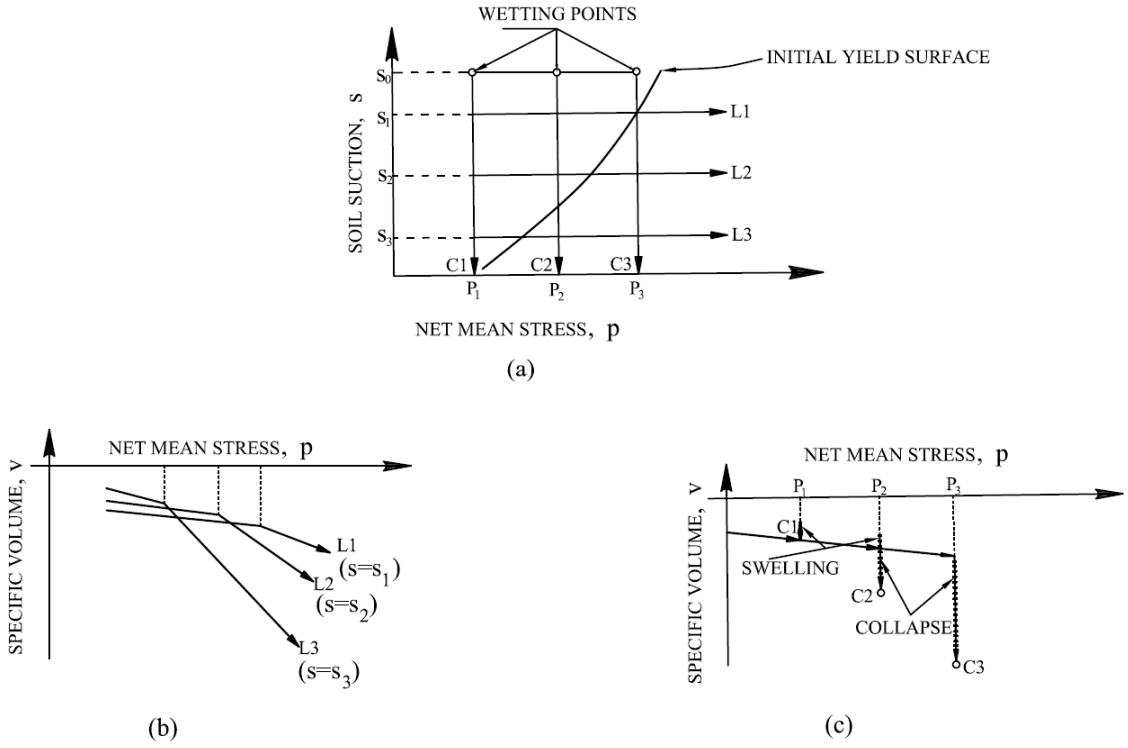

Figure 2-13 Load Collapse (LC) yield surface concept, b) and c) represents change in specific volume corresponding to L's and C's in a) respectively (Alonso et al., 1990).

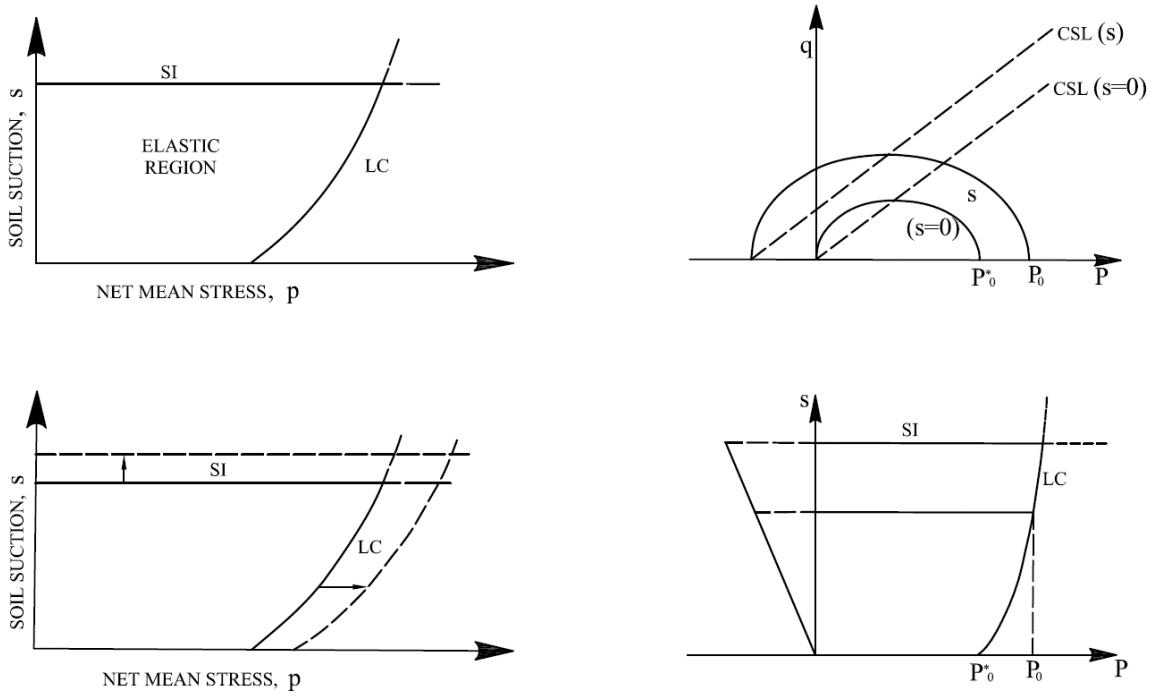

Figure 2-14 Elastic zone bounded by Load Collapse (LC) and Suction Increase (SI) curves (Alonso et al., 1990).

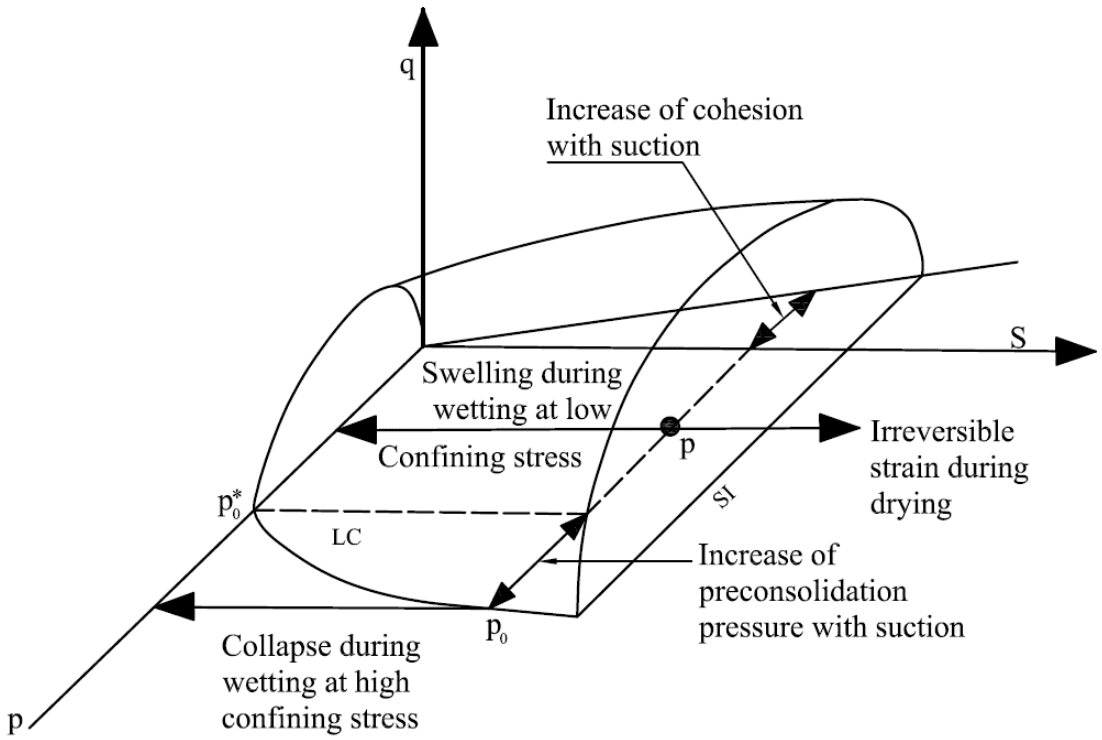

Figure 2-15 3-D yield surfaces in p-q-s space (Alonso et al., 1990).

hysteresis has been incorporated in the model. In spite of its basic nature, BBM was quite able to define several typical behaviors of unsaturated soils such as the variation of wetting-induced swelling or collapse strains depending on the magnitude of applied stresses, the reversal of volumetric strains observed during wetting-induced collapse, the increase of shear strength with the increase in suction, stress path independency associated with wetting paths and the opposite when the stress path involves drying or the apparent increase of pre-consolidation stress with suction. BBM became a basis for its specific and advanced model for the expansive soils, BExM.

As BBM was developed for the non-expansive or slightly expansive soils, Gens and Alonso (1992) provided a breakthrough in the provision of a conceptual model encompassing the behavior model for expansive clays. The model was based on the behavior of an extension of the BBM. This model covers the limitation of the BBM to model the large strain behavior of expansive soils and hence introduced a microstructure model to be coupled with the macrostructure model of Alonso et al. (1990). In their coupled models, soil structure has been divided into two distinct levels i.e. micro and macro. Microstructure consists of quasi-crystals, particles assemblages, and pore spaces, while assemblages together formulate matrix in which large sized sand and silt particles are embedded. The extended model incorporates a microfabric of clay particles and aggregations embedded into an overall macrofabric of silt and sand size particles. The elementary particles group together to form aggregations and resulting in granular type of structure. The pores sizes in the formulated structure are present both as intra and inter aggregations. They considered microfabric to be only affected by the local stresses and hence effective stress principles may be applicable and volume change in microfabric to be reversible and

unaffected by strain in the macrofabric. This assumption leads to the fact that if sum of net stress and suction (p+s) remains constant, then no change in overall volume would occur and the stress state moves on a line known as neutral line (Figure 2-16). The microfabric in their model is essentially considered saturated even if the overall saturation of the soil fabric is not achieved. Although, micro structural level behavior remains generally independent of the macrostructure behavior and is basically controlled by the physicochemical processes causing volume variations, there is an obvious interaction and this has been covered in the extended model by coupling of the micro and macro structure (Figure 2-17). Therefore, the extended model for expansive clays should consist of three essential elements as soil behavior at macroscale, behavior at microscale, and the coupling between the two levels. One of the major limitations of the Gens and Alonso (1992) model was the assumption regarding the permanent saturation of the microfabric as that does not seem to be realistic as microvoids / inter platelet voids may remain unsaturated as well. The permanent saturation of the microfabric may be considered valid only for the intraplatelet fabric only. Moreover, this model was mainly conceptual in nature and no detailed mathematical formulation was provided till a complete mathematical model by Alonso et al. (1999), named as Barcelona Expansive Model (BExM).

Up to this stage, it is clear that modeling of expansive clays require consideration of three basic elements: microstructure model, macrostructure model and the interaction in the form of coupling functions. From Gens and Alonso (1992) model onwards, both the micro and macro level models of the unsaturated soils were mostly handled independently by several researchers. However, most of the researchers worked towards the development and improvement of the unsaturated soil model for non-expansive soils, while only few

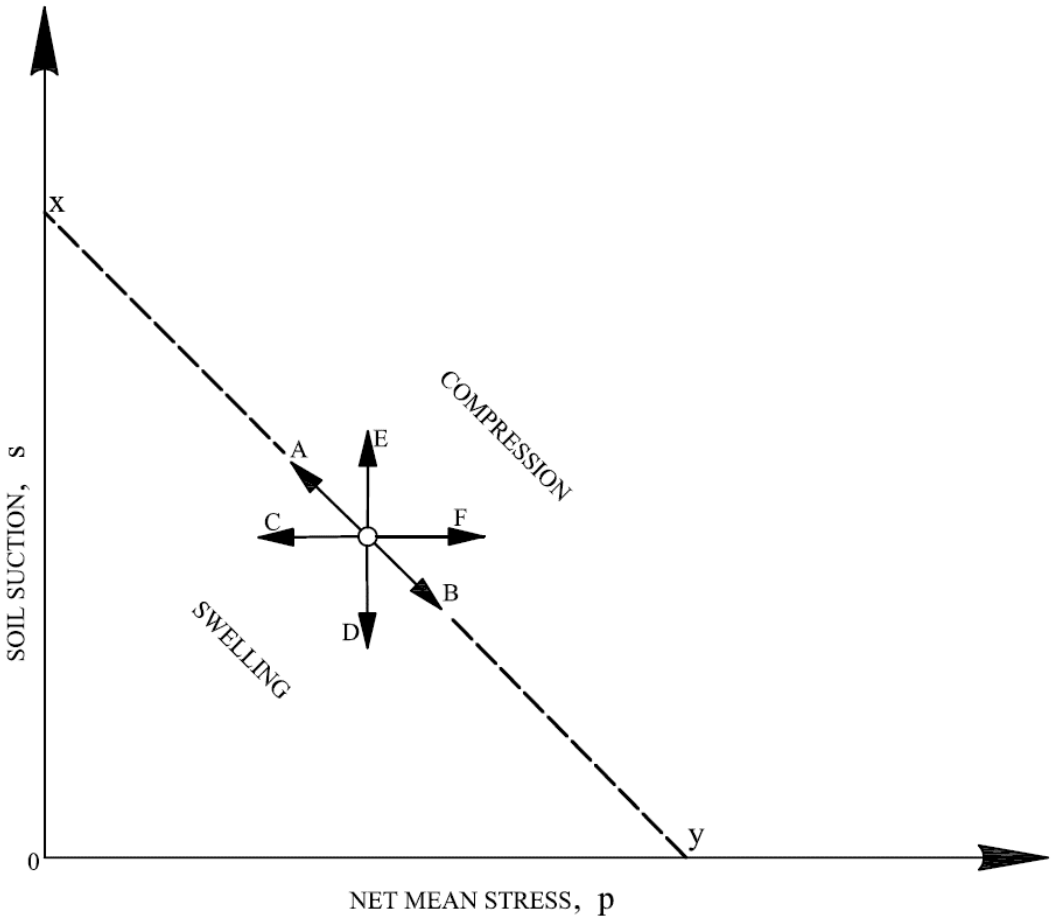

Figure 2-16 Neutral line representing microstructure in model (Gens and Alonso, 1992).

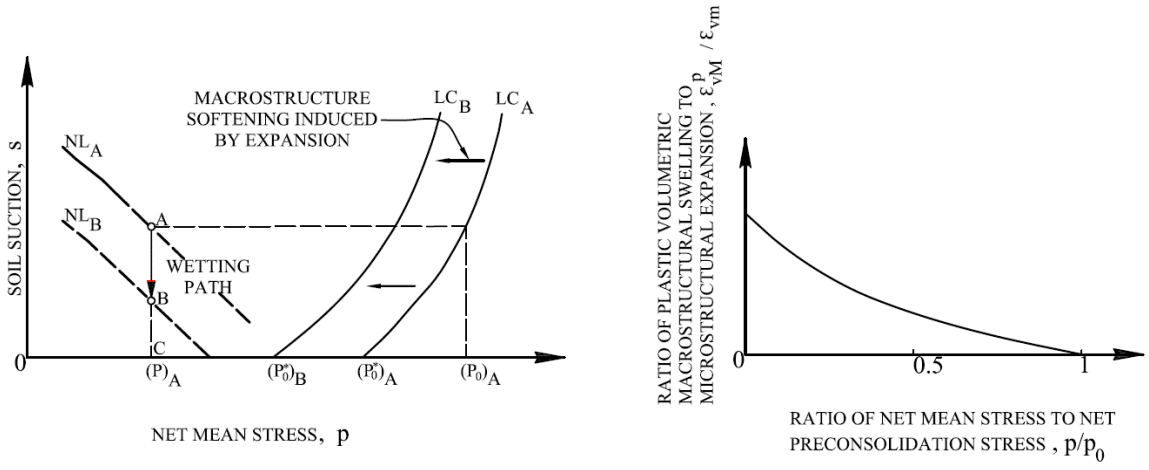

Figure 2-17 Coupling function in the expansive clay model (Gens and Alonso, 1992).

accomplished some improvements and variations in the expansive clays model. The rest of the discussions on the evolution of both the non-expansive model by Alonso et al. (1990) and expansive model by Gens and Alonso (1992) are presented mostly in the chronological order.

Alonso et al. (1999) had a landmark contribution in expansive clays model by developing a mathematical model for expansive clays based on the concepts developed in the models of Alonso et al. (1990) and Gens and Alonso (1992). Two additional yield surfaces, one for plastic yielding caused by suction increase (SI) and the other by suction decease (SD), were introduced (Figures 2-18 and 2-19). These surfaces are parallel to the neutral loading line in the space of net mean stress versus suction, and are coupled to the LC surface through two experimentally determined functions. The model by Alonso et al. (1999) is able to predict the irreversible expansion caused by wetting at low stresses and shrinkage at high stresses. In this model, macro-structural plastic volumetric change causes a corresponding change in the location of the LC. When the macro-structure becomes looser, the macro-structural yield surface shrinks. When the structure becomes denser, the elastic domain increases and LC expands. A coupling therefore exists between yield surfaces LC, SI and SD (Figures 2-18 and 2-19). However, irreversible change of degree of saturation during cyclic wetting and drying was not considered in the model of Gens and Alonso (1992) or of Alonso et al. (1999) and this has remained one the major limitation of these models even to the present.

After Alonso et al. (1999) BExM, major contribution towards the development of the expansive clay models was done by Sanchez et al. (2005) who formulated an expansive

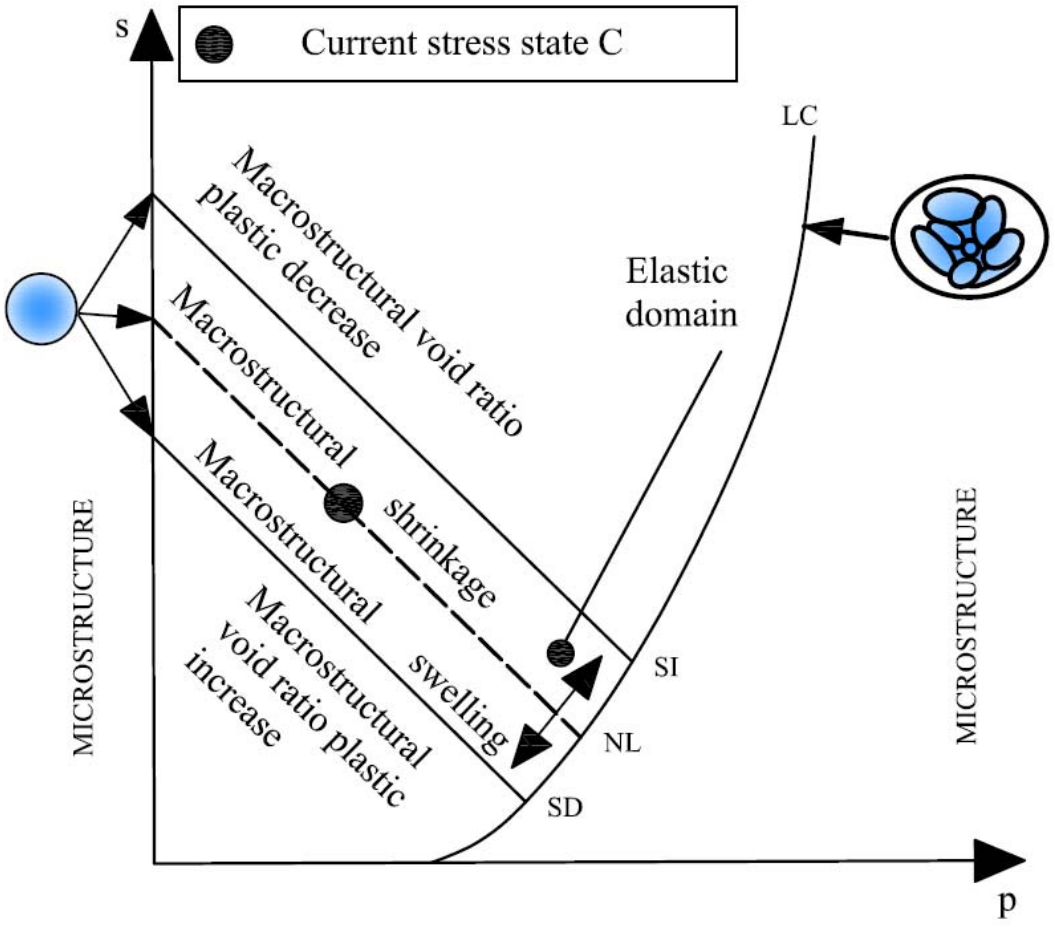

Figure 2-18 Barcelona Expansive Model (BExM) (Alonso et al., 1999).

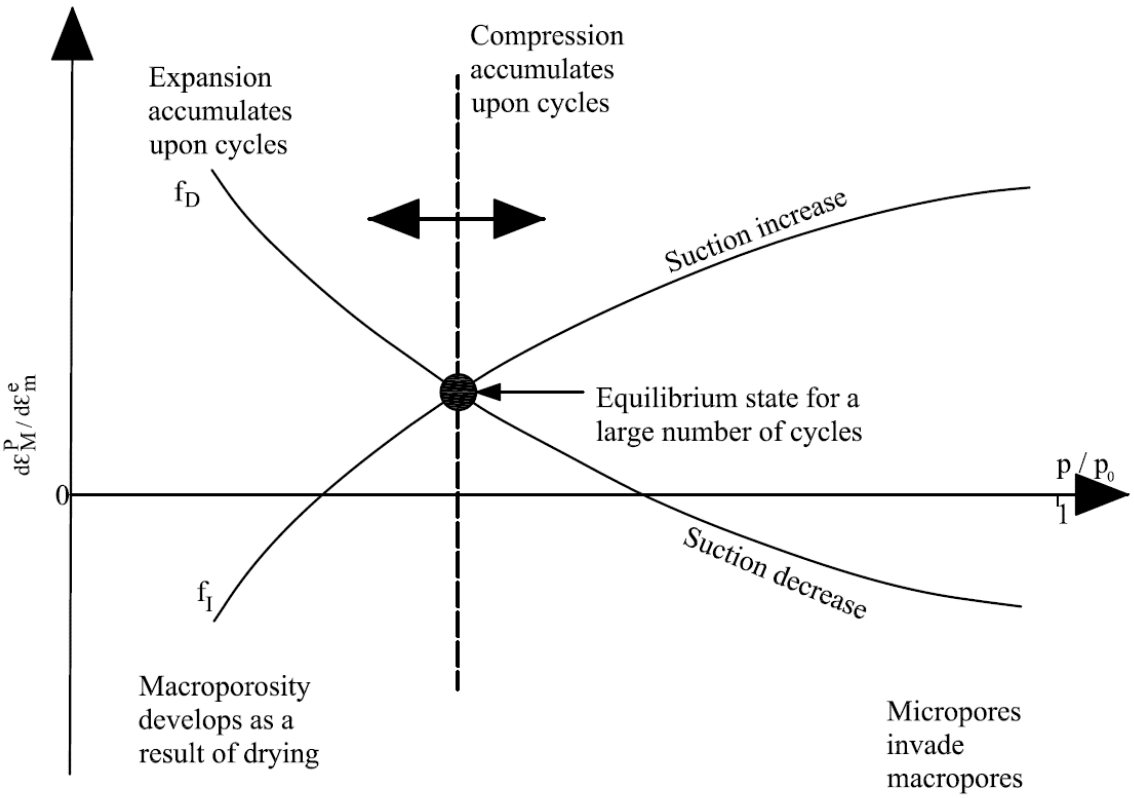

Figure 2-19 Interaction and coupling functions in BExM (Alonso et al., 1999).

clays model considering concepts of classical and generalized plasticity theories and is shown in Figure 2-20. They developed generalized stress–strain rate equations from the concept of a framework of multi-dissipative materials. This framework provides a consistent and formal approach when there are several sources of energy dissipation and is well suited for the modeling of generalized stress reversals. They used a generalized plasticity model for the materials that show irrecoverable deformations upon reloading and also to include the behavior of soils under cyclic loading when they exhibit irreversible deformation in loading, unloading, and reloading. They were successful in modeling the typical aspects of the behavior observed in expansive soils under generalized stress paths including suction and stress changes. The authors attributed significant advantages in using generalized plasticity theory to model the plastic mechanism related to the interaction between two levels of pores structures.

Sanchez et al. (2005) formulated the model in the space of stresses, suction and temperature; and implemented the double structure approach in a finite element program CODE BRIGHT. The mechanical law of this model is able to model the macropore invasion induced by microstructure expansion, when conditions of high confinement prevail considering negative values of the function fs for high values of $p=p_o$ (Figures 2-20 and 2-21). In Figure 2-21, point at which both interaction curves meet, indicated as E; is the equilibrium point. This point represents the state of the material for which no cumulative deformations are observed after cycles of suction changes.

Next major contribution in the modeling of expansive clays could be considered by Pinyol et al. (2007) who investigated the dual nature of Claystone by developing independent constitutive models for their rock-like and clay-like behavior. Claystone acts like a Rock

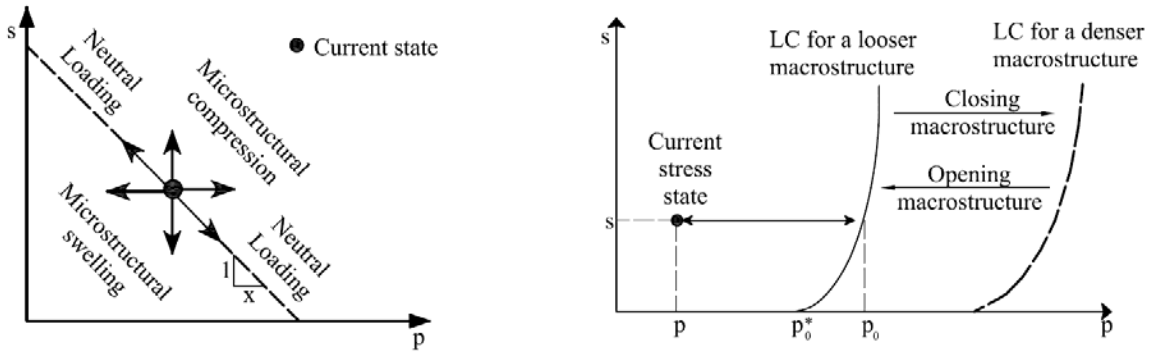

Figure 2-20 Constitutive surface for expansive clay in the model (Sanchez et al., 2005).

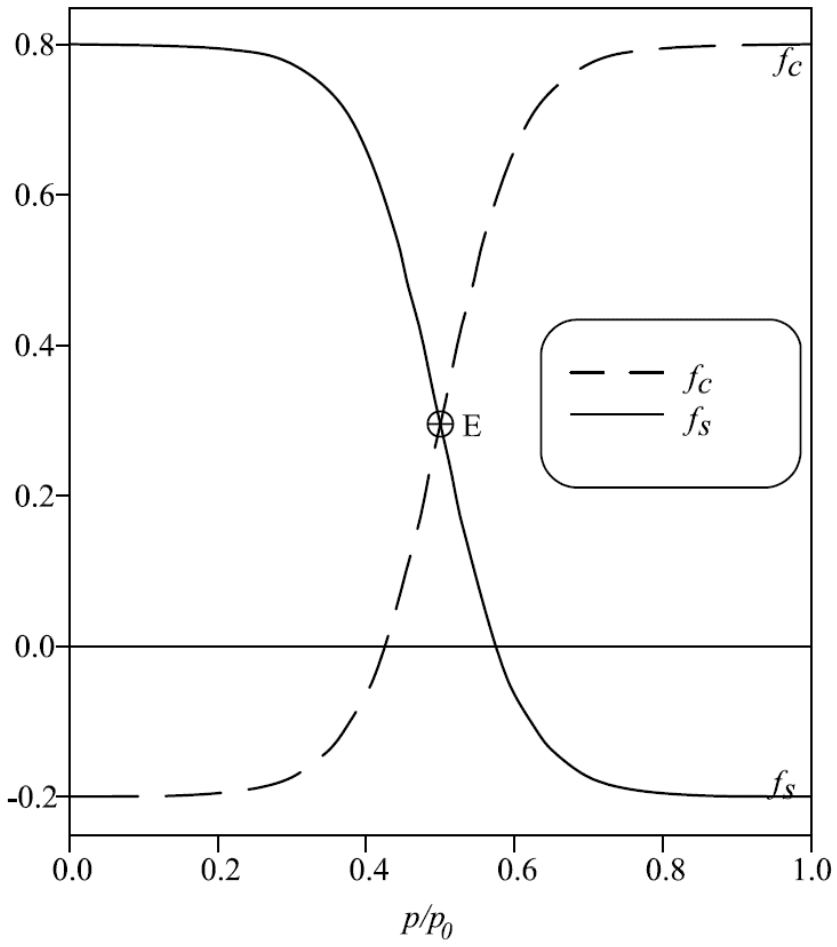

Figure 2-21 Coupling functions between macro and micro structure in the model (Sanchez et al., 2005).

when present in the unweathered state while it behaves as Soil in its weathered state. The authors attributed this dual behavior to the presence of basic clay matrix and the quasi-brittle cementation at the microstructure level. They considered the matrix behavior by the elasto-plastic double structure model proposed by Gens and Alonso (1992) and Alonso et al. (1999), while cementation / bonding was modeled using the damage mechanics based model. They demonstrated the effectiveness of the developed integrated models through the data generated through experimentation. Models by Pinyol et al. (2007) could also be considered a substantial contribution in modeling the natural homogenous types of clay.

The challenge with BExM is that the micro parameters and the function coupling the micro and macro structural strains are difficult to determine experimentally. Moreover, BExM is mainly concentrating on the stress-strain and strength behavior without considering the water retention behavior of the expansive soils. In this respect, several models have been developed for unsaturated soils but no such effort has been made for expansive soils. Sun and Sun (2011) developed an elasto-plastic constitutive model for predicting the hydraulic and mechanical behavior of unsaturated expansive soils based on an existing hydro-mechanical model for unsaturated non-expansive soils. They basically developed the first macroscopic elastoplastic model for unsaturated expansive soils and also introduced the concept of equivalent void ratio curve to distinguish between the yield curve and plastic potential curve. Basis is the experimental data and the model developed for unsaturated non-expansive soils. This model incorporates the coupled hydro-mechanical effect of degree of saturation on the mechanical behavior and void ratio on the water-retention behavior. Sun and Sun (2011) argued that compression index of swelling clays have been found to be increasing with increase in suction while it decreases with increase in suction

for unsaturated non-expansive soils. This is a fundamental difference among the compressibility behavior of the unsaturated non-expansive and expansive soils. Their hydro-mechanically coupled elastoplastic model can predict the hydraulic and mechanical behavior of unsaturated expansive soils. While developing that model, they assumed that pore air and pore-water are continuous throughout the soil voids which are basically true for some regime of water content (degree of saturation) only. Besides being a macroscopic model, this is in fact a major limitation of the model.

Guimaraes et al. (2013) may be considered as the pioneer in the formulation of a chemo-mechanical model for the expansive clays with due consideration of the contribution from cation content, osmotic suction, and the cation exchange. Their model is a contribution to the microstructure model in the double-structure approach used by Sanchez et al. (2005). Their main assumption regarding the elastic or reversibility of the microstructure behavior remains the same. They introduced additional parameters for the microstructure to be incorporated into the constitutive model. Although, the model is quite capable of predicting the behavior of saturated and unsaturated behavior, but most of the basis is through the indirect inferences from macro level studies and no input from molecular level has been incorporated.

2.3.2 Nano / Molecular level modeling and simulations

Expansive clay minerals are nano-materials and nano-mechanics concepts can be used to improve fundamental understanding of the behavior and predict the volumetric changes under the desired boundary and stress conditions. By obtaining molecular-scale material properties, the macro-scale material behavior can be obtained, with limited input

parameters and with great accuracy and details. Following discussions will initially address the general approach being adopted for the molecular simulations followed by the presentation of some of the relevant and key contributions to the nano simulation of the expansive clay minerals.

For the purpose of molecular / nano level simulations, most commonly adopted technique is the Molecular Dynamics (MD). MD is a computational method which calculates the time dependent behavior of a molecular system. MD is based on Newton's second law of motion and provides a trajectory which specifies the variation of position and velocity of individual atoms in a molecular system with time. In this technique, Individual atoms are characterized by balls with bonds represented as springs. A variety of springs are introduced that capture stretching, angular rotation, and torsion non-bonded interactions are modeled as van der Waals and electrostatic. In MD, individual atoms would be represented by the balls and the connecting major bonds as springs, while non-bonded interactions among the molecules would be represented by the van der Waal's and electrostatics. The potential energy of the system is then calculated using a force-field and is used to calculate the trajectory of the atoms in a molecular system. Force-field (Brooks et al., 1983) is generally given by:

$$E_{Total} = E_{Coul} + E_{VDW} + E_{Bond\ Stretch} + E_{Angle\ Bend} + E_{Torsion} \qquad 2\text{-}1$$

where

$$E_{Coul} = \frac{e^2}{4\pi\varepsilon_o}\sum_{i\neq j}\frac{q_i q_j}{r_{ij}}$$

$$E_{VDW} = \sum_{i\neq j} D_o\left[\left[\frac{Ro}{r_{ij}}\right]^{12} - 2\left[\frac{R_o}{r_{ij}}\right]^{6}\right]$$

$$E_{Bond\ Stretch} = k_1(r - r_o)^2$$

Skipper et al. (1995a, 1995b) performed the swelling simulation of various clay minerals using Monte Carlo (MC) simulation technique. They used MONTE (Skipper 1992) software for the purpose. They explained the methodology and the simulation details in two of their consecutive papers (Skipper et al. 1995a and 1995b), respectively. They defined the atomic positions and the corresponding effective charges of the clay minerals for the simulation purpose. The outcome of the study showed that Monte Carlo simulations of the Wyoming-type montmorillonite and vermiculite have resulted in layer spacings, average potential energies, and molecular structure that are consistent with the experimental findings.

Karaborni et al. (1996) was one of the early researchers who adopted MD for the nano level simulations. They performed molecular dynamics and Monte Carlo simulations to study the lattice expansion mechanism of the Na-montmorillonite (Figure 2-22). The simulation results revealed and confirmed the generally accepted theory of four stable states at lattice basal spacings of 9.7, 12.0, 15.5 and 18.3 Å respectively. They also proved that swelling percentages and the swelling sites in the stable form of the Na-montmorillonite are generally in good quantitative agreement with the previous studies. The swelling process resulted in the development of one, three, and then five water layers. This anomalous behavior has been found to be contradicting the general concept of formation of hydrated cations layers of one, two, three, four etc. in Na-montmorillonite. They also theorized that relative amount of water adsorbed by Na-montmorillonite is a result of the balance between the hydrogen bonding between water and the tetrahedral sheets of the clay and water adsorption in the clay hexagonal cavities. Based on this theory, they defined the stable states to be those where one of the interaction becomes dominant, while an unstable state

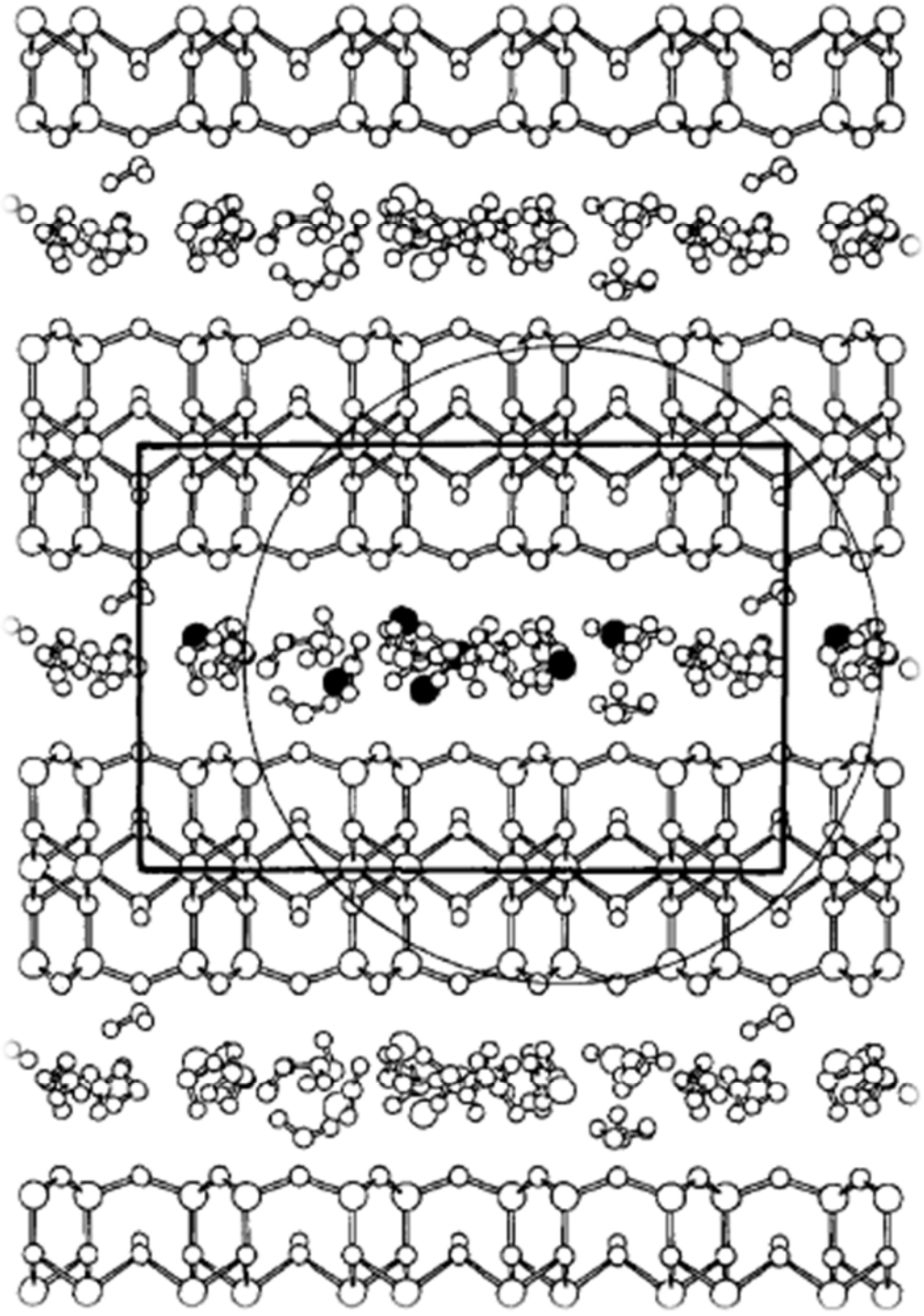

Figure 2-22 Molecular Simulation of the Hydration of Na Montmorillonite (Karaborni et al., 1996).

to be one where a 'frustration effect' is created due to the predominance of both the phenomena simultaneously. They attributed higher swelling potential of Na-montmorillonite to this phenomenon. Therefore, a transition would be required from one optimal orientation of water molecules to a second in order to cause expansion to the clay structure. Clearly, this transition requires lesser free volume of water and is quite easy to take place than the one with the addition of the simultaneous complete layers of water molecules.

Katti et al. (2005) conducted Molecular Dynamics (MD) study of the interlayer response of pyrophyllite under the influence of water and cations in the interlayer. They used NAMD (Phillips et al., 2005) and VMD software to perform interactive simulations and these were simulated on the North Dakota State University 32 processor parallel computer system. One of the major parts of the study was to transform the Consistent Force Field (CFF) parameters earlier developed by Teppen et. al. (1997) to CHARMm force field parameters. These were later on used with the NAMD software. Basic pyrophyllite model and the force applied model developed by the authors are respectively shown in Figures 2-23 and 2-24. In this study, forces were applied on the clay surfaces ranging from 0 pN to 160 pN simulating an equivalent stresses of 0 to 1.65 GPa. The authors concluded that deformation of the clay layers observed in this stress range is only ~1.6% compared to ~12.9% for the interlayer. The modulus of the interlayer and the two-clay-layer unit were found to be 13.18 GPa and 54.56 GPa, respectively.

Wang et al. (2007) studied the elastic properties of several minerals including quartz, albite, calcite, montmorillonite, kaolinite and palygorskite through MD technique. They modeled these minerals using both bonded and non-bonded interatomic contributions. The

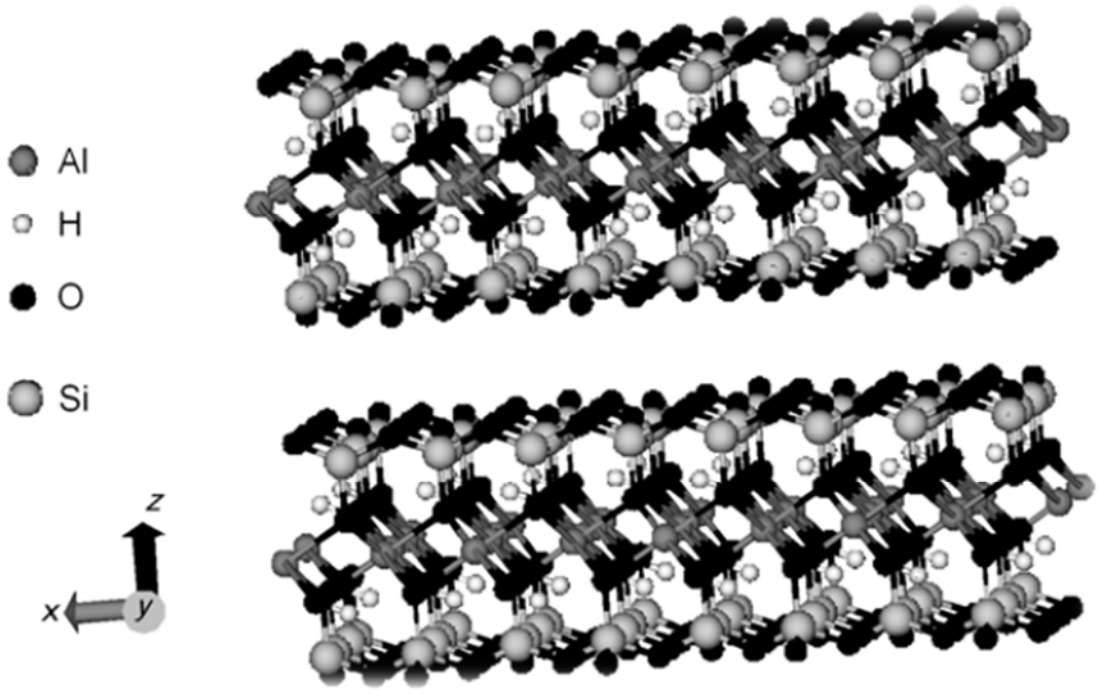

Figure 2-23 Perspective view of two pyrophyllite layers comprising 2 x 4 unit cells each (Katti et al., 2005).

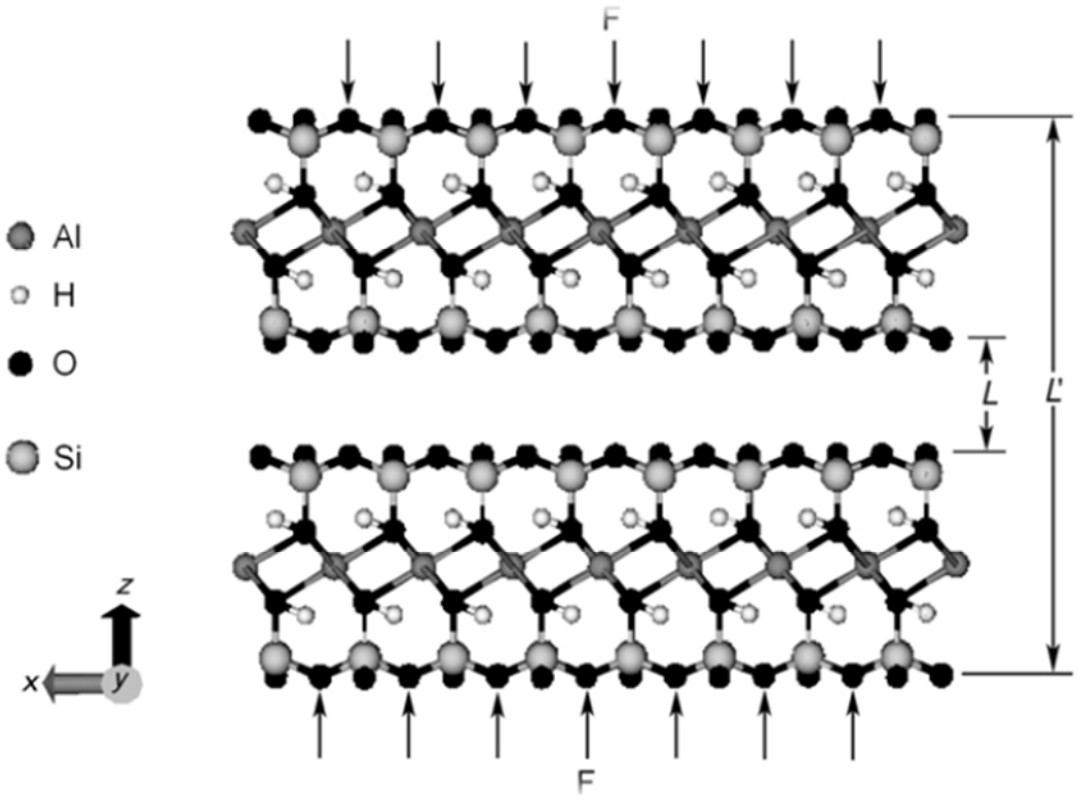

Figure 2-24 Forces applied normal to the simulation cell (Katti et al., 2005).

interatomic bonding energies, used in the molecular simulation, are expressed in the following Newtonian form as below:

$$m_i \frac{d^2\mathbf{r}_i}{dt^2} = \mathbf{F}_i \qquad 2\text{-}2$$

The force F_i acting on a particle i is calculated from the interatomic potential function U ($r, r_1, r_2, r_N \ldots$):

$$\mathbf{F}_i = \frac{\partial U(\mathbf{r}_1, \mathbf{r}_2, \ldots \mathbf{r}_N)}{\partial \mathbf{r}_i}, \quad i = 1,2,\ldots N \qquad 2\text{-}3$$

Dynamics of the system is dominated only by the interatomic potential function U that is representative of the atomic interaction owing to the complex quantum effects occurring at the subatomic level. They utilized the most commonly adopted pair-wise potentials inclusive of Lennard-Jones (LJ) and Morse potentials, as in the following equations:

$$U(\mathbf{r}_i, \mathbf{r}_j) = U(r) = 4\varepsilon\left[\left(\frac{\sigma}{r}\right)^{12} - \left(\frac{\sigma}{r}\right)^{6}\right], \quad r = |\mathbf{r}_{ij}| = |\mathbf{r}_i - \mathbf{r}_j|, \qquad \text{(LJ potential)} \quad 2\text{-}4$$

$$U(r) = \varepsilon\left[e^{2\beta(\rho - r)} - 2e^{\beta(\rho - r)}\right]. \qquad \text{(Morse potential)} \qquad 2\text{-}5$$

The potential function used by Sato et al. (2001) and Ichikawa et al. (2002) for the simulation of several clay minerals was used to simulate the specific minerals. The function is composed of several potentials such as Coulomb (attractive or repulsive), Born-Mayer-Higgins short range repulsion, van der Waals, and Morse terms. They used TINKER software (Ponder, 2011) for carrying out MD simulations. Data input included the initial configuration of the atomic structures and the interatomic potentials assigned to the specific mineral. An NPT (constant number of particles N, pressure P, and temperature T) ensemble was used to acquire the stress-strain behavior of the simulated minerals. The

results of the simulations as shown in Figure 2-25 reveal a general agreement between the measured and known values of modulli for the minerals except Kaolinite. The authors have attributed the anomalously higher modulus value of Kaolinite to the molecular arrangement at the crystal lattice level.

Wang and Gutierrez (2007) conducted a molecular simulation study of dehydrated 2:1 clay minerals by changing the MD cell size and shape under the general applied stress conditions. The molecular simulation method adopted by the authors considered the basic relationship between the atomic level stress tensors, including internal, external, and the simulation stress tensor. They thoroughly investigated the relaxation behavior of the dehydrated mica sheets by the incorporation of varying boundary conditions on the simulation cell. It was concluded that the degree of freedom of the simulation cell is directly related to the formation of the final crystal structure. One of the important conclusions was the shear deformation of the crystal structure in the absence of any boundary constraint. They also showed that the interlayer spacing could either be reduced or completely removed by application of the high normal pressures.

Katti et al. (2009) studied the effect of swelling and swelling pressure of the montmorillonite clay using the experimental set up and further validated the results using numerical techniques. They used a specially designed swelling device to control the swelling and swelling pressure of the sample and studied the clay fabric created at each specified level. They concluded that there is breakdown of the clay particles / assemblages as the swelling of the clay particles increases as a result of intake of water. They used Fourier Transform Infrared Spectroscopy (FTIR) and X-ray diffraction (XRD) techniques

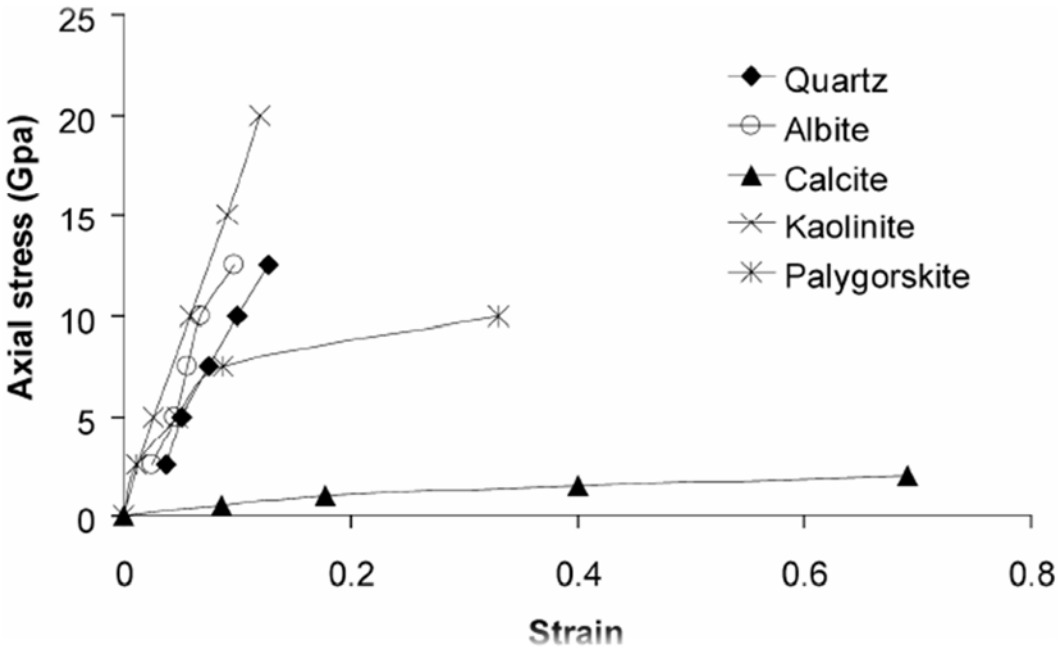

Figure 2-25 Modulli values for various minerals obtained from the Nano-scale modelling (Wang et al., 2007).

to study the microstructure of the swollen clays. They also used Discrete Element Method (DEM) and Steered MD based numerical techniques to model the swelling behavior of clay soils. Basic model of Na-montmorillonite with 3 water layers is shown in Figure 2-26, while the plots of stress vs. interlayer strain with the variation of water content is shown in Figure 2-27. Based on the experimental and numerical simulation, main conclusion of their study was there is increase in d-spacing of the clay particles as a result of the swelling and beyond certain d-spacing, particle assemblage breakdown takes place and more and more particles are exposed to swelling.

Tao et al. (2010) performed molecular dynamics simulations to investigate the role of the cations K, Na, and Ca on the stability and swelling of montmorillonite. They used CLAYFF force field (Cygan et al., 2004) to predict the basal spacing as a function of the water content in the interlayer. All MD simulations were carried out using the LAMMPS software package (Plimton, 1995). The results of the simulations showed that the swelling pattern of these simulated Montmorillonite is different than that by the corresponding K^+, Na^+, and Ca^{2+} montmorillonite (Figure 2-28). The authors discovered that Ca-montmorillonite exhibits less swelling than Na- and K-montmorillonite for a given water content. The results of this study also showed that the higher the hydration energy of the interlayer cation, the greater is this difference. In particular, these results indicated that the valence of the cations has the larger impact on the behaviour of clay – water systems.

Katti et al. (2011) presented the results of modeling of molecular interactions between swelling clay and fluids and their effects on the mechanical and flow characteristics. In this study, MD simulations were conducted to study the possible interactions among clay, water, and cations present in the interlayer using MD based software NAMD

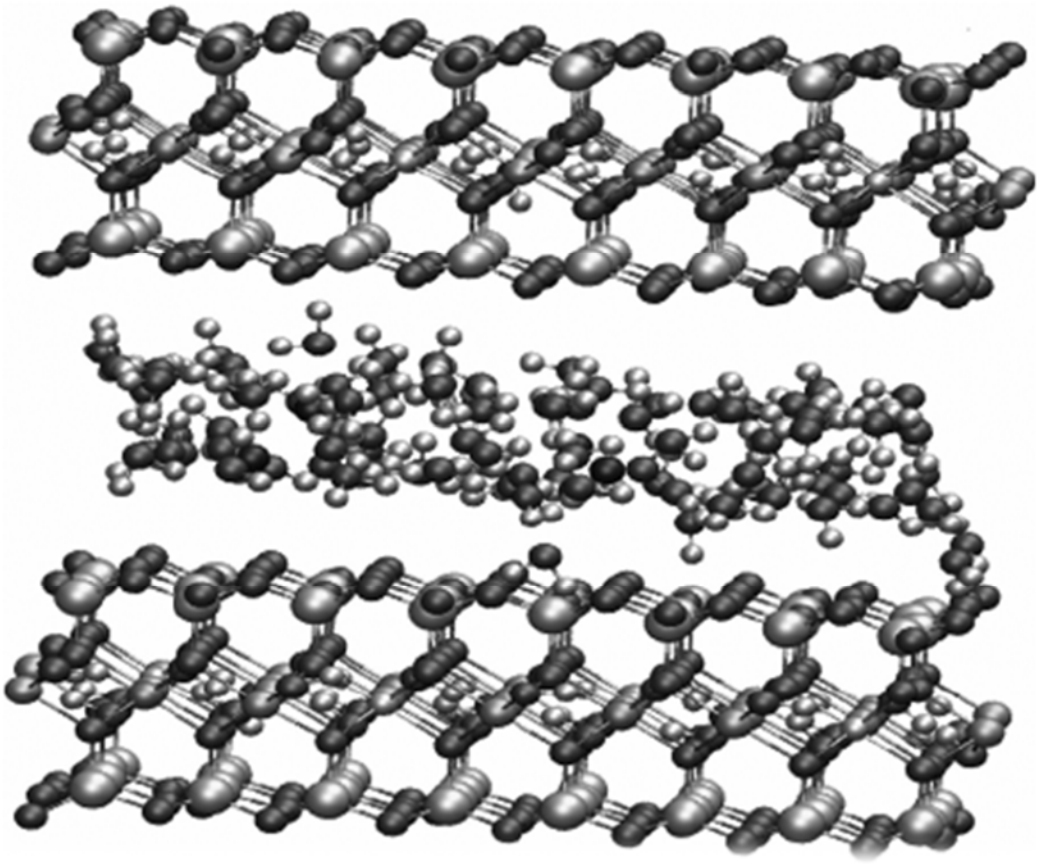

Figure 2-26 Snapshot of Na-montmorillonite with 3 water layers in the interlayer (Katti et al., 2009).

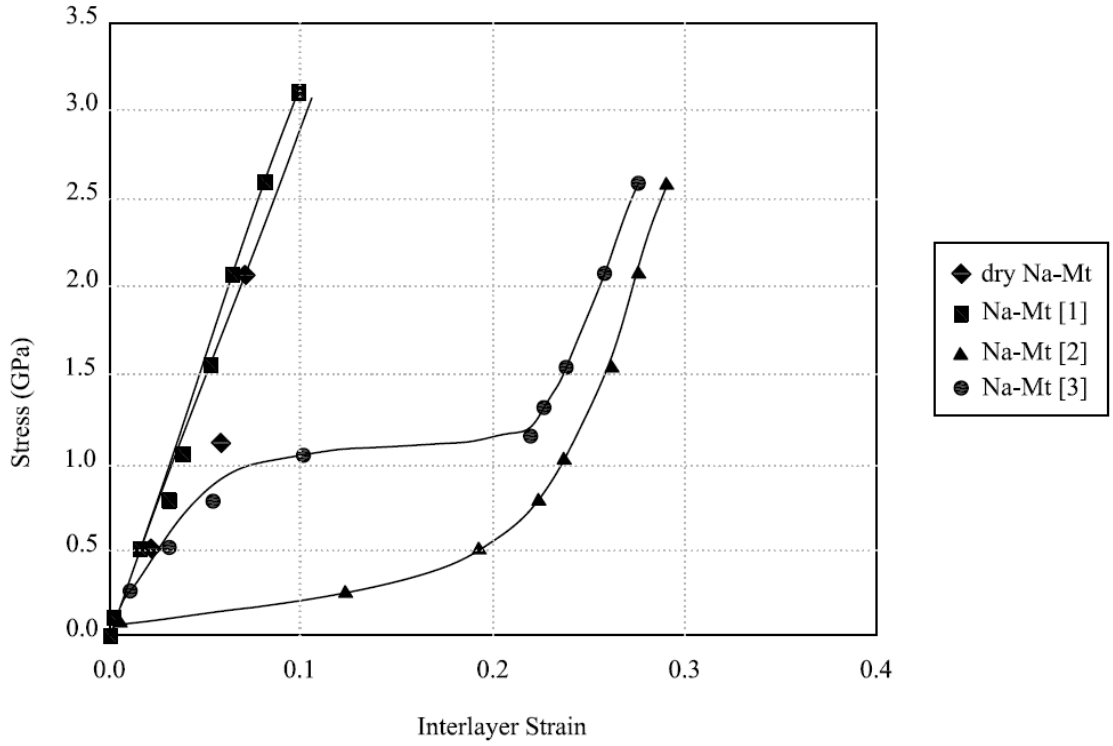

Figure 2-27 Stress vs. interlayer strain plots for various level of hydration in the interlayer (Katti et al., 2009).

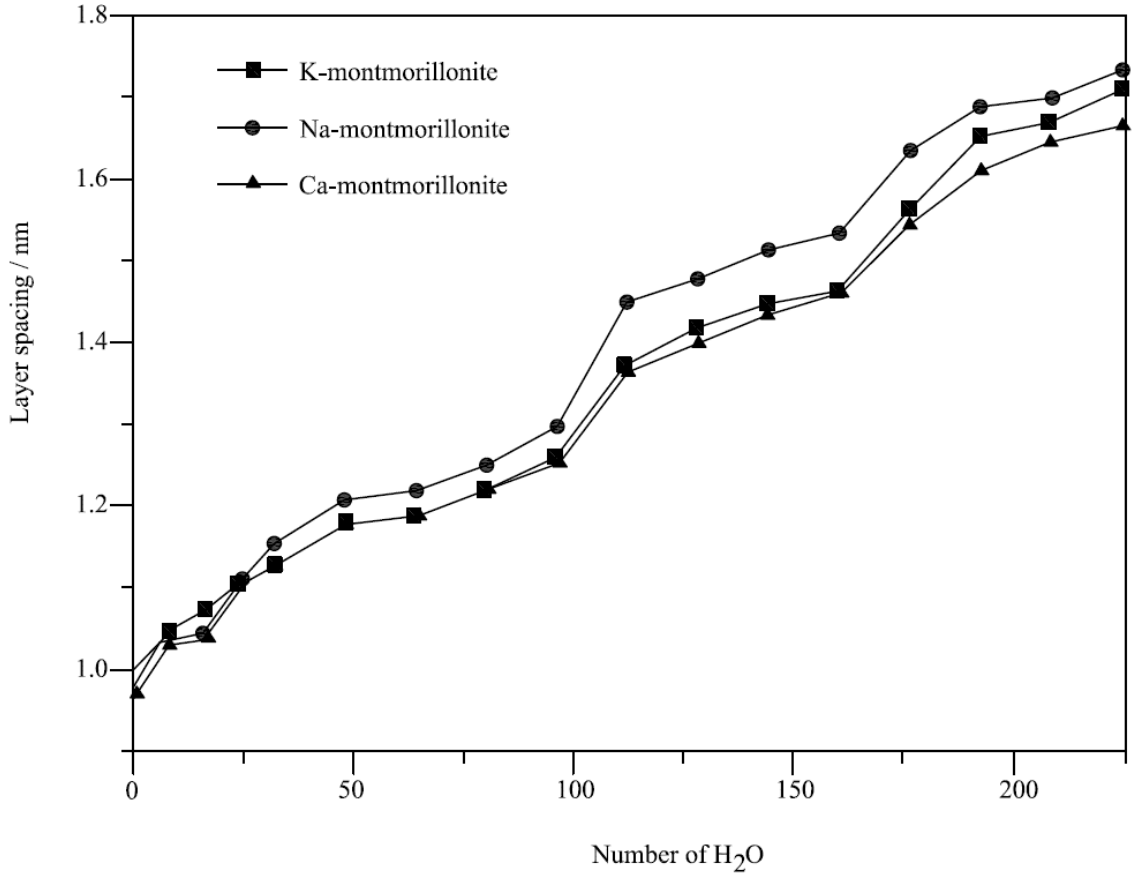

Figure 2-28 Swelling curves of the potassium, sodium and calcium-montmorillonite clay showing the dependence of the layer spacing on the water molecules of the clay (Tao et al., 2010).

(Philips et al., 2005) and the visualization software VMD (Humphrey et al. 1996). The results of the study showed an increased breakdown of the aggregated particles and their corresponding contributions towards the enhanced swelling and the swelling pressure. Generally, their results showed an agreement with the well-established and determined concepts related to the swelling mechanism of the clay minerals. They discovered that the fact that the forces among clay sheets and Na+ cations are attractive in nature in the dry state. As per their results, these attractive forces / interactions among Na+ and clay surfaces are quite pronounced even up to the presence of 8 water layers in the interlayer and water is still contributing to the attractive forces among hydrated Na+ cations and the water bounded to the clay surfaces even more than 8 water layers (Figure 2-29).

2.4 Conclusive remarks

Based on the deliberations in the above sections, it could be inferred that nano or molecular level processes play a central role in the understanding of the volume change behavior of the expansive clays. Although some studies have been conducted to simulate the swelling and / or water absorption behavior of the single or isolated expansive clay minerals, but modeling of the real / natural expansive soil fabric and its interaction with pore fluids at molecular level is still lacking. Moreover, no efforts have been directed even to couple the macro and micro scale material behavior to the findings of these molecular simulations. Based on all the above deliberations on the modeling of expansive clay soils, following are the conclusive remarks:

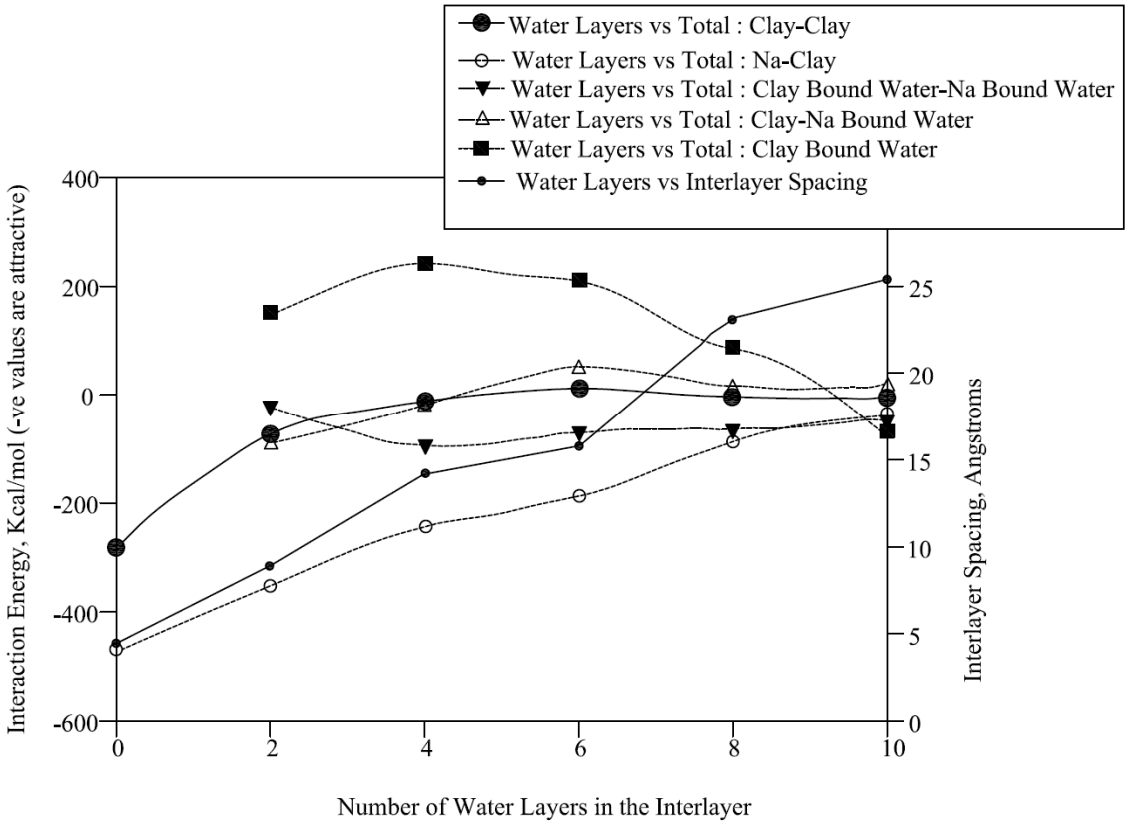

Figure 2-29 Plot of interaction energies versus number of water layers in the interlayer (Katti et al., 2011).

- More efforts and emphasis have been placed by the researchers towards the development and enhancement of the unsaturated non-expansive soils models, while much lesser contributions have been made towards the expansive clay modeling.
- Almost all the researchers involved in the unsaturated soils research have considered expansive soils as an extreme case of the unsaturated soils; rather it should be considered both as a special case of saturated soils and unsaturated soils under the complete moisture regime.
- Micro and nano level fabric, believed to have a central role in the overall behavior of expansive clays, is only partially considered in the modeling concepts. Even the partial consideration of the micro and nano level fabric is for the clays compacted / constructed under highly controlled conditions; natural clay fabrics with multiple clay minerals, silt and sand inclusions, micro fissures, cementation, over-consolidation, induration, and other such features have never been considered.
- The boundary between expansive and non-expansive soils is not well defined, and more consideration is needed to better understand the behavior of slightly expansive clay soils such as broadly graded soils with small Smectite (and Illite) contents and soil dominated by non-swelling clays such as Kaolinite.
- Molecular level research, at present, has just concentrated mostly on one mineral only; interaction with other minerals and macro particles is lacking.
- It has been observed that the macroscopic behavior of clay mass may differ considerably from their nano-scale response, which is the major motivation for characterizing and modeling these materials using multiscale simulations.

CHAPTER 3

METHODOLOGY

This research constituted three major levels of activities; macro level testing, micro level imaging and analysis, and molecular level simulation and modeling. The research methodology generally involved formulation of several types and nature of fabrics / structures of expansive clays through preparation and compaction of mixes of expansive clay minerals and non-expansive / non-clay minerals in various proportions at several moisture and density conditions, mapping and analysis of the fabric and structure of the laboratory compacted expansive clays specimens using nano / micro level imaging laboratory techniques at the pre and post swelling states. This was achieved through advanced imaging techniques such as X-ray diffraction (XRD), Environmental SEM (ESEM), Fourier Transform Infrared Spectroscopy (FTIR), and Computerized X-ray Tomography (Micro CT). Finally, to precisely model the behavior of natural and compacted fabric and structure of the expansive clays, molecular scale simulation of the swelling behavior of the above mentioned natural and compacted fabric and structure was carried out using the concepts of molecular mechanics (MM) / molecular dynamics (MD) and Monte Carlo (MC) simulation techniques. This chapter provides the details of the material acquisition, specimen preparation, testing, and modeling involved in the study.

3.1 Materials

One of the objective of this study is to compare the behavior of the natural expansive clay deposits and the laboratory reconstituted specimens using controlled proportions of the standard soil constituents with the simulation models. Therefore, to constitute the control samples besides obtaining undisturbed samples from natural expansive soil deposits, individual soil constituents were also acquired from standard / known sources.

3.1.1 Undisturbed expansive soils samples

Qatif and Hofuf areas in the eastern region of Saudi Arabia (Figure 1-1) are well known for the presence of problematic shallow subsurface expansive soils deposits. Sampling plan was prepared to acquire representative undisturbed samples from some of the sites in Hofuf and Qatif known for their volume change behavior. For the purpose, test pits were excavated in the shallow subsurface to expose the expansive soil layers. Large lumps / pieces of expansive clayey soils were acquired from the excavated test pits and were immediately sealed to preserve the natural moisture content of these samples. Two samples each representative of two different expansive clay deposits were acquired from Qatif area, while one sample was obtained from Hofuf area. Samples from Qatif area were obtained from a site in the housing area next to Qatif Central Hospital, while sample from Hofuf area was acquired from a site in National Guard. The samples were characterized using various laboratory index tests and XRD and the results are summarized in Tables 3-1, 3-2, and 3-3.

Table 3-1 Summary of index tests on the acquired samples and materials

Material	Designation	Source	Classification	Atterberg Limits			Specific Surface Area (m^2 / g)	CEC (meq / 100g)
				LL	PL	PI		
Na-Montmorillonite (SWy-1)	NaM	The Clay Mineral Society, US	CH	612	36	576	31.82	76.4
Ca-Montmorillonite (SAz-1)	CaM	The Clay Mineral Society, US	MH	129	55	74	97.42	120.0
Kaolinite (KGa-1)	K	The Clay Mineral Society, US	MH	58	36	22	10.05	2.0
Bentonite	B	Kanoo Est., KSA	CH	480	44	436	-	54.8
Qatif Clay - *Source 1*	Q-1	Qatif, KSA	CH	155	53	102	-	51.0
Qatif Clay - *Source 2*	Q-2	Qatif, KSA	CH	69	29	40	-	20.7
Hofuf Clay	H-1	Hofuf, KSA	CH	70	27	43	-	12.7
Calcium Carbonate	Ca	Techno Pharmchem, India	-	-	-	-	-	-
Gypsum	G	Phosphate Plant, RIC, KSA	-	-	-	-	-	-
Sand	S	Jubail, KSA	SP	NP	NP	NP	-	-
	CH: High Plastic CLAY MH: Elastic SILT SP: Poorly graded SAND NP: Non Plastic		RIC: Ras al-Khair Industrial City KSA Kingdom of Saudi Arabia					

Atterberg Limits methodology: ASTM D 4318

Specific Surface Area methodology: Brunauer, Emmett and Teller (BET) Method

CEC methodology: Rayment and Higginson (1992)

3.1.2 Materials for laboratory control samples

In order to precisely isolate and study the relative contribution of various non-swelling clay particles / minerals to the behavior of swelling clay minerals, several standard materials were acquired from the known sources. These materials were further characterized to define the pertinent properties and complete compositional details. For the purpose,

samples of standard clay minerals of different composition were obtained from Clay Mineral Society (2013). Na-montmorillonite (SWy-1), Ca-montmorillonite (SAz-1), and Kaolinite (KGa-1) are the three standard clay samples obtained from Clay Mineral Society.

Table 3-2 Exchangeable and total cations analysis of the Clay samples

Soil	Designation	CEC (meq / 100g)	Exchangeable Cations				Total Cations		
			Type	meq/100g	mg/kg	% of CEC	Type	mg/kg	% of Fixed Cations
Bentonite	B	54.8	Ca	35.2	7054	64	Ca	16300	22
			Mg	2.4	292	4	Mg	869	1
			K	2.0	782	4	K	1200	1
			Na	15.2	3496	28	Na	24300	49
Qatif Clay - *Source 1*	Q-1	51.0	Ca	25.0	5004	49	Ca	101000	68
			Mg	17.0	2002	33	Mg	32400	22
			K	7.0	2963	14	K	6280	2
			Na	2.0	496	4	Na	840	0
Qatif Clay - *Source 2*	Q-2	20.7	Ca	10.0	2004	48	Ca	118000	54
			Mg	7.0	851	34	Mg	89600	41
			K	3.0	1173	14	K	6920	3
			Na	0.7	161	3	Na	1540	1
Hofuf Clay	H-1	12.7	Ca	7.2	1443	57	Ca	28000	54
			Mg	4.1	510	32	Mg	8900	17
			K	1.2	469	9	K	6880	13
			Na	0.2	46	2	Na	5790	12

Total Cations methodology: APHA 21st ed., USEPA SW 846 – 6010 (ICPAES)

Table 3-3 Mineralogical analysis of Clay samples

Soil	Designation	Smectite	Kaolinite	Illite	Palygorskite	Quartz	Calcite	Dolomite	Gypsum
Na-Montmorillonite (SWy-1)	NaM	97	-	-	-	3	-	-	-
Ca-Montmorillonite (SAz-1)	CaM	95	-	-	-	5	-	-	-
Bentonite	B	95	-	-	-	5	-	-	-
Qatif Clay - *Source 1*	Q-1	32	-	21	7	9	22	-	9
Qatif Clay - *Source 2*	Q-2	15	-	25	9	15	-	24	12
Hofuf Clay	H-1	-	5	35	5	15	40	-	-

As only small quantities of samples are available with Clay Mineral Society and large quantities were required to perform the required experimentation, commercially available bentonite samples were also obtained from Kanoo establishment, one of the bentonite (drilling mud) suppliers in KSA. As per information provided by the supplier, the source of this bentonite is from the shale deposits in Gujrat city of India. The bentonite is quarried from these deposits, crushed to fine powder (passing Sieve No. 200), homogenized, and marketed in 50 lbs bags. For this study, five bentonite bags were obtained from the supplier and were stored in controlled temperature and humidity rooms. Several samples were collected from different parts of the bags for the characterization and further verification of the homogeneity and uniformity of the bag samples. The test results indicate a uniformly distributed material throughout the bags.

In addition to the standard clay minerals from Clay Mineral Society and commercial bentonite, sand samples were acquired from the general sand dune deposits near Jubail area of KSA. Bulk sand samples were sampled and were washed through the sieves (No. 4 to No. 200). The relative amount of material retained on each sieve was collected and reconstituted to a standard gradation (Table 3-4).

In any typical natural expansive clayey soil deposit, in addition to swelling and non-swelling clay minerals, other common inclusions are quartz (sand), gypsum and calcite. In order to constitute control laboratory samples, these inclusions such as gypsum and calcium carbonate were also acquired from the known / standard sources. Each of these materials were further characterized using XRD and chemical testing techniques for verification of the composition. Gypsum samples were acquired in powdered form from Ma'aden's

Table 3-4 Standard gradation for the Sand sample

ASTM Sieve No.	10	20	40	60	100	200
% passing	100	92	58	35	19	2

Phosphoric Acid Plant at Ras al-Khair on the east coast of KSA. Calcium carbonate was obtained from the local market manufactured by Techno Pharmchem, India. Characterization results for these materials are presented in Tables 3-1, 3-2, and 3-3.

The control laboratory specimens were prepared at various moisture contents using the distilled water and compacted at various densities using both static and dynamic compaction techniques. Detailed steps and procedures for the sample preparations in the laboratory are provided in the next section.

3.2 Laboratory preparation of specimens

In order to formulate the various forms of fabric and structure, control specimens with known proportions of clay minerals and non-clay minerals / particles were prepared at various known densities and moisture contents. Type of clay and non-clay constituents and the corresponding proportions used for preparing the controlled specimens are listed in Table 3-5.

In this study, baseline mixtures were prepared using bentonite and sand in various proportions (10, 30, 60, and 100% bentonite) and the moisture-density relationships were

developed for each of the proportion using modified Proctor Test procedure (ASTM D 1557). Proctor test provides a relationship between moisture and density with its peak density at optimum moisture content (OMC) and further marking different zones such as dry and wet side of optimum moisture content. Results of Proctor compaction tests are

Table 3-5 List of control samples with the details of the respective compositions of various constituents.

Sample No	Moisture Content State	NaM	CaM	Bentonite	Sand	Gypsum	Calcite	Kaolinite
1	Dry of OMC	-	-	100	-	-	-	-
2	Wet of OMC	-	-	100	-	-	-	-
3	Dry of OMC	-	-	60	40	-	-	-
4	Wet of OMC	-	-	60	40	-	-	-
5	Dry of OMC	-	-	30	70	-	-	-
6	Wet of OMC	-	-	30	70	-	-	-
7	Dry of OMC	-	-	10	90	-	-	-
8	Wet of OMC	-	-	10	90	-	-	-
9	Dry of OMC*	-	-	30	70	-	-	-
10	Dry of OMC*	-	-	30	60	10	-	-
11	Dry of OMC*	-	-	30	40	30	-	-
12	Dry of OMC*	-	-	30	20	50	-	-
13	Dry of OMC*	-	-	30	40	-	30	-
14	Dry of OMC*	-	-	30	20	-	50	-
15	Dry of OMC*	-	-	30	40	-	-	30
16	Dry of OMC*	-	-	-	-	-	-	100
17	Dry of OMC*	-	-	-	40	-	-	60
18	Dry of OMC*	-	-	-	70	-	-	30
19	Dry of OMC*	100	-	-	-	-	-	-
20	Dry of OMC*	60	-	-	40	-	-	-
21	Dry of OMC*	30	-	-	70	-	-	-
22	Dry of OMC*	-	100	-		-	-	-
23	Dry of OMC*	-	60	-	40	-	-	-
24	Dry of OMC*	-	30	-	70	-	-	-
	* Static Compaction							

provided in Figure 3-1. To formulate specimens with different fabric conditions, specimens were prepared at 95% of maximum dry density both on dry and wet side of OMC. For the purpose, samples were prepared by mixing the required proportions of clay, sand, and water and were left over in sealed plastic bags for a minimum period of twenty four hours. This is to ensure the proper and uniform distribution and adsorption of the moisture throughout the clay and sand particles. These loose mixed samples were then compacted to 95% maximum dry density in the Proctor mold. Oedometer circular steel rings of 70 mm diameter and 19 mm height were then hydraulically pushed into the compacted samples to obtain the required specimens. The compacted specimens along with the rings were sealed against moisture loss for onward testing for the swelling tests. Among these specimens, one with 30% bentonite and compacted at 95% maximum dry density on the dry side of the OMC was selected as a reference specimen for the further variation in the clay and non-clay constituents.

As samples of standard materials other than bentonite could not be obtained in ample quantities for the dynamically compacted specimens, it was decided to use static compaction technique for the rest of the variation in constituents. For the comparison purpose, reference specimen (30% bentonite) was also compacted to the required density (95% of maximum dry density) on dry side of OMC using static compaction technique in the oedometer rings. The specimens were compacted in two layers through the piston of the compression machine having almost the same diameter as of the oedometer ring (Figure 3-2). Equivalent static pressure to achieve the same density in oedometer rings as in Proctor compaction was determined to be 1500 kPa. This equivalent pressure was used to compact the mixes in which sand was partially replaced with other constituents, several

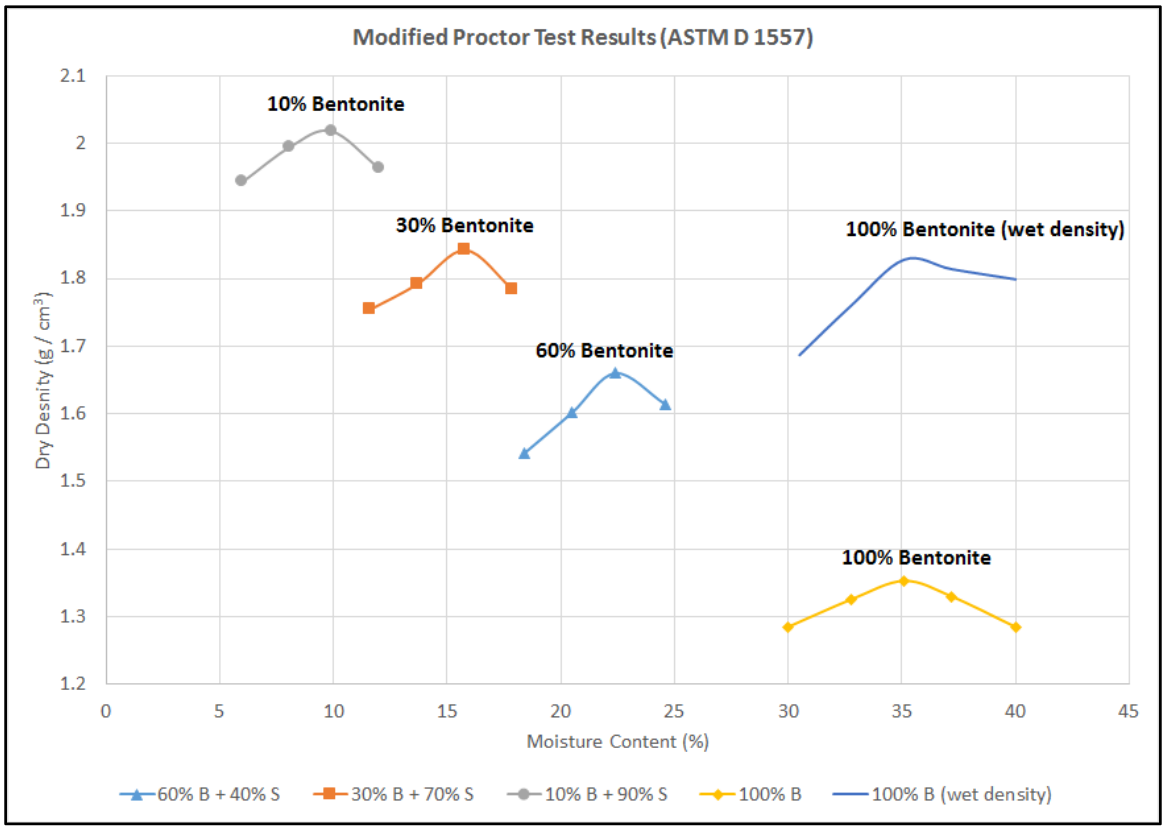

Figure 3-1 Proctor Moisture-Density relationships for various bentonite-sand proportioned mixes.

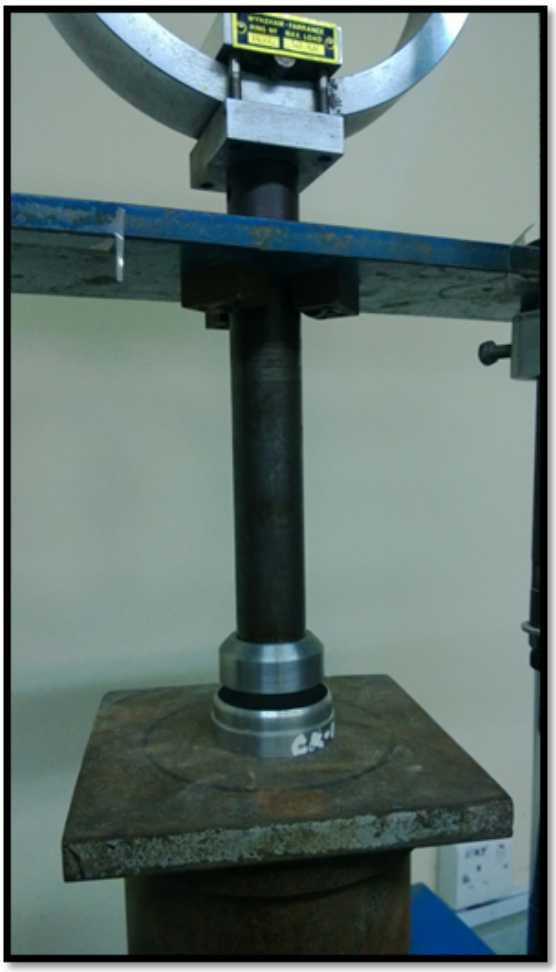

a)

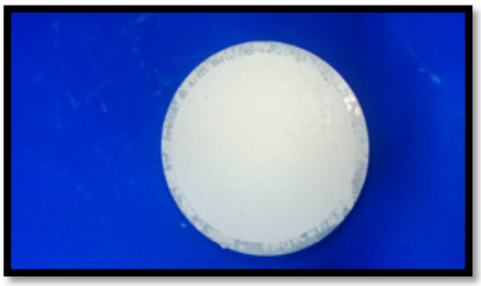

b)

Figure 3-2 Typical views of the a) Static compaction equipment b) Compacted specimen for the compacted clay and other soil constituents mixtures.

combinations used are listed in Table 3-5. In order to achieve the required density and moisture conditions, the samples were compacted to a pressure of 1500 kPa. In order to preserve the moisture conditions, the compacted specimens were immediately sealed with several wraps of plastic cling film and cased in polythene bags. In addition to the specimen compacted for swelling test, additional similar specimens were prepared for the micro investigation on the pre swell samples. These pre swell samples, taken from the compacted layer, were later on evaluated using molecular / nano level investigation and imaging techniques. All the laboratory prepared specimens were subjected to swell potential tests as detailed in the next section.

3.3 Swell potential tests

As mentioned in the previous section, specimens for the swell potential tests were prepared with various proportions of bentonite, sand, and / or gypsum, calcite, and kaolinite. Similarly, standard clays were also mixed with 40 % and 70 % sand and compacted to the maximum density corresponding to 1500 kPa static pressure. In order to ensure that specimens of standard clays be compacted on the dry side of OMC, it was assessed from the PL of these clay samples. Swell potential tests were carried out in general agreement with ASTM D 5890 and compacted specimens were subjected to free swell testing in the oedometer test equipment. In order to magnify the relative influence of each change in type and percentage of non-swell particles, the specimens were surcharged with a low surcharge pressure of 2 kPa and flooded with distilled water in the oedometer specimen holder. Increase in height of the specimen was recorded at regular time intervals till no further noticeable change in height of the specimen is recorded. Maximum change in the

height of the specimen divided by the original height was recorded and expressed in percent swell for each tested specimen. After the swelling test, samples for moisture content were cut from the middle of the ring and rest was preserved for the post-swell micro level imaging and tests. The results of the swell tests carried out on bentonite, sand, and other inclusions are summarized in Table 3-6 and plotted in Figure 3-3.

3.4 Micro level testing and imaging of fabric and structure

Micro level fabric testing and visualization of the pre and post swell samples was carried out using X-ray Diffraction (XRD), Fourier Transform Infrared Spectroscopy (FTIR), Micro Computed Tomography Scan (CT), and Environmental Scanning Electron Microscopy (ESEM). XRD and CT were performed at Center of Excellence in Nanotechnology of KFUPM, while FTIR tests were conducted at the Center for Refining and Petrochemicals of the Research Institute (RI) of KFUPM. ESEM were conducted at R&D Center of Saudi Aramco at Dhahran, KSA. The main objectives achieved through this laboratory study were the soil fabric visualization, variation in interlayer spacing with change in moisture regime, assessment of crystallite size, and interaction among swelling and non-swelling soil particles in the fabric on the dry and wet side of optimum moisture content both in pre and post swell state. The molecular level information acquired from these tests are presented in next sections and were used as an input in the molecular level modeling schemes.

Table 3-6 Summary of swell potential tests results

Sample No	Moisture Content State	NaM	CaM	Bentonite	Sand	Gypsum	Calcite	Kaolinite	Swell (%)	Initial Dry Density (g/cm^3)	IMC (%)	Initial Wet Density (g/cm^3)	FMC (%)	Final Dry Density (g/cm^3)	Final Wet Density (g/cm^3)
1	Dry of OMC	-	-	100	-	-	-	-	184	1.290	29.5	1.67	136.0	0.45	1.07
2	Wet of OMC	-	-	100	-	-	-	-	132	1.290	39.0	1.79	174.0	0.56	1.52
3	Dry of OMC	-	-	60	40	-	-	-	153	1.577	19.5	1.88	93.0	0.62	1.20
4	Wet of OMC	-	-	60	40	-	-	-	111	1.577	26.0	1.99	103.0	0.75	1.52
5	Dry of OMC	-	-	30	70	-	-	-	89	1.750	11.3	1.95	72.0	0.93	1.59
6	Wet of OMC	-	-	30	70	-	-	-	53	1.750	18.8	2.08	82.0	1.14	2.08
7	Dry of OMC	-	-	10	90	-	-	-	32	1.917	5.2	2.02	18.0	1.45	1.71
8	Wet of OMC	-	-	10	90	-	-	-	5	1.917	13.4	2.17	22.0	1.83	2.23
9	Dry of OMC*	-	-	30	70	-	-	-	121	1.750	12.0	1.96	108.0	0.79	1.65
10	Dry of OMC*	-	-	30	60	10	-	-	21	1.750	12.0	1.96	56.0	1.45	2.26
11	Dry of OMC*	-	-	30	40	30	-	-	11	1.750	12.0	1.96	27.0	1.58	2.00
12	Dry of OMC*	-	-	30	20	50	-	-	6	1.750	12.0	1.96	19.0	1.65	1.96
13	Dry of OMC*	-	-	30	40	-	30	-	74	1.750	12.0	1.96	80.0	1.01	1.81
14	Dry of OMC*	-	-	30	20	-	50	-	68	1.750	12.0	1.96	66.0	1.04	1.73
15	Dry of OMC*	-	-	30	40	-	-	30	95	1.750	12.0	1.96	115.0	0.90	1.93
16	Dry of OMC*	-	-	-	-	-	-	100	4	1.512	23.1	1.86	27.0	1.45	1.84
17	Dry of OMC*	-	-	-	40	-	-	60	3	1.828	13.3	2.07	16.0	1.77	2.06
18	Dry of OMC*	-	-	-	70	-	-	30	1	1.845	8.1	1.99	11.0	1.83	2.03
19	Dry of OMC*	100	-	-	-	-	-	-	96	1.436	3.8	1.49	87.0	0.73	1.37
20	Dry of OMC*	60	-	-	40	-	-	-	59	1.673	10.0	1.84	50.0	1.05	1.58
21	Dry of OMC*	30	-	-	70	-	-	-	25	1.889	8.0	2.04	25.0	1.51	1.89
22	Dry of OMC*	-	100	-		-	-	-	49	1.298	1.5	1.32	90.0	0.87	1.66
23	Dry of OMC*	-	60	-	40	-	-	-	18	1.567	16.3	1.82	42.0	1.33	1.89
24	Dry of OMC*	-	30	-	70	-	-	-	9	1.591	11.5	1.77	33.7	1.46	1.95
25	NMC	Qatif (Q-1)							29	1.367	7.2	1.47	55.6	1.06	1.65
26	NMC	Qatif (Q-2)							8	1.557	5.2	1.64	40.0	1.44	2.02
27	NMC	Hofuf (H-1)							5	1.507	3.9	1.57	29.3	1.44	1.86

* Static Compaction

NMC: Natural Moisture Content
IMC: Initial Mositure Content
FMC: Final Mositure Content

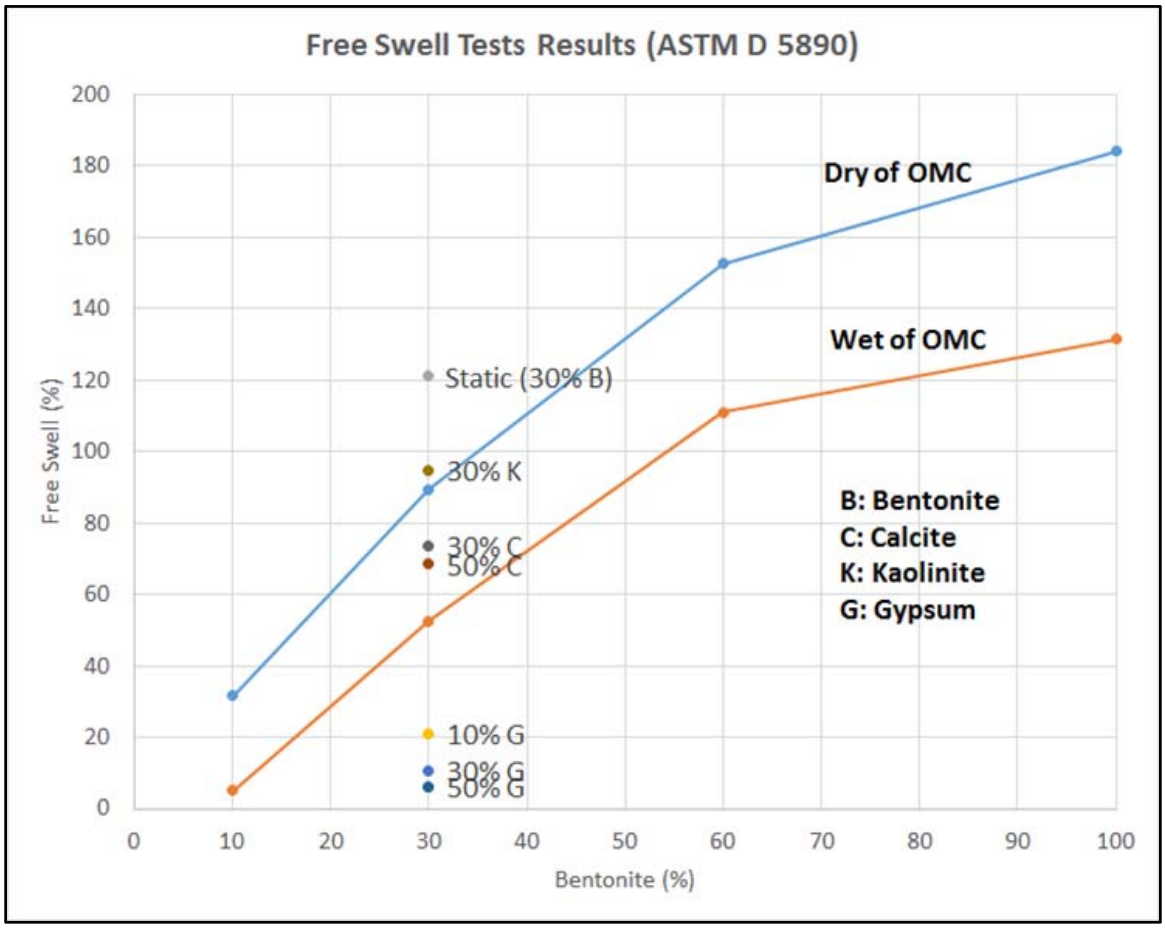

Figure 3-3 Swell potential test results using laboratory oedometer tests

3.4.1 X-Ray Diffraction

Pre and post swell specimens were tested for mineralogical analysis and change in interlayer / lattice space at various moisture regimes using Rigaku Miniflex II X-ray Diffraction (XRD) equipment. XRD equipment is equipped with a 40keV X-ray tube, radiation safe enclosure, water chiller, and a monochromator.

For the testing purpose, few grams of representative specimen were taken from the corresponding samples and were pulverized / smeared to the fine powder or was used in paste form for high moisture content samples. The pulverized or paste sample was then placed in a sample holder creating a flat upper surface and assuring random distribution of lattice orientation. The specimen was subject to XRD testing from the diffraction angles 2θ varying from 3^o to 90^o. During the test, intensity of diffracted X-rays was continuously recorded as the sample and detector rotate through their respective angles. A peak in intensity occurs when the mineral contains lattice planes with d-spacings appropriate to diffract X-rays at that value of θ. The data was analyzed to determine the presence of various minerals and their approximate percentages. Results are presented as peak positions at d spacings and X-ray counts (intensity) in the form of x-y plots in Appendix A. These plots were also used to determine the changes in lattice / d-spacing upon change in moisture content in the pre and post swell state.

In addition to the knowledge of type and proportions of various minerals and the changes in the lattice spacing of clay minerals, crystallite size was also approximately assessed from XRD data. For the purpose, Scherrer (1918) method was used and procedure is shown in

Figure 3-4. The line broadening caused by small crystal size, B, is calculated using the relation suggested by Warren (1941),

$$B^2=B_M^2 - B_S^2 \qquad 3\text{-}1$$

where

B_M = measured montmorillonite peak breadth

B_S = average measured aluminum peak breadth in radians

The Scherrer's formula relating peak breadth to crystal size is,

$$D=0.9\lambda/(B \cos \theta_B) \qquad 3\text{-}2$$

where λ=1.542 Å and θ_B=diffraction angle at maximum intensity

3.4.2 Fourier Transform Infrared Spectroscopy (FTIR)

Fourier Transform Infrared Spectroscopy (FTIR) was carried out using Nicolet 6700 FTIR spectrometer at Center for Refining and Petrochemicals at Research Institute (RI) of KFUPM. The equipment is equipped with OMNIC software and is capable of recording the wavelengths in the range of 400 cm^{-1} and 4000 nm.

For the analysis, few grams of representative sample was obtained from each of the pre and post swell samples. These samples were mixed with potassium bromide (KBr) and mixed thoroughly in a stone dish using the marble pestle. After achieving a uniform color, the mix was placed in a steel mold and the mold was compressed to form a thin slice / pellet. The pellet was carefully removed from the mold and placed in a vertical

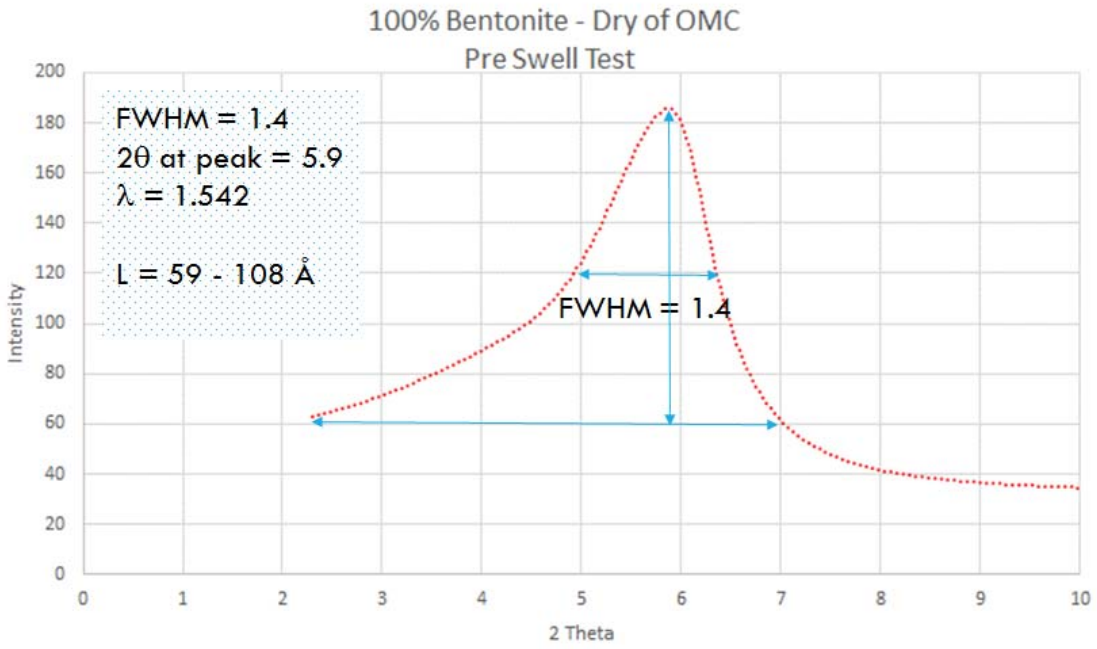

Figure 3-4 Typical crystallite size determination using Scherrer (1918) method

stand in the specimen chamber of the equipment. The sample holder was placed in such a way that the incident laser beam focuses on the specimen. OMNIC software is used to control the data acquisition. To exclude the other possible interferences in the sample chamber, background data is acquired using the software before placing the specimen. For each specimen, data was acquired for a wavelength range of 400 to 4000 cm^{-1}. The data acquired for the specimen is corrected by subtracting the background from the collected data. The data was acquired in absorbance units and the final results are presented as wavelength versus absorbance. The results are appended in Appendix B.

3.4.3 Environmental Scanning Electron Microscope

The pre and post swell samples obtained from the swell test specimens were viewed, examined, and studied using Environmental Scanning Electron Microscope (ESEM). FEI-Phillips ESEM-FEG Quanta 400 available at R&D center of Saudi Aramco was used for the purpose.

In ESEM, electron guns are used to produce a fine, controlled beam of electrons which are then focused at the specimen surface. ESEM mode in the instrument applies high pressure to ensure prevention of moisture during the test. In this study, a pressure up to 0.55 torr was used. The electron gun emits electrons from field-emission gun to produce an image representing the morphology of the sample. Moreover, it also facilitates in the spot and general elemental analysis at the selected points / surface of the specimen.

Representative sample particles / particle assemblage of the pre and post-swell specimens were placed on the copper strips pasted on the specimen holders. The specimens were

scanned in the ESEM at 20 keV to acquire the high contrasting micrographs at different resolutions varying from 100x to 30,000x. Spot and general area level elemental analysis was also carried out using Energy Dispersive Spectroscopy (EDS) at the selected locations and / or areas of the specimens using 20 keV energy electron beams. EDS spectrums of several spots on the selected specimens were obtained to assess the elemental composition of the specimen. ESEM results are presented in Appendix C.

3.4.4 X-ray Computerized Tomography

X-ray Computed Tomography (Micro CT) of the compacted and the natural clay samples was carried out using Micro CT SkyScan 1172 equipment. This equipment is capable of providing tomographic sections of the specimens in 2-D and 3-D with a resolution of 1 micron. The equipment is equipped with an X-ray source of 100 keV to focus on a spot size of less than 5 micron. The associated acquisition and analysis software aid in the acquisition of the data and further analyzing and presenting the data in 2-D and 3-D tomographic sections.

Cubical to cylindrical specimens of about 15 mm x 25 mm size were used for the CT scanning of the pre and post swell samples. The specimens were fixed on the sample holder placed in the sample chamber of the equipment. Through the acquisition software, the specimens were focused to scan the middle section of the specimen without any dried end effects. The specimens were scanned using X-ray energy of 72 keV and scans were obtained every 2^{o} of the specimen. After the complete scan, data was loaded in the analysis software for display and development of tomographic sections. The raw data was reconstructed to formulate a series of tomographic sections of the entire height of the

specimen. These series of sections were converted to a video form that shows the slides / slices of the variation in the X-ray attenuated sections along the height of the scanned specimen. Attenuation of the X-rays, while travelling through the specimen, is a result of several factors including density and the nature of the particles. During reconstruction of the specimen tomographic sections, each level of X-ray attenuation was designated with a different color. Colored CT sections of all the tested specimens, before and after the swell tests are provided in Appendix D.

3.5 Molecular level modeling and simulation

The main objective of this research is to simulate and study the processes and interactions occurring at the molecular level in the natural and compacted fabrics of the expansive soils. A typical natural microstructure of expansive soils consists of clay and non-clay particles assemblages, pores varying from nano to micro level, and the water present in all these pore levels. A particle assemblage further consists of various sizes of the unit crystallites or quasi-crystals of each constituent. In this study, molecular mechanics (MM), molecular dynamics (MD), and Monte Carlo (MC) based simulation techniques were used to study the interactions between clay and non-clay particles in the presence of various combinations of interlayer and intra layer cations, anions, and water under various fabric and structure conditions. Materials Studio software (2013) have been used in this simulation study. Due to large volume of computations involved in the simulations, these calculations were carried out through the high performance computing facilities at KFUPM and King Abdullah University of Sciences and Technology (KAUST), KSA; HPC at KFUPM and NESER at KAUST were used for the purpose.

The general essentials for any molecular simulation scheme are the choice of the representative crystallites, formulation of the representative unit cells with periodic boundary conditions, and running the appropriate ensemble using an applicable forcefield. This study also involved the modifications to the existing Universal forcefield inbuilt in the software to adapt it to the simulations involved in this study. The steps adopted for the formulation of unit cells and the subsequent simulations are described in the following sections.

3.5.1 Selection and formulation of basic molecule units

In order to formulate the basic unit cells of the soil fabric, individual clay and non-clay crystallites / molecules were acquired from several sources. Unit molecules used in the formulation are Na-montmorillonite of three different Cation Exchange Capacity (CEC), pyrophyllite, kaolinite, calcite (Calcium Carbonate), Calcium Sulfate (Gypsum), Potassium Chloride, and water. Most of these basic molecular units including two CEC Na-montmorillonite, kaolinite, Calcium Carbonate, and Calcium Sulfate were acquired from Nanoscale Simulation Lab at University of Akron, US (2013), while other molecules were prepared using the drafting tools of the software. The molecules acquired from Nanoscale simulation lab are already in charged state and their charges were verified using charge equilibration method QEq of the Materials Studio software. Other molecules formulated in the software were charged using QEq module of the software. In order to study the relative effect of CEC on the simulation behavior, Na-montmorillonite molecules of three different CECs of 54, 90, and 144 meq/100g were used. A typical Na-montmorillonite model with CEC of 90 meq/100g and Na as interlayer cations is shown in

Figure 3-5. In addition, pyrophyllite (CEC=0) known for its non-swell nature, was also used as a reference to verify the parameters in the simulation technique. A typical pyrophyllite crystallite is shown in Figure 3-5. In addition to the verification through pyrophyllite behavior, knowledge of several other well-known behaviors have been used to verify the parameters and other procedures adopted in the software. Calcite and gypsum unit cells and water molecule are also shown in Figure 3-6.

The simulation study consisted of several steps starting from sorption of water molecules on the individual crystallite, assemblage of crystallites through natural randomness concepts, compaction to the maximum density, relaxation to simulate stress relief, and finally volume change upon sorption of water molecules in the pore spaces. The procedure is repeated for all the three CEC varied Na-montmorillonite and further variations in the exchangeable cations and the cementation due to the interactions with other soil constituents (Tables 3-7, 3-8, and 3-9). All the simulations as per combinations in Table 3-7 were carried out on Na-montmorillonite with Na as the sole exchangeable cation. MCEC Na-montmorillonite was then selected to simulate the cementation effects due to potassium chloride, gypsum, and calcite as per permutations in Table 3-8. LCEC montmorillonite was finally selected for the simulations by changing the type and amount of exchangeable cations as given in Table 3-9.

The detailed procedures involved in all these steps are provided for a typical complete case for MCEC (90 meq/100g) montmorillonite and one case of change in exchangeable cations in LCEC (54 meq/100g) montmorillonite in the following sections. Complete results are provided in Appendix E and are discussed in detail in Chapter 4 of this thesis.

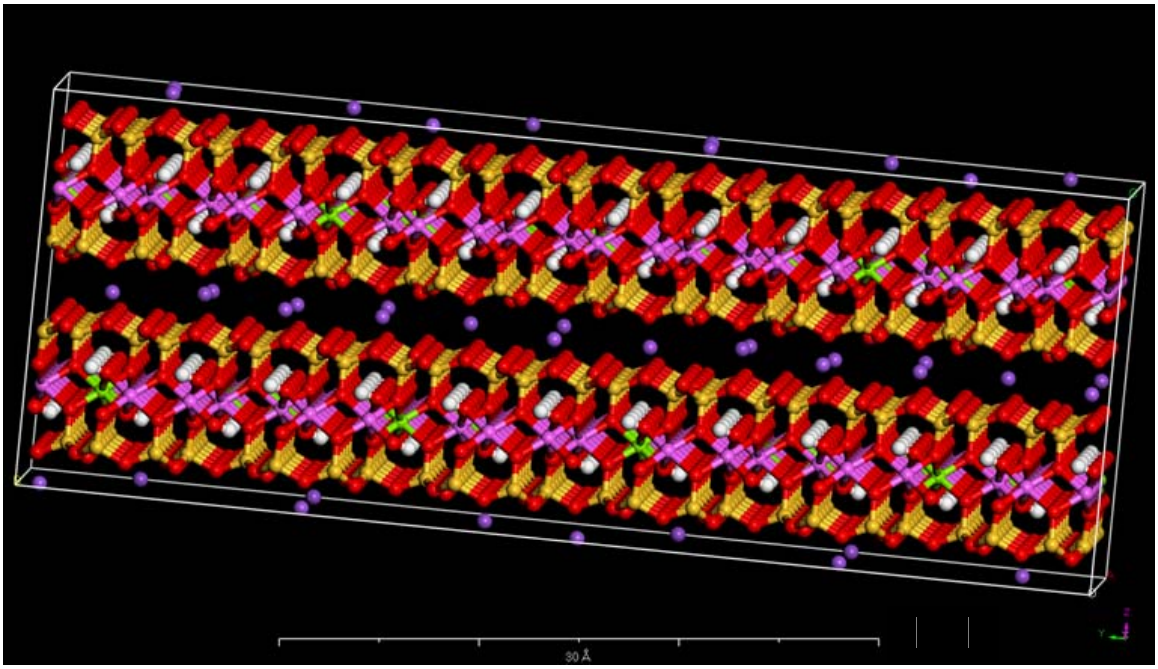

(a)

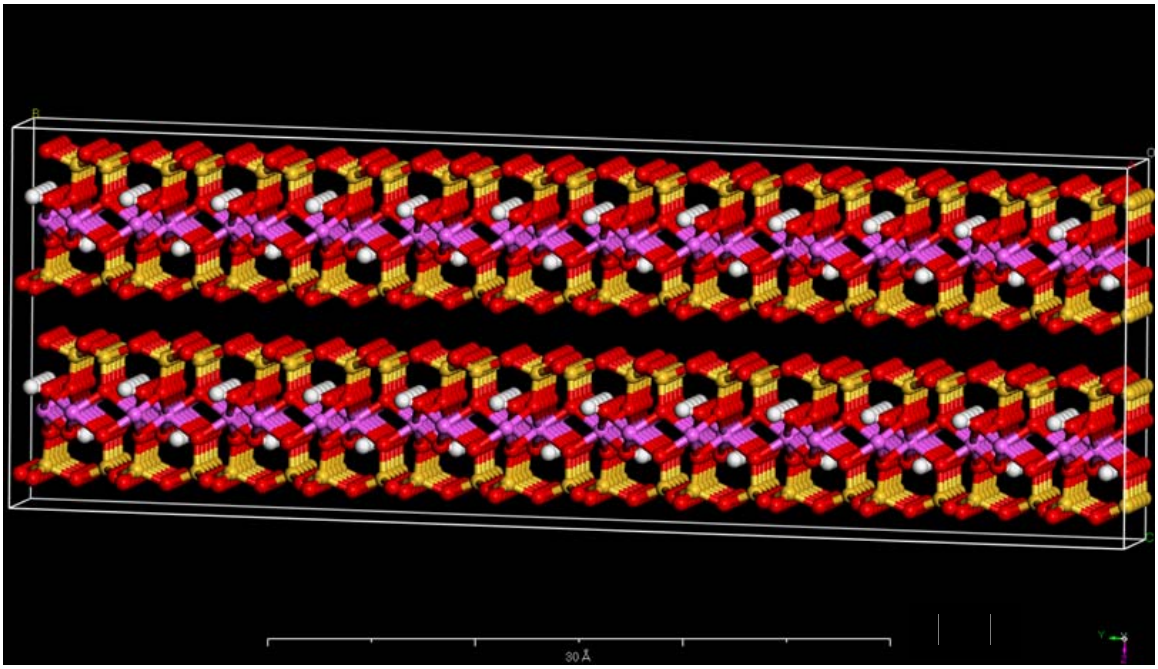

(b)

Figure 3-5 Typical crystallite unit cell (26 x 54 x 20 Å) of a) Na-montmorillonite with CEC=90 meq/100g b) Pyrophyllite with CEC=0.

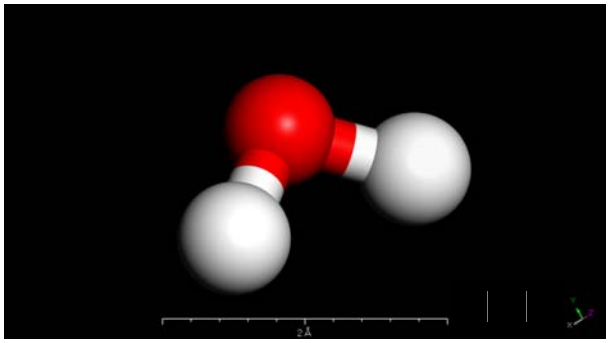

(a)

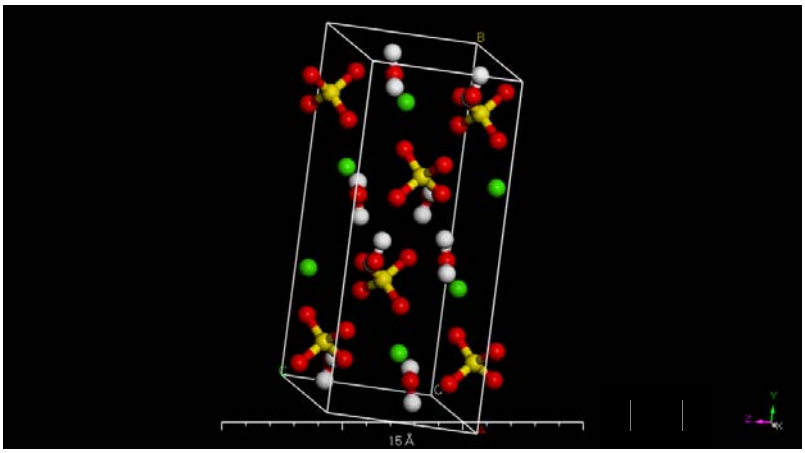

(b)

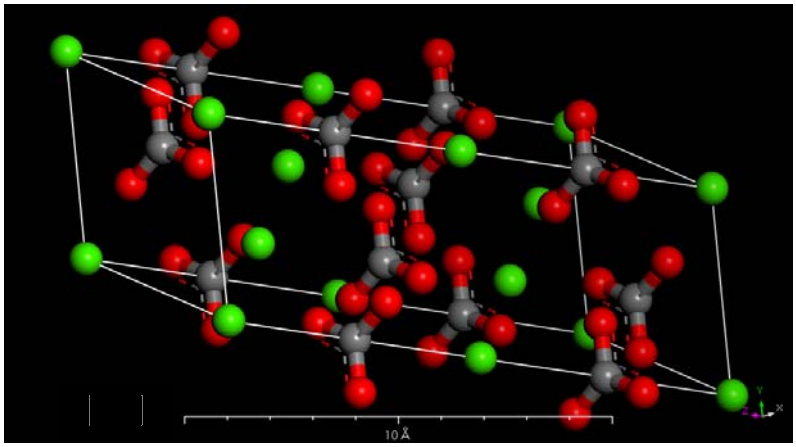

(c)

Figure 3-6 Typical views of a) water molecule b) Gypsum unit cell c) Calcite unit cell.

Table 3-7 Summary of various variations and combinations used in simulations for Na-montmorillonite (Na as 100% exchangeable cation).

CEC (meq/100g)	Designation	Density conditions*	Moisture conditions
54	LCEC	Stress relieved at 1000 kPa	10, 20, 30, and 40 %
90	MCEC	Stress relieved at 1000 kPa	10, 20, 30, and 40 %
144	HCEC	Stress relieved at 1000 kPa	10, 20, 30, and 40 %

***** compacted at 1, 0.1, and 0.01 GPa

Table 3-8 Simulation permutations of cementation agents for MCEC Na-montmorillonite.

Cementation Agent	Percentage	Density conditions	Moisture conditions
Gypsum ($CaSO_4.2H_2O$)	Max 20	Stress relieved at 1000 kPa	10 and 30 %
Calcite ($CaCO_3$)	Max 10	Stress relieved at 1000 kPa	10 %
Potassium Chloride (KCl)	Max 10	Stress relieved at 1000 kPa	10 %

Table 3-9 Simulation permutations for various combinations of exchangeable cations for LCEC montmorillonite.

Combinations	Exchangeable Cations			
	Na^{+}	K^{+}	Mg^{+2}	Ca^{+2}
1	40	60	-	-
2	40	-	60	-
3	40	-	-	60
4	40	20	40	-
5	40	20	-	40
6	40	20	20	20

3.5.2 Water sorption on individual Na-montmorillonite crystallites

This step simulates the sorption of water molecules on the individual montmorillonite crystallites. It represents the processes of water mixing with the clay in the laboratory conditions or the interaction of clay particles with water during the geological depositional processes. Based on the knowledge from the literature and the findings of XRD results of the samples with similar densities on the moisture density plots in this research, a basic crystallite size of a x b x c: 26 x 54 x 20 Å was chosen as the fundamental particle / crystallite for Na-montmorillonite in the simulation.

Water molecules sorption on the individual montmorillonite crystallites were simulated using Sorption and Forcite modules of Materials Studio software. Sorption module is based on Monte Carlo simulation technique in which water molecules get sorbed on the clay particle on its surfaces, interlayer, and edges. In Sorption module, sorbate (single water molecules) is absorbed in the sorbent framework of clay molecule. Fixed loading was used to find the global minimum energy sites for the water molecules in a clay crystallite by running cycles of fixed loading simulation series where the temperature is steadily reduced over the series. Metropolis Monte Carlo method (Metropolis et al., 1953) used in the Sorption module is a conventional Monte Carlo method in which trial configurations are generated without bias. This method was selected for the simulations as it treats the sorbate structure as rigid and only rigid body translations and reorientations are incorporated. In the sorption module, ratios for exchange, conformer, rotate, translate, and regrow have been selected as 0.39, 0.2, 0.2, 0.2, 0.2 respectively, while the corresponding probabilities are 0.39, 0.2, 0.2, 0.2, and 0.2. Amplitudes adopted for rotation and translation are 5^{o} and 1 Å respectively. These selected parameters in Monte Carlo simulations have been verified through the findings and results of certain well known baseline facts. Facts such as formation of 3 Å thick water layers upon absorption of about 10 % water and hydration radius of sodium cation have been used in the verification of the choice of the parameters.

The simulation is based on the concept of finding locations in the unit cell where water molecules would cause the maximum lowering in the energy. The water molecules get to the locations in the unit cell based on the lowering of the energy principle and the sorption is continued till an energy cut off is reached. After experimenting several energy cut off

levels, 25000 steps cut off was adopted as the threshold limit for the realistic sorption. Simulation beyond 25000 steps resulted in the occupation of higher energy sites by water molecules and an unrealistically high volume change occurred. Moreover, pyrophyllite was also shown to be adsorbing water and showing high swell potential at steps more than 25000. After sorption of the water molecules in 25000 steps, equilibration was achieved in 15000 steps to a temperature of 298°K. Universal forcefield, one of the built in forcefield in the software was modified and used in the simulation and using the current charges associated with the molecules. Details of the modifications to the Universal forcefield are provided in Section 3.5.11. Ewald summation method was adopted for the electrostatic forces, while atom based summation was used for van der Waals forces with cubic spline cut off at 12.5 Å. The final result of the Sorption simulation was a lowest energy frame with the water molecules sorbed at the most desired locations of the unit crystallite of montmorillonite; a typical sorption result is shown in Figure 3-7.

After performing each sorption cut off, the unit crystallite with water sorbed molecules was stabilized through molecular dynamics simulation. Forcite module of the Materials Studio software was used for the purpose. In Forcite, NPT (constant number of particles, pressure, and temperature) ensemble was used and simulations were performed using modified Universal forcefield for a period of 5 to 30 ps in 0.5 fs intervals or till a constant volume is achieved. Berendsen thermostat with a decay constant of 0.1 ps was used to control the temperature during the simulation. During the molecular dynamics simulation, temperature was kept constant at 298°K. Simulations were carried out at atmospheric pressure (100 kPa) and Berendsen barostat with decay constant of 0.1 ps was used to control the pressure of the system. Berendsen methodology was found as the most suitable

for the single crystallites after several trials with other thermostats and barostats available in the software. A typical post molecular dynamics molecule is shown in Figure 3-7.

As evident from Figure 3-7, water molecules are getting sorbed on the surface, edges, and the interlayer of the montmorillonite crystallite. The water sorbed in the interlayer causes the lattice expansion. The entire process of sorption and dynamics is repeated and the lattice expansion is noted with each increase in water content. A total of 277 water molecules sorption is equivalent to 10% water content of the unit crystallite of montmorillonite of 26 x 54 x 20 Å size. The simulation was continued to a maximum water content of 40%. Lattice expansion (d-spacing) for MCEC Na-montmorillonite is plotted against sorbed water content in Figure 3-8. Change in lattice spacing with moisture content of the loose bentonite as determined through XRD is also plotted in Figure 3-8. The verification of sorption parameters have been carried out using the pyrophyllite crystallite of the same size as Na-montmorillonite as described in the next section. These water sorbed crystallites were then used to model the loose soil mix using natural randomness process through Monte Carlo simulation.

3.5.3 Calibration of Sorption parameters using pyrophyllite

Pyrophyllite is the clay mineral in which no isomorphous substitution takes place and hence its CEC is zero. In order to verify the combination of parameters being used for the sorption of the water molecules in a montmorillonite crystallite, pyrophyllite crystallite of the same size (54 x 26 x 20 Å) was also used for the simulation. Adopting the same parameters in the sorption simulation, pyrophyllite did not show any adsorption of the water molecules.

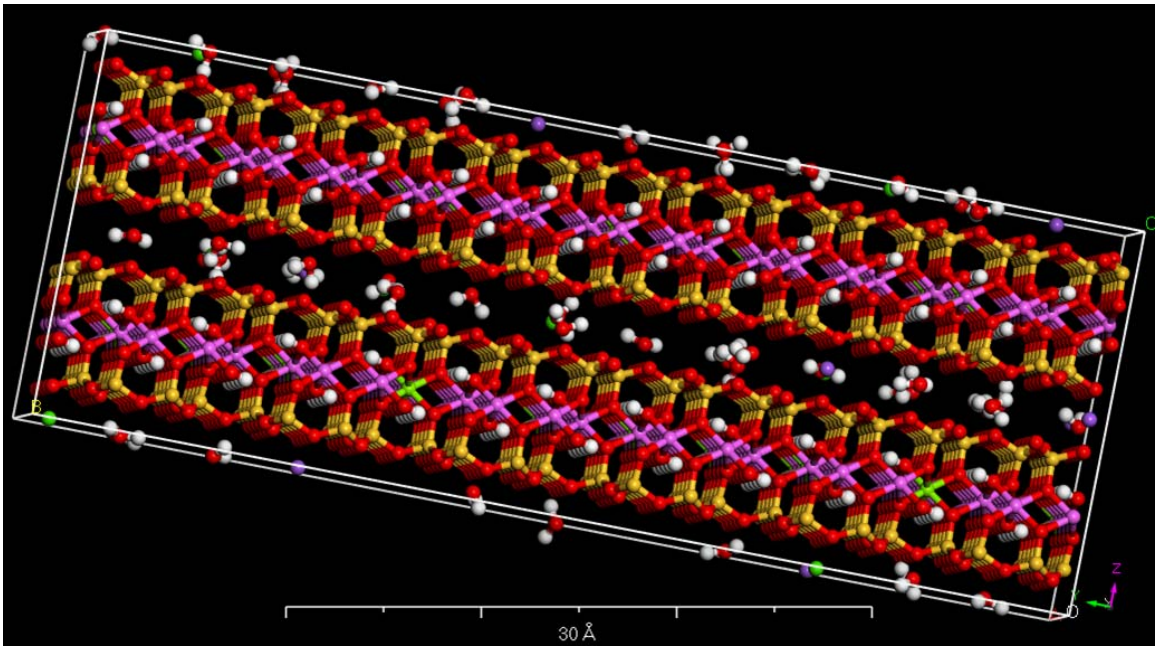

(a)

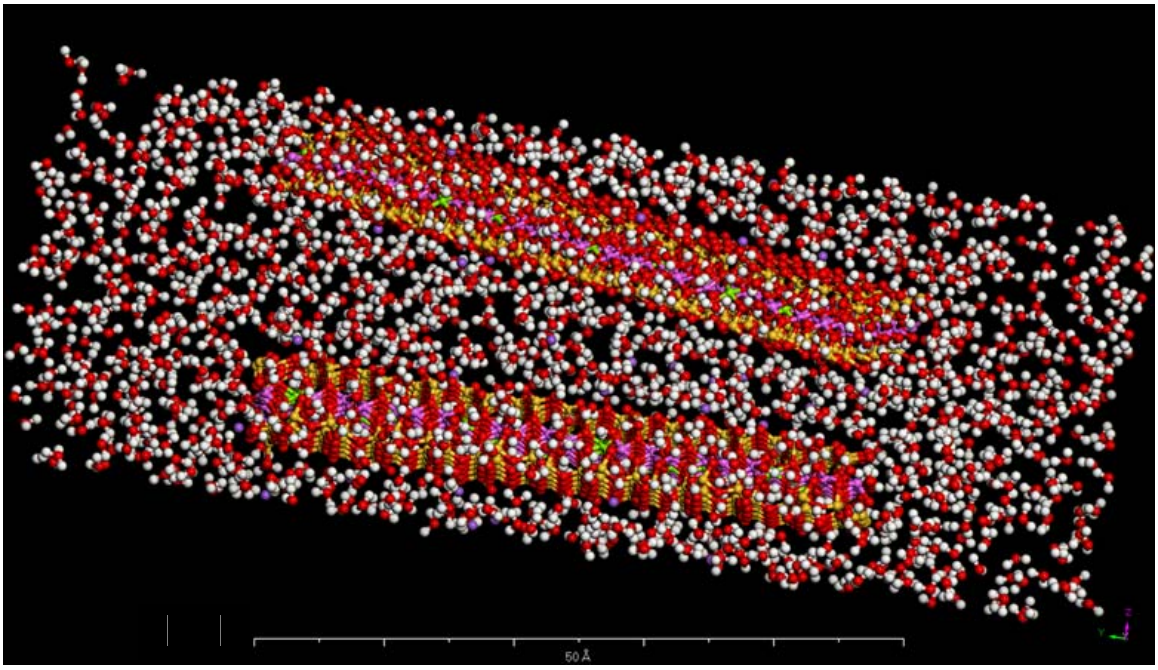

(b)

Figure 3-7 (a) Typical initial water sorption in a dry MCEC Na-montmorillonite and (b) the final picture of the molecule after sorption of 30 % water and the subsequent molecular dynamics.

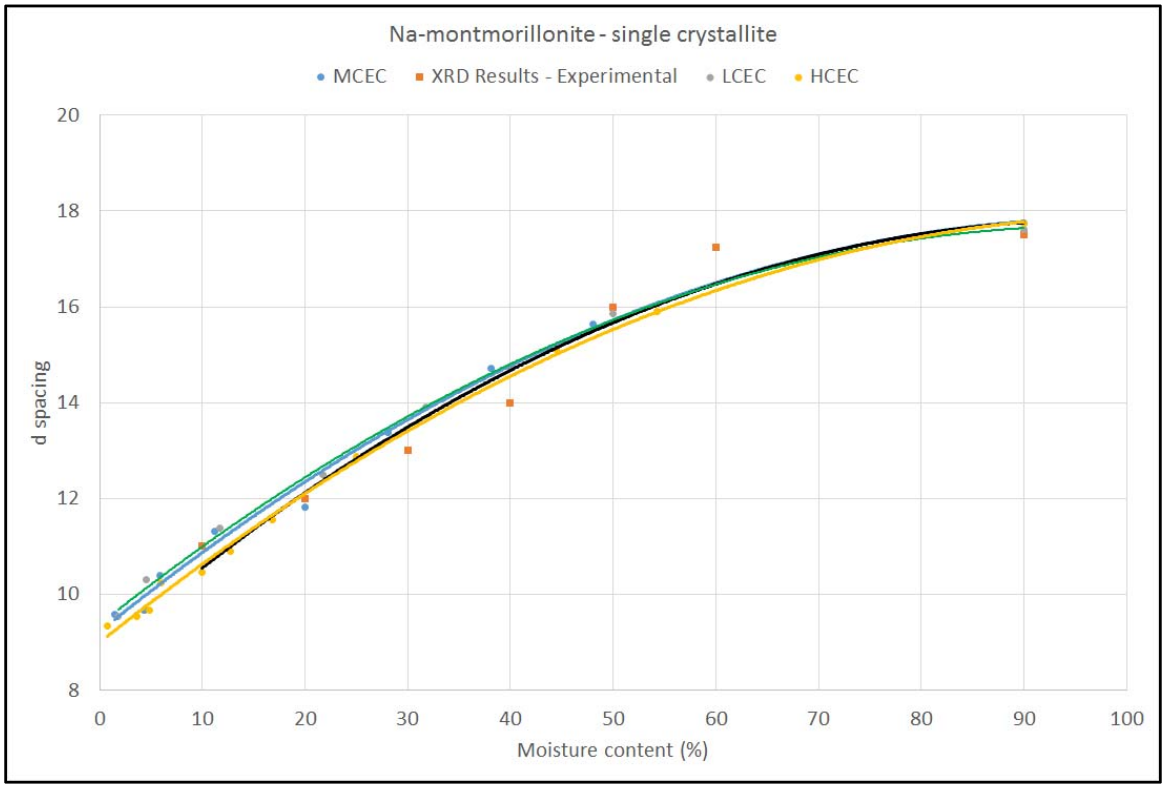

Figure 3-8 Variation in d-spacing of MCEC Na-montmorillonite single crystallite during the water sorption process

So parameters selected for sorption module got further calibration and verification through this process.

3.5.4 Formulation and animation of loose mix of clay particles

Sorption module was used to simulate the assemblages of water sorbed crystallites when mixed together in the loose form before the compaction process. For the purpose, four crystallites were randomly sorbed in a 125 x 125 x 125 Å cubic unit cell (Figure 3-9). Several cubic unit cells sizes ranging from 100 Å to 200 Å were experimented and 125 Å was finally selected. Bigger unit cells resulted in distances larger than the crystallite themselves and smaller ones caused overlapping of the crystallites. Based on the randomness analogy and the parameters used in the Monte Carlo simulation in Sorption module for the single crystallite, these four crystallites occupy relative positions in the cubic space (Figure 3-9). The relative positions are taken up by the crystallites either parallel to faces, edge to edge, edge to the face, or an intermediate form depending on the charge distribution on each crystallite and the moisture content. These unit cells repeat infinitely in space with the superposition of the periodic boundary conditions. In this way, several possible fabrics during the loose mix state were created using Sorption module of the software. As a next step, simulation of the creation of the fabric and structure due to compaction was performed using molecular dynamics Forcite module as detailed in the next section.

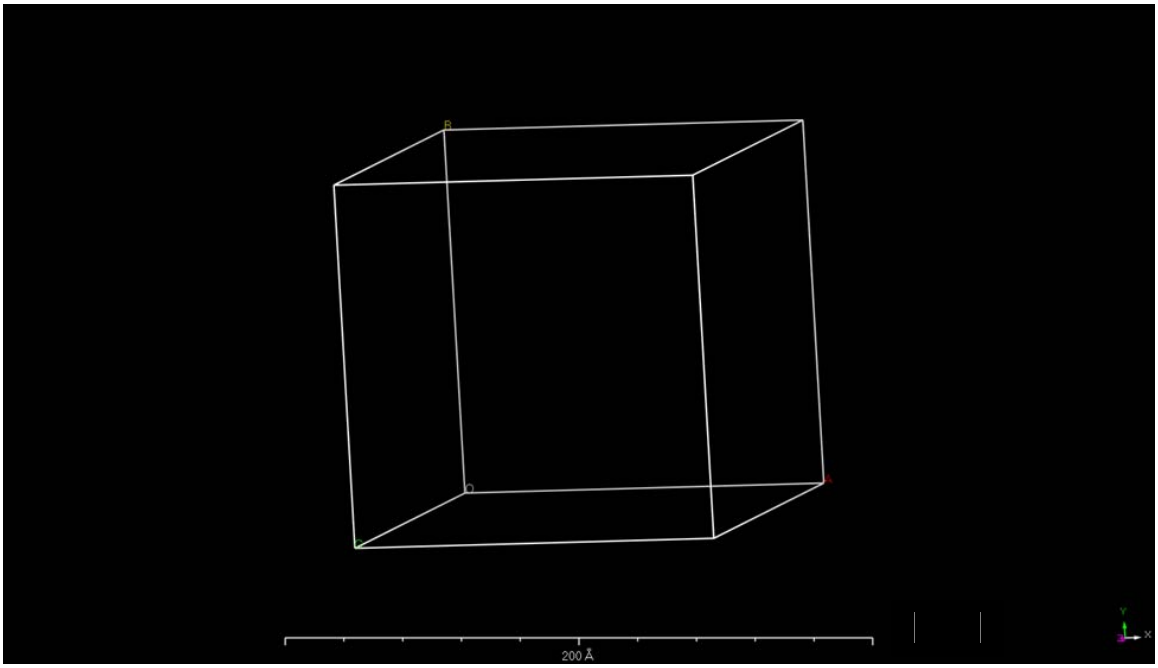

(a)

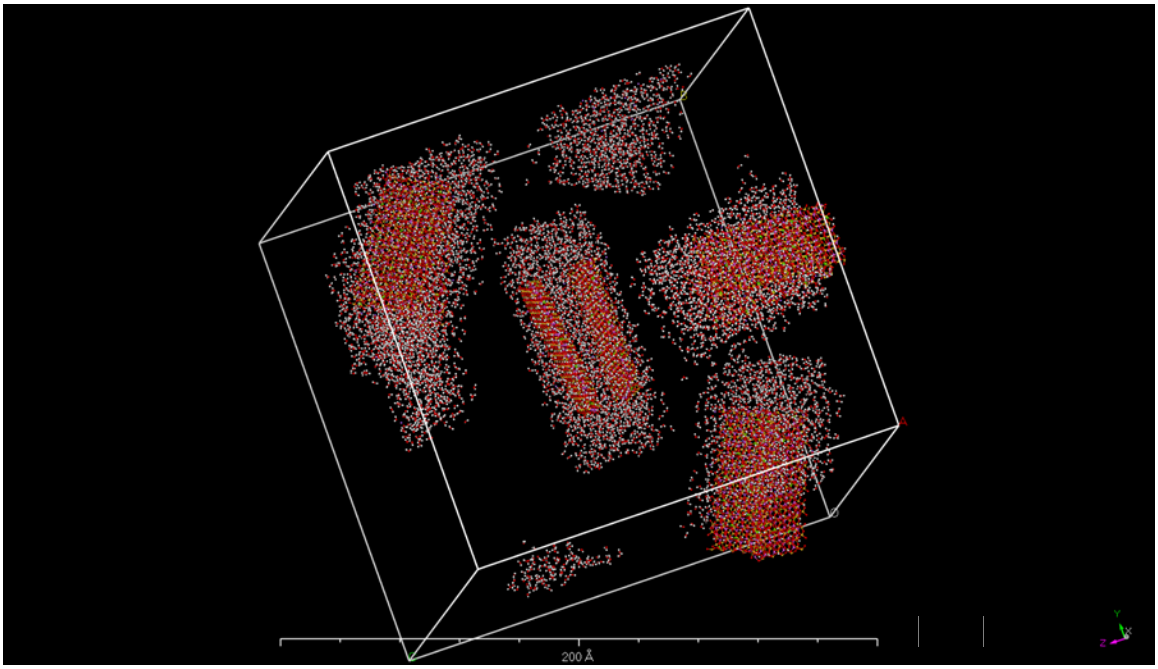

(b)

Figure 3-9 Simulation of loose clay minerals mix using Sorption module (a) empty unit cell (54 x 26 x 20 Å) (b) four water sorbed MCEC Na-montmorillonite crystallites occupying random positions in the unit cell.

3.5.5 Formulation and animation of compacted clay particles mix

To simulate the fabric and structure in the compacted specimens, unit cells consisting of the loose clay crystallites created in the previous step were compressed to the required density using Forcite molecular dynamics module. NPT ensemble was used to compress the unit cell to high density at different confining pressures of 0.01, 0.1, and 1 GPa. Different confining pressures were used to simulate the several levels of geological and laboratory compaction pressures. A comparison of the maximum density achievement at different pressures is shown in Figure 3-10. The simulations were run to 30 ps or more at an interval of 0.5 fs to achieve the maximum density. In this simulation, Berendsen thermostat was used as in Sorption module, while barostat was replaced by Parrinello. As Berendsen barostat applies pressure in all the directions in such a way to keep the unit cell dimensions equal and the corresponding uniform reduction of volume on all the faces of the periodic boundary cell. As Berendsen barostat does not simulate the real compaction process in which stresses vary along the faces under a uniform pressure compaction process. The dynamics compaction simulation was continued till a maximum density is achieved. A 3-D view of several combined unit cells in Figure 3-11 provide a clear visualization of the created fabric. The compacted unit cell and the corresponding compaction curve is shown in Figure 3-12.

To simulate the overconsolidation process by the removal of geological overburden, next step in the simulation process was the relaxation of the compacted structure at low confining pressure and is detailed in the next section.

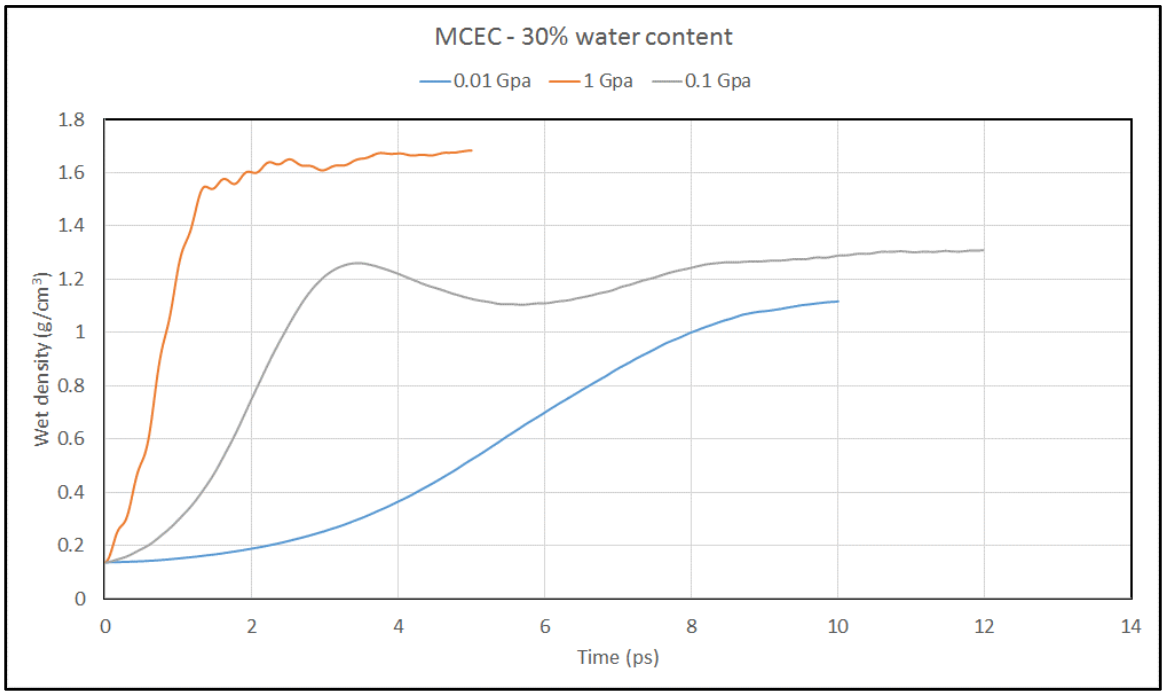

Figure 3-10 Comparison of compaction to maximum density levels at different confining pressures

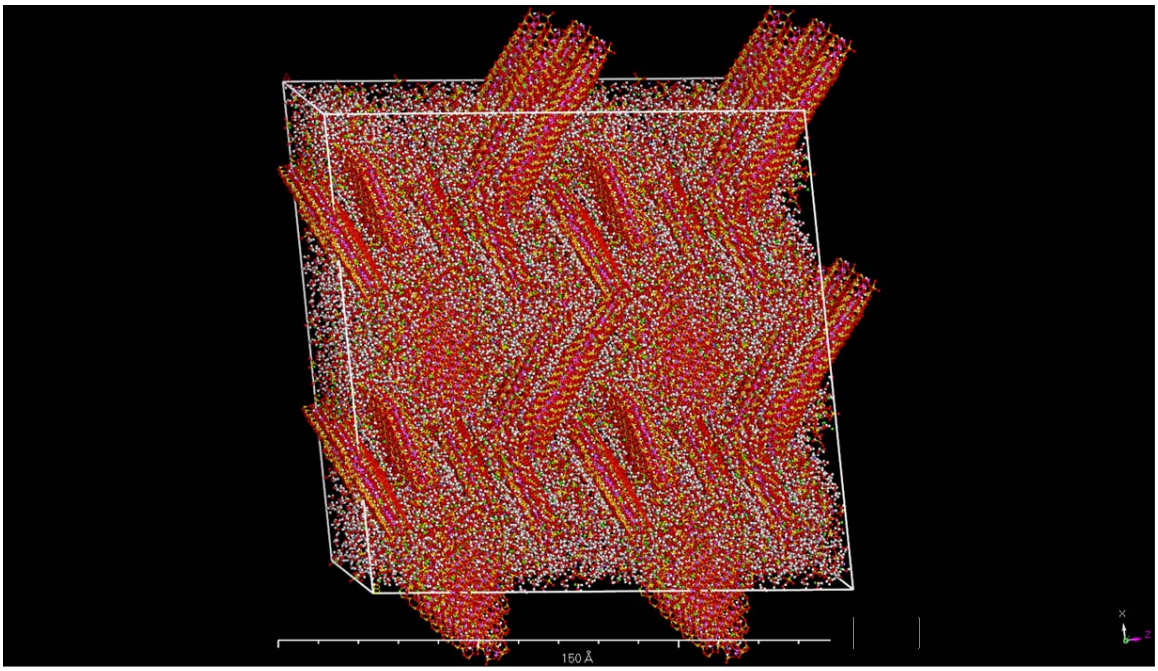

Figure 3-11 3-D view of multiple unit cells showing the continuity of fabric in the compacted MCEC Na-montmorillonite structure.

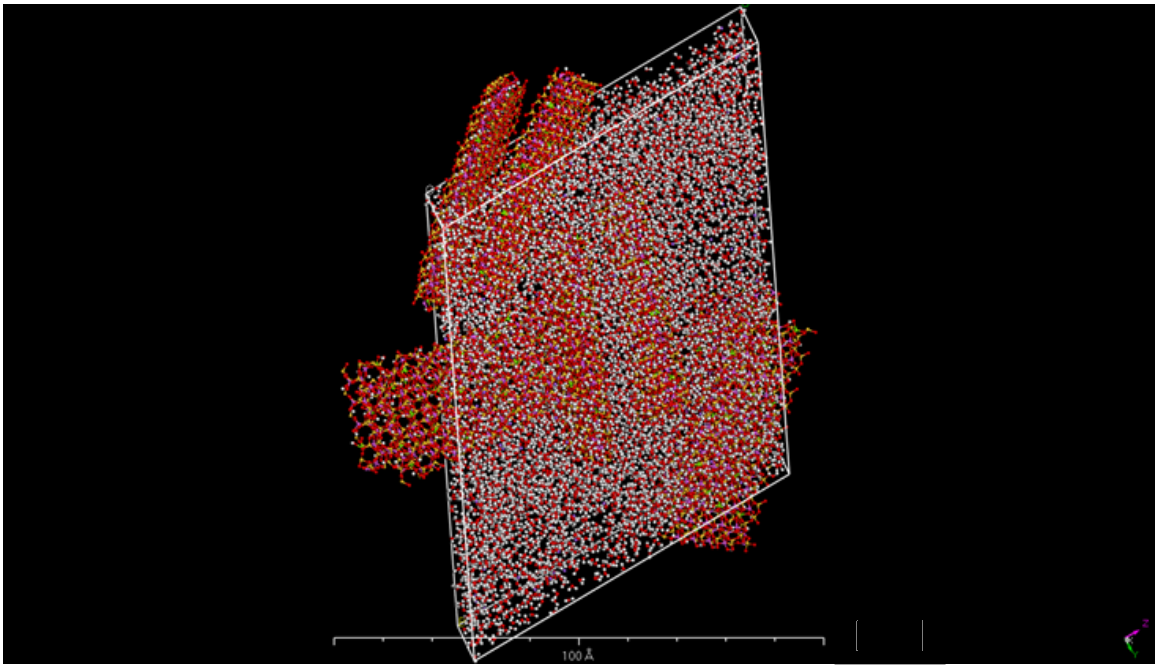

(a)

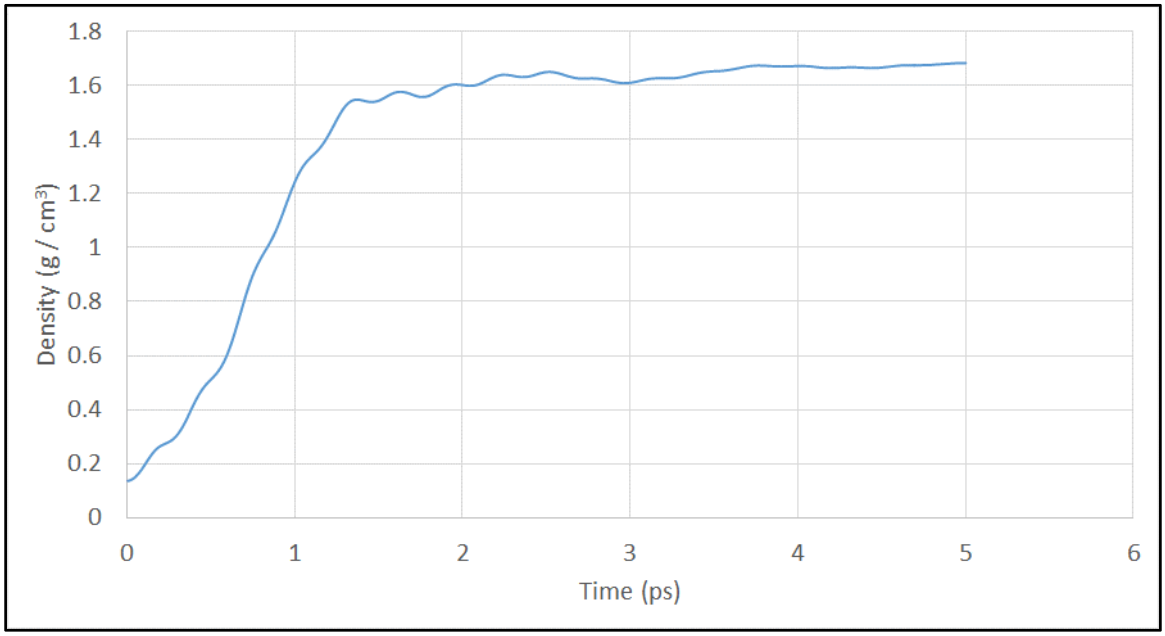

(b)

Figure 3-12 Simulation of compaction process of loose crystallites (a) compacted crystallites (b) compaction curve showing density change with time

3.5.6 Animation of soil structure relaxation at low confining pressure

Expansive clay deposits present at shallow subsurface level have suffered a stress relief due to removal of high geological pressures initially responsible for the creation of highly compacted soil structure. This process causes overconsolidation in the compacted expansive clay layers. To simulate the process of overconsolidation on the compacted unit cell, dynamics through Forcite module of the software was used at a confining pressure of 0.001 GPa. Due to a representative overconsolidation pressure in most of the expansive clay deposits in the area, a confining pressure of 0.001 GPa has been selected as the confining pressure for the relaxation simulation. The relaxed structure of the unit cell after the dynamics simulation and the corresponding relaxation curve is shown in Figure 3-13. The stress relaxed unit cell is now ready to be simulated for the water intake and the corresponding simulation of the swell / volume change behavior. The details of water sorption in the pores of the unit cell and the volume change behavior simulation is provided in the next section.

3.5.7 Water sorption and volume change simulation of compacted clay particles

The stress relaxed unit cell was sorbed with water molecules in the intra and interlayer of the crystallites / particles using sorption module of the software. A maximum number of 25000 steps for the sorption of water molecules were used to apply the energy cutoff. Figure 3-14 shows the sorbed water molecules in the stress relaxed cell.

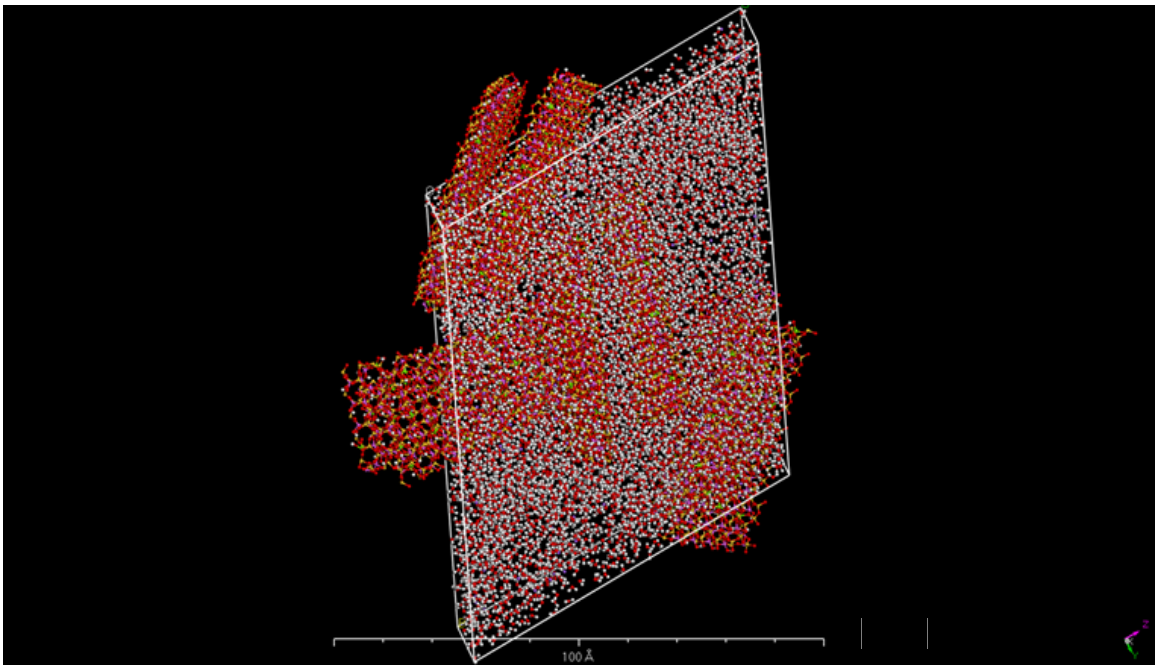

(a)

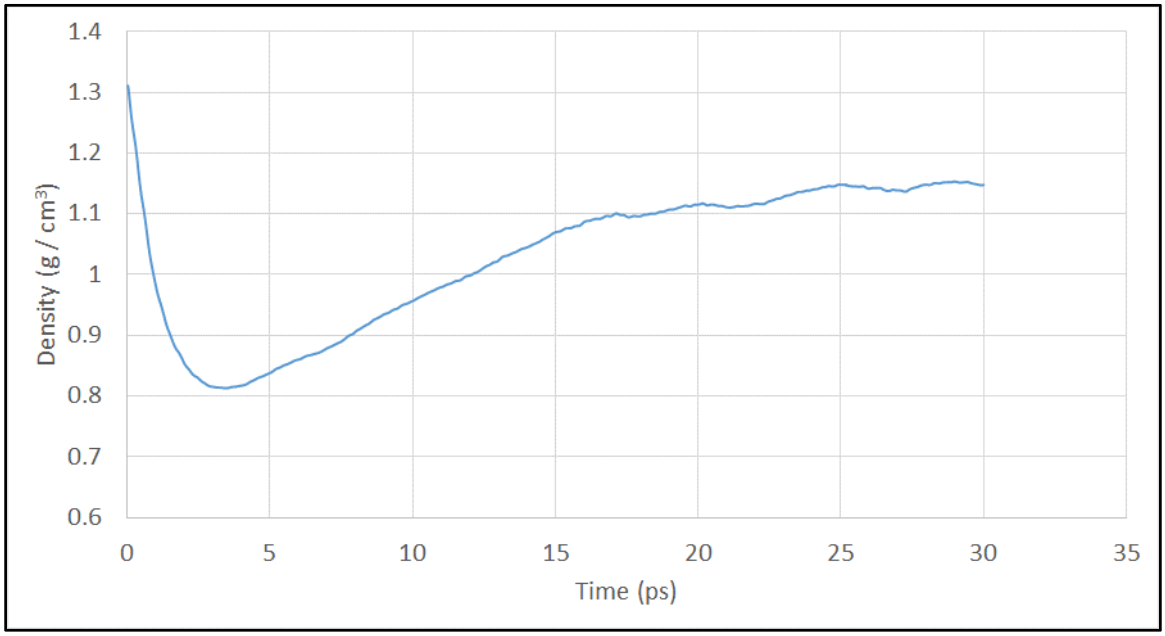

(b)

Figure 3-13 Simulation of stress relief (overconsolidation) (a) expanded MCEC Na-montmorillonite structure against a stress relief of 0.001 GPa (b) density change during the stress relief process

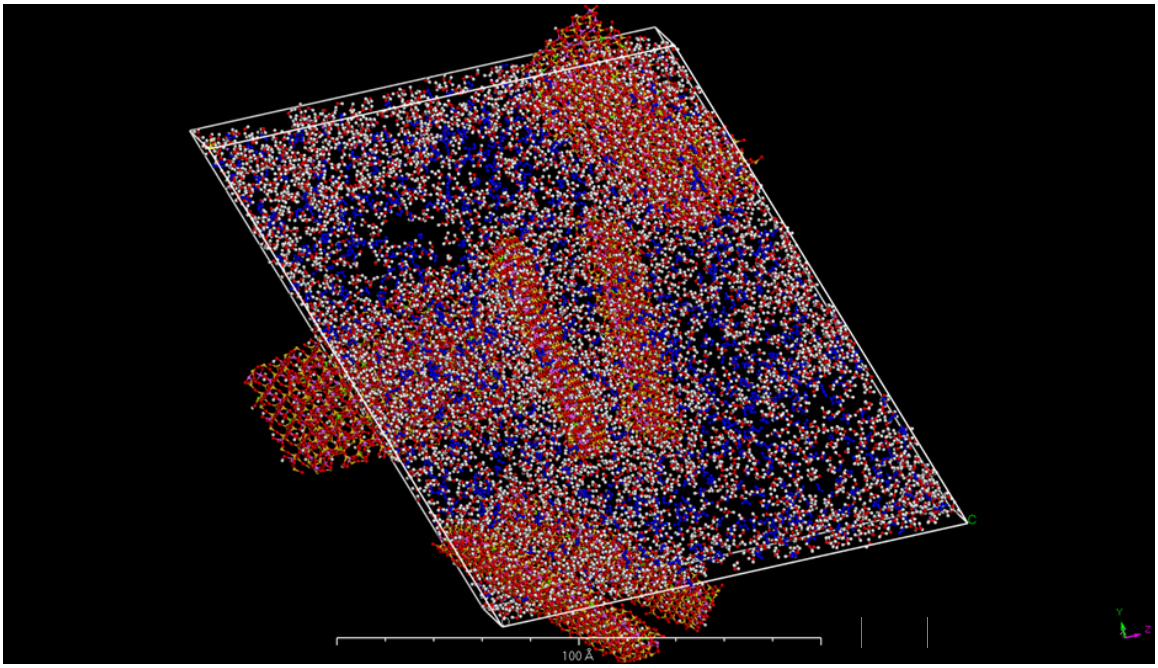

Figure 3-14 Water sorption simulation in a stress relaxed MCEC Na-montmorillonite using Sorption module

Upon the completion of sorption step, dynamics was performed on the water sorbed unit cell. The dynamics was continued till a stabilized volume / density is obtained. The unit cell after the volume change process simulated through dynamics and the corresponding volume change curve are shown in Figure 3-15.

The process of water molecules sorption and the subsequent dynamics leading to a stabilized volume was repeated till a dry density of 0.5 g/cm^3 was obtained. A dry density of 0.5 g/cm^3 is considered a terminal point for the swelling process. Equivalently, this can also be determined once cohesive energy density of 6x10^8 J/m^3 is reached during the dynamics simulation process. In this study, cohesive energy density concept is applied to the behavior of expansive clays and have been used for the volume change model formulation. Use of cohesive energy density concept and its application to the formulation of volume change behavior of expansive clays is discussed in Section 3.5.9. Volume change versus water content curve for MCEC Na-montmorillonite with initial moisture content of 30 % is shown in Figure 3-16.

In addition to the simulations with Na-montmorillonite, simulations were also carried out using other inclusions resulting in the cementation / cohesion effects. The simulations considering these variations are discussed in the next section.

3.5.8 Simulation of adding gypsum, calcite, and potassium chloride

In addition to the presence of non-clay inclusions in the expansive clay deposits as an inert materials, gypsum, calcite, and other salts are also responsible for the cementation /

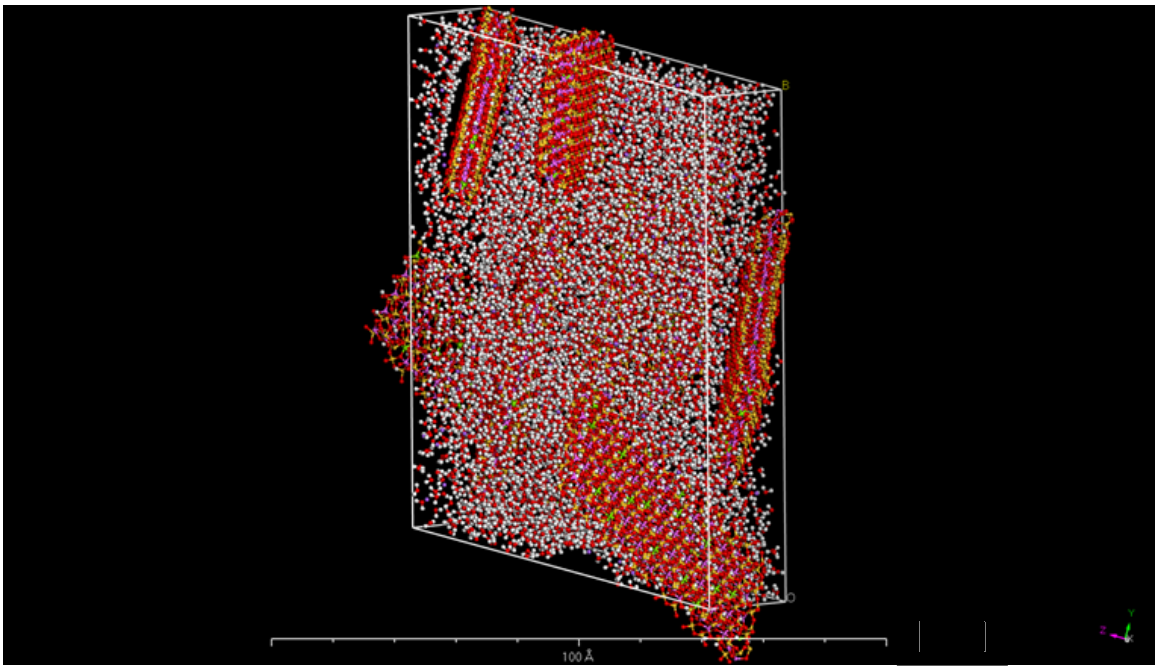

(a)

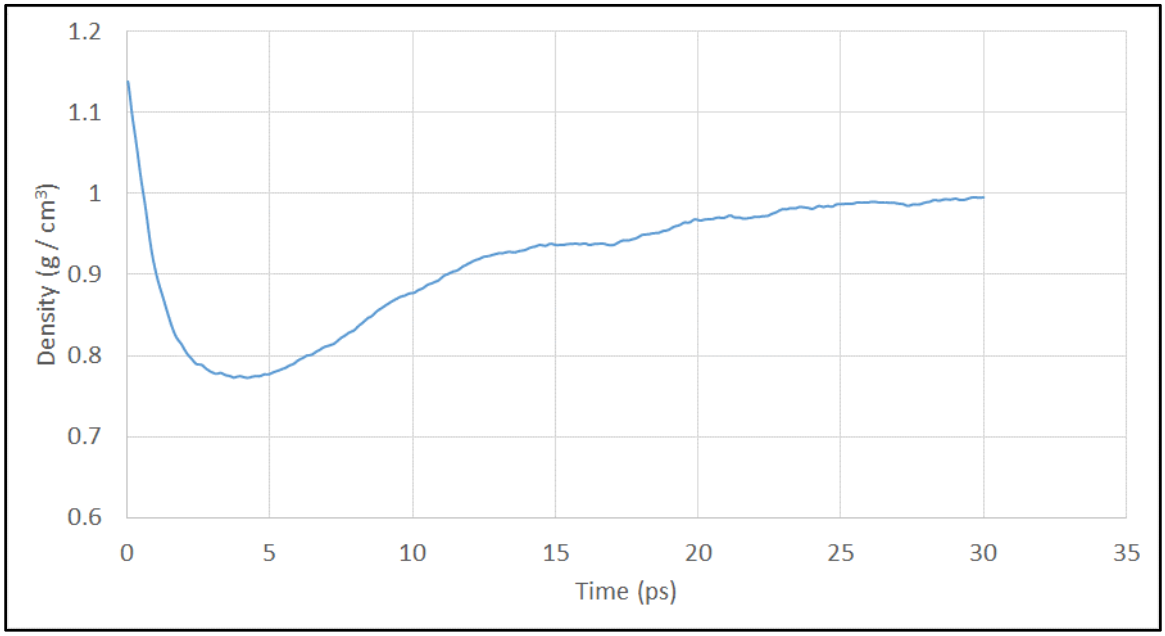

(b)

Figure 3-15 Swelling simulation of water sorbed MCEC Na-montmorillonite (a) expanded structure (b) swelling curve.

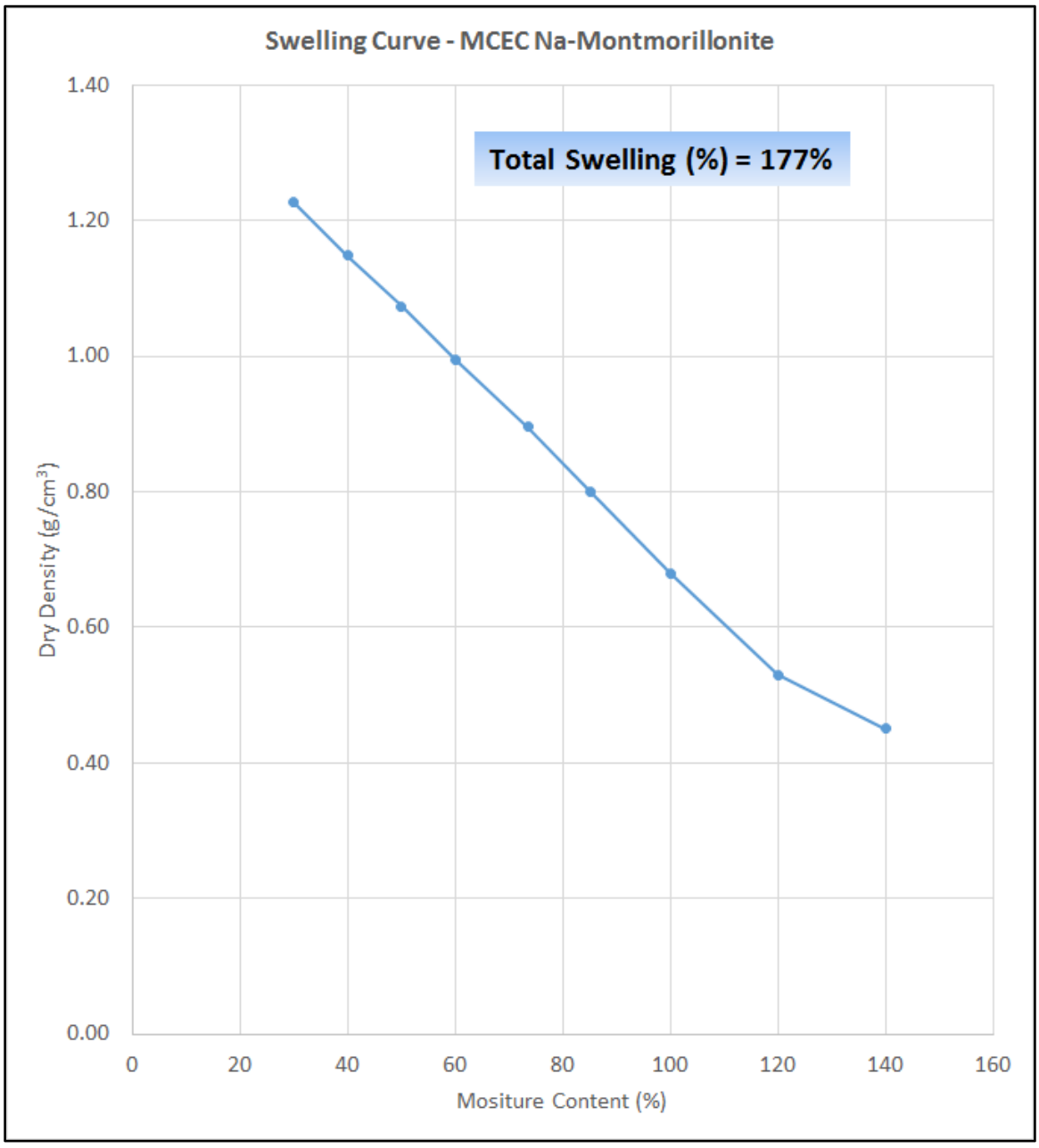

Figure 3-16 Swelling versus moisture content plot for MCEC Na-montmorillonite compacted at an initial moisture content of 30 %.

cohesion among the clay particles. In order to simulate this process, individual atoms / molecules such as Ca^{+2}, SO_4^{-2}, K^+, Cl^-, and CO_3^{-2} were sorbed in the water bearing montmorillonite crystallites. For the purpose, 10 % water was sorbed onto the montmorillonite crystallite with a CEC of 90 meq/100 g. Sorption of 10 % water was performed in order to create a media in which other minerals can get dissolved. To simulate the dissolution of gypsum in the sorbed water layer, Ca^{+2} and SO_4^{-2} were sorbed in and around the crystallite using Sorption module of the software. About 20 % Gypsum was added to the clay crystallite, creating an envelope of Ca^{+2} and SO_4^{-2} around the molecule (Figure 3-17).

Similarly to simulate the adsorption of potassium chloride and calcite in the sorbed water of clay crystallite, K^+ / Cl^- and Ca^{+2} / CO_3^{-2} were respectively sorbed using the Sorption module of the software. These processes led to the formulation of the individual crystallites containing the respective molecules.

Rest of the procedure including the simulation of loose mix of crystallites, compaction, stress relief, water sorption, and the swelling is same as described for the MCEC Na-montmorillonite in the above sections. The final unit cell after swelling simulation for the Gypsum sorbed case is shown in Figure 3-17. A swell cutoff selected for these cases is the quantity of water adsorbed in any single step. Water sorption as low as 2.0 to 4.0 % is indicative of extremely small size of pores and the corresponding extremely low permeability. Therefore, such low values of water adsorption are practically not possible in such highly densified / cemented mass of expansive clay structure. Rest of the simulation results using potassium chloride and calcite are provided in Appendix E.

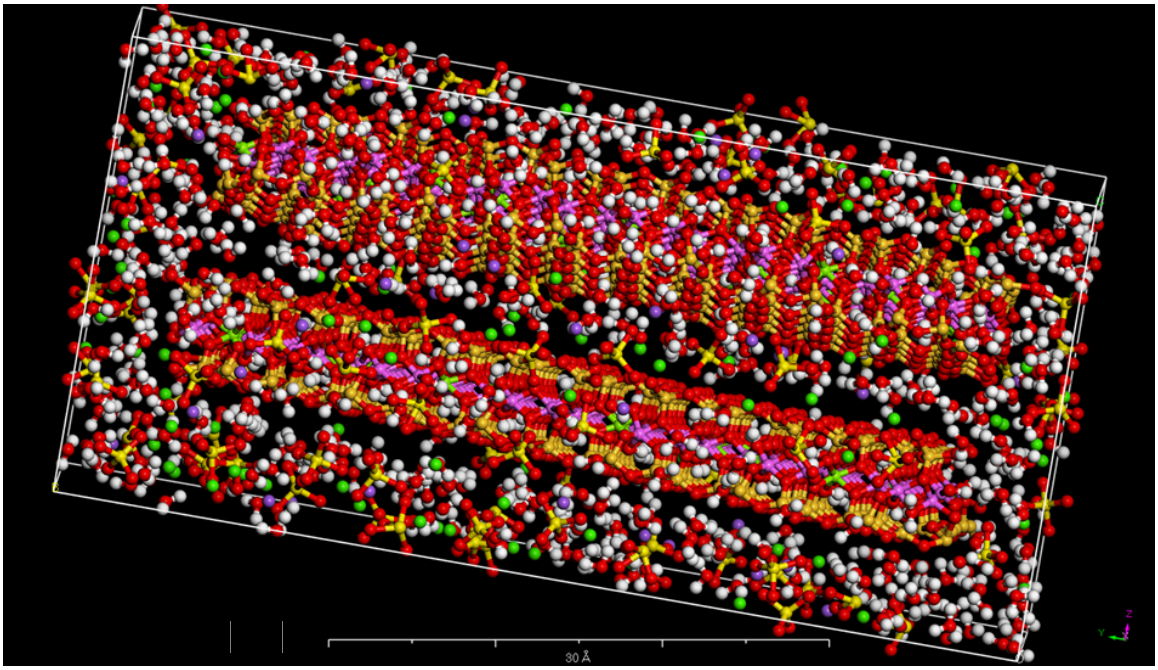

(a)

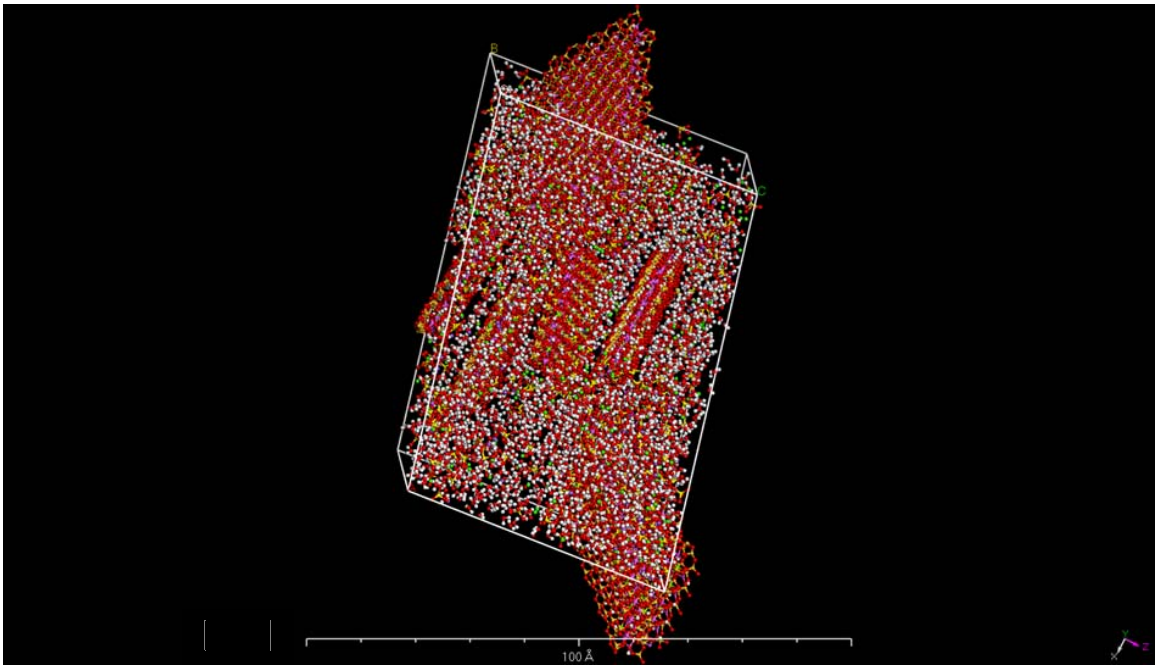

(b)

Figure 3-17 (a) adsorption of Ca^{+2} and SO_4^{-2} on the individual clay crystallite (b) final fabric of the compacted four crystallites unit cell after swelling simulation.

3.5.9 Simulation of change in type of exchangeable cations

All the above simulations were carried out using montmorillonite having sodium as the only exchangeable cation. To study the influence of varying type and proportion of the exchangeable cations, LCEC montmorillonite was subjected to changes in type and number of exchangeable cations. For this purpose, Na^+ cations in LCEC montmorillonite were partially replaced with K^+, Mg^{2+}, and Ca^{2+} cations as per the permutations in Table 3-9. Rest of the process followed for such cases was same as adopted for MCEC Na-montmorillonite in the above sections. The results for various exchangeable cations combinations are provided in Appendix E.

3.5.10 Cohesive energy density correlation to swelling potential

The concepts of cohesive energy and cohesive energy density were first introduced into the theoretical treatment of mixtures by Hildebrand (1916, 1919, 1933, 1970) and Scatchard (1931). In their theories, the cohesive energy is used to estimate the energy change on mixing two species. When supplemented with the entropy of mixing it allows the prediction of the phase behavior of simple mixtures.

The cohesive energy density concept is first time used in this study in relating the swelling behavior of expansive clay minerals to the various variants such as moisture, density, CEC, type, and proportion of exchangeable and total cations etc. Cohesive energy is indicative of how strongly the molecules / crystallites are coherent with each other due to the inherent CEC or cementation effects. Higher the cohesive energy density of the expansive clay structure, lesser the swelling potential of the clay minerals. A swell cutoff selected for

these cases is the quantity of water adsorbed in any single step. Water sorption as low as 2.0 to 4.0 % is indicative of extremely small size of pores and the corresponding extremely low permeability. Therefore, such low values of water adsorption are practically not possible in such highly densified / cemented mass of expansive clay structure. Moreover, swell cutoff for these cases also derives from the fact that swell will take place for the cohesive energy density corresponding to its original counterpart (without cementation and with Na cations only). Using these both concepts, swell potential was evaluated for these cases.

Cohesive energy density was measured for all the simulation cases using Forcite module of the software. Total cohesive energy density was plotted against the moisture content for all the steps in each simulation case as loose mix, compaction, relaxation, and swelling / volume change with water. Typical variation of cohesive energy density for HCEC, MCEC, and LCEC Na-montmorillonite are shown in Figures 3-18, 3-19, and 3-20. Rest of the results are provided in Appendix E and are discussed in detail in Chapter 4.

3.5.11 Modification to Universal Forcefield (UFF)

Forcefield plays a vital role in any molecular simulations study. It provides the relative interaction among the particles by defining the energy relationship for the system. Usually, studies involved in the simulations of clay minerals, CLAYFF forcefield (Cygan et al., 2004) and some others specifically prepared for the purpose have extensively been used.

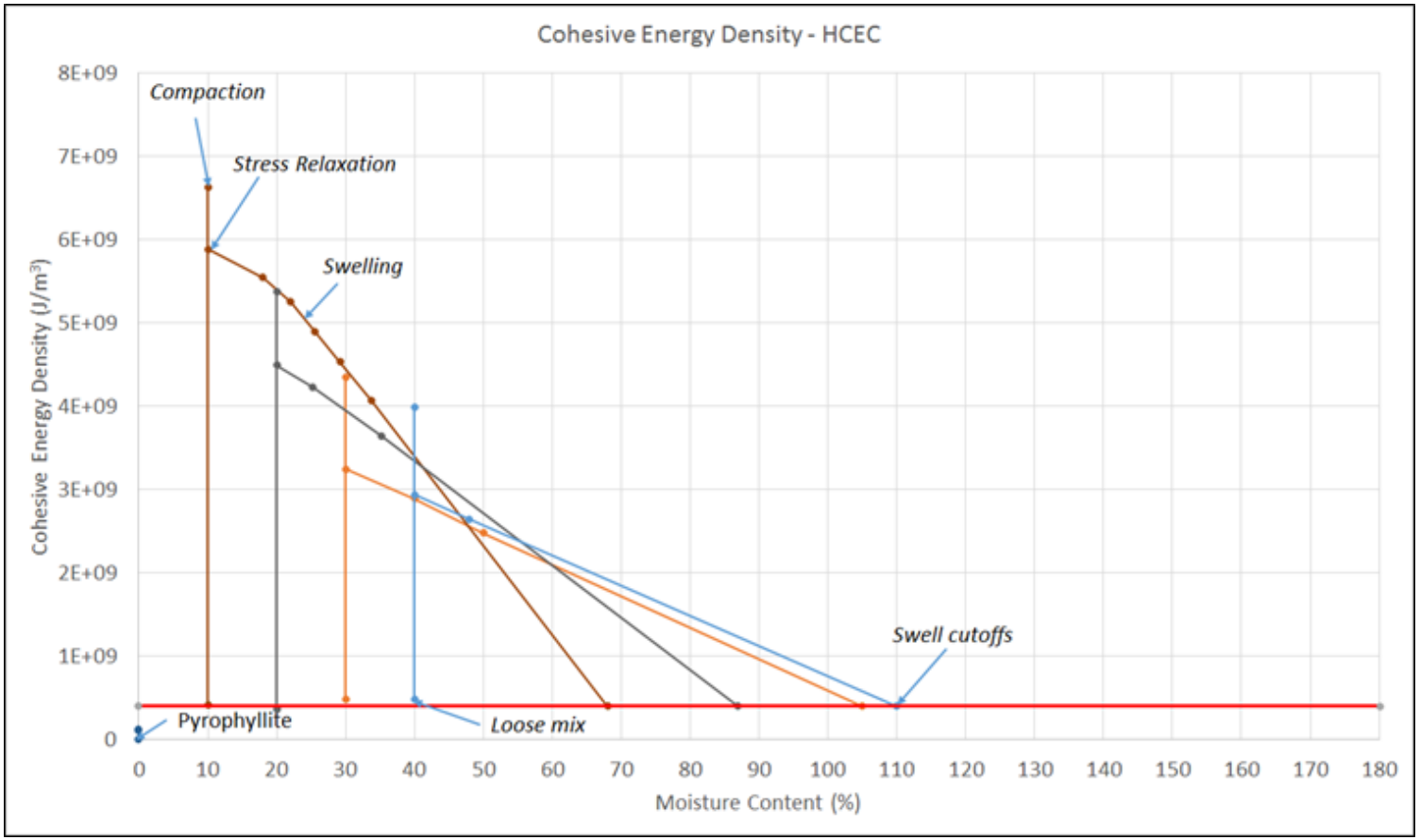

Figure 3-18 Variation of cohesive energy density with moisture and density conditions for HCEC Na-montmorillonite.

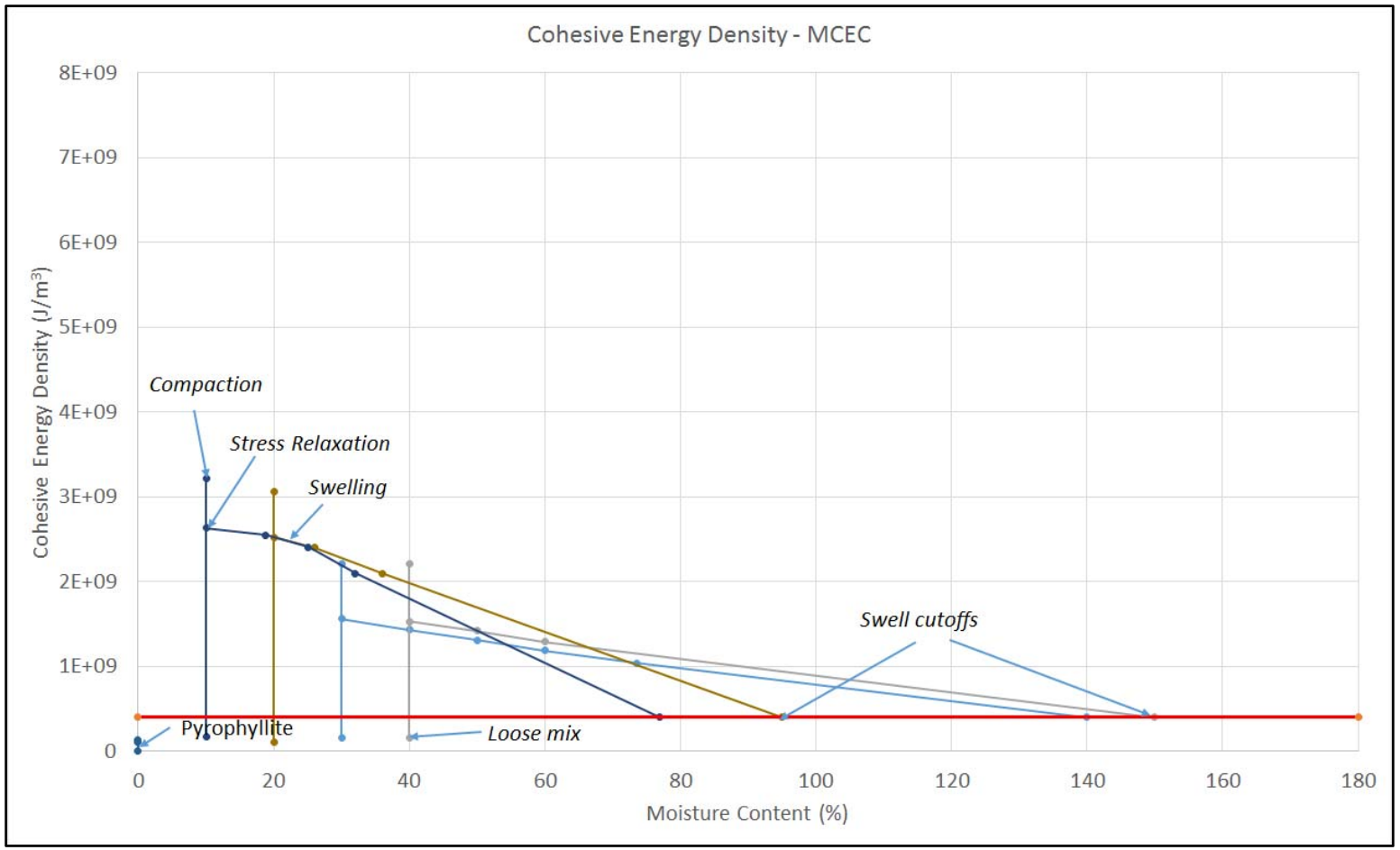

Figure 3-19 Variation of cohesive energy density with moisture and density conditions for MCEC Na-montmorillonite.

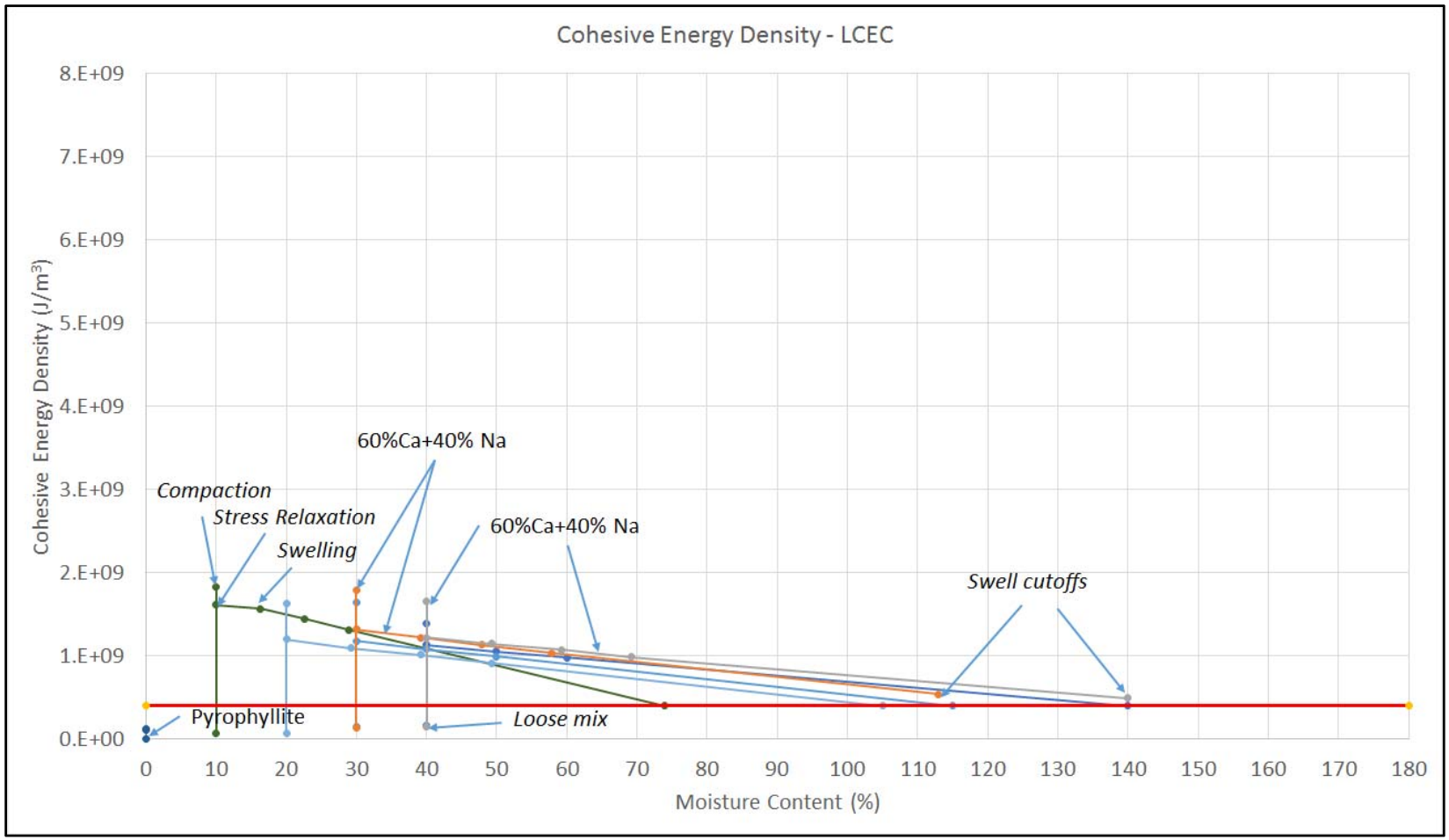

Figure 3-20 Variation of cohesive energy density with moisture and density conditions for LCEC Na-montmorillonite.

But all of these have been applied exclusively for a single clay unit molecule cell. For the scenarios of several crystallites in a unit cell as used in this study, these forcefields have limitations especially when the unit cells / single crystallites are converted to non-periodic superstructure for sorption purpose. Universal forcefield (UFF), the forcefield embedded in the software consists of universal parameters to cover the entire periodic table and may be used for such scenarios. When UFF was applied to several scenarios formulated in this study, several well-known facts could not be verified. Therefore, it was planned to do changes and modifications to the UFF as per the requirements of a typical forcefield applicable to clay minerals interaction with water. So, several forcefield parameters in UFF were modified in the light of the parameters suggested in CLAYFF forcefield. The parameters for Na, Ca, Mg, Al, and Si were accordingly modified. The original and the corresponding modified parts of UFF are provided in Appendix F, while the comparison of the results of typical swell of Na-montmorillonite crystallite of the original and modified UFF are shown in Figure 3-21.

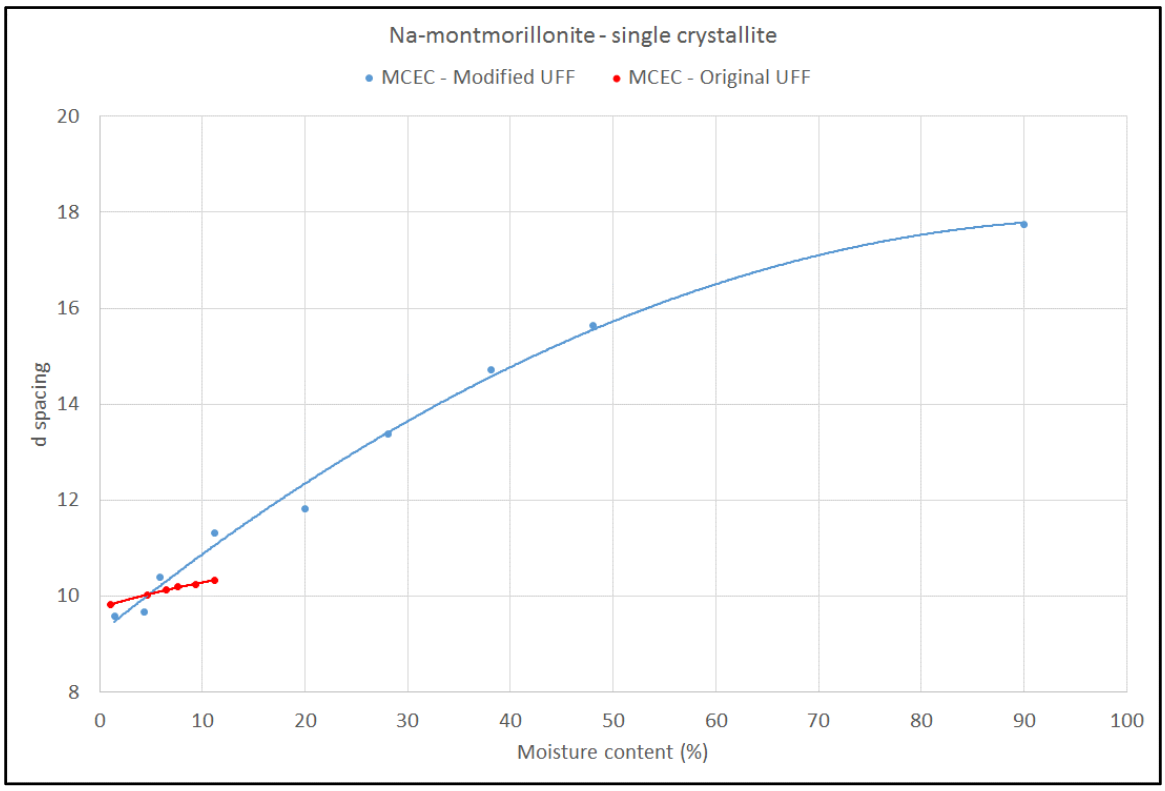

Figure 3-21 Comparison of d-spacing change of a single Na-montmorillonite crystallite using original and modified UFF.

CHAPTER 4

RESULTS AND DISCUSSIONS

This research is composed of three major activities; macro level testing, micro level imaging and analysis, and molecular level simulation and modeling. These activities have led to the formulation of a volume change behavior model for the molecular / nano level structure of expansive clayey soils. The nano level model can be coupled with micro and macro level models to formulate a comprehensive volume change model for the expansive soils. This chapter discusses the results of each level of activity and the corresponding contribution to the other activities. As the main intent of this research was to study, analyze, and model the molecular / nano level structure of the expansive clays, main focus of the discussions are the molecular level processes. This chapter contains the major findings and the corresponding discussions for all three activities of this research.

4.1 Macro level tests

The macro level behavior of the expansive soils have been studied through the free swell potential tests on various combinations of clay and non-clay minerals, undisturbed natural samples, compacted at various moisture and density conditions (Table 3-5). Free swell tests results tabulated in Table 3-6 and plotted in Figure 3-3 reveal that there is a general increase in swell potential with increase in bentonite content, rate of increase in swelling is reduced as bentonite content increases to the maximum value of 100 %. This decrease rate of swell could be attributed to the reduced permeability or water intake capacity of the

fabric of the compacted clay and sand mixes. As the swelling increases, more swollen particles start occupying the bigger pores, thus further impeding the water flow rate in the clay fabric. This fact can be qualitatively confirmed through the ESEM results of the typical fabrics of sand-bentonite mixes in Figure 4-1. This figure reveals very small size of pores for the 100 % bentonite case while a relatively open fabric containing relatively large sized pores in case of higher percentages of sand. Based on the above facts, the aspect of permeability of the fabric should have a special consideration besides density, in the modeling of total swell potential of closed fabrics composed otherwise of high swell potential clay minerals. Relatively lower permeability may not allow the permeation of enough water required for the complete swelling of all the clay mineral particles present in the soil fabric. This phenomenon needs to be translated into a significant factor in the volume change modeling of the expansive clays. Permeability characteristics of the micro fabric should also be coupled with the macro fabric features such as fissures and stress cracks to define the water intake potential of the entire structure of the expansive clayey soils.

Use of static compaction to prepare the samples with the same density achieved through dynamic Proctor compaction has led to an equivalent static pressure of 1500 kPa. As the fabric created using the static compaction is less dispersed in nature (agglomerates are obvious in Figure C-21), it has resulted in higher swelling (121 %) than it's dynamically (Proctor) compacted counterpart (89 %). Although kaolinite is a non-expansive clay mineral, replacing sand partly with kaolinite resulted in reduced swelling (95 %) as compared to the one with no replacement. This phenomenon may again be attributed to

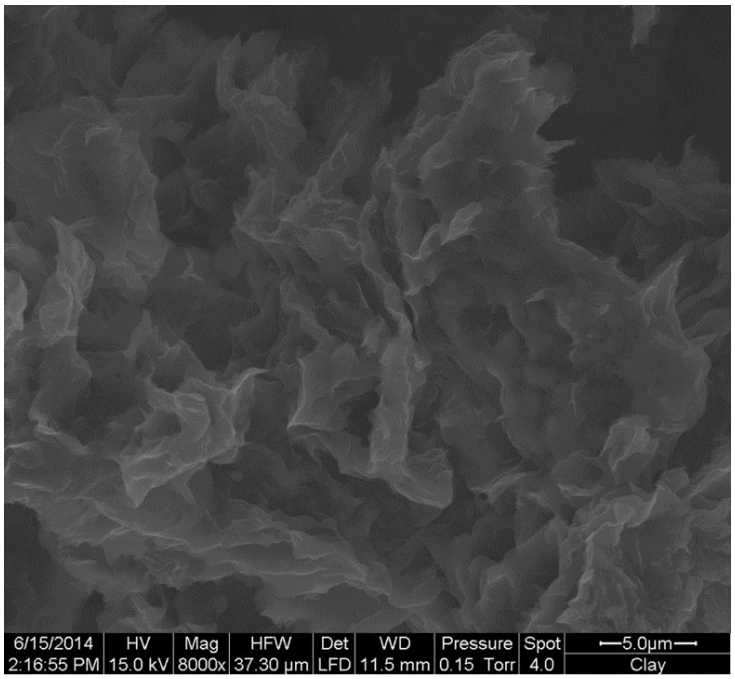

(a)

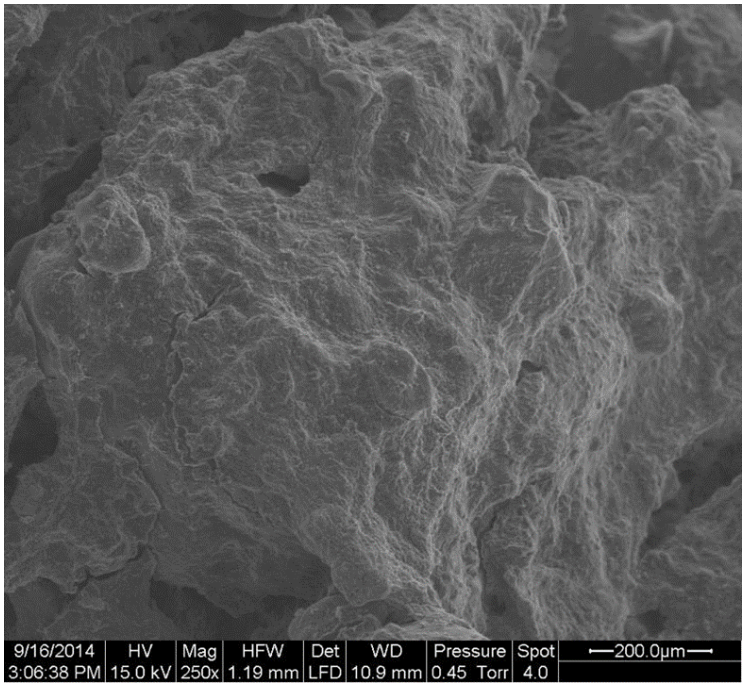

(b)

Figure 4-1 Comparison of a closed and open fabric in post swell samples respectively for (a) 100 % bentonite (b) 30 % bentonite and 70 % sand.

the low permeability of the fabric containing high percentage of fine grained kaolinite replacing part of coarse grained sand.

Replacing part of the sand by calcite and gypsum have resulted in substantial reduction in swelling. There is a reduction of 82, 90, and 95 % in the swelling potential when gypsum was added 10, 30, and 50 %, respectively. Similarly, there is reduction of 40 and 44 % in swelling upon part of sand replaced by calcite of 30 and 50 %, respectively. The phenomenon of decrease in swelling by addition of calcite and gypsum might be resulting from the binding effects produced by these compounds to the individual or group of clay particles. As calcite and gypsum in their powdered form were mixed with bentonite and water, these minerals get dissolved in the molding water to varying degree of dissolution. The resulting cations and anions dissolved in water get adsorbed on the surface and interlayer of the clay particles. This phenomenon provides additional binding forces to the individual and group of clay particles. As solubility of powdered gypsum in water is generally higher than calcite, it is causing more reduction in the swelling when added in equivalent quantities. This theory of the additional binding effects or cohesion provided by these compounds can be visualized through ESEM results in Figures C-23 and C-24 for gypsum and Figures C-31 and C-32 for calcite, respectively. These figures clearly show the closed fabrics due to additional bonding or cohesion created as a result of the presence of these compounds. As it is difficult to visualize the dissolved salts causing cohesion to the clay particles, this bonding / cohesion theory was further verified through molecular level simulations.

Presence of bonding / cohesion can also be imagined from the fact that although CEC of and the percentage of smectite in the natural undisturbed sample of Qatif-1 is almost same

as of the commercial bentonite (30/70 sand-bentonite mix), the difference in percent swell is large, i.e., 29 % vs. 121 %. This difference may be attributed to the cementation effects provided by the calcite, gypsum, and other similar compounds or salts present in the soil. To further investigate these results, in addition to the exchangeable cations, total cations were also determined for the bentonite and undisturbed samples. The results are provided in Table 3-2 and are further discussed in Section 4.2.4 under micro investigations.

4.2 Micro level tests and analysis

The reasoning provided in the previous section for the various phenomena responsible for the macro level behavior were further confirmed through micro level investigations. Some of the interpretations were confirmed through direct imaging techniques and other through the analysis of the data and results of these tests. The results acquired through these tests and the corresponding discussions and explanations are provided in the next sections.

4.2.1 X-Ray Diffraction

X-Ray Diffraction (XRD) test is primarily used for the mineralogical analysis of crystalline samples. In this study, XRD has not only been used for the determination of the mineralogical composition of the laboratory compacted specimens and the undisturbed samples obtained from the natural deposits but also for the study of change in lattice d-spacing in crystal lattice of clay mineral with water content. Change in d-spacing in the clay mineral structure was determined both on the specimens from the loose mix and the compacted samples.

Loose mixture of bentonite samples were prepared by mixing the soil with different water contents ranging from 10 to 100 %. XRD tests were performed on each of these samples and the resultant d-spacing as a function of water content is shown in Figure 3-8, which is evident that there is an increase in lattice spacing with water content to a spacing of 17.5 Å at 60 % water content and remains constant afterwards to a water content of 100 %. As d-spacing of dry bentonite is 10 Å and each water layer occupies an approximate thickness of about 2.5 Å in the interlayer space, 17.5 Å indicates the presence of three water molecules layers in interlayer. Each water layer of about 2.5 Å in the interlayer constitutes about 10 % water content. This indicates that the maximum water content accommodated in the interlayer space in clay minerals is about 30 % and the rest of the water is adsorbed on the ends and edges of the clay mineral crystallites. This fact constitutes a significant aspect in the molecular level simulation and modeling.

In addition to the XRD tests on the specimens from the loose mixture at various water contents, these tests were also conducted on the samples compacted on the dry and wet side of OMC. Figures 4-2 and 4-3 indicate that d-spacing of about 15 Å (equivalent to two water layers or 20 % water content) exists in the clay crystallites on the dry side of OMC while d-spacing of 17.5 Å occurs (equivalent to three water layers or 30 % water content) on wet side of OMC. As the molding water content is respectively 30 and 40 % for the dry and wet side of OMC, it is established that rest of the 10 % water content for both the cases is adsorbed on the edges and ends of the crystallites. This fact has played an essential role in the assessment of the fundamental size of the crystallite in the molecular level simulation.

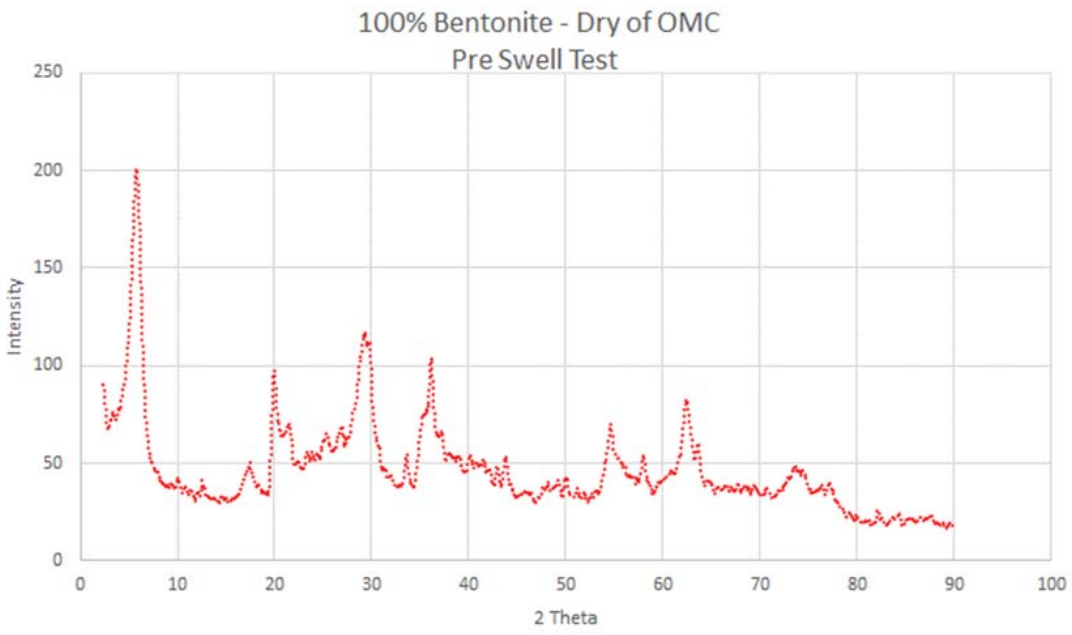

(a)

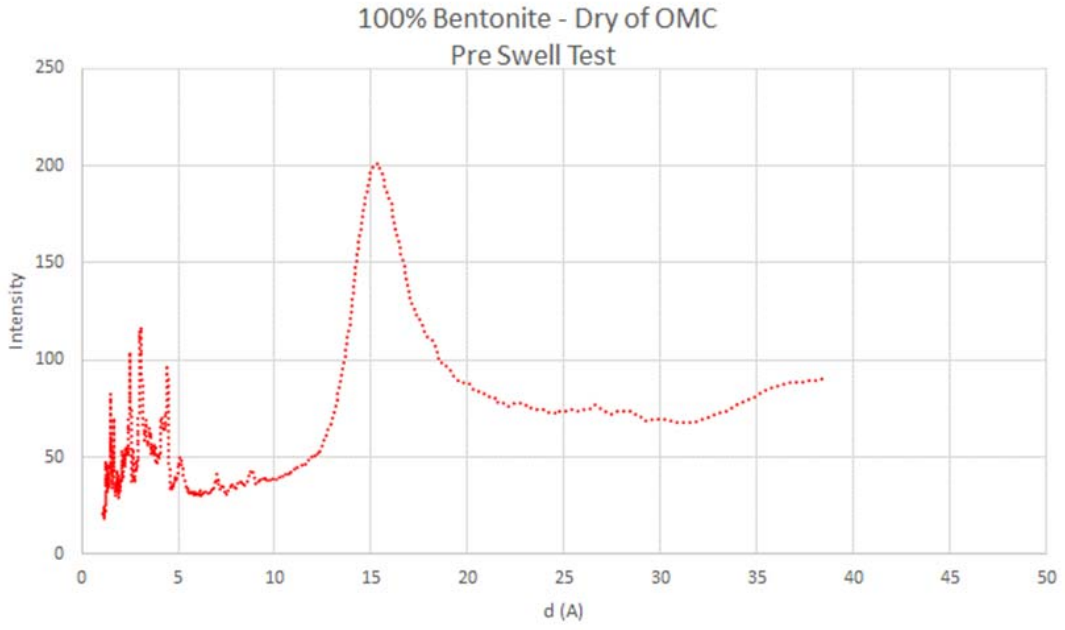

(b)

Figure 4-2 Analysis of d-spacing in compacted 100 % bentonite – dry of OMC (a) XRD pattern (b) d-spacing.

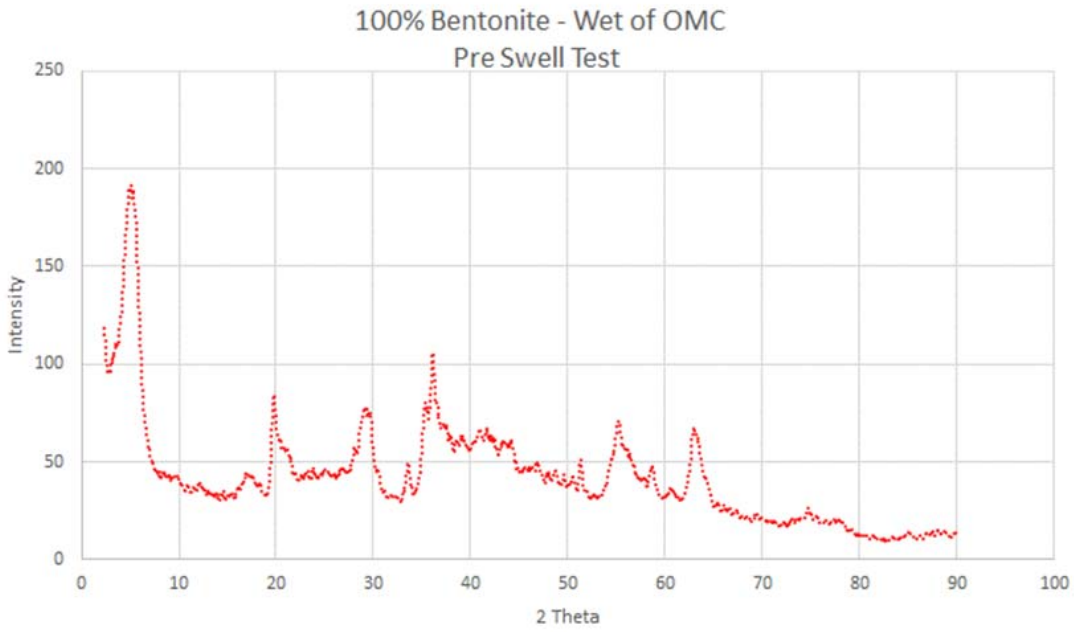

(a)

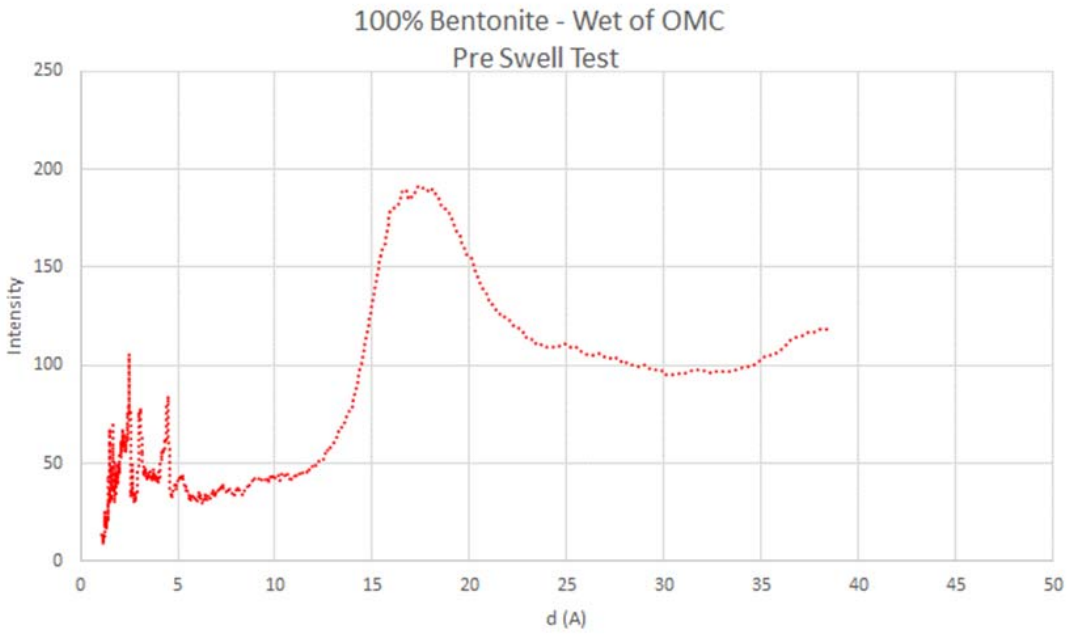

(b)

Figure 4-3 Analysis of d-spacing in compacted 100 % bentonite - wet of OMC (a) XRD pattern (b) d-spacing.

Fundamental crystallite size was also assessed from the XRD data using Debye-Sherrer's method (Sherrer, 1918). The mechanism based on the concept of inverse relationship between width of an X-Ray diffraction peak and the crystallite size is shown in Figure 3-4. Using the Full Width at Half Maximum (FWHM) of the corresponding peaks in the XRD data, removal of background to obtain the net peak intensity have resulted in the assessment of the crystallite size in the range of 59 to 108 Å. This knowledge has been used in the selection of the size of the crystallite in molecular level modeling.

4.2.2 Environmental Scanning Electron Microscopy

Environmental Scanning Electron Microscopy (ESEM) results have provided a clear conception of several features of the fabric of the pre and post swell samples. For the samples with 100 % bentonite, particles have shown greater spacing in the post swell state (Figure C-4), while the ones having other minerals such as calcite and gypsum have shown closed fabric of the nano clay particles in the microstructure. These two features support several explanations regarding the specific behavior observed during the swell potential tests. For example, high swelling of 100 % bentonite samples and highly reduced swelling for the samples containing gypsum or calcite.

Energy Dispersive Spectroscopy (EDS) was performed both on specific area or focused points of the specimens during the performance of ESEM. EDS results indicate the presence of Na^{+} and Ca^{+2} as two major cations in the bentonite. From the Figures C-7 to C-10, it can be observed that although intensity of peak for Na^{+} cations is present both in pre and post swell samples, Ca^{+2} peak is present in pre swell samples only and it diminishes in the post swell samples. Based on this observation, it could be inferred that not all the

Ca^{+2} cations may be exchangeable in nature, rather most of these may be associated with clay crystallites as non-exchangeable cations. These non-associated Ca^{+2} cations after getting dissolved in water might have drained away in the free water and thus not appearing the EDS results of post swell samples.

In case of samples containing sand and other non-clay inclusions, clay particles have found to be coating the bigger non-clay particles. For the samples containing gypsum, ESEM in Figures C-23 and C-24 reveal the clay layers to be present as cohesive assemblages. On the other hand, ESEM of the samples containing Ca (Figures C-31 and C-32), calcite has been found in crystal form on the specimens. From these results, relatively higher dissolution of gypsum in water as compared to calcite may be inferred.

4.2.3 Fourier Transform Infrared Spectroscopy

Fourier Transform Infrared Spectroscopy (FTIR) has been extensively used for the investigations of the molecular level behavior contributing to the macro behavior of the expansive clays (Katti and Katti, 2010). In case of clays interacting with water, H-O-H bending vibration and O-H stretching vibration bands provide the vital information on the level of interactions at various interlayer water contents. Both the vibration bands under stable / dry form are 1694 cm^{-1} and 3634 cm^{-1}, respectively (Katti and Katti, 2010). When water enters the interlayer of the clay crystallites, H-O-H bending band shifts to lower energy levels depending on the water content. In Figure B-6, it can be noticed that there is a reduction in H-O-H bending band from 1694 to 1650 in bentonite loose mixed samples with moisture content from 40 to 60 % and remains same at higher moisture contents. This confirms the trend as observed in the XRD analysis of the bentonite samples mixed with

varying percentages of water. Moreover, O-H stretching band achieves higher energy from 3634 to 3650 cm^{-1} as a result of the addition of water. A similar trend of reduction in the H-O-H bending band and O-H stretching band have been observed in all the post swell specimens. FTIR have proven to be a complementary technique for the investigations of nano level changes in the clay structure due to the interaction with water.

4.2.4 Exchangeable and Total Cations

Presence of non-clay minerals and constituents in any natural or compacted expansive soils play a vital role towards the total swell potential. Most of the non-clay minerals such as calcite, gypsum, and other compounds or salts of sodium and potassium exist in cations and anions form when present in pore solution of these deposits. Part of the cations such as Na^{+}, K^{+}, Ca^{+2}, and Mg^{+2} get adsorbed on the surfaces and interlayer of the charged clay mineral crystallites, while others exist either as isolated fabric or associated with the individual or group of clay crystallites by covering them on the surfaces, ends, and edges.

During the swell potential testing phase, it was observed that presence of non-clay minerals such as calcite and gypsum act as swell retarders. It was hypothesized at that stage that these non-clay minerals provide a sort of additional binding / cohesion to the individual and group of expansive clay particles. To find out a correlation among the type, nature, and quantity of non-clay cations and the swelling potential, both total and exchangeable cations were determined as described in Section 3.1.1.

Results of the total and exchangeable cations, summarized in Table 3-2 provide an estimate of the non-exchangeable cations present in the samples. Comparison of the percentage of

non-exchangeable cations with the percent of expansive clay minerals may provide a very close estimate of the swell retardation percent. These estimated numbers are further discussed in Section 4.3.11.

4.2.5 Micro Computed Tomography

Owing to its micron level resolution, Micro Computed Tomography (Micro CT) is limited in its use for the nano / molecular level studies. In this study, micro CT has been used only to visualize and evaluate the micron level fabric of the pre and post swell samples using the contrasting attenuation property of the clay particles before and after the swell test. This concludes that CT could be used as a general tool for the assessment of the factors contributing to the swell potential of any compacted or natural clay matrix. Micro CT results indicate the agglomeration of the fine grained clay particles in the pre swell state while these become more dispersed in their post swell state (Figures D-1 to D-7 in Appendix D). Conclusion drawn in swell potential tests regarding the swell retardation caused by the non-clay constituents and visualized in ESEM results are also indicative through CT results. In Figures D-1 to D-7 of Appendix D, pre and post swell CT scans indicating several parts of the specimens showing no change in attenuation color are indicative of the particle assemblages restrained from swell through cohesion / bonding created by non-clay constituents such as calcite, gypsum, and other salts present in soils.

4.3 Molecular level modeling and simulations

Molecular level modeling and simulations performed in this study are divided into various steps. The results of each of these steps are discussed individually followed by the consolidated conclusions. As explained in the previous chapter, molecular level modeling techniques such as molecular mechanics (MM), molecular dynamics (MD), and Monte Carlo (MC) simulations have been used to study the processes and interactions occurring at the molecular level in the natural and compacted fabrics of the expansive clayey soils. These simulation techniques were used to study the interactions between clay and non-clay particles with various combinations of CEC, interlayer and intra layer cations, anions, and water under various fabric and structure conditions. Basic clay mineral was represented by a montmorillonite crystallite of 54 x 26 x 20 Å size.

In Section 3.5.10, cohesive energy density (CED) concept has been used to explain various molecular level processes and interactions occurring at different levels of the volume change in expansive clayey soils. CED has been found sensitive to all the possible changes in the clay structure due to variation in CEC, interlayer and intra layer cations, anions, water, and density conditions. Total CED of any combination of molecules is contributed from two components, i.e., electrostatic and van der Waals forces. Contribution from van der Waals could either be repulsion or attraction in nature, while it is always attraction in nature from electrostatic forces. The results of each step are discussed and interpreted in the light of the CED concept.

4.3.1 Water sorption and swell simulation – single montmorillonite crystallite

The simulation of the sorption of water molecules onto a single crystallite of montmorillonite was carried out using Sorption module of the software. Each sorption phase consisted of 25,000 steps of Monte Carlo simulation followed by molecular mechanics and dynamics using Forcite module to achieve a stable configuration of the sorbed water molecules, cations, and the crystallite layers. It is evident from first sorption phase shown in Figure 4-4 that water molecules start occupying the locations next to Na^+ cations present in the interlayer. This phenomenon reveals that water molecules start hydrating the interlayer cations in the first instance. Completely hydrated Na^+ are shown in Figure 4-5. It was observed in the subsequent phases that water molecules start making bonds with the edges, ends, and interlayer to satisfy the crystalline swelling. It is important to observe that not all the water molecules occupy the interlayer, rather these equally get sorbed on the edges and ends of the crystallite. For instance, when the total sorbed water content on a single crystallite reaches 20 %, lattice expansion (d-spacing) in Figures 3-7 and 3-8 reveals only 10 % water to be present in the interlayer. Similarly, this lag continues for the rest of the higher moisture contents and the water molecules sorption continues equally on the edges and the interlayer. This fact visualized in the molecular simulations have also been confirmed through the variation in lattice d-spacing with moisture content in XRD results shown in Figure 3-8. Comparison between the lattice expansion in the modeling and the experimental values from XRD are showing an excellent agreement. This phenomenon leads to an important conclusion that clay mineral particles might exist in the form of bigger size crystallites of an order of 1000+ Å in the dry form, but start

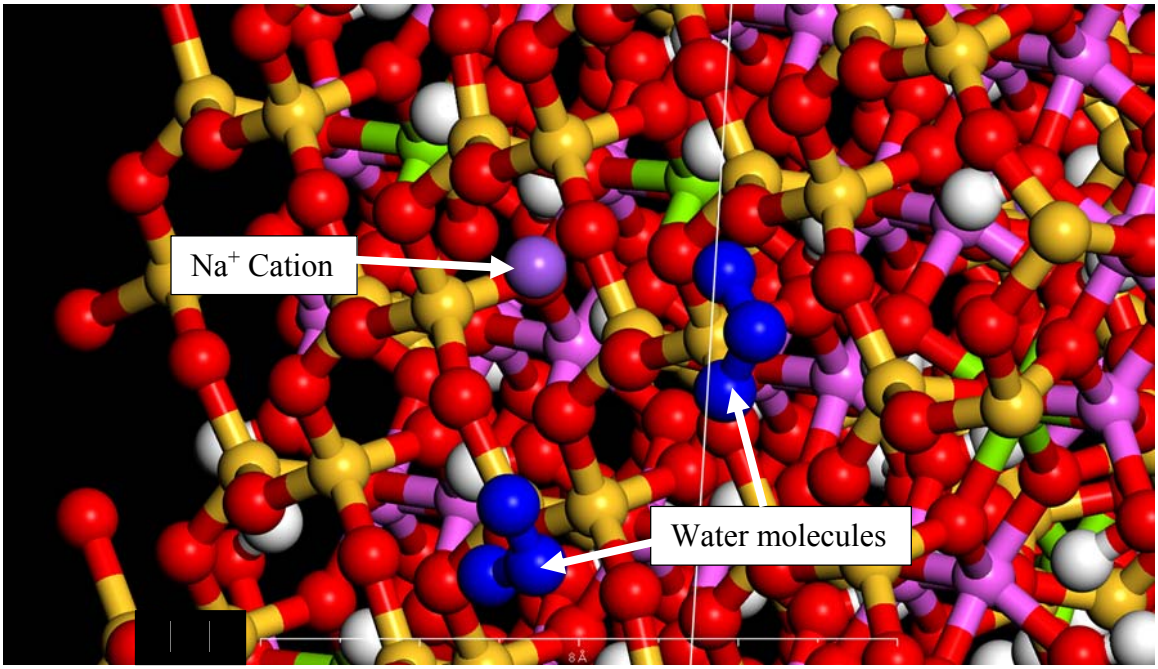

(a)

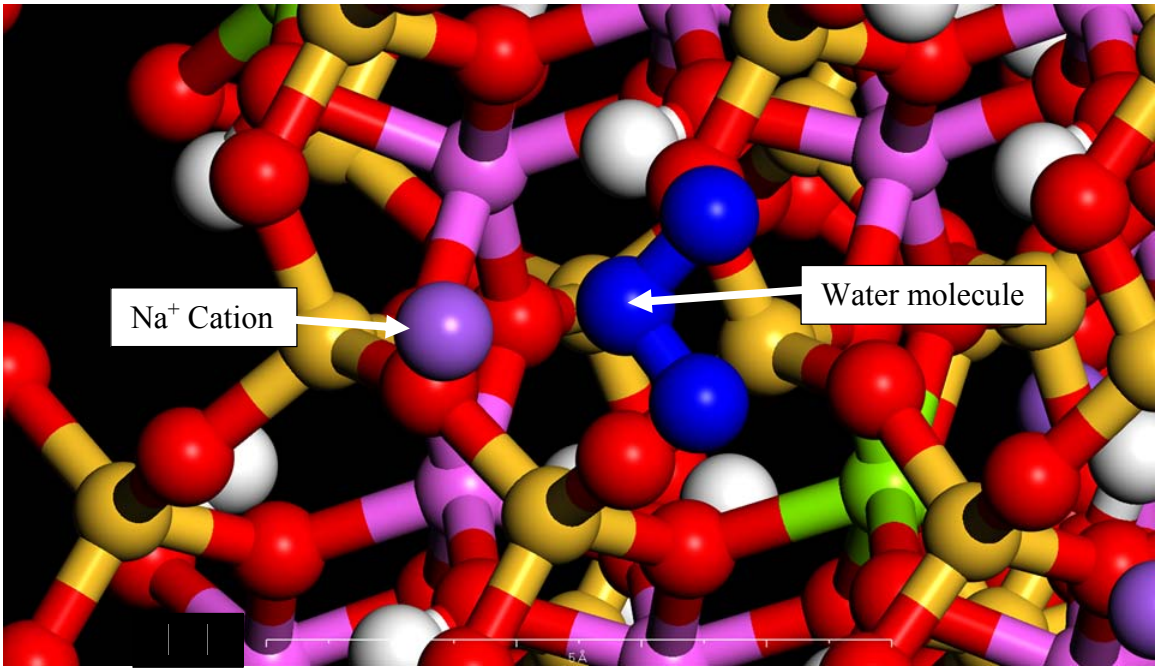

(b)

Figure 4-4 Initial stage of sorption of water molecules onto montmorillonite crystallite (a) Na^+ cation surrounded by two water molecules, (b) a closer view of Na^+ cation with sorbed water molecule.

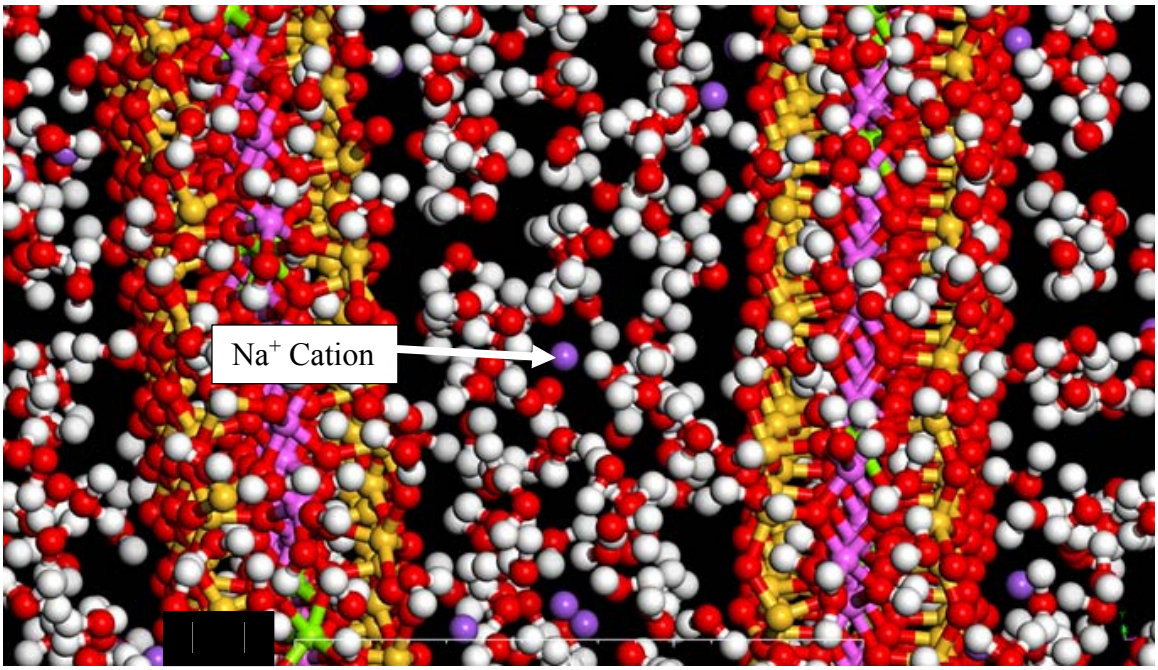

(a)

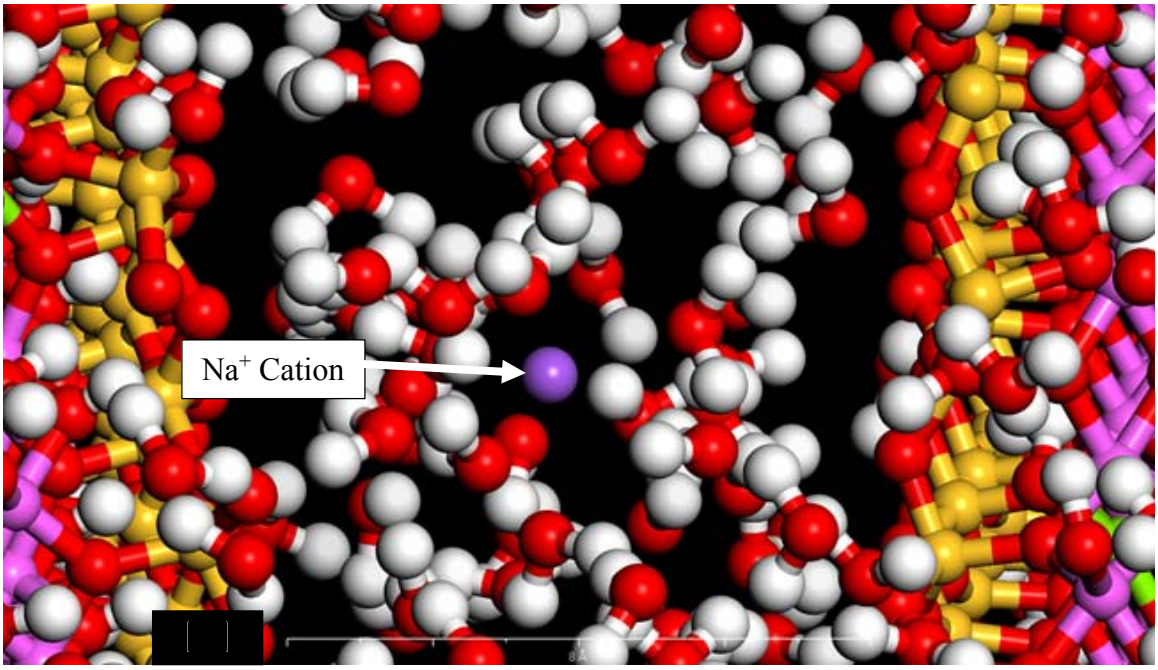

(b)

Figure 4-5 Completely hydrated Na^+ cations (a) general view showing all the cations in the interlayer, (b) close up view of a single hydrated Na^+ cation.

breaking up into much smaller crystallites once come in contact with water. During the compaction phase, these smaller crystallites join at the edges and ends to become larger particles with the water present in between the joined parts. Fabric created after the compaction process is discussed in Section 4.3.5.

Based on the previous discussions, the parameters selected in the Sorption and Forcite modules including the modified Universal forcefield are confirmed. A comparison of the swelling results from the original and the modified Universal forcefields is shown in Figure 3-21. The comparative plots clearly indicate the disability of the original Universal forcefield to predict the real swell behavior of single montmorillonite crystallite. Moreover, concept of using 25,000 steps as threshold for the water molecules sorption and other parameters in Sorption Monte Carlo simulation have also proven to be accurate. To further confirm and verify the parameters and the procedure, same process of water sorption was adopted for the pyrophyllite crystallite. The procedure and parameters further confirms as no water molecule could be sorbed in pyrophyllite crystallite of the same size (54 x 26 x 20 Å) during the 25,000 steps of Monte Carlo simulation.

General trend and the quantitative change in lattice d-spacing is very similar for all the CECs in Figure 3-8, but anomalously, LCEC has shown a slightly higher expansion than HCEC and MCEC especially at lower water contents. Difference is small; however, this anomalous behavior most probably owes to the availability of more space in the interlayer of LCEC due to lesser number of interlayer cations. This allows more water molecules to wedge in the interlayer and consequently causing a little higher expansion in the initial stages of water intake. On the other hand, amount of water molecules intake in the interlayer of HCEC in the initial stages is offset by more water intake required for the

hydration of the more number of cations. This results in almost the same lattice expansion at higher water contents. Another important conclusion drawn from this study is that lattice expansion becomes constant to maximum of three layers of interlayer water (17.5 Å) after a certain total water content (60 % in case of this study). Any further increase in water content takes place at the edges and ends of the crystallites. This phenomenon may be theorized by assuming that the swelling or hydration forces at this water content becomes smaller enough to cause the movement of the particles against the friction existing in the soil mix.

For the molecules where cations / anions from other compounds such as calcite, gypsum, and KCl were sorbed show a general trend of sorption both in the interlayer and on the surfaces. Cations of relatively small sizes such as Ca^{+2} enters the interlayer while bigger anions such as SO_4 , Cl, and CO_3 remain enveloping the surface (Figure 4-6).

4.3.2 Sorption of non-clay molecules – single Na-montmorillonite crystallite

To simulate the effects of presence of the generally available non-swell particles in the expansive soils, calcite, gypsum, and potassium chloride molecules were formulated. These molecules were then sorbed onto the montmorillonite crystallite at different water contents. The montmorillonite crystallite with previously sorbed water molecules was further sorbed with equal number of cations and anions from these minerals as shown in Figure 4-6. From the Figure 4-6 that Ca^{+2} cations got sorbed to some extent in the interlayer while rest of Ca^{+2} cations and the anions got sorbed around the crystallite surface. This

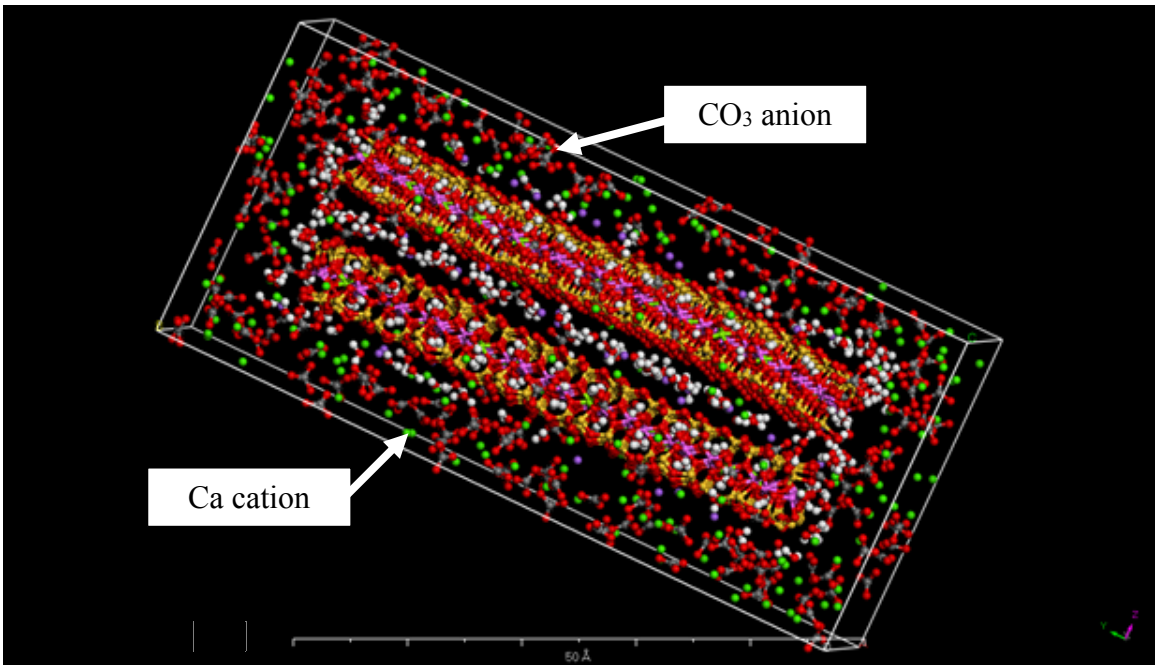

(a)

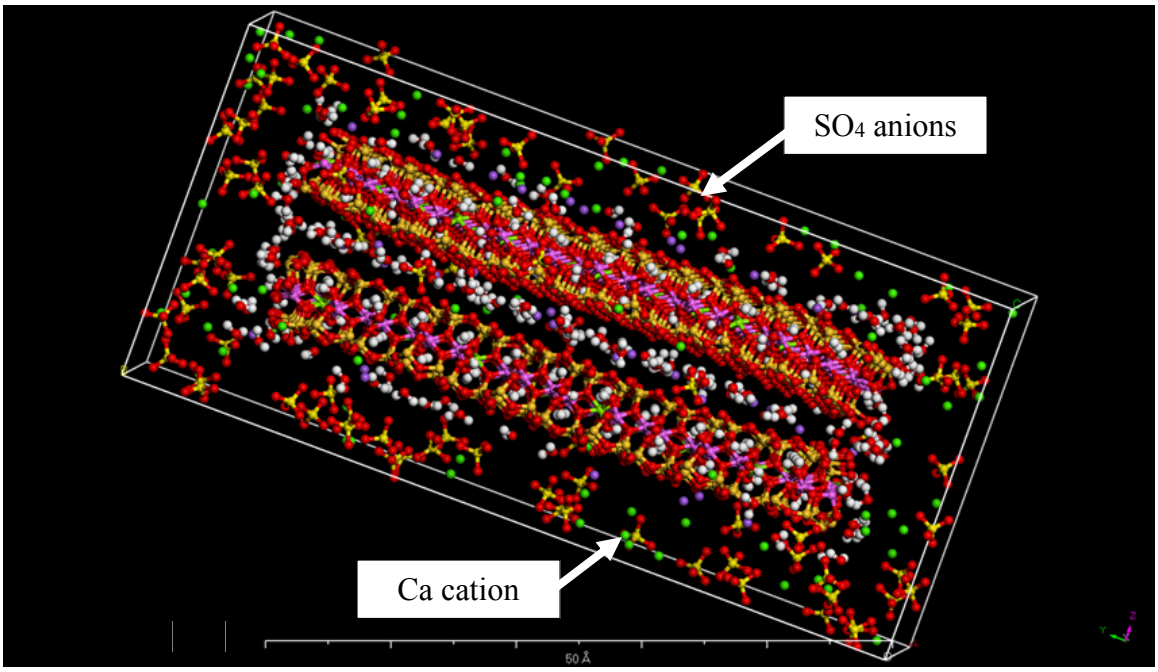

(b)

Figure 4-6 Interaction of montmorillonite with other compounds (a) calcite, (b) gypsum.

scenario could be considered as closely representative of the generally imagined cementation effects produced by these particles in any soil mix. These non-swelling minerals sorbed crystallites were further used to create the compacted mass followed by the water sorption and the subsequent swelling simulation.

4.3.3 Sorption of water molecules – exchangeable cations variations

It is rare in nature to find montmorillonite with Na^+ as the sole exchangeable cation, rather a combination of Na^+, K^+, Ca^{+2}, and Mg^{+2} exist naturally with at least one of these as the predominant exchangeable cation. Basic montmorillonite crystallite was transformed into various combinations of exchangeable cations as per Table 3-9. Sorption of water molecules was performed on these combinations in a similar way as was done for Na-montmorillonite (Figure 4-7). It was observed that general behavior of water molecules sorption was same for these crystallites with multiple exchangeable cations. However, some angular shift of the crystallite in space was observed in case of multiple cations. This phenomenon most probably owes to the presence of exchangeable cations of different charges, sizes, and hydration radii and positioned at random locations in the interlayer. These cations while getting hydrated might generate different level of forces in the crystallite interlayer space and consequently causing an angular shift in the crystallite position in space.

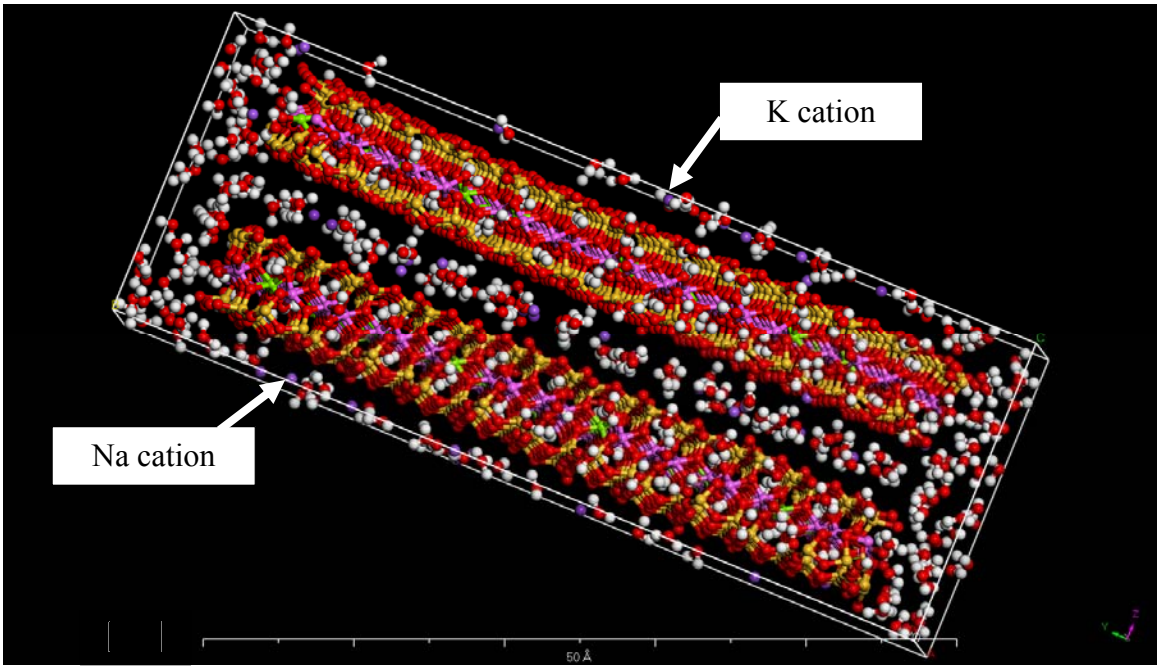

(a)

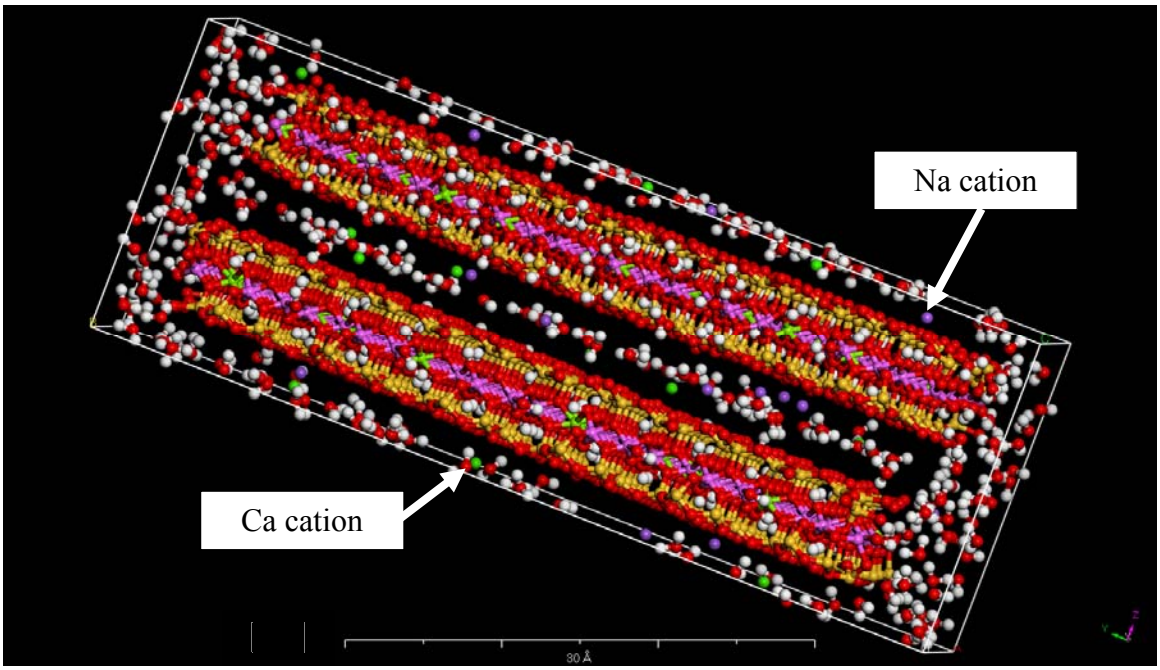

(b)

Figure 4-7 Water molecules sorption (10 %) to montmorillonite with (a) 40%Na+60%K, (b) 40%Na+60%Ca.

4.3.4 Simulation of formation of loose mix of clay particles

Sorption module was used to simulate the assemblages of water sorbed crystallites when mixed together in the loose form before the compaction process. For the purpose, four crystallites were randomly sorbed in a 125 x 125 x 125 Å cubic unit cell (Figure 3-9). Several cubic unit cells sizes ranging from 100 Å to 200 Å were experimented and 125 Å was finally selected. Bigger unit cells resulted in distances larger than the crystallite themselves and smaller ones caused overlapping of the crystallites. Based on the randomness analogy and the parameters used in the Monte Carlo simulation in Sorption module for the single crystallite, these four crystallites occupy relative positions in the cubic space (Figure 3-9). The relative positions are taken up by the crystallites either parallel to faces, edge to edge, edge to the face, or an intermediate form depending on the charge distribution on each crystallite and the moisture content. Typical fabric formation in loose mix form are shown in Figure 4-8. It could be noted that crystallite arrangement at lower water contents are more random and generally follows the face to edge / end configuration, while it becomes more oriented and adopts parallel configuration at higher water contents.

In this study, CED have been considered as a good indicator of the interaction of the soil structure to the water sorption and the consequent volume change. Simulated loose mixes of the soil was determined through the Forcite module of the software and plotted in the corresponding graphs in Figures 4-9 to 4-14. Total CED of the loose mixes varies from $1x10^8$ to $8x10^8$ J/m^3. A general trend observed is that low CEC crystallites produce lesser

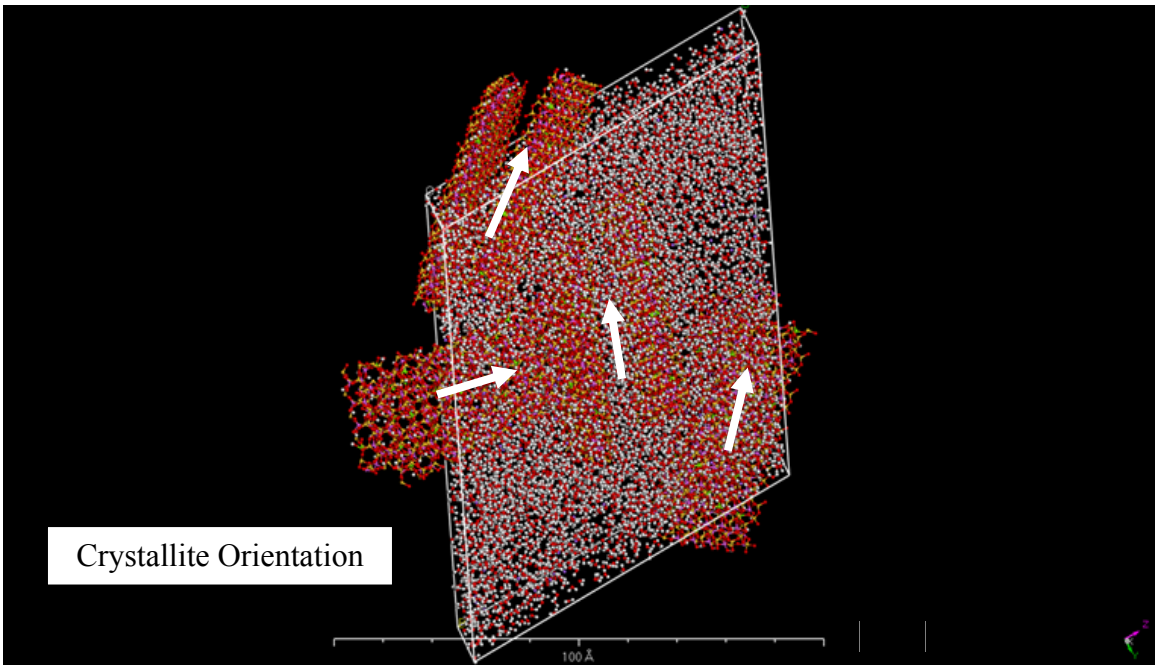

(a)

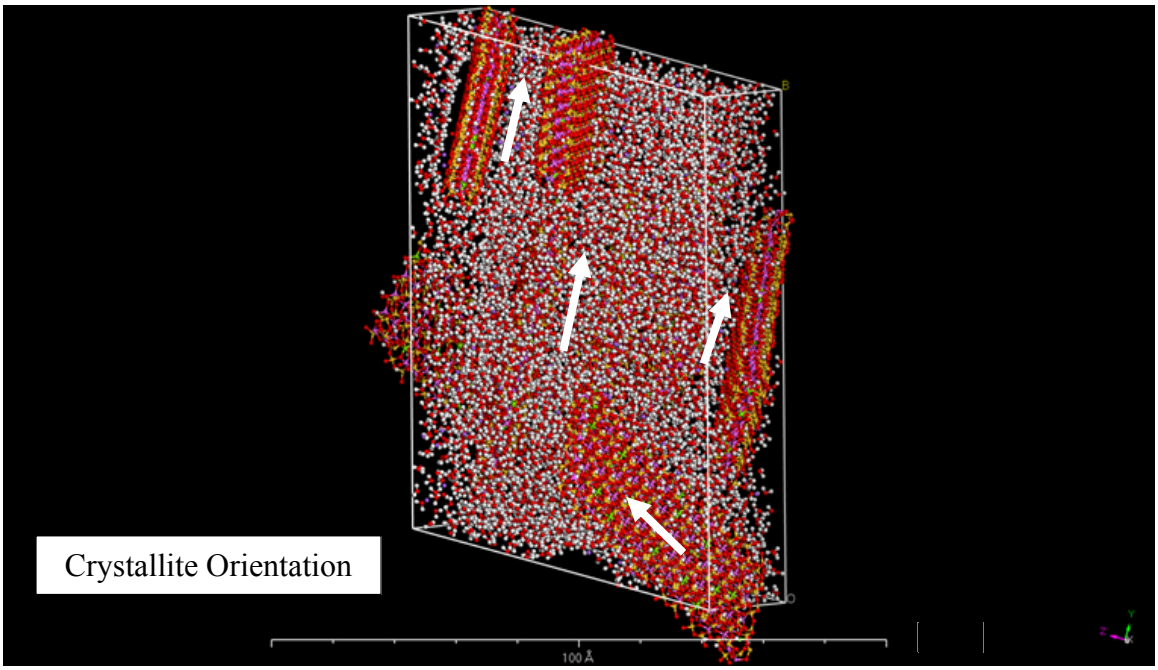

(b)

Figure 4-8 Typical fabric of Na-montmorillonite after compaction at (a) 30 % water content, (b) 40 % water content.

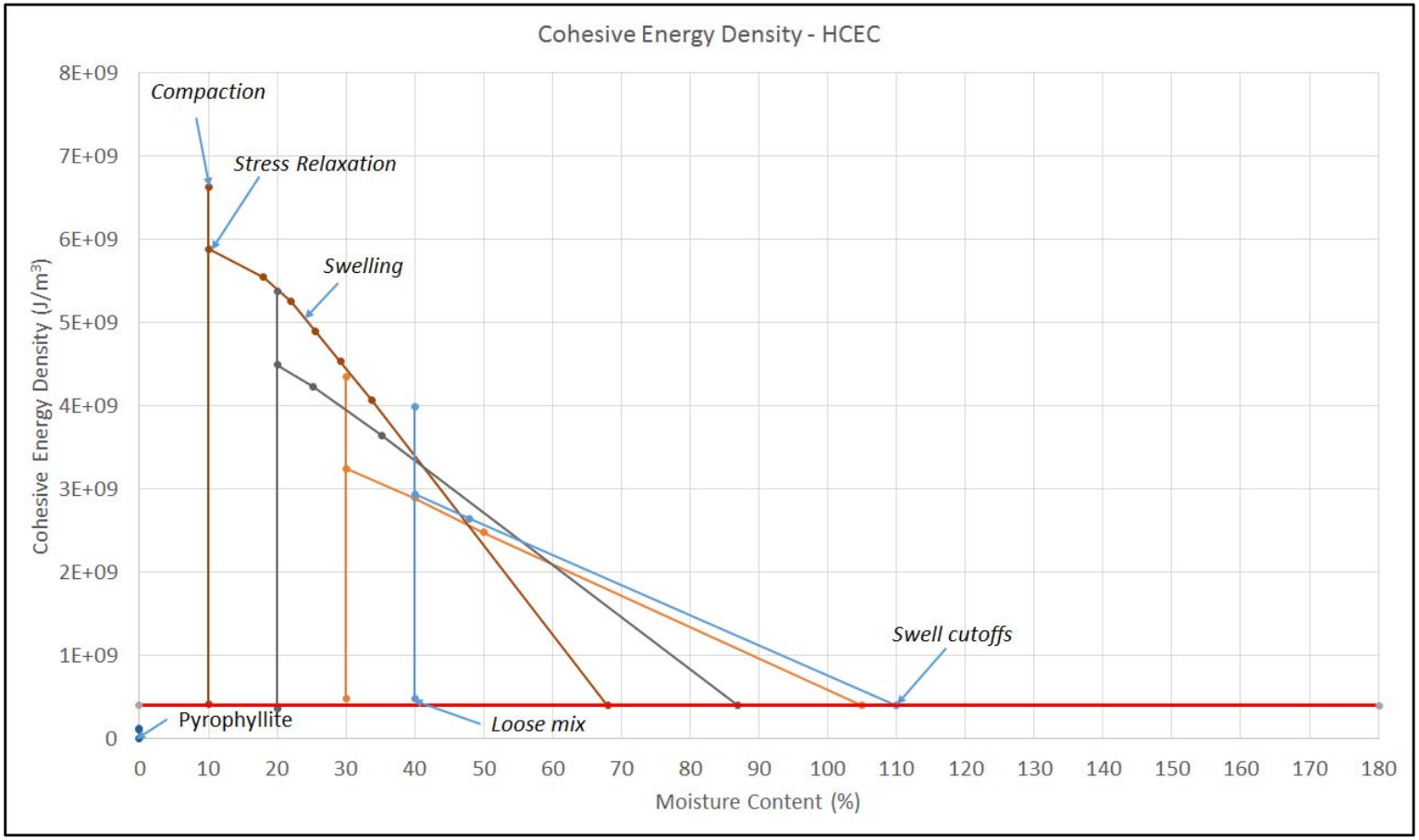

Figure 4-9 Cohesive energy density plots for crystallites for all stages of simulations (loose, compacted, relaxed, and swelling) for HCEC.

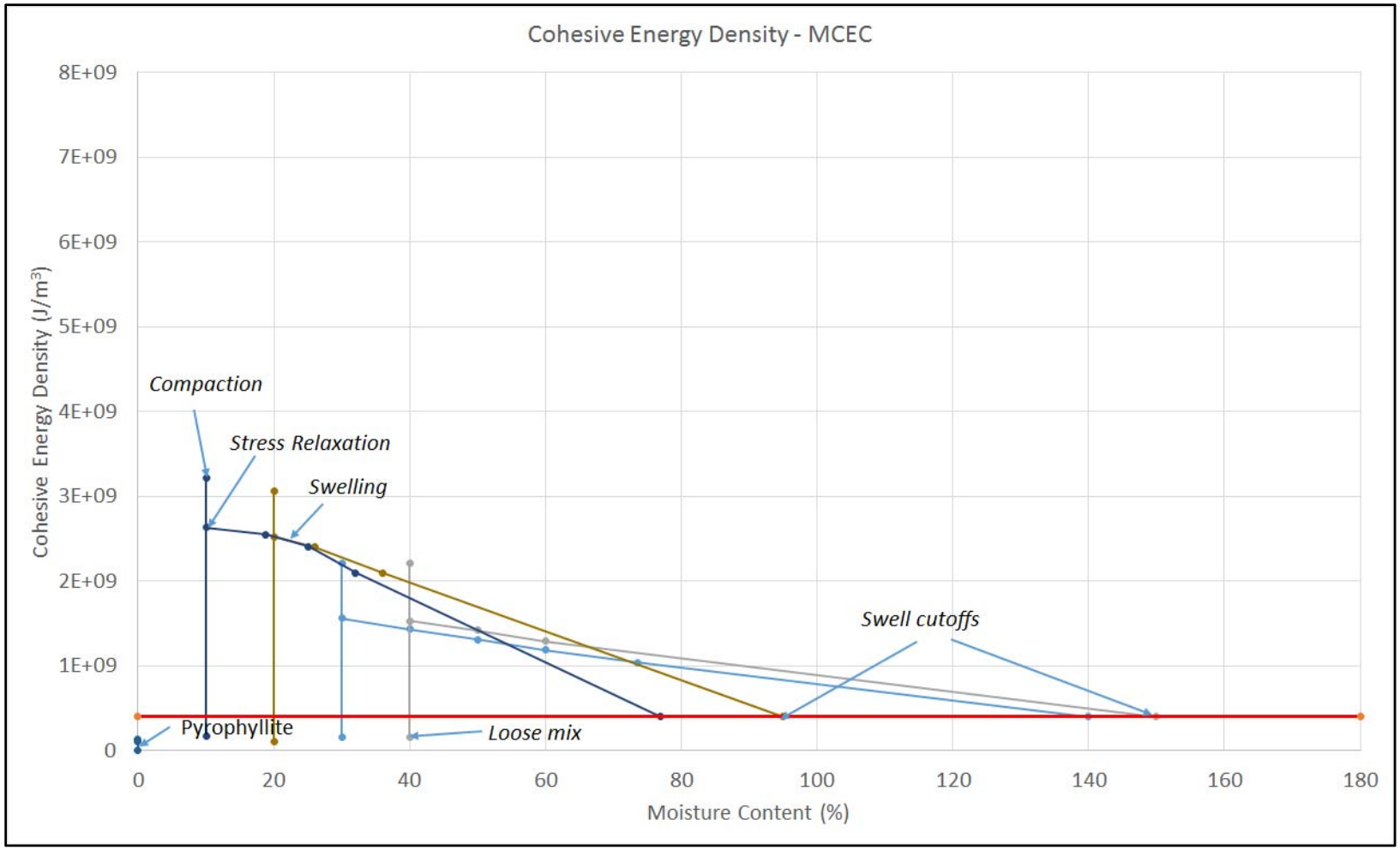

Figure 4-10 Cohesive energy density plots for crystallites for all stages of simulations (loose, compacted, relaxed, and swelling) for MCEC.

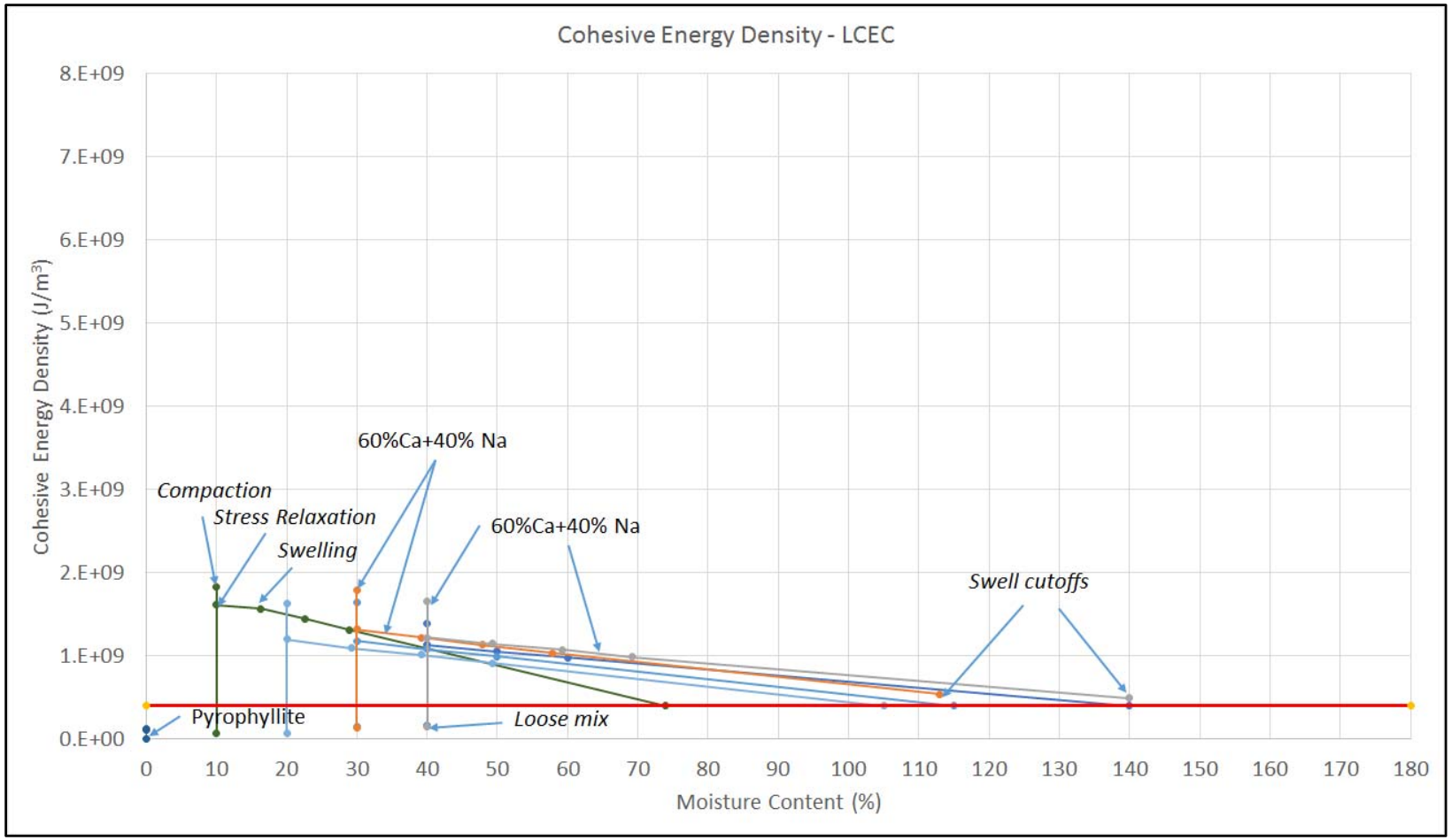

Figure 4-11 Cohesive energy density plots for crystallites for all stages of simulations (loose, compacted, relaxed, and swelling) for LCEC.

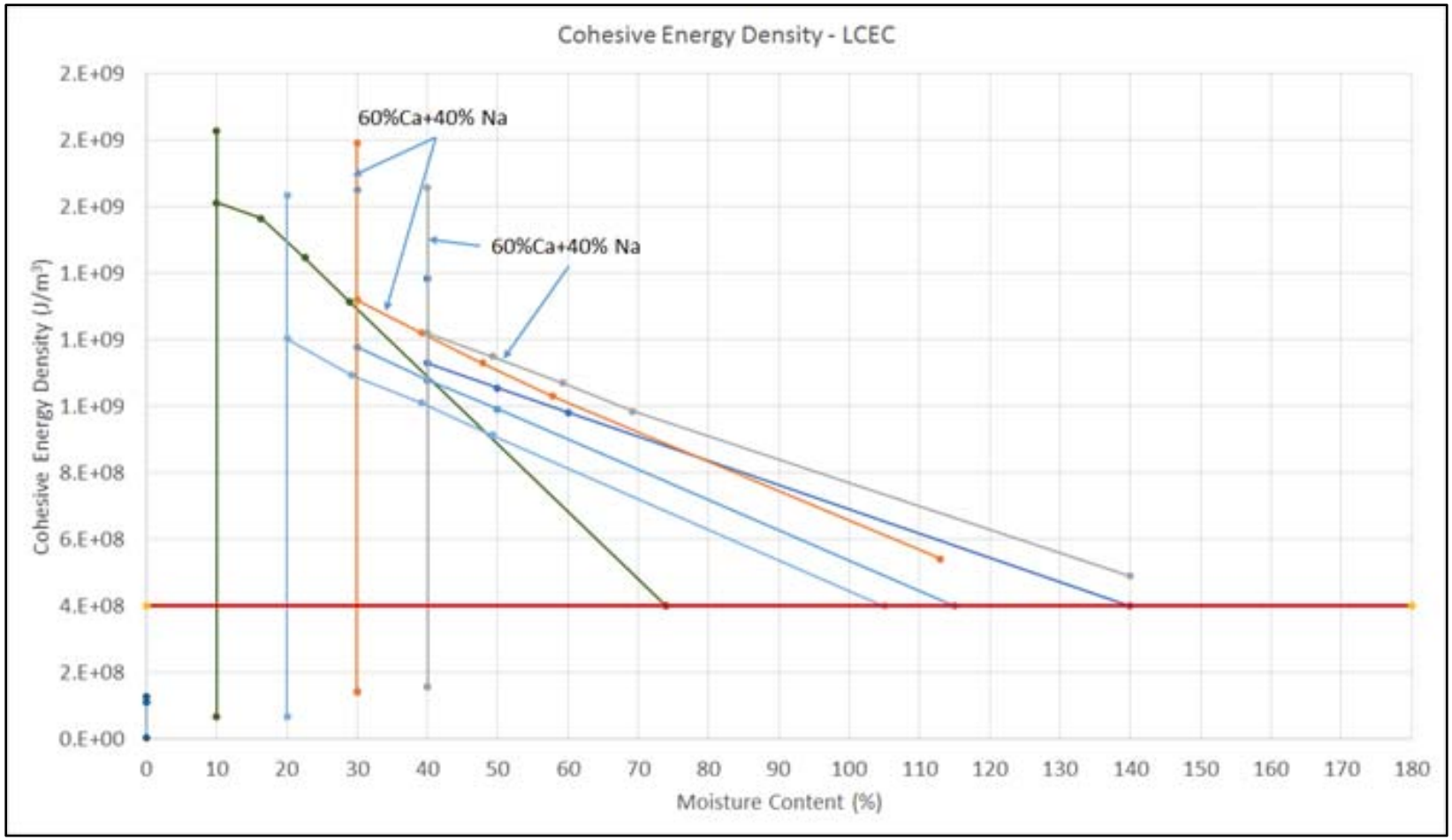

Figure 4-12 Cohesive energy density plots for crystallites for all stages of simulations (loose, compacted, relaxed, and swelling) for LCEC (same as Figure 4-11 with y scale).

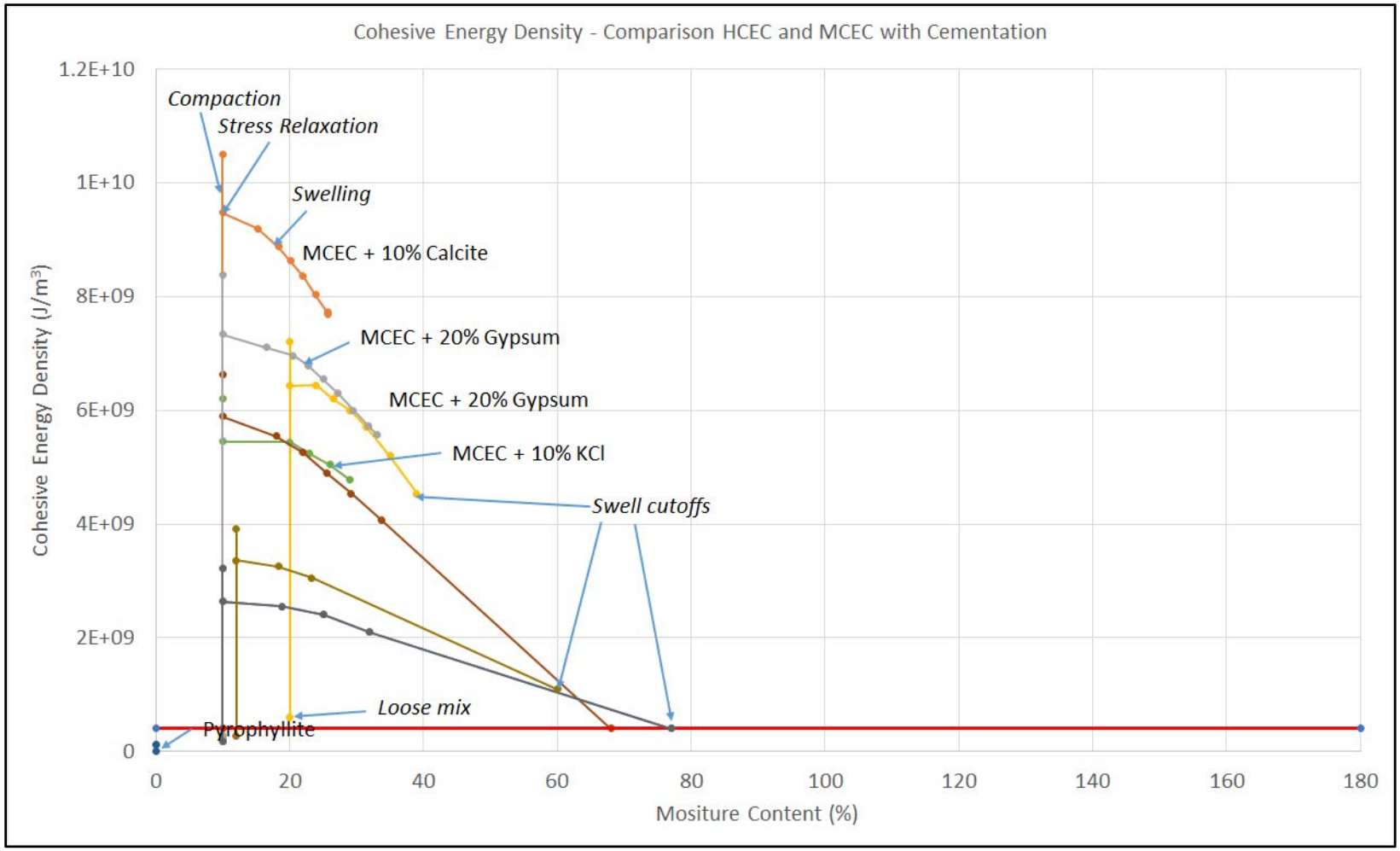

Figure 4-13 Cohesive energy density plots for crystallites for all stages of simulations (loose, compacted, relaxed, and swelling) for changes in cementation compounds.

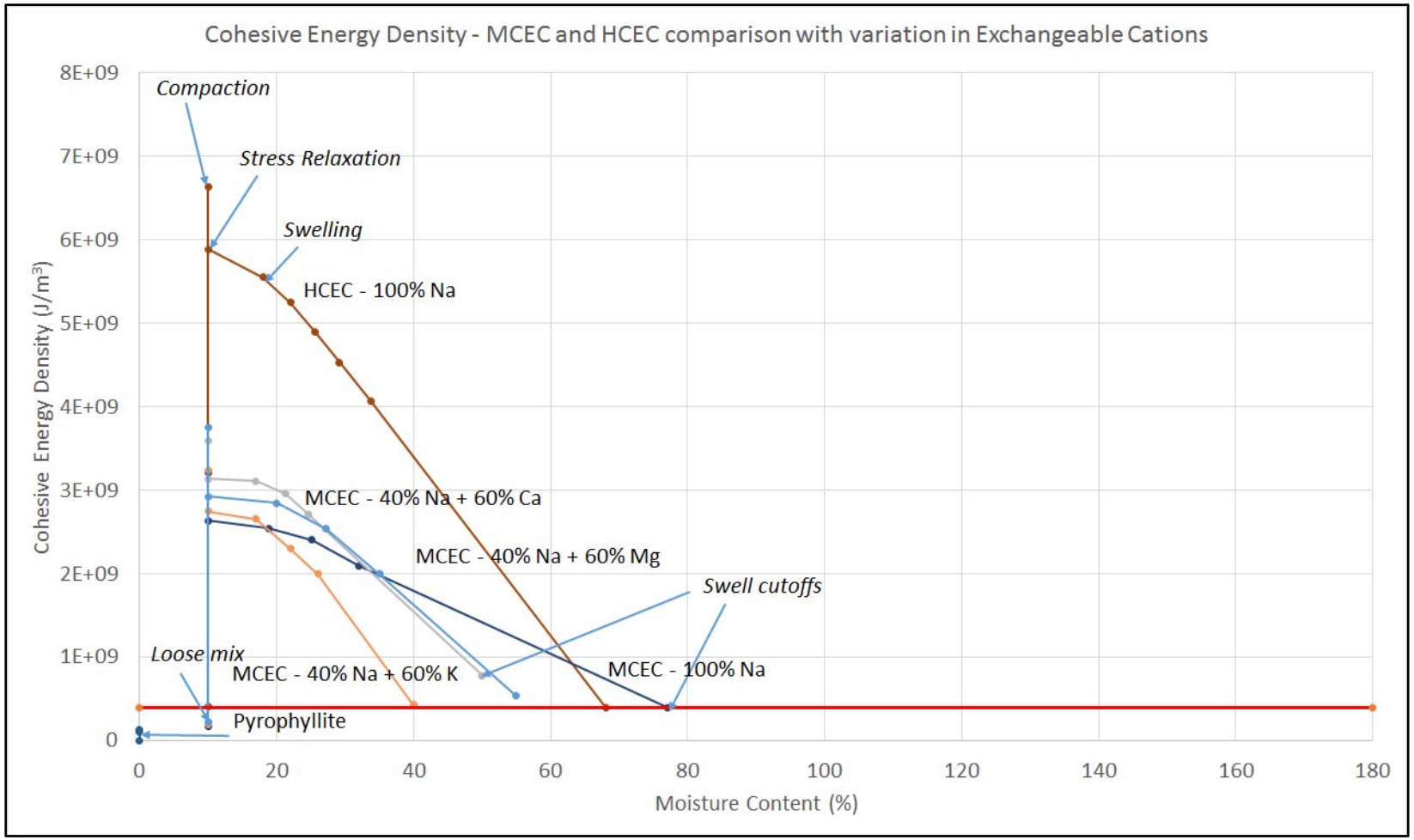

Figure 4-14 Cohesive energy density plots for crystallites for all stages of simulations (loose, compacted, relaxed, and swelling) for changes in exchangeable cations.

cohesive energy while higher CEC and the crystallites sorbed with other compounds showed higher numbers.

4.3.5 Simulation of the compaction of clay particles

To simulate the fabric and structure in the compacted specimens, unit cells consisting of the loose clay crystallites created in the previous step were compressed to the required density using Forcite molecular dynamics module. There are several barostats provided in the software for the control of applied pressure on the unit cell; Berendsen and Parrinello are two that could be considered suitable for the compaction simulation of naturally or manually compacted soil samples. In the compaction simulation, Berendsen thermostat was used as in the simulation of single crystallite, while barostat was replaced by Parrinello. As Berendsen barostat applies pressure in all the directions in a way to keep the unit cell dimensions equal, the corresponding reduction of volume on all the faces of the periodic boundary cell remains uniform. Therefore Berendsen barostat does not simulate the real compaction process in which stresses vary along the faces under a uniform compaction pressure process. A comparison of the compressed / compacted unit cells using Berendsen and Parrinello is shown in Figure 4-15. On the other hand, using Parrinello barostat has resulted in more realistic way of compaction by varying the stresses on the faces depending on the shear stresses generated in the unit cell. The resulting fabric is also more random and face to edge fabric on lower moisture content while more oriented and parallel fabric is created on higher moisture contents. The variation in relative positioning or configurations of the crystallites with water content is a well-established fact

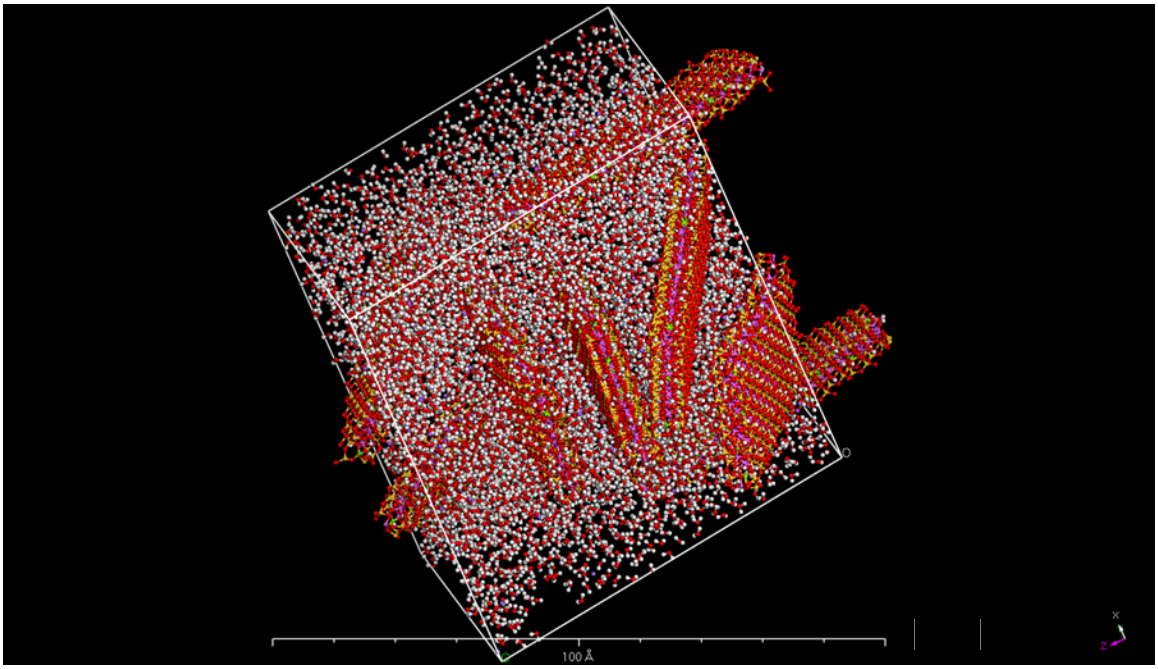

(a)

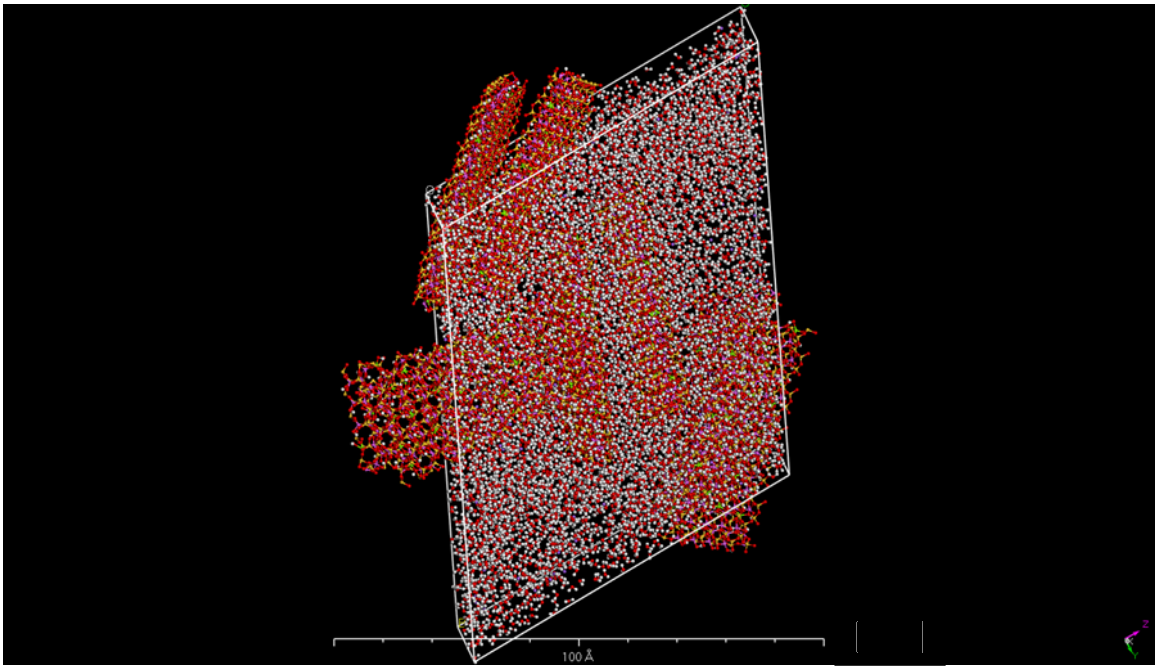

(b)

Figure 4-15 Comparison of the compacted fabric created for Na-montmorillonite at 30 % water content using (a) Berendsen barostat, (b) Parrinello barostat.

in compacted clays. Figure 3-11 provides a 3-D view of the repetition of the unit cell in three dimensions in space. The repetition of unit cell provides the continuity of the crystallites to form soil particles. Since formulation of compacted crystallites / particles resemble the actual fabrics schematically visualized, it further confirms the selected parameters and procedures for the formulation and simulation of compacted fabric of soil particles.

Different confining or compaction pressures were used to simulate the several levels of geological and laboratory compaction pressures. Different pressures have resulted in different maximum densities of the unit cells (Figure 3-10). It is evident from Figure 3-10, high pressures of an order of 1 GPa causes quick compaction and may be closely representative of dynamic and static quick type of compaction using the laboratory and field equipment. On the other hand, low confining pressures of an order of 0.01 to 0.1 GPa result in slow compaction and hence may be simulating more closely slow compaction / consolidation pressures for the geological deposits. It could be noted from the plots that densities are also closely representative of the general range of field and laboratory densities.

Both total and van der Waals CED for each of the case were determined using Forcite module. Total cohesive energy density is plotted in the respective plots (Figures 4-9 to 4-14), while both total and van der Waals cohesive energy density are tabulated in Table 4-1. From the plots, it could be inferred that total CED for any compacted mix is sensitive to all the parameters being considered such as water content, density, CEC, cementation, and type and percentages of exchangeable and total cations.

From Table 4-1 and Figures 4-9 to 4-15, total CED has been found to be increasing with increase in CEC, density, cementation, and bivalent cations and decreasing with water content, while van der Waals cohesive energy density reduces and becomes repulsion in nature with the same variation of the above parameters.

For the same CEC, lesser water content results in higher cohesive energy, but for same density / moisture, higher CEC crystallites achieve much higher cohesive energy. As cohesion in clay particles are a result of the hydrogen bonding between their surfaces and the water, more number of charge deficiency centers in higher CEC clay results in more number of hydrogen bonds and consequently raising the electrostatic attraction cohesive energy density. However, van der Waals repulsions increase due to the high vicinity of the crystallites. Therefore, higher total CED mixes have corresponding higher repulsion van der Waals. These additional repulsion forces play an important role in the expansion / swell behavior of the clay particles in addition to the hydration by water molecules. Similarly, interaction with gypsum and calcite also causes an increase in cohesive energy density due to the extra bonding created by the cations and anions. Although there is an increase in repulsion due to van der Waals forces, but increase in attraction forces due to electrostatic component has much higher value and far outweighs the repulsion forces in these cases.

4.3.6 Simulation of stress relaxation / overburden relief

As natural expansive clay deposits usually form at deeper depths under consolidation pressures from the overlying geological formations. These clay layers exposed closer to the ground surface due to removal of overlying layers. As a result of this stress relief, these

layers become overconsolidated in nature. Moreover, fabric and structure of these clay deposits also change as a result of the stress relief and several other features such as fissures and voids develop in the structure of these overconsolidated layers. To simulate the process of overconsolidation, compressed / compacted unit cells at higher pressures were dynamically run in the Forcite module using Parrinello barostat under a stress level of 1000 kPa. The pressure of 1000 kPa is very close representation of the generally measured preconsolidation pressures of such deposits in the shallow subsurface. It is also representative of the compaction pressures of 1500 kPa used for the preparation of laboratory samples. As a result of stress relief simulation, the unit cells achieved a lesser density due to more void space and the corresponding change in lattice spacing of the crystallite layers. Figures 4-16 show typical unit cells before and after the stress relief simulation. Comparing the fabric before and after the stress relief shows not only an increase in pore space but also an increase in the d-spacing of the crystallites. CED results in Figures 4-9 to 4-15 and Table 4-1 show a drop in cohesive energy as the structure relaxed. There is also a decrease in the repulsion forces due to van der Waals. This drop is indicative of the elastic recovery of the soil structure upon overburden stress relief.

4.3.7 Water sorption simulation – compacted and relaxed clay particles structure

Relaxed unit cell for each of the case under study was then sorbed with water molecules. A typical water sorption of water molecules in Na-montmorillonite crystallites compacted with 30 % water content is shown in Figure 4-17. Figure 4-17 shows that water molecules

Table 4-1 Summary of swell potential results for all the simulation cases

Case no	Case			Initial water content (%)	Maximum desnity		Relaxed density		Final water content (%)	Maximum density (g/cm^3)		Relaxed density (g/cm^3)		Terminal density (g/cm^3)		Swell (%)
					Total cohesive energy density (J/cm^3)	van der Waals cohesive energy density (J/cm^3)	Total cohesive energy density (J/cm^3)	van der Waals cohesive energy density (J/cm^3)		Wet	Dry	Wet	Dry	Wet	Dry	
1	HCEC	Na100	-	10	6636	-145	5890	-98	68	2.432	2.211	2.132	1.938	0.571	0.340	470
2				20	5379	-80	4500	-33	87	2.112	1.760	1.762	1.468	0.617	0.330	345
3				30	4360	-35	3250	2	105	1.831	1.408	1.382	1.063	0.656	0.320	232
4				40	3988	-11	2945	20	110	1.731	1.236	1.309	0.935	0.651	0.310	202
5	MCEC	Na100	-	10	3213	-102	2640	-62	77	2.359	2.145	1.903	1.730	0.602	0.340	409
6				20	2750	-50	2110	-18	95	2.226	1.855	1.600	1.333	0.663	0.340	292
7				30	2206	5	1615	28	140	1.683	1.295	1.260	0.969	0.792	0.330	194
8				40	2212	5	1530	39	150	1.686	1.204	1.204	0.860	0.800	0.320	169
9	LCEC	Na100	-	10	1828	-77	1612	-49	74	2.441	2.219	2.073	1.885	0.592	0.340	454
10				20	1634	-15	1333	-1	105	1.967	1.639	1.677	1.398	0.697	0.340	311
11				30	1650	-13	1180	45	115	2.000	1.538	1.444	1.111	0.710	0.330	237
12				40	1386	-10	1130	59	140	1.700	1.214	1.290	0.921	0.768	0.320	188
13	MCEC	Na100	G20	10	8385	-305	7336	-224	33	2.510	2.282	2.195	1.995	1.820	1.368	46
14	MCEC	Na100	C10	10	10507	-497	9476	-425	26	2.636	2.396	2.367	2.152	2.050	1.630	32
15	MCEC	Na100	G20	20	7200	-245	6437	-162	39	2.218	1.848	1.955	1.629	1.700	1.223	33
16	HCEC	Na100	G20	10	11808	-348	10586	-260	29	2.588	2.352	2.459	2.236	1.727	1.368	53
17	LCEC	Na100	G20	10	7000	-280	6308	-211	32	2.597	2.361	2.391	2.174	1.789	1.368	51
18	LCEC	Ca60Na40	G20	12	3909	-151	3363	-105	60	2.294	2.048	1.947	1.738	2.168	1.355	28
19	MCEC	Na100	KCl10	10	6210	-125	5450	-79	29	2.225	2.023	1.923	1.748	1.790	1.388	26
20	MCEC	Ca60Na40	-	10	3593	-118	3138	-87	50	2.422	2.202	2.075	1.886	0.915	0.610	209
21	MCEC	K60Na40	-	10	3246	-100	2748	-64	40	2.454	2.231	2.037	1.852	0.574	0.410	352
22	MCEC	Mg60Na40	-	10	3750	-164	2930	-121	55	2.408	2.189	1.815	1.650	0.791	0.510	224
23	HCEC	Ca60Na40	-	10	7016	-161	6388	-123	44	2.497	2.270	2.325	2.113	0.868	0.610	240
24	LCEC	Ca60Na40	-	30	1791	-31	1320	-4	113	1.969	1.515	1.480	1.138	0.843	0.396	187
25	LCEC	Ca60Na40	-	40	1658	-7	1207	18	138	1.798	1.284	1.343	0.959	0.935	0.393	144

Na: Sodium G: Gypsum
Ca: Calcium C: Calcite
K: Potassium KCl: Potassium Chloride
Mg: Magnesium

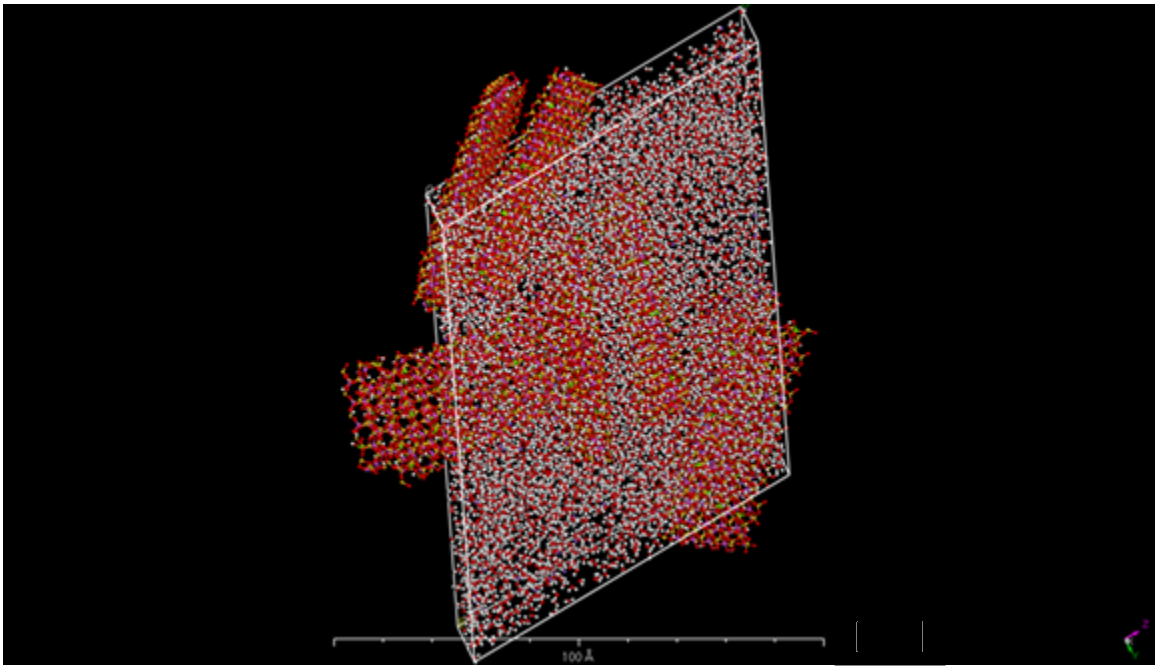

(a)

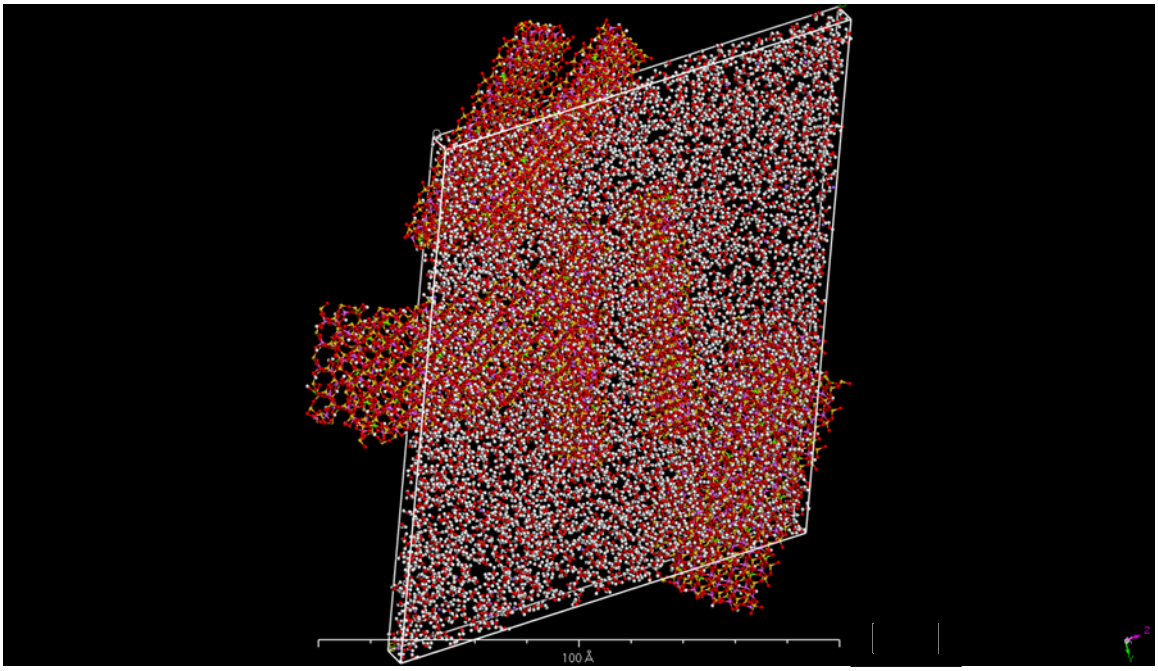

(b)

Figure 4-16 Comparison of fabrics a) before, and b) after the stress relief for Na-montmorillonite.

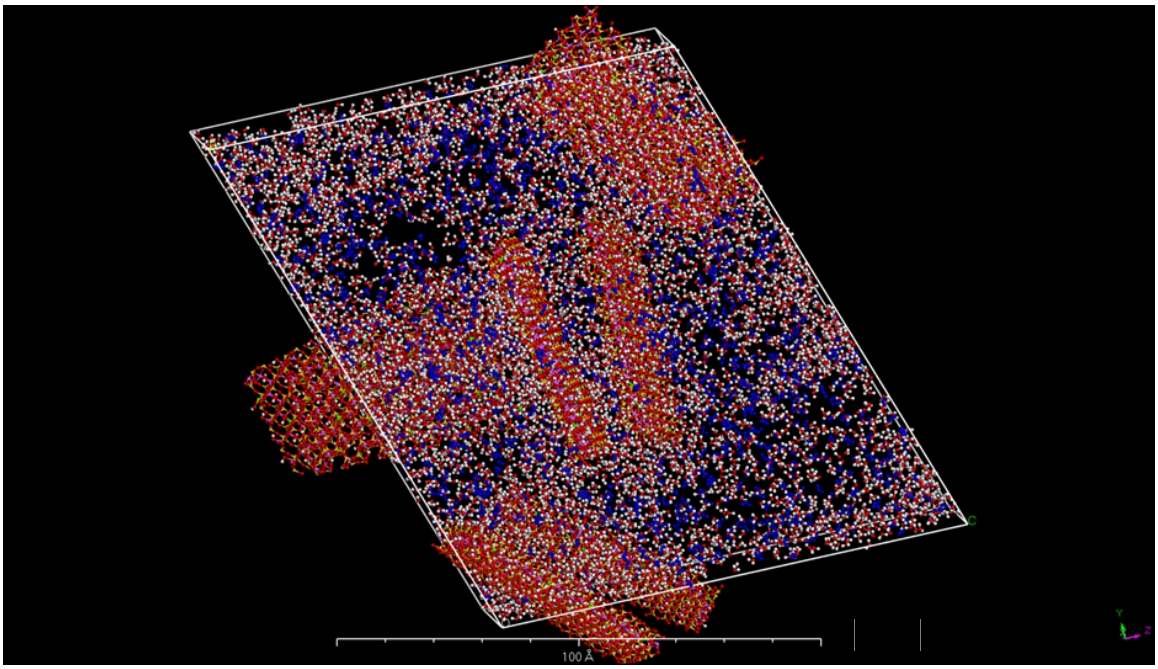

Figure 4-17 Typical water molecules sorption in Na-montmorillonite crystallites compacted at 30 % water content (blue colored water molecules indicate the sorption in the current sorption step).

have occupied both inter and intra crystallite space. For each step of Sorption, 25,000 steps were adopted to sorb the maximum number of water molecules. Depending on the initial water content, density, and other factors such as cementation and exchangeable cations, water sorption for a single step varied from as low as 2 % to maximum of 10 %. Very low water content is indicative of structure with very small pore space created either due to high density or cementation. Higher water content sorption on the other hand indicates an open pore space fabric and high interlayer deficiency. At the end of each sorption phase, the unit cell of crystallites were dynamically stabilized using Forcite module. Sorption steps were repeated in steps followed by stabilization through molecular dynamics till the swell cutoff was reached. Swell cutoffs have been defined based on the cohesive energy concept and are explained in the next Sections on swelling of water sorbed various forms of crystallites.

4.3.8 Swelling simulation – Na-montmorillonite

Each unit cell consisting of four crystallites and sorbed with the maximum number of water molecules in 25,000 steps in the Sorption module, was subjected to molecular dynamics using Forcite module. The dynamics module causes the movement of molecules to stable positions and result in a stable expanded structure under a pressure of 1000 kPa (Figure 4-18). It could be noted from Figure 4-18 that the volume change occurs both in the interlayer and intracrystallite space. The maximum expansion occurs in the intracrystallite space while the interlayer space continues to expand at slow pace till it reaches a maximum value of about 17.5 Å.

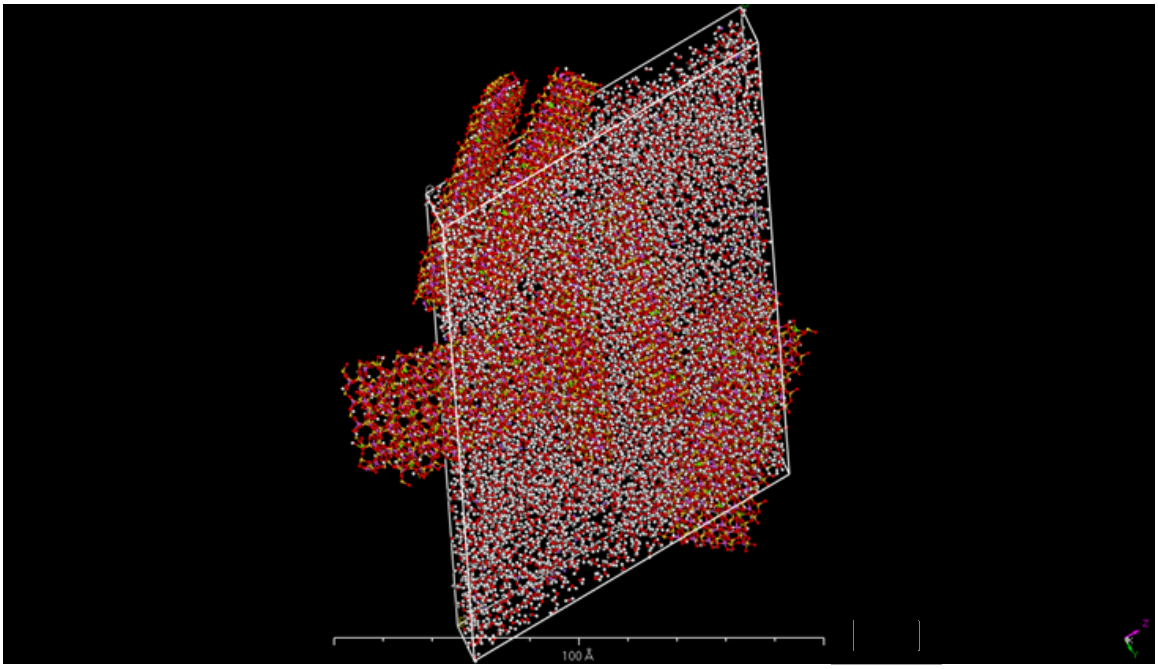

(a)

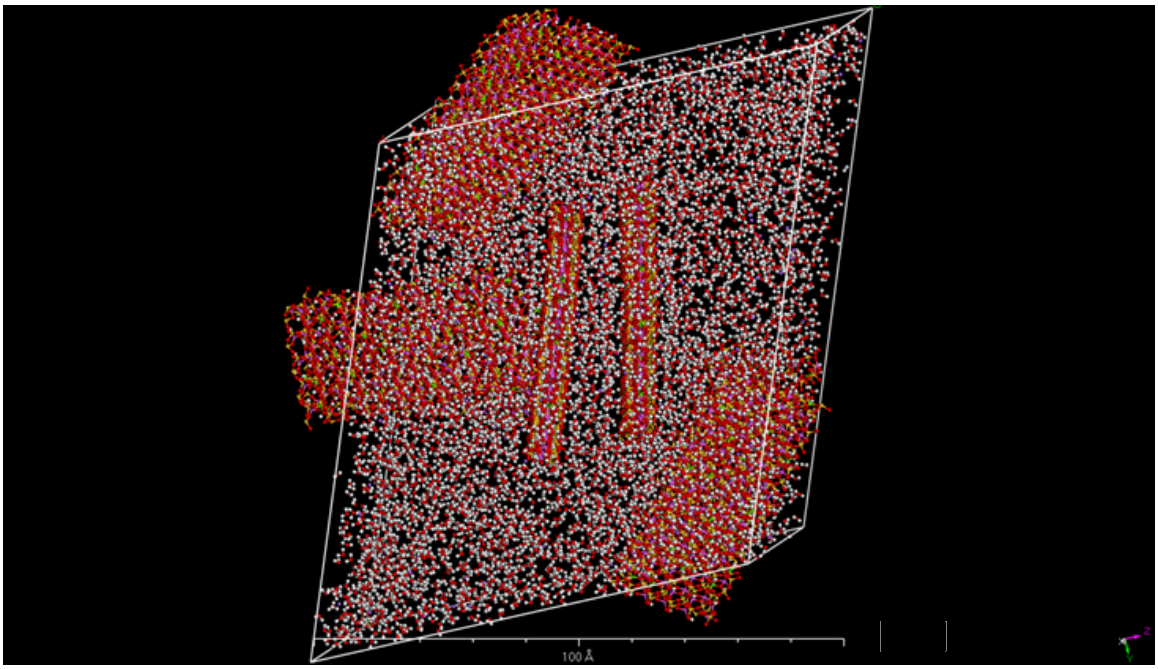

(b)

Figure 4-18 Swelling simulations of crystallites unit cell of Na-montmorillonite (a) pre swell fabric at 30 % water content, (b) post swell fabric at 40 % water content.

From cohesive energy density plots, it is noted that each swelling phase causes reduction in cohesive energy density at a uniform rate for each CEC of Na-montmorillonite except for HCEC at 10 % water content. All the cases, except those with cementation and exchangeable cations other than Na^+, a straight line plot between CED and water content is continued till it reaches a swell cutoff or terminal point. Swell cutoff points for all such cases were found to be terminating at a cohesive energy density of an order of 300 to 500 J/cm^3. By looking at the swell potential test results, terminal dry densities were found to be about 0.45 to 0.55 g/cm^3 for 100 % bentonite samples. In the dynamics simulation, this density range has been found equivalent to the cohesive energy density range of 300 to 400 J/cm^3. In the absence of any other factor causing an early termination of swelling process such as cementation and / or exchangeable cations other than Na^+, all the swell lines terminate at a cohesive energy density of 400 J/cm^3. The termination points also indicate the terminal or post swell moisture content. For the other cases, terminal or swell cutoffs are discussed in the next respective sections.

It could be observed from the Figures 4-9 to 4-14 that terminal moisture content for high swell cases for each CEC is lesser than their low swell counterparts. For instance, swell line for 30 % initial water content LCEC terminates at 113 % while the one for 40 % initial water content LCEC falls at 138 %. A similar observation was also made during the swell potential tests (Table 3-6); terminal moisture content for initial moisture contents of 30 % and 40 % are 136 % and 174 % respectively. This anomalous phenomenon can be explained using the contribution of van der Waals to the cohesive energy density (Figure 4-19). For these cases, in addition to the expansion caused by water molecules, the

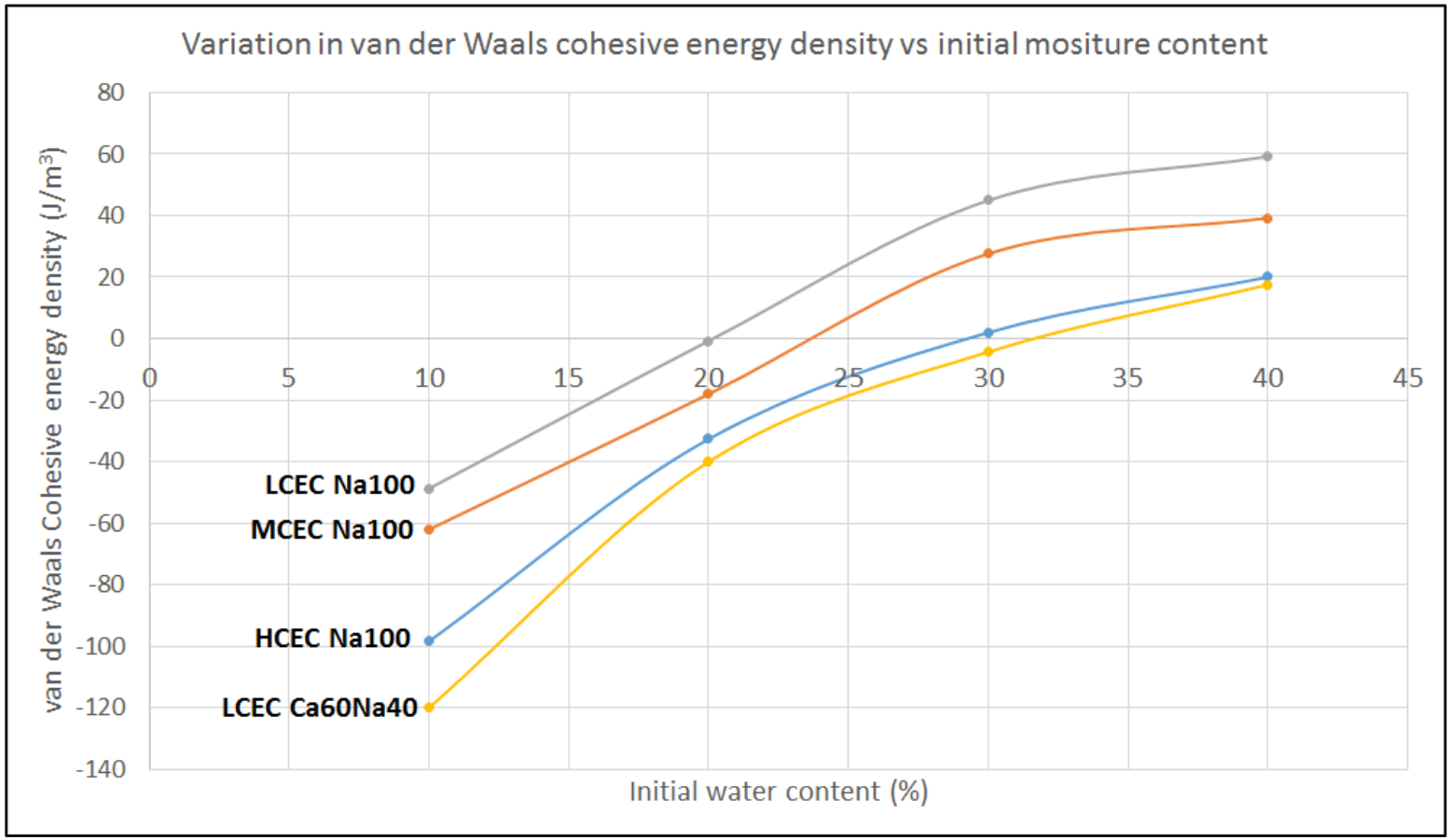

Figure 4-19 Variation of van der Waals cohesive energy density with initial water content.

the repulsion force due to van der Waals result in pushing the particles apart. Since these forces are higher in case of highly compacted specimens or lesser moisture contents, relatively higher swelling takes place at lower water content for such cases. The resulting swell potential determined from the swell simulations for all the cases under study are summarized in Table 4-1.

4.3.9 Swelling simulation – cementation effects

The most common types of cementation produced in natural soil deposits are by calcite, gypsum, and potassium chloride. From Figures 4-9 to 4-14, it can be observed that there is a substantial increase in the cohesive energy density of an order of 20 to 300 %. The CED contribution from van der Waals is repulsion in nature and is also higher than their counterparts. For all these cases, unlike Na-montmorillonite, the plot between CED and moisture content is not a straight line. The plot has an initial straight portion followed by a curvature and a straight line to the terminal or swell cutoff. Swell cutoff for these cases have been determined to be the point up to cohesive energy density equivalent to $4x10^{-8}$ J/m^3 plus CED difference between the specific case and its Na-montmorillonite counterpart. Figures 4-13 and 4-14 shows the typical curved plots and the corresponding terminal or swell cutoff points and the corresponding swell potential are summarized in Table 4-1.

4.3.10 Swell simulation – exchangeable cations variation

Several combinations of exchangeable cations shown in Table 3-9 were transformed into respective unit cells and were simulated for swelling using all the steps described in the

previous sections. Figure 4-14 provides the corresponding cohesive energy plots for these various combinations. Replacing 60 % of exchangeable Na^+ cation with K^+ cation causes a reduction in swell by about 15 %, while 60 % replacement with Ca^{+2} and Mg^{+2} cations result in a reduction by 50 and 45 % respectively. These results also indicate the sensitivity of these models to the change in percent and type of exchangeable cations. Bivalent cations such as Ca^{+2} and Mg^{+2} result in extra binding to the crystallite layers and hence cause a reduction in swell potential. Similarly, as compared to bivalent cations, monovalent K^+ cation does not provide binding forces enough to cause substantial reduction in swell potential.

Based on the CEC and the type of major exchangeable cations, LCEC with 60 % Ca+40 % Na could be considered as a close representative of the bentonite used in this study. Swell potential results of this combination very closely match the values obtained from swell potential tests. Considering that some part of post swell water content resides in the macro pores, the terminal moisture contents as assessed from simulations are also very close to the ones determined experimentally.

4.3.11 Nano / molecular level swell behavior model for expansive clays

The results of the molecular level simulations of different CECs, moisture, density, exchangeable cations, and cementation effects were compiled to form two unified sets of plots. One set of plots consists of graphs between two state variables i.e., water content and the total CED for all the possible variations of the parameters for each CEC (Figures 4-20 to 4-23). Similarly, plots were prepared between CED and the third state variable, swell potential, for the various cases considered in Table 4-1 (Figures 4-24 and 4-25). In

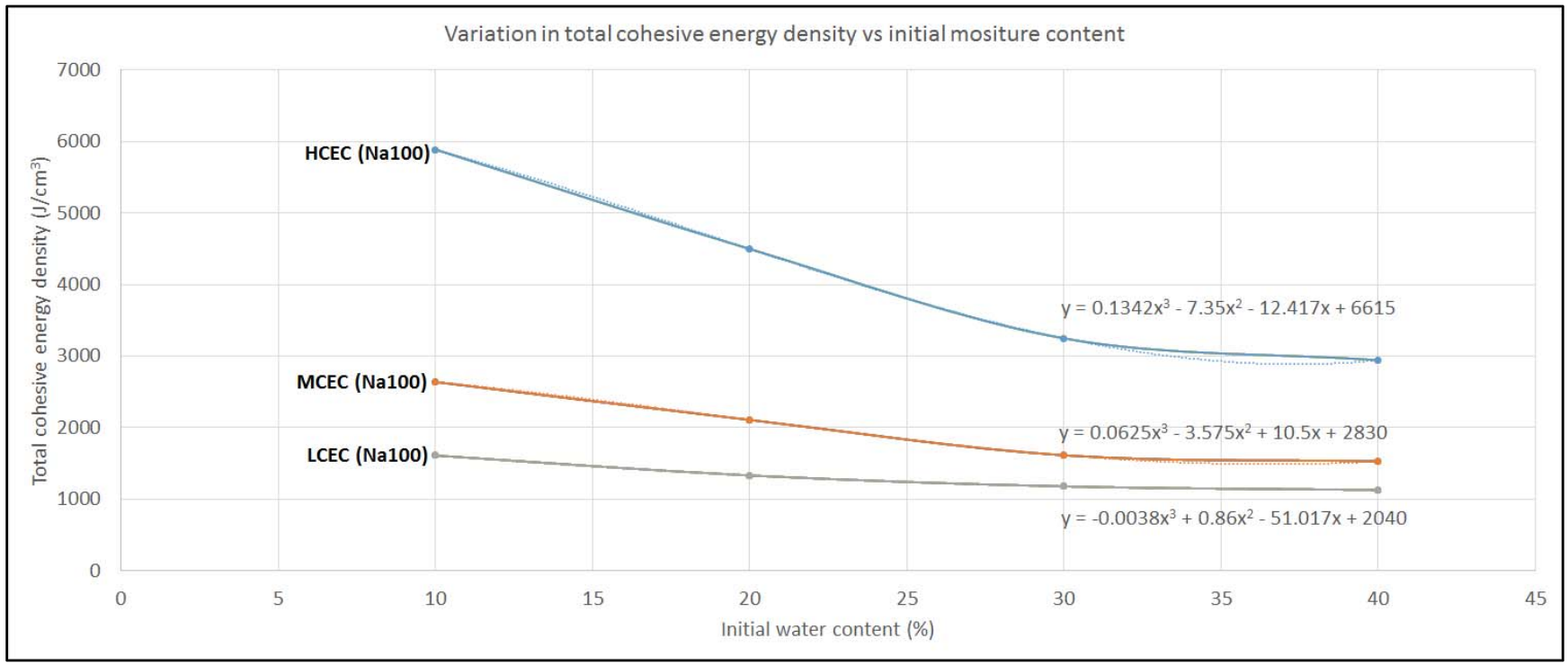

Figure 4-20 Variation of total cohesive energy density of Na-montmorillonite crystallites of different CECs compacted at a range of initial water content.

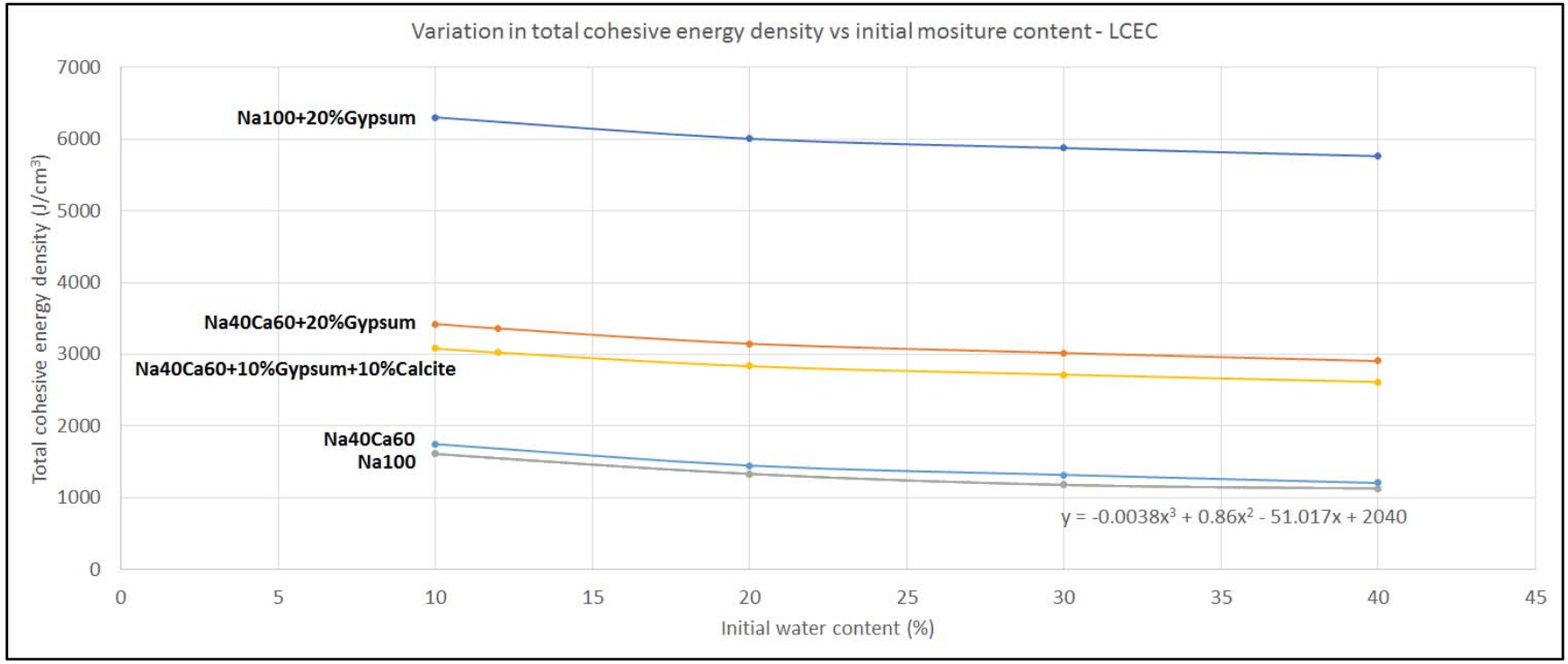

Figure 4-21 Variation of total cohesive energy density of montmorillonite crystallites of LCEC compacted at a range of initial water content.

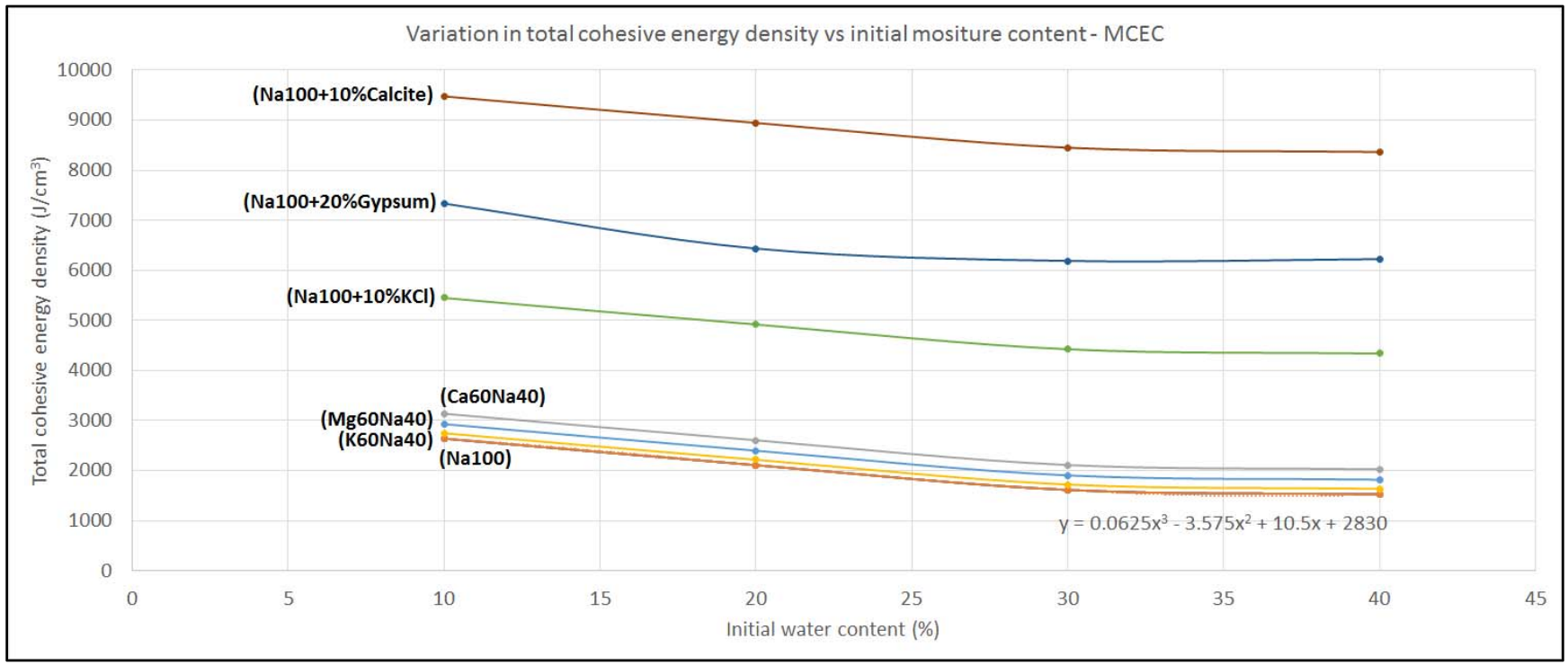

Figure 4-22 Variation of total cohesive energy density of montmorillonite crystallites of MCEC compacted at a range of initial water content.

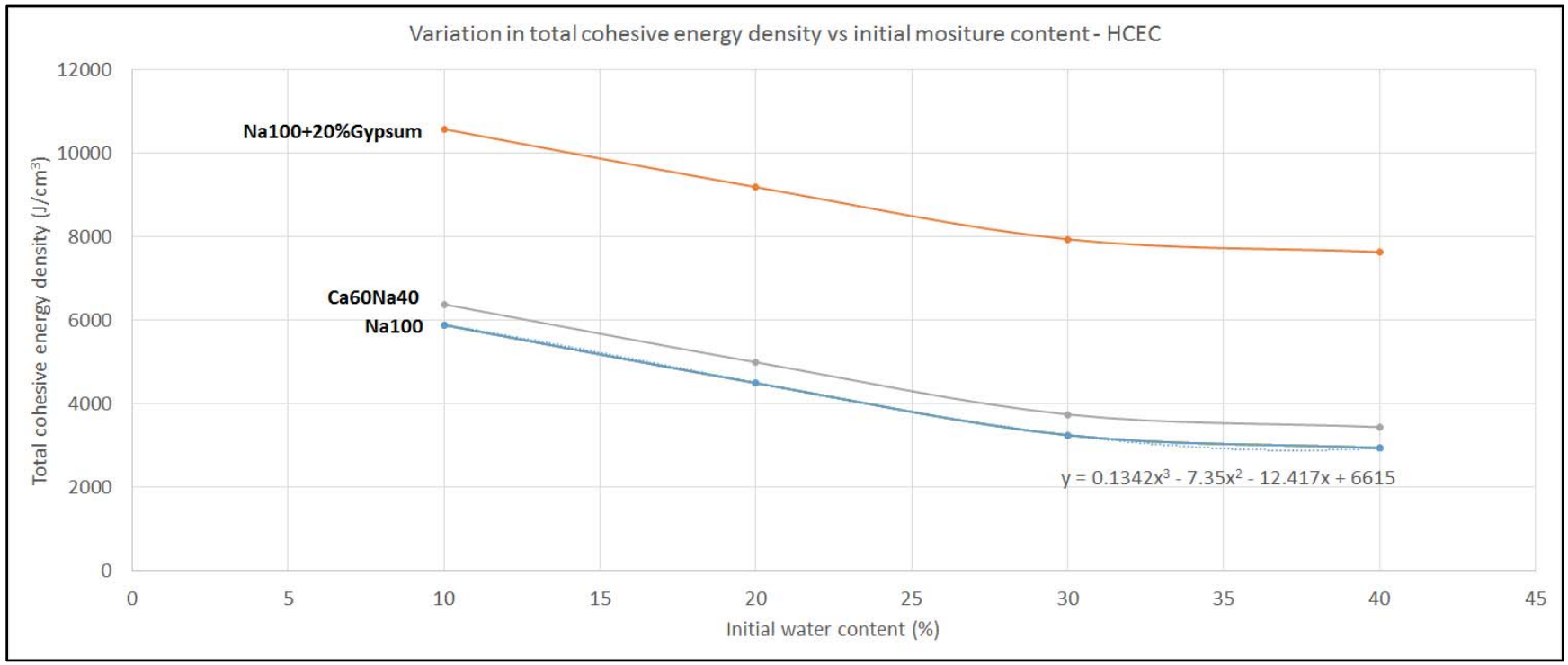

Figure 4-23 Variation of total cohesive energy density of montmorillonite crystallites of HCEC compacted at a range of initial water content.

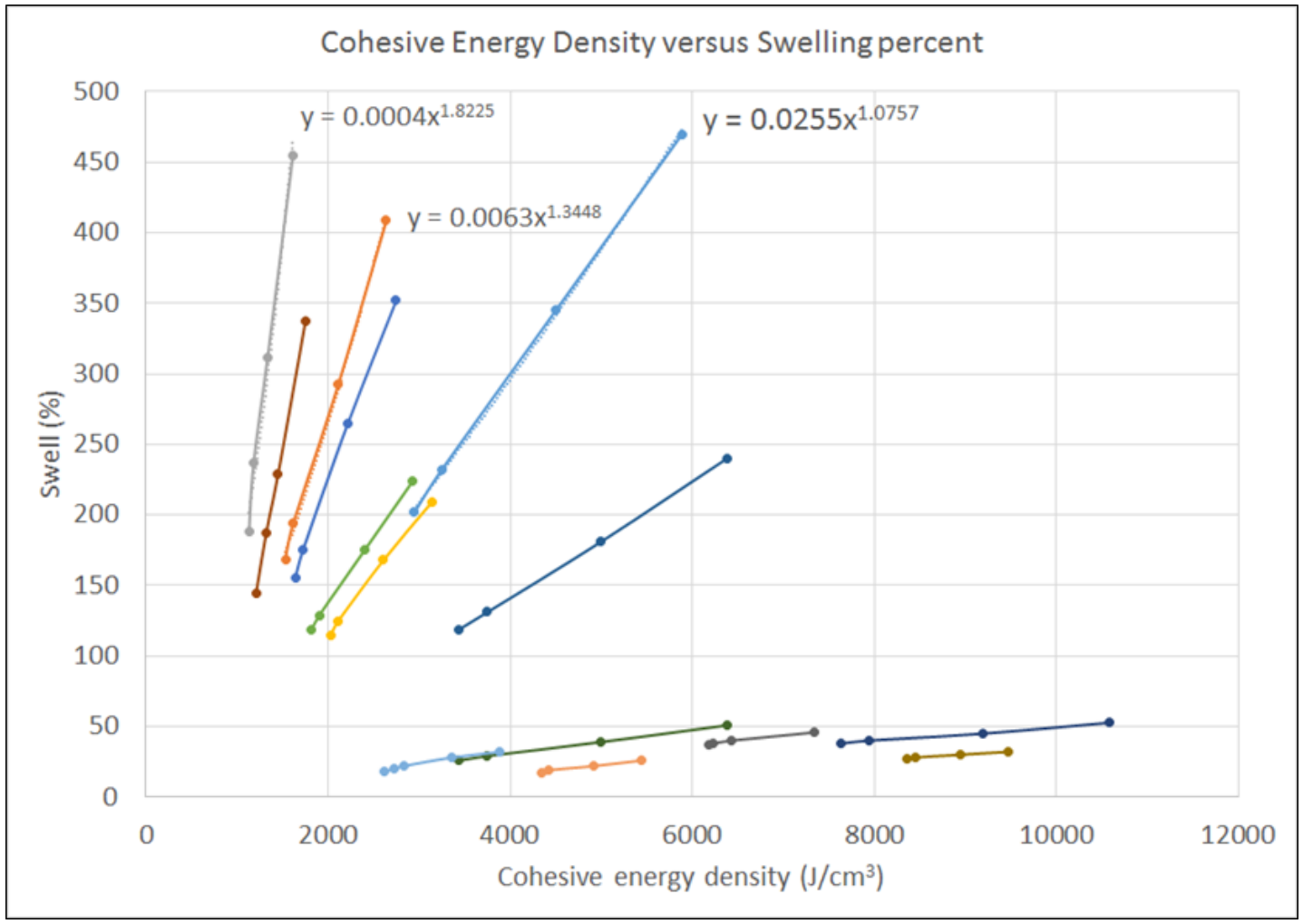

Figure 4-24 Relationships between total cohesive energy density and swell potential for different cases of montmorillonite with variation in cations and non-clay cementation compounds.

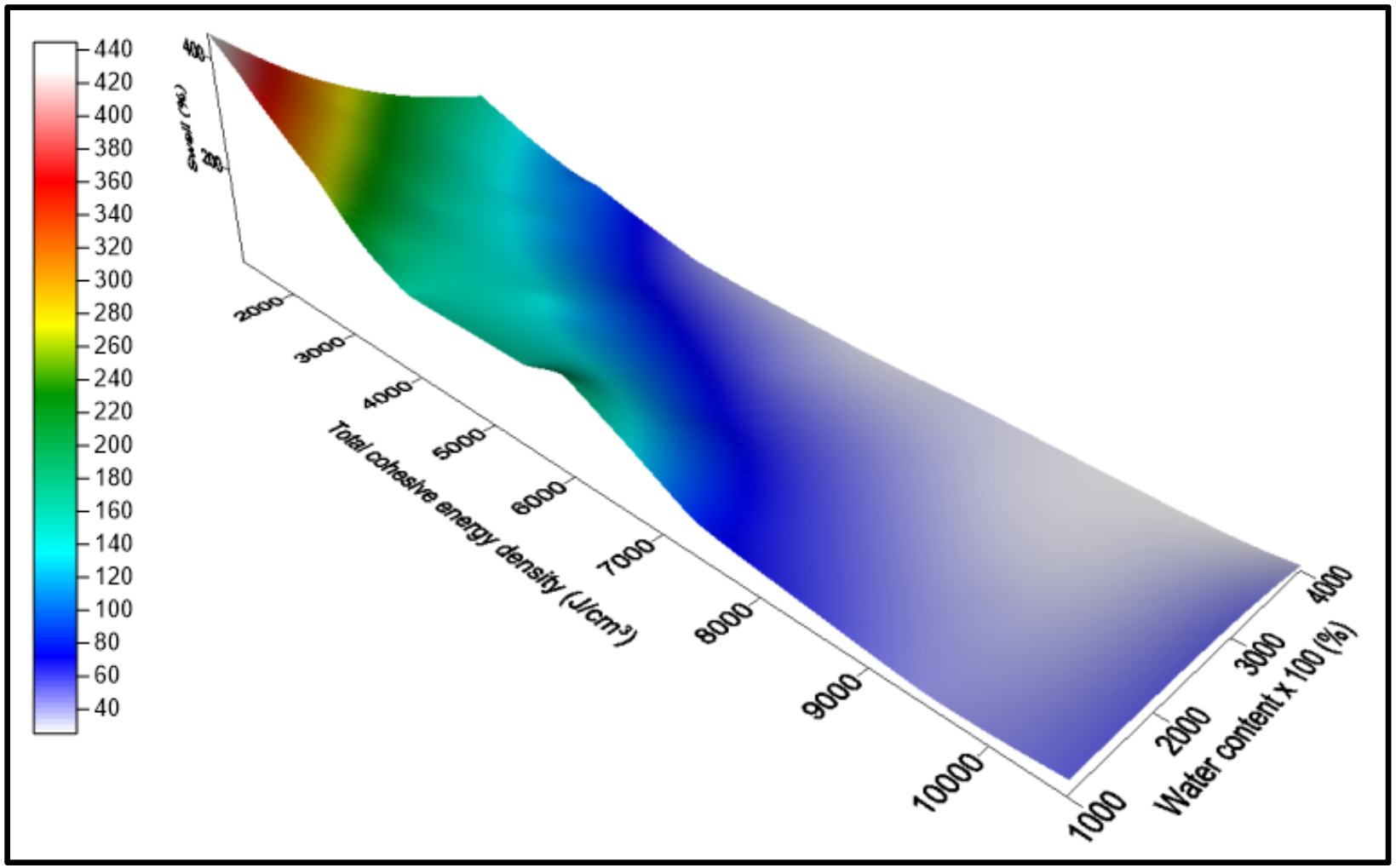

Figure 4-25 3-D representation of constitutive surface of the Nano level model for expansive clays.

combination, these plots serve as a nano level constitutive model, a 3-D representation is provided in Figure 4-25. These surfaces can be used to determine the swell potential of any natural or compacted expansive clays using the basic input parameters such as initial moisture content, CEC, exchangeable cations, and total cations / non-clay minerals.

The plots in Figures 4-20 to 4-23 show a general trend of decreasing CED with the water content till 30 % and afterwards it remains almost constant. Any change in parameters like CEC, cementations, cations, causes a shift in total CED and the shift remains constant throughout the moisture content range. To avoid cluttering of the data and for better visualization, several plots have been omitted in these figures. Development of an incremental form of constitutive relations is detailed in next Section 4.3.12.

4.3.12 Nano level constitutive model

In addition to the total swell potential determination, the molecular level simulation results for all the parameters such as CEC, water content, density, exchangeable cations, and cementation compounds have also been used to develop the constitutive equations of a nano model relating the incremental intake water content to the corresponding change in the volume as:

d_v = (slope for straight line or hyperbolic for curved plots) d_{wc} 4-1

where

d_v and d_{wc} are change in volume and water content respectively

slope or slope change (hyperbolic) = (ID-FD)/(FWC-IWC)

ID=initial density, FD=final density, FWC=final water content, IWC=initial water content

A basic equation relating the initial water content and the total cohesive energy density (TCED) is developed from Figure 4-26 and is expressed as:

$$TCED = 0.0625\,(IWC)^3 - 3.575\,(IWC)^2 + 10.5\,(IWC) + 2830 \qquad 4\text{-}2$$

Considering a constant shift in total cohesive energy density by change in exchangeable cations and by addition of cementing agents, equation 4-2 has been modified as:

$$TCED = 0.0625\,(IWC)^3 - 3.575\,(IWC)^2 + 10.5\,(IWC) + 2830 + 7100\,(C/0.1) + 5050\,(G/0.2) + 3010\,(KCl/0.1) + Ca\,(500) + Mg\,(300) + K\,(100) \qquad 4\text{-}3$$

where

C=Calcite, G=Gypsum, KCl=Potassium chloride, Ca=Calcium exchangeable cation, Mg=Magnesium exchangeable cation, K=Potassium exchangeable cation

Using this comprehensive relationship for total cohesive energy density, other required start and end points in the equation 4-1 could be obtained from the relationships developed from Figures 4-27 to 4-29. The corresponding relationships for Initial Density (ID), Final Density (FD), and Final Water Content (FWC) are provided below:

$$ID = \{-2E\text{-}15(TCED)^4 + 5E\text{-}11(TCED)^3 - 5E\text{-}07(TCED)^2 + 0.0023(TCED) - 1.5378\} * 1.85 * (ABS(CEC-90)/90) \qquad 4\text{-}4$$

$$FD = = -2E\text{-}22(TCED)^6 + 5E\text{-}18(TCED)^5 - 6E\text{-}14(TCED)^4 + 3E\text{-}10(TCED)^3 - 7E\text{-}07(TCED)^2 + 0.0005(TCED) + 0.3747 \qquad 4\text{-}5$$

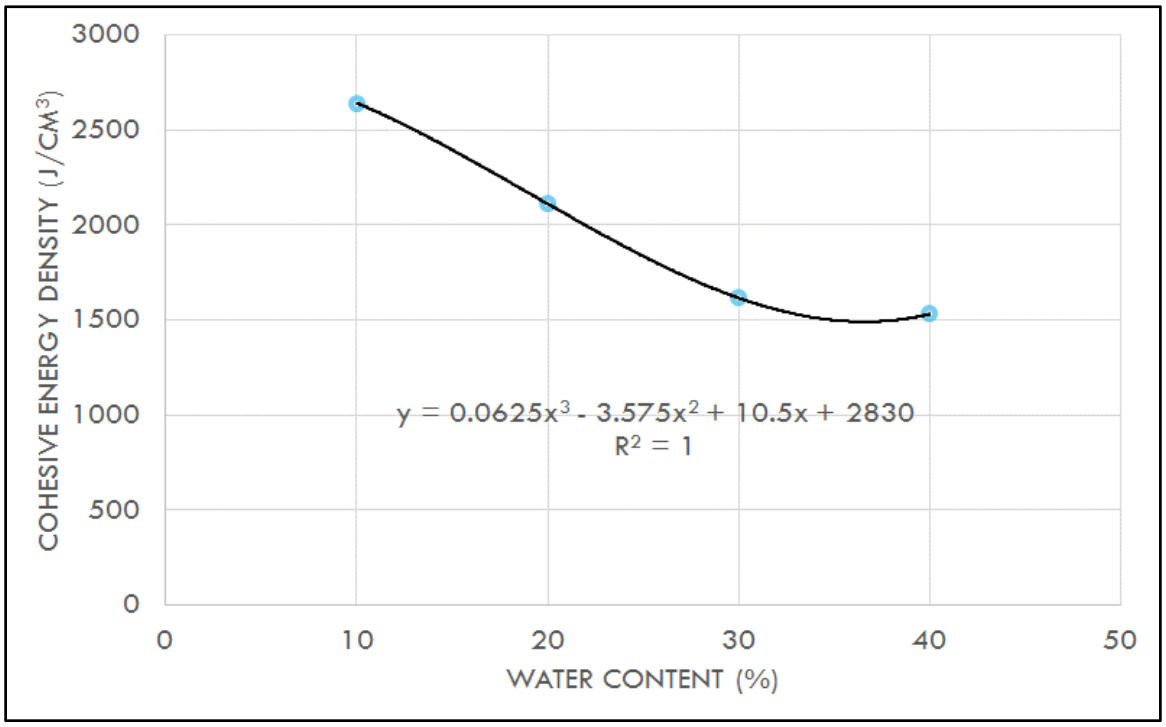

Figure 4-26 Basic relationship between total cohesive energy density and initial water content

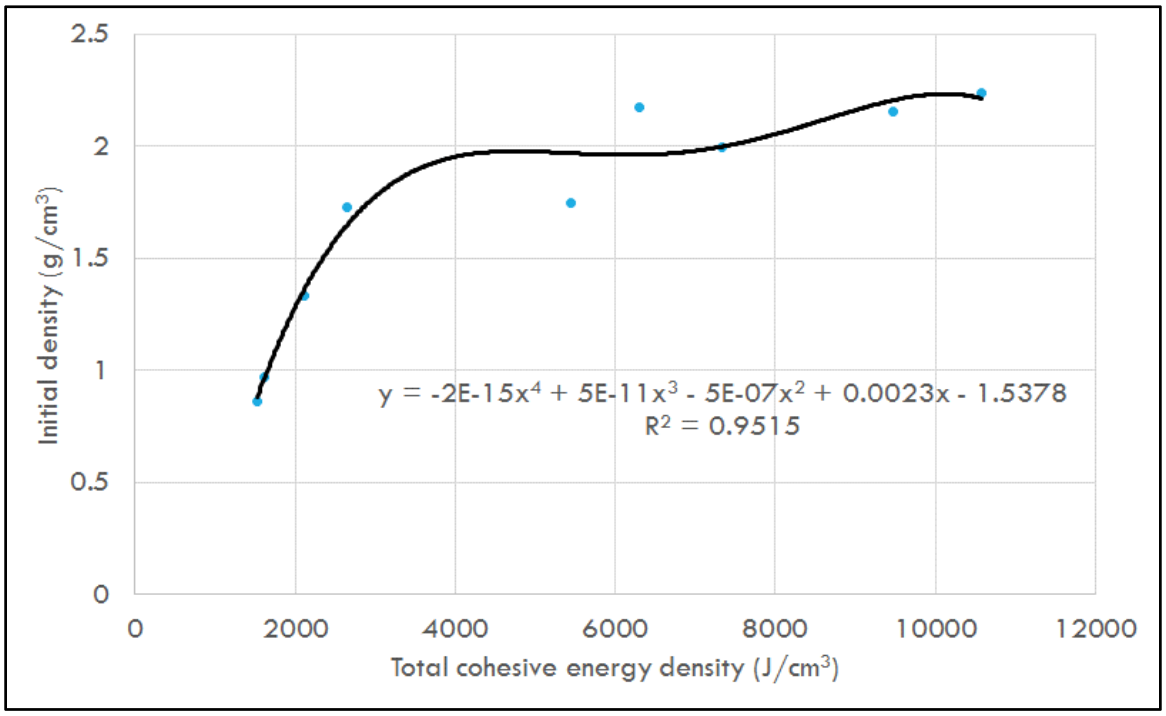

Figure 4-27 Variation of initial density with total cohesive energy density

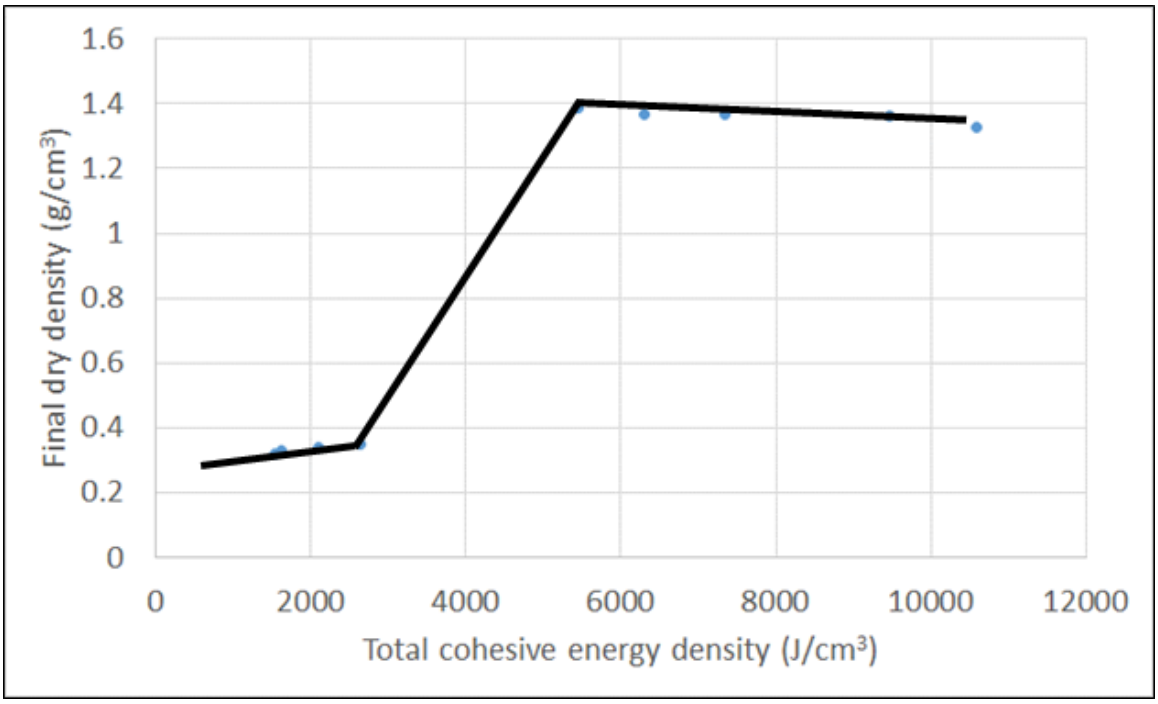

Figure 4-28 Variation of final density with total cohesive energy density

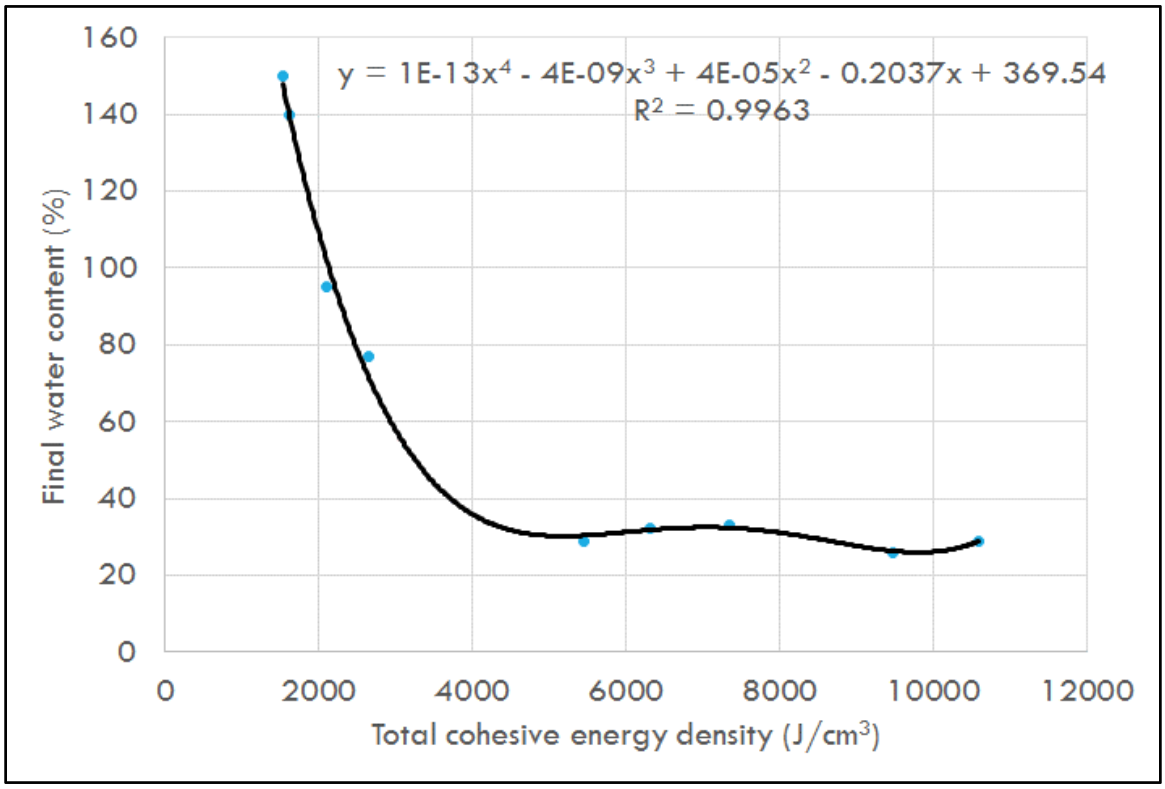

Figure 4-29 Variation of final water content with the total cohesive energy density

$$FWC = = \{1E\text{-}13(TCED)^4 - 4E\text{-}09(TCED)^3 + 4E\text{-}05(TCED)^2 - 0.2037\ TCED + 369.54\} * ABS(CEC^2\text{-}90)/CEC^2 * 0.82 \quad 4\text{-}6$$

The constitutive surface shown in Figure 4-5 can be expressed in the form of equations 4-4 to 4-6 to develop the equation for the constitutive surface:

$$Swell\ (\%) = (FD - ID) / FD * 100 \quad 4\text{-}7$$

Using the above equations of the nano model, swell potential was determined for all the samples tested using swell potential tests in this study and are tabulated in Table 4-2. Similarly, swell potential was also assessed for the undisturbed samples from the Eastern region of KSA tested by Hameed (1991) and the results are tabulated in Table 4-3 and plotted in Figure 4-30.

As observed from Tables 4-2 and 4-3, predictions of swell potential, final dry densities, and moisture contents for most of the cases are very close to the values obtained from the macro level tests. It can also be observed that major difference exists only in the measured and predicted values for samples with calcite as a non-clay mineral. This deviation can be attributed to very low solubility of calcite in distilled water as compared to gypsum that has a moderate solubility in water. As distilled water was used for the swell potential tests, very low percentages of calcite would have got interacted with the clay particles consequently causing only small reduction in swell potential. On the other hand, the molecular simulations for this case considers the interaction of entire 10 % calcite with the clay crystallite. Therefore, the extent of the percent of non-clay mineral interacting with clay mineral in laboratory or natural samples should always be considered.

Table 4-2 Summary of comparison of swell potential tests results in the current study and nano / molecular model predictions

Sample No	Moisture Content State	NaM	CaM	Bentonite	Sand	Gypsum	Calcite	Kaolinite	Swell Tests							Nano Model Prediction		
									Swell (%)	Initial Dry Desnity (g/cm^3)	IMC (%)	Initial Wet Desnity (g/cm^3)	FMC (%)	Final Dry Desnity (g/cm^3)	Final Wet Desnity (g/cm^3)	Swell (%)	Final Dry Desnity (g/cm^3)	FMC (%)
1	Dry of OMC	-	-	100	-	-	-	-	184	1.290	29.5	1.67	136.0	0.45	1.07	187	0.396	113
2	Wet of OMC	-	-	100	-	-	-	-	132	1.290	39.0	1.79	174.0	0.56	1.52	144	0.393	138
3	Dry of OMC	-	-	60	40	-	-	-	153	1.577	19.5	1.88	93.0	0.62	1.20	155	-	-
4	Wet of OMC	-	-	60	40	-	-	-	111	1.577	26.0	1.99	103.0	0.75	1.52	121	-	-
5	Dry of OMC	-	-	30	70	-	-	-	89	1.750	11.3	1.95	72.0	0.93	1.59	90	-	-
6	Wet of OMC	-	-	30	70	-	-	-	53	1.750	18.8	2.08	82.0	1.14	2.08	58	-	-
7	Dry of OMC	-	-	10	90	-	-	-	32	1.917	5.2	2.02	18.0	1.45	1.71	33	-	-
8	Wet of OMC	-	-	10	90	-	-	-	5	1.917	13.4	2.17	22.0	1.83	2.23	5	-	-
10	Dry of OMC*	-	-	30	60	10	-	-	21	1.750	12.0	1.96	56.0	1.45	2.26	28	1.355	60
11	Dry of OMC*	-	-	30	40	30	-	-	11	1.750	12.0	1.96	27.0	1.58	2.00	9	-	-
12	Dry of OMC*	-	-	30	20	50	-	-	6	1.750	12.0	1.96	19.0	1.65	1.96	6	-	-
13	Dry of OMC*	-	-	30	40	-	30	-	74	1.750	12.0	1.96	80.0	1.01	1.81	32	1.63	26
14	Dry of OMC*	-	-	30	20	-	50	-	68	1.750	12.0	1.96	66.0	1.04	1.73	29	-	-
25	NMC	Qatif (Q-1)							29	1.367	7.2	1.47	55.6	1.06	1.65	28	1.355	60

* Static Compaction

NMC: Natural Moisture Content
IMC: Initial Mositure Content
FMC: Final Mositure Content

Table 4-3 Summary of comparison of swell potential tests results from Hameed (1991) and nano / molecular model predictions

Sample No.	Location	BH / TP No.	Depth (m)	Smectite (%)	Non-swell cementitious minerals (%)	Non-swell cementitious associated (%)	Swell (%) from Swell tests*	Swell (%) from Nano Model**
1	Al-Khars, Al-Hasa	BH-9	2.5-2.7	7	50	3.5	2.2	4.7
2	Mahasen-Aramco, Al-Hasa	BH-13	2.0-2.25	4	34	1.4	6.28	10.3
3	Al-Hamadiya	BH-11	1.0-1.3	8	35	2.8	7.16	11.0
4	Al-Salehiya	BH-12	2.4-2.7	6	64	3.8	4.84	3.9
5	Al-Khars, Al-Hasa	TP-7	1.1	6	39	2.3	8.4	8.4
6	Al-Naathel, Al-Hasa	TP-11	2.0-2.2	6	27	1.6	16.38	18.0
7	Mahasen-Aramco, Al-Hasa	TP-11	2.0-2.2	4	32	1.3	13.11	14.2
8	Housing Area	BH-1	3.8	30	40	12.0	29	24.5
9	Housing Area	BH-3	1.8-2.1	13	48	6.2	4.06	4.6
10	Umm Al-Sahek	BH-6	0.45-0.6	25	32	8.0	14.35	13.0
11	Umm Al-Hammam	BH-8	5.6-5.75	39	39	15.2	12.88	13.9

* Hameed (1991) ** Current study

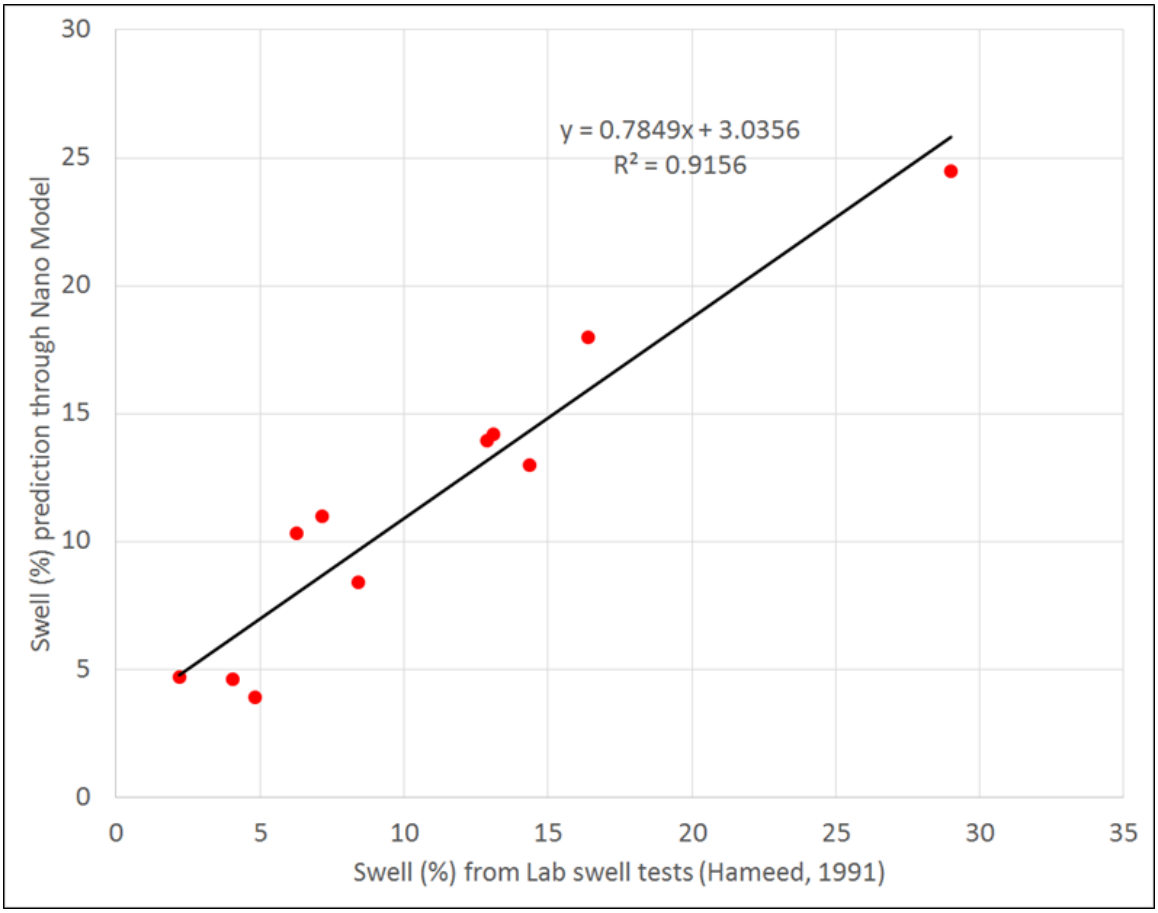

Figure 4-30 Comparison of swell potential tests results from Hameed (1991) and nano / molecular model predictions

Minor deviations in some other cases could be attributed to the contributions from the macro level features in the samples. So for the cases where macro features dominate in controlling the water in flow and the volume change, it is required to consider the coupling of this nano model with micro and macro level models to assess the total swell potential of the real fabric and structure of the expansive clays.

Application of the nano model to the natural soils requires a knowledge of the quantity and distribution of the non-clay minerals in the matrix. This knowledge can be acquired from the XRD results and total cations analysis of these samples. Based on this close confirmation of swell potential for undisturbed samples by nano model, it can also quite effectively be used for the assessment of swell potential of natural expansive clay deposits.

Using equation 4-1, typical plots showing swell versus water have been plotted using straight line and hyperbolic variation in density are shown in Figures 4-30 to 4-32. Figure 4-30 typically represents the swell behavior of Na-montmorillonite without any other constraint and it shows a complete separation of particles at higher water contents. On the other hand, Figures 4-31 and 4-32 depict the volume change response of expansive clay minerals restrained by other factors such as additional binding from very high CEC, cementation from non-clay salts, and / or exchangeable cations other than sodium. These typical behaviors also mark the validity of the developed model and the constitutive relationships.

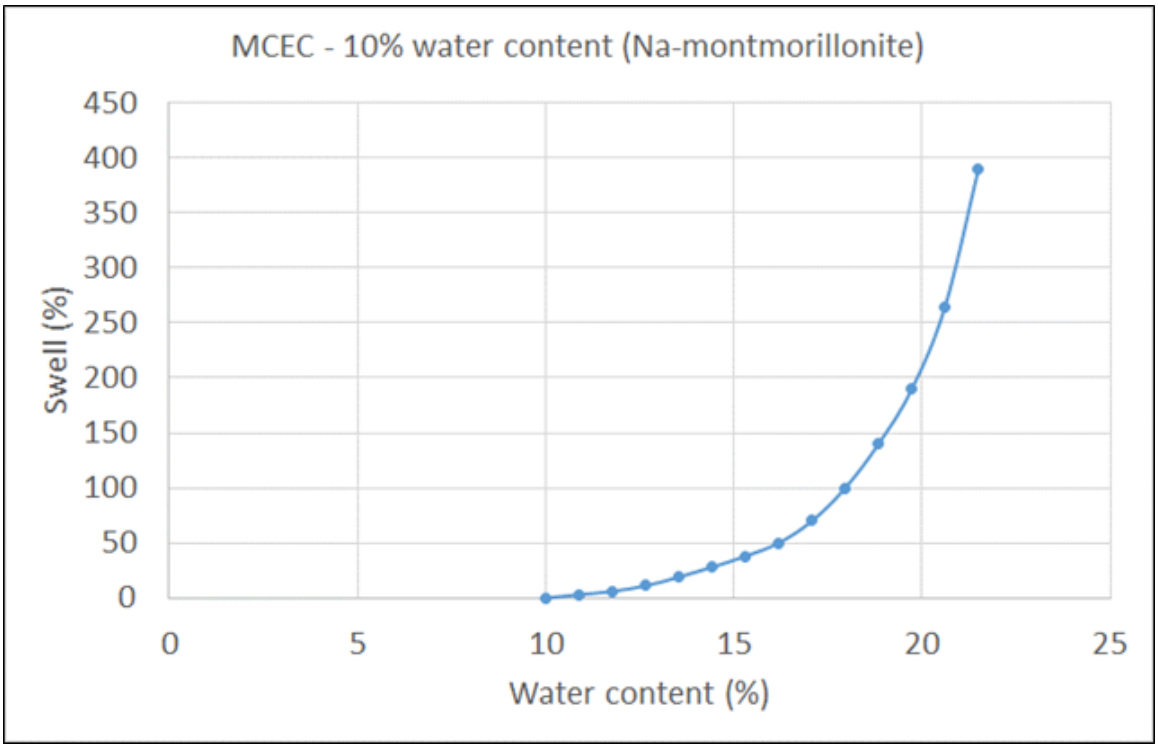

Figure 4-31 Water content – swell relationship for Na-montmorillonite (MCEC)

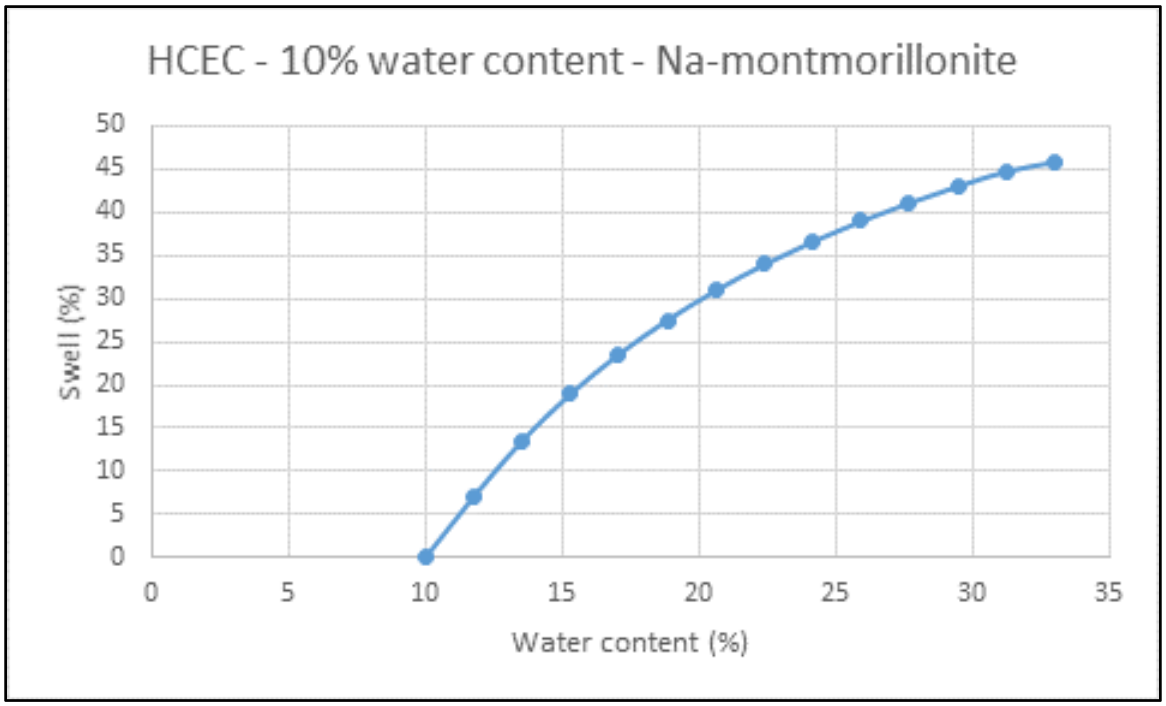

Figure 4-32 Water content – swell relationship for Na-montmorillonite (HCEC)

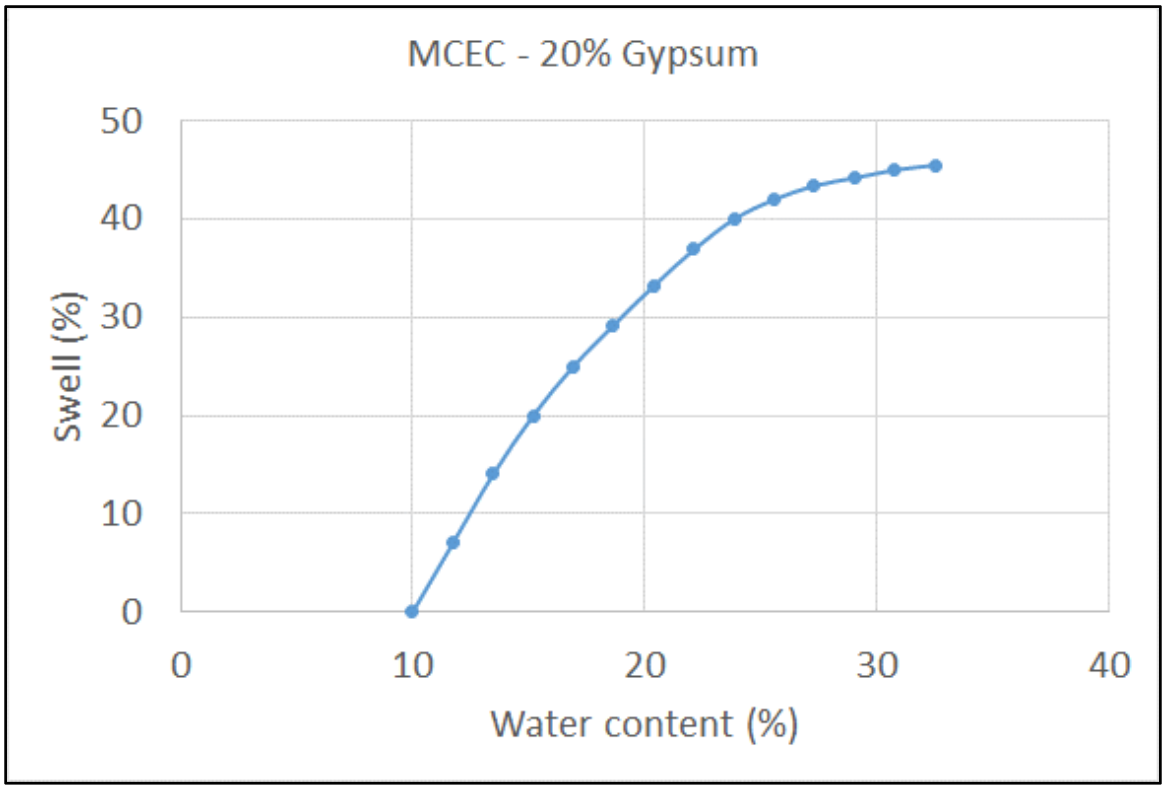

Figure 4-33 Water content – swell relationship for 20% Gypsum (MCEC)

CHAPTER 5

CONCLUSIONS AND RECOMMENDATIONS

This research constituted three major levels of activities including macro level testing, micro level imaging and analysis, and molecular level simulation and modeling to develop a volume change behavior model for the nano/molecular level fabric and structure of expansive clayey soils. This chapter provides a summary of the conclusions of this study and also provides recommendations for the future research.

5.1 Conclusions

In this research, several conclusions have been made at each level of investigations followed by the key conclusions formulated at the end of the research. Based on the nature of the conclusions, these have been divided into three major groups and are briefed in the next sections:

5.1.1 Confirmation and better explanation of existing concepts

(i) Among micro investigation techniques for the determination of the input parameters in the molecular level simulations, powder XRD have provided vital information on the crystallite size and the relationship of the lattice (d-spacing) expansion with water content. Results from CT, FTIR, and ESEM are more qualitative in nature and provide complementary information to XRD results.

(ii) Replacing part of the sand by calcite and gypsum in the swell potential test on bentonite / sand samples have resulted in substantial reduction in swelling. There is a reduction of 82, 90, and 95 % in the swelling potential when 10, 30, and 50 % gypsum was added, respectively. There is also reduction of 40 and 44 % in swelling upon part of sand replaced by 30 and 50 % of calcite, respectively. The phenomenon of decrease in swelling by addition of calcite and gypsum might be resulting from the binding effects produced by these compounds to the individual or group of clay particles.

(iii) Although CEC and the percentage of smectite in the natural undisturbed sample of Qatif-1 is almost the same as of the commercial bentonite (30/70 sand-bentonite mix), the difference in percent swell is large, i.e., 29 % vs. 121 %. This difference might be closely attributed to the cementation effects provided by the calcite, gypsum, and other similar compounds or salts present in the soil.

(iv) For the determination of the fundamental crystallite size from the XRD data using Debye-Sherrer's method, various widths of the corresponding peaks in the XRD data, removal of background, and leveling of the peaks have resulted in the assessment of the crystallite size in the range of 59 to 108 Å. This knowledge has been used in the selection of the size of the crystallite in molecular level modeling.

(v) XRD tests conducted on the specimens at various water contents conducted on the samples compacted on the dry and wet side of OMC indicated that d-spacing of about 15 Å (equivalent to two water layers or 20 % water content) exists in the clay crystallites on the dry side of OMC while d-spacing of 17.5 Å occurs (equivalent to three water layers or 30 % water content) on wet side of OMC. As the molding water content is respectively 30

and 40 % for the dry and wet side of OMC specimens, it is established that rest of the 10 % water content for both the cases is adsorbed on the edges and ends of the crystallites. This fact has played an essential role in the assessment of the fundamental size of the crystallite in the molecular level simulation.

(vi) Owing to its micrometer level resolution, micro CT testing is limited in its use for the nano/molecular level studies. Therefore, in this study, micro CT has been used to visualize and evaluate only the micron level fabric of the pre and post swell samples using the contrasting attenuation property of the clay particles before and after the swell test.

5.1.2 New concepts and developments

(i) For the static compaction of the specimens to the modified Proctor density in the Odometer rings, an equivalent static pressure has been determined as 1500 kPa. To achieve the modified Proctor density, a static pressure of 1500 kPa could be used to compact the specimens in two layers in the Odometer rings of 70 mm diameter and 19 mm height.

(ii) In addition to the exchangeable cations, total cations have also been determined for the natural and bentonite samples. Non-exchangeable cations, which are difference of these two, provide useful information on the contribution of non-clay minerals in the soil to the molecular level volume change behavior.

(iii) In Sorption simulation in the Materials studio software, optimum number of Monte Carlo steps to cause a realistic number of water molecules adsorption have been determined to be 25000. After experimenting several energy cut off levels, 25000 steps cut off was adopted as the threshold limit for the realistic sorption. Simulation beyond 25000 steps

resulted in the occupation of higher energy sites by water molecules and consequently occurrence of an unrealistically high volume change.

(iv) For the simulation purpose, Metropolis Monte Carlo method has been selected in the Sorption module of Materials Studio software. In this method, parameters selected for ratios of exchange, conformer, rotate, translate, and regrow have been selected as 0.39, 0.2, 0.2, 0.2, 0.2 respectively, while the corresponding probabilities are 0.39, 0.2, 0.2, 0.2, and 0.2. Amplitudes adopted for rotation and translation are 5^{o} and 1 Å respectively.

(v) Universal force field, one of the force fields in-built in the Materials Studio software has been modified in this research. Several force field parameters in UFF such as atom types, atom typing rules, diagonal van der Waals, and generators were modified for Na, Ca, Mg, Al, and Si in the light of the parameters suggested in CLAYFF force field. Modified Universal force field has successfully been used for carrying out sorption and molecular dynamics simulations on clay minerals during this research.

(vi) Different confining or compaction pressures used to simulate the several levels of geological and laboratory compaction pressures have shown that high pressures of an order of 1 GPa causes quick compaction and may be closely representative of dynamic and static quick type of compaction using the laboratory and field equipment. On the other hand, low confining pressures of an order of 0.01 to 0.1 GPa result in slow compaction and hence might be simulating more closely slow compaction / consolidation pressures for the geological deposits.

(vii) In this study, cohesive energy density (CED) has been considered as an excellent indicator of the interaction of the soil structure to the water sorption and the consequent

volume change. CED has been found highly sensitive to various volume change variables such as water content, density, CEC, type and percentage of exchangeable and non-exchangeable cations.

(viii) A general trend observed during this study is that low CEC crystallites produce lesser CED, while higher CEC and the crystallites sorbed with other compounds showed higher values.

(ix) Total CED has been found to be increasing with increase in CEC, density, cementation, and bivalent cations and decreasing with water content, while van der Waals CED reduces and becomes repulsion in nature with the same variation of the above parameters.

(x) For the same CEC, lesser water content results in higher cohesive energy, but for same density / moisture, higher CEC crystallites achieve much higher cohesive energy. As cohesion in clay particles is a result of the hydrogen bonding between their surfaces and the water, more number of charge deficiency centers in higher CEC clay result in more number of hydrogen bonds and consequently raising the electrostatic attraction CED. However, at the same time, van der Waals repulsions increase due to the high vicinity of the crystallites. Therefore, higher total cohesive energy mixes have corresponding higher repulsion van der Waals. These additional repulsion forces play an important role in the expansion / swell behavior of the clay particles in addition to the hydration by water molecules. Similarly, interaction with gypsum and calcite also causes an increase in cohesive energy density due to the extra bonding created by the cations and anions. Although there is an increase in repulsion due to van der Waals forces, but increase in attraction forces due to electrostatic component has much higher value and far outweighs the repulsion forces in these cases.

(xi) All the combination cases, except those with cementation and exchangeable cations other than Na, a straight line plot between CED and water content is continued till it reaches a swell cutoff or terminal point. Swell cutoff points for all such cases were found to be terminating at a CED of an order of 300 to 500 J/cm^3. By looking at the swell potential test results, terminal dry densities were found to be about 0.45 to 0.55 g/cm^3 for 100 % bentonite samples. In the dynamics simulation, this density range has been found equivalent to the cohesive energy density range of 300 to 400 J/cm^3. Therefore, in the absence of any other factor causing an early termination of swelling process such as cementation and / or exchangeable cations other than sodium, all the swell lines terminate at a cohesive energy density of 400 J/cm^3. The termination points also indicate the terminal or post swell moisture content.

(xii) For all the cases with cations other than Na and ones with non-clay minerals, plots between CED and moisture content is not a straight line. The plot has an initial straight portion followed by a curvature and a straight line to the terminal or swell cutoff. Swell cutoff for these cases have been determined to be the point up to CED equivalent to $4x10^{-8}$ J/m^3 plus CED difference between the specific case and its Na-montmorillonite counterpart.

(xiii) Terminal moisture content for high swell cases for each CEC is lesser than their low swell counterparts. For instance, swell line for 30 % initial water content LCEC terminates at 113 % while the one for 40 % initial water content LCEC falls at 138 %. A similar observation was also made during the swell potential tests; terminal moisture content for initial moisture contents of 30 % and 40 % are 136 % and 174 %, respectively. This anomalous phenomenon can be explained using the contribution of additional expansion

caused by the repulsion van der Waals forces. For these cases, in addition to the expansion caused by water molecules, the repulsion van der Waal forces result in an additional expansion. As swelling progresses, the repulsion force due to van der Waals result in pushing the particles apart. Since these forces are higher in case of highly compacted specimens or lesser moisture contents, relatively higher swelling takes place at lower water content for such cases.

5.1.3 Key contributions

(i) The results of the molecular level simulations of different CECs, moisture, density, exchangeable cations, and cementation effects were compiled to form a nano model to determine the swell potential of expansive soils. Predictions of swell potential, final dry densities, and final moisture contents using the nano model have been found to be very close to the values obtained from the macro level tests both for laboratory control samples and undisturbed natural samples. Therefore, these constitutive surfaces and equations can be comprehensively used for the expansive soils with both clay and non-clay minerals and all the possible combinations of CEC, water content, density, total cations, and exchangeable cations.

(ii) Molecular level models have been developed for the fabric and structure of both natural and compacted soils containing both clay and non-clay minerals. These molecular level models with the suggested parameters and procedures can be used for any combination of clay minerals and other interacting compounds. These models can also be used to model the soil behavior in other industrial fields such as pharmaceutical, agriculture, petroleum, and waste management.

5.2 Further research recommendations

To continue the development of the nano model into a constitutive nano level model, following are the suggestions for the future research:

(i) Nano level constitutive model for expansive soils developed in this study should be formulated into a numerical model using Finite Element Method (FEM) technique.

(ii) Although predictions of final dry densities and moisture contents using the nano model are very close to the values obtained from the macro level tests, deviations in some of the cases could be attributed to the contributions from the macro level features in the samples. Therefore, it is required to consider the coupling of nano model with micro and macro level models to assess the total swell potential of the real fabric and structure of the expansive clays.

(iii) The contribution of non-exchangeable cations and anions associated with the clay mineral particles to the swelling behavior have been well established in this research. Although total cations measurement could provide a general and close estimate of the type and percentage of these cations and anions contributing to the volume change behavior, this aspect requires further investigations and the development or modification of tests to determine a precise estimate.

References

Abduljauwad, S. N. and Al-Sulaimani, G. J. (1993), "Determination of Swell potential of Al-Qatif Clay", Geotechnical Testing Journal, ASCE, December 1993, pp. 469-484

Abduljauwad, S. N., Al-Sulaimani, G. J., Basunbul, I. A., and Al-Buraim, I. (1998), "Laboratory and field studies of response of structures to heave of expansive clay", Geotechnique, 48(1): 103-121

Alonso, E. E., Gens, A. and Hight, D. W. (1987), "Special Problem Soils, General Report", Proceedings 9th European Conference on Soil Mechanics, Dublin, Vol. 3, 1087-1146

Alonso, E. E., Gens, A. and Josa, A. (1990), "A constitutive model for partially saturated soils", Geotechnique, Vol. 40(3), 405-430

Alonso, E. E., Vaunat, J., Gens, A. (1999), "Modeling the mechanical behavior of expansive Clays", Eng Geol 1999; 54:173–83

Alymore, L. A. G. and Quirk, J. P. (1962), "The structural status of clay systems", In: Swineford, A. (Ed.), Proceedings of the 9th National Conference on Clays and Clay Minerals, Lafayette, Ind., pp. 104–130

ASCE (2013), http://geology.com/articles/expansive-soil.shtml

Bolt, G. H. (1956), "Physico-chemical Analysis of the Compressibility of Pure Clays", Geotechnique, Vol. 6, No. 2, pp.86-93

Brooks, B. R., Bruccoleri, R. E., Olafson, B. D., States, D. J., Swaminathan, S., Karplus, M. (1983), "CHARMM: A program for macromolecular energy, minmimization, and dynamics calculations", J. Comp. Chem. 4, 187-217

Cabidoche, Y. M. and Ruy, S. (2001), "Field shrinkage curves of a swelling clay soil: analysis of multiple structural swelling and shrinkage phases in the prisms of a vertisol", Australian Journal of Soil Research 39, 143–160

Chapman, D. I. (1913), "A contribution to the theory of electrocapillarity", Philosophical magazine, Vol. 25 (6), 475-481

Clay Minerals Society (2013), "Source Clays Physical / Chemical Data", http://www.clays.org/SOURCE%20CLAYS/SCdata.html

Cygan, R. T., Liang, J. J. and Kalinichev, A. G. (2004)," Molecular Models of Hydroxide, Oxyhydroxide, and Clay Phases and the Development of a General Force Field", J. Phys. Chem. B 108 1255

Dafalla, M. A. and Shamrani, M. A. (2012), "Expansive Soil Properties in a Semi-Arid Region", Research Journal of Environmental and Earth Sciences 4(11): 930-938, 2012

Delage, P. and Graham, J. (1996), "Mechanical behavior of unsaturated soils: understanding the behavior of unsaturated soils requires reliable conceptual models", In: Alonso EE and Delage P. (eds) , Proceedings of 1st International conference on Unsaturated Soils, Paris, vol. 3, Balkema Presses des Ponts et Chaussees pp. 1223–1256

El Sohby, M. A. and Rabba, E. A. (1981), "Some Factors affecting the swelling of clayey soils", Geotechnical Engineering, Vol 12, page 19-39

Fityus, S. and Buzzi, O (2008), "The place of expansive clays in the framework of unsaturated soil mechanics", Applied Clay Science, Vol. 43, Issue 2, page 150-155

Fredlund, D. G. and Morgenstern, N. R. (1977), "Stress state variables for unsaturated soils", Journal of Geotechnical Engineering Division, ASCE, Vol. 103(GT5), 447-466

Fredlund, D. G. (1979), "Appropriate concepts and technology for unsaturated soils", Canadian Geotechnical Journal, Vol. 16, 121-139

Gens, A. and Alonso, E. E. (1992), "A framework for the behavior of unsaturated expansive clays", Canadian Geotechnical Journal 29, 1013-1032 (1992)

Gouy, G. (1910), "Sur la constitution de la charge electrique a la surface d'un electrolyte", Annales de Physique (Paris), Serie 4, 9, 457-468

Guimares, L. D., Gens, A., Sanchez, M., and Olivella, S. (2013), "A chemo-mechanical constitutive model accounting for cation exchange in expansive clays", Geotechnique 63, No. 3, 221-234

Hameed, R. A. (1991), "Characterization of Expansive Soils in the Eastern Province of Saudi Arabia", MS Thesis, KFUPM, Dhahran, Saudi Arabia, July 1991

Hildebrand, J. H. (1916), "Solubility", J. Am. Chem. Soc., 38, 1452

Hildebrand, J. H. (1919), "Solubility III. Relative Values of Internal Pressures and their Practical Application", J. Am. Chem. Soc., 41, 1067

Hildebrand, J. H., Prausnitz, J. M., and Scott, R. L. (1970), "Regular and Related Solutions", van Nostrand: New York

Hildebrand, J. H., Scott, R. L. (1933), "Solubility of Non-Electrolytes", 3rd Edition, Reinhold: New York

Hueckel, T. A. (1992), "Water-mineral interaction in hygromechanics of clays exposed to environmental loads: a mixture-theory approach", Workshop on Stress Partitioning in Engineered Clay Barriers, May 29-31, 1991, Duke University, Durham, N.C. 1071-1086

Humphrey, W., Dalke, A., and Schulten, K (1996), "VMD: Visual molecular dynamics", Journal of Molecular Graphics, 14(1), 33–35

Ichikawa, Y., Kawamura, K., Fuji, N. and Nattavut, T. (2002), "Molecular dynamics and multiscale homogenization analysis of seepage-diffusion problem in bentonite clay", International Journal of Numerical Methods in Engineering 2002; 54:1717–1749

Karaborni, S., Smit, B., Heidug, W. Urai, E. and van Oort, (1996), "The Swelling of Clays: Molecular Simulations of the Hydration of Montmorillonite", Science, Vol. 271, 23 February, 1996, 1102-1104

Katti, D. R., Schmidt, S., Ghosh, P., and Katti, K. S., (2005), "Modeling Response of Pyrophyllite Clay Interlayer to Applied Stress Using Steered Molecular Dynamics", Clays and Clay Minerals, Vol. 52, n2, 171-178

Katti, D. R., Matar, M. I., Katti, K. S. and Amarasinghe, P. M. (2009), "Multiscale Modeling of Swelling Clays: A Computational and Experimental Approach", KSCE Journal of Civil Engineering (2009) 13(4): 243-255

Katti, K. S. and Katti, D. R. (2010), "Fourier Transform Infrared Spectroscopy Studies of Clay and Shales", Indian Geotechnical Conference – 2010, GEOtrendz, December 16-18, 2010, 267-270

Katti, D. R., Katti, K. S., Amaasinghe, P. M. and Pradhan, S. M. (2011), "An insight into role of clay-fluid molecular interactions on the microstructure and Macroscale

properties of swelling clay", Alonso and Gens (eds), Unsaturated Soils, 2011 Taylor and Francis Group, London

Lambe, T. W. (1958), "The structure of compacted clay", Journal of Soil Mechanics and Foundations Division, ASCE, Vol. 84 (SM2), 1654

Lambe, T. W., Whitman, R. V. (1959), "The role of effective stress in the behavior of expansive soils", First Annual Soil Mechanics Conference, Colorado School of Mines, pp. 33–65

Likos, W. J. and Lu, N. (2006), "Pore scale analysis of bulk volume change from crystalline swelling in Na+- and Ca2+-smectite", Clays and Clay Minerals, Vol. 54, No. 4, pp. 516 - 529

Likos, W.J., Wayllace, A. (2010), "Porosity Evolution of Free and Confined Bentonites During Interlayer Hydration" Clays and Clay Minerals, Vol. 58 (3), pp. 399-414.

Lloret, A. and Alonso, E. E. (1985), "State surfaces for partially saturated soils", Proc 11th Conference on Soil Mechanics and Foundation Engineering, Sand Francisco, Vol. 2, 557-562

Longuet-Escard, J., Mering, J., and Brindley, G. (1960), "Analysis of hk bands of montmorillonite", C. R. Acad, Sci, Paris 251, 106-108

Madsen, F. T. and Muller-Vonmoos, M. (1989), "The swelling behavior of clays", Applied Clay Science4:143–56

Marshall, C. E. (1949) "The Colloid Chemistry of the Silicate Minerals", New York: Academic Press, P. 54.

Matyas, E. I. and Radhakrishna, H. S. (1968), "Volume change characteristics of partially saturated soils", Geotechnique, Vol. 18 (4), 432-448

Metropolis, N.; Rosenbluth, A. W.; Rosenbluth, M. N.; Teller, A. H.; Teller, E. J. (1953), "cccc" Chem. Phys., 21, 1087

Meunier, A. (2006) "Why are clays minerals small", Clay Minerals 41, 551–566

Miller, D. J. (1996) "Osmotic suction as a valid stress state variable in unsaturated soils" Ph.D. dissertation, Colorado State University, Fort Collins, CO

Mitchell, J. K. (2005), "Fundamentals of soil behaviour", 3rd Edition, John Wiley and Sons, Inc., New York

Nanoscale Simulation Lab at University of Akron, US (2013) (http://www2.uakron.edu/cpspe/dpe/web/nsl/interface-force-field.php

Norrish, K. (1954), "The Swelling of Montmorillonite", Transaction Faraday Society 18: pp. 120-134

Oades, J.M. and Waters, A.G., (1991), "Aggregate hierarchy in soils", Australian Journal of Soil Research, 29, 815–828

Phillips, J. C., Braun, R., Wang, W., Gumbart, J., Tajkhorshid, E., Villa, E., Chipot, C., Skeel, R. D., Kale, L., and Schulten, K (2005), "Scalable molecular dynamics with NAMD", Journal of Computational Chemistry, 26(16), 1781–1802

Pinyol, N., Vaunat, J. and Alonso, E. E. (2007), "A constitutive model for soft clayey rocks that includes weathering effects", Geotechnique 57, No. 2, 137–151

Plimpton, S. J. (1995), "Fast Parallel Algorithms for Short-Range Molecular Dynamics", J Comp Phys., 117, 1-19

Ponder, J. W. (2011), http://dasher.wustl.edu/, Washington University, US

Pons, L. J. and Van der Molen, W. H. (1977), "Soil genesis under dewatering regimes during 1000 years of polder development", Soil Science 116, 228–235

Quirk, J. P. and Murray, R. S. (1991), "Towards a model for soil structural behavior", Australian Journal of Soil Research 29, 829–867

Robertson, H. E., Weir, A. H. and Woods, R. D. (1968), "Morphology of particles in size fractionated Na montmorillonite", Clays and Clay Minerals 16, 239–247

Sa´nchez, M., Gens, A., Guimaras, L. N. and Olivella, S. (2005), "A double structure generalized plasticity model for expansive materials", International Journal for Numerical and Analytical Methods in Geomechanics, 2005, 29:751–787

Sato, H., Yamagishi, A. and Kawamura, K. (2001), "Molecular simulation for flexibility of a single clay layer", Journal of Physics Chemistry, vol. B 105, 7990-7997

Sharma, R. S. (1998), "Mechanical Behavior of Unsaturated Highly Expansive Clays", PhD Thesis, Oxford University, UK

Scatchard, G. (1931), "Equilibria in Non-Electrolyte Solutions in Relation to the Vapor Pressures and Densities of the Components", Chem. Rev., 8, 321

Scherrer, P. (1918), “Bestimmung der Grösse und der inneren Struktur von Kolloidteilchen mittels Röntgenstrahlen” Nachr. Ges. Wiss. Göttingen 26 (1918) pp. 98-100

Skipper, N. T. (1992), “MONTE User's Manual”, Technical Report, Department of Chemistry, University of Cambridge, UK

Skipper, N. T., Sposito, G., and Chang, F. R. (1995a), “Monte Carlo simulations of interlayer molecular structure in swelling clay minerals 1. Methodology”, Clays and Clay Minerals, Vol. 43, No. 3, pp. 285-293

Skipper, N. T., Sposito, G., and Chang, F. R. (1995b), “Monte Carlo simulations of interlayer molecular structure in swelling clay minerals 1. Monolayer Hydrates”, Clays and Clay Minerals, Vol. 43, No. 3, pp. 294-303

Snethen, D. R., Johnson, L. D. and Patrick, D. M. (1977), “An Investigation of the Natural Microscale Mechanisms That Cause Volume Change in Expansive Clays” Federal Highway Administration Report No. FHWA-RD-77-75

Sridharan, A., Venkatappa R. G. (1973), “Mechanisms controlling volume change of saturated clays and the role of the effective stress concept”, Geotechnique 23, 359–382

Stern S. (1924), “Modification in Diffuse Double Layer Theory”, Z. Elektrochem., Vol. 30, p. 508

Sun, W. and Sun, D. (2011), “Coupled modeling of hydro-mechanical behavior of unsaturated compacted expansive soils”, International Journal of Numerical and Analytical Methods in Geomechanics, Vol. 36, Issue 8, page 1002-1022

Tao, L., Xiao-Feng, T., Yu, Z. and Tao, G. (2010), “Swelling of K^+, Na^+ and Ca^{2+} - montmorillonites and hydration of interlayer cations: a molecular dynamics simulation", Chin. Phys. B Vol. 19, No. 10 (2010)

Teppen, B. J., Rasmussen, K., Bertsch, P. M., Miler, D. M., and Schafer, L. (1997), “Molecular dynamics modeling of clay minerals. 1. Gibbsite, kaolinite, pyrophyllite, and beidellite”, Journal of Physical Chemistry B, 101, 1579–1587

Thomasson, A. J. (1978), “Towards an objective classification of soil structure”, Journal of Soil Science 29, 38–46

Van Olphen, H. (1963), “Compaction of Clay Sediments in the Range of Molecular Particle Distances”, Clays and Clay Minerals, Vol. 11, pp.178-187

Van Olphen, H. (1977), “An introduction to clay colloid chemistry”, 2nd ed. New York: John Wiley and Sons.

Villar, M. V. (2000), “Thermo-hydro-mechanical characterization of a bentonite from Cabode Gata”, PhD Thesis, Universidad Complutense, Madrid, Spain

Wang, J., Sharma A. and Gutierrez, S. M. (2007), “Nanoscale Simulations of Rock and Clay Minerals”, ASCE Geotechnical Special Publication 173: Advances in Measurement and Modeling of Soil Behavior Geo-Denver 2007: New Peaks in Geotechnics

Wang, J. and Gutierrez, S. M. (2010), “Structural Transformation of 2:1 Clay Minerals by a constant pressure molecular dynamics simulation method”, Journal of Nanomaterials, 2010

Wayllace, A. (2008), “Volume change and swelling pressure of expansive clay in the Crystalline swelling regime”, PhD Thesis, University of Missouri, US

Scherrer, P. (1918), “Analysis of external and internal structure of colloidal particles by means of X-rays”, Nachrichten von der Konig, Gesellsch. Wissensch, zu Guttingen-Math., Physics, Kl., 98-100

Warren, B. E. (1941), “X-ray methods”, Jour. Applied Physics 12, 375-83

Appendix A - XRD Results

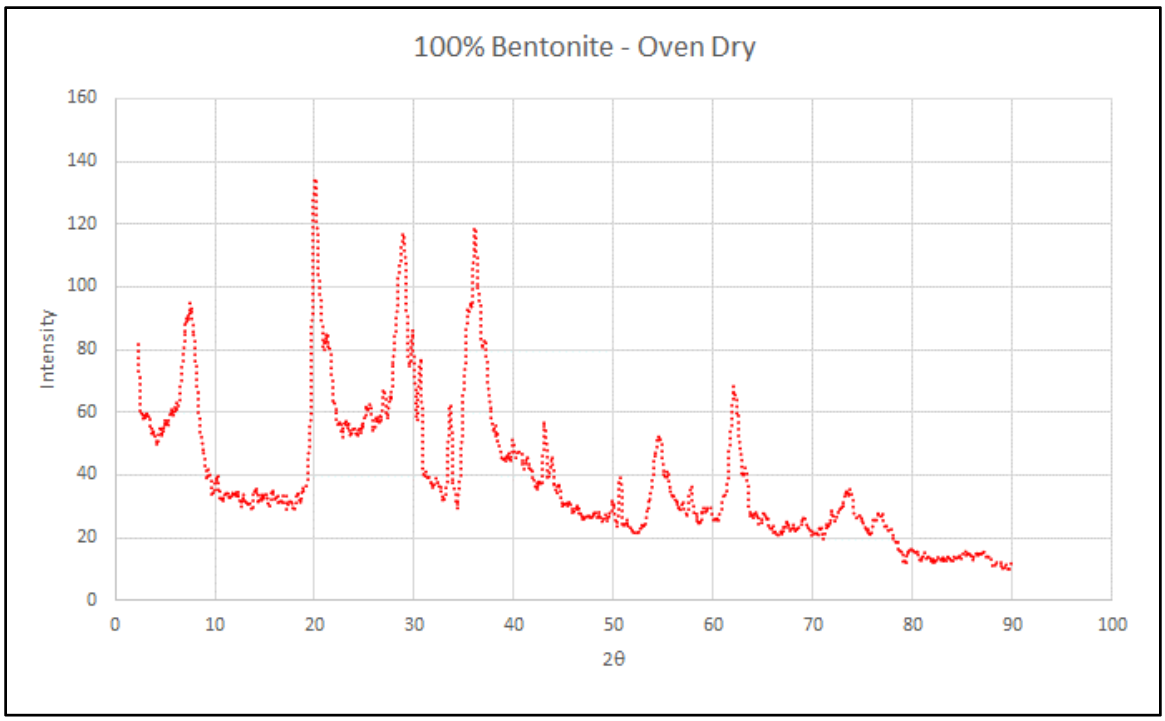

Figure A-1 XRD results of dry bentonite sample

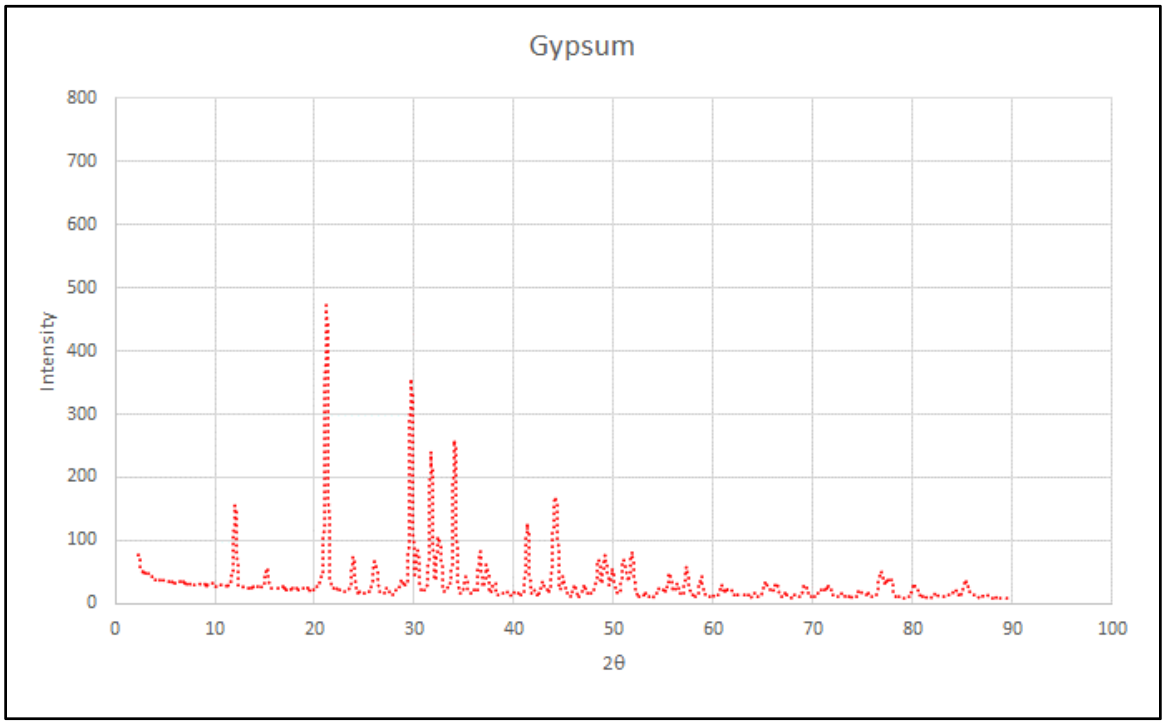

Figure A-2 XRD results of gypsum sample

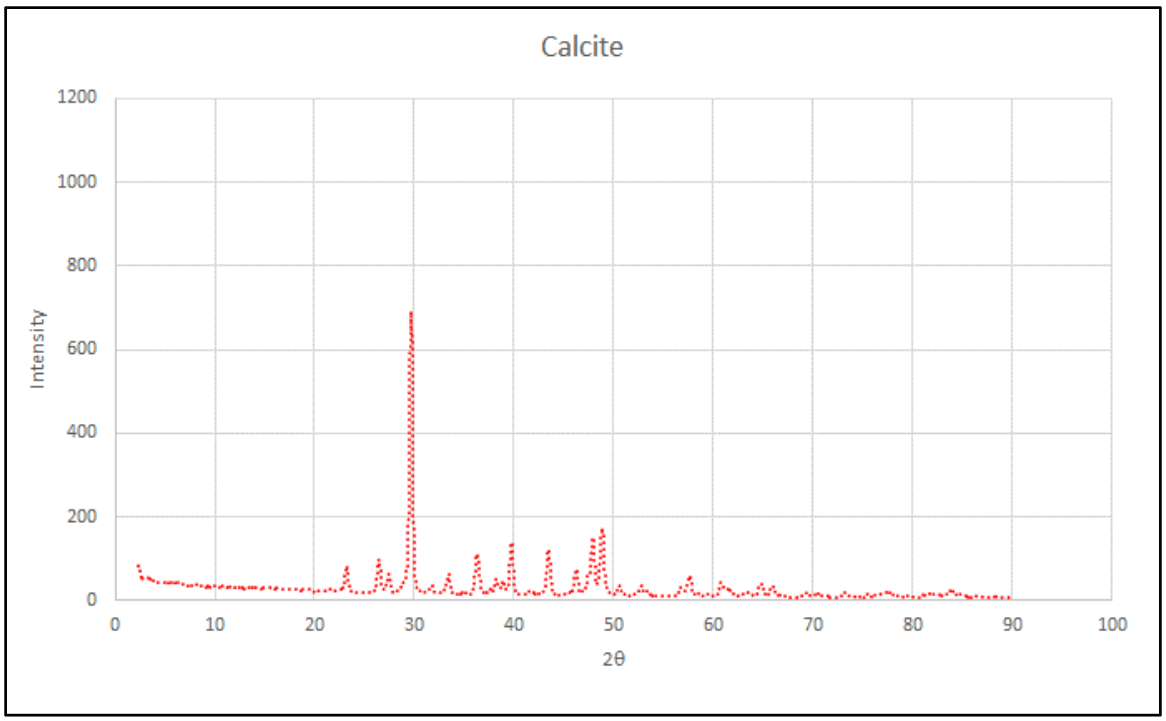

Figure A-3 XRD results of Calcium Carbonate sample

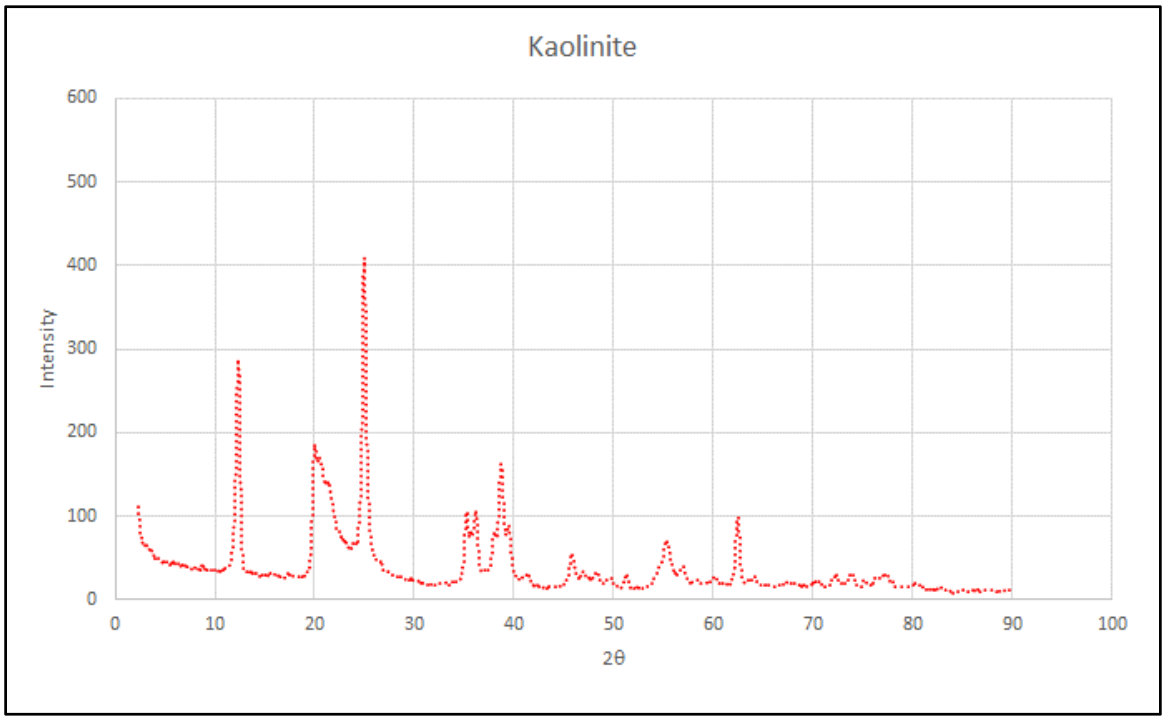

Figure A-4 XRD results of kaolinite sample

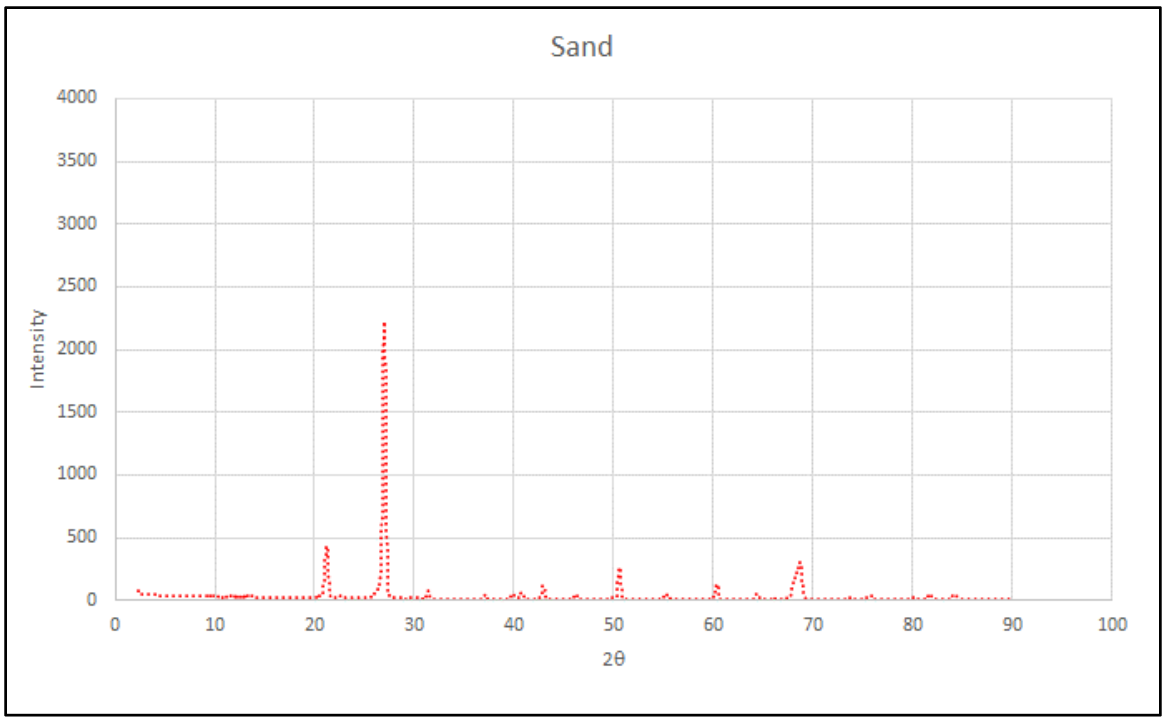

Figure A-5 XRD results of sand sample

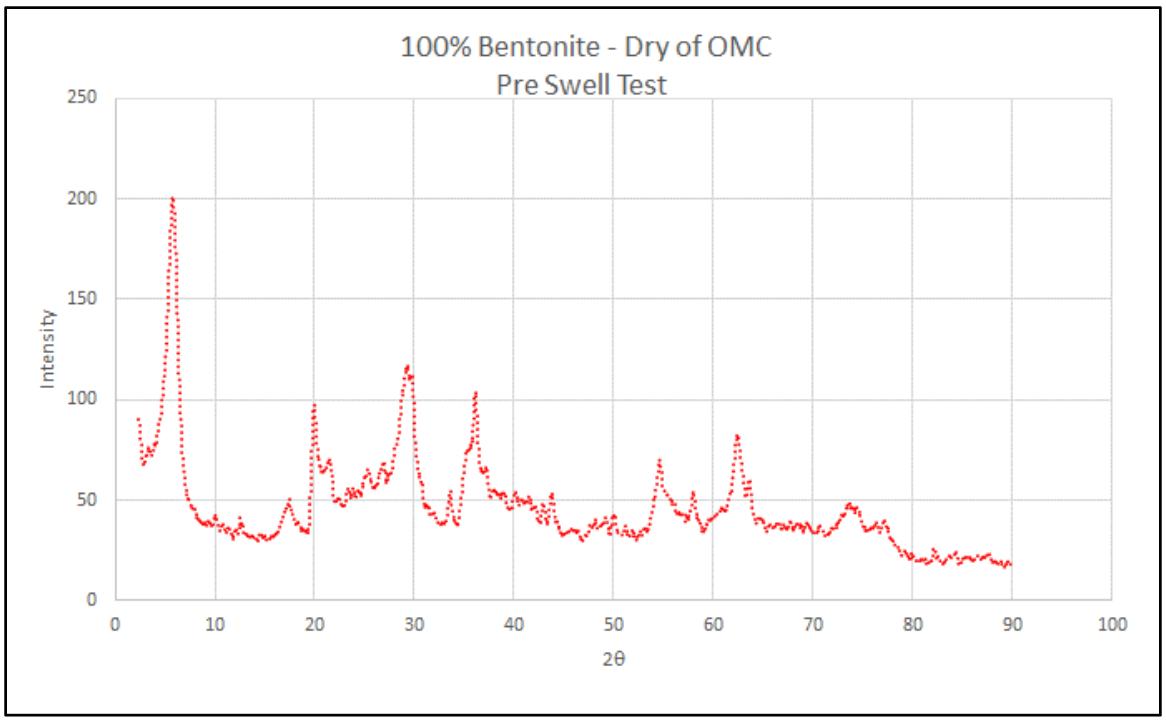

Figure A-6 XRD Results of 100 % bentonite compacted on dry of OMC – pre swell conditions

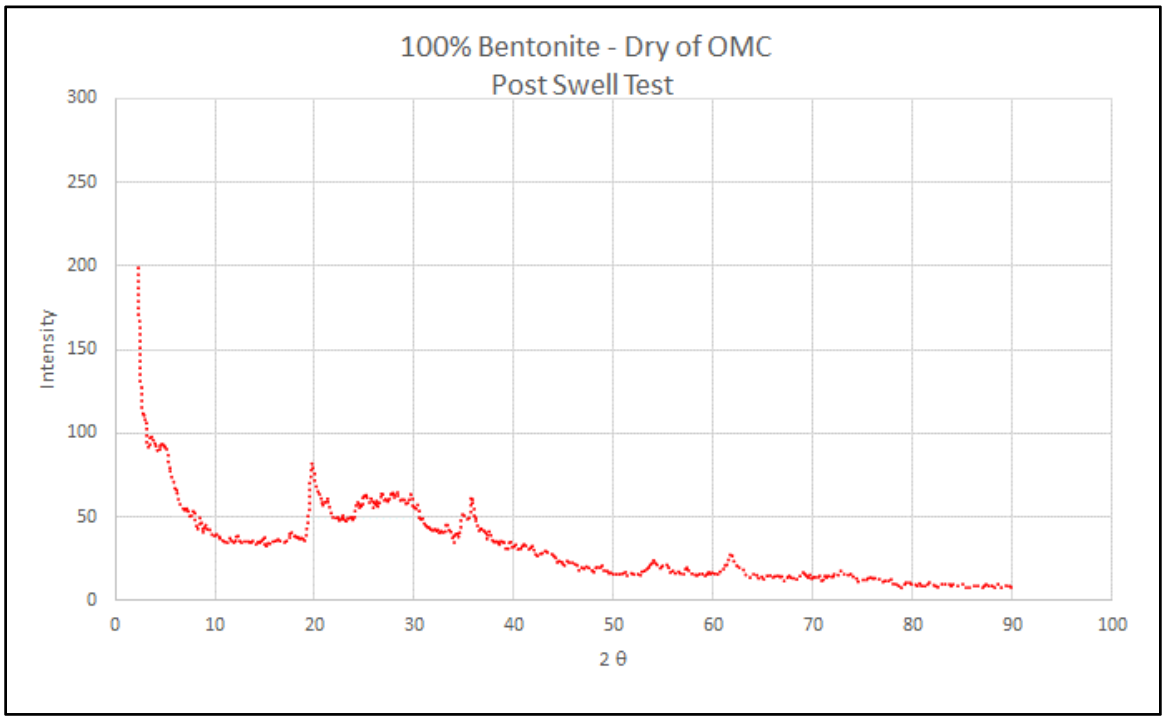

Figure A-7 XRD Results of 100 % bentonite compacted on dry of OMC – post swell conditions

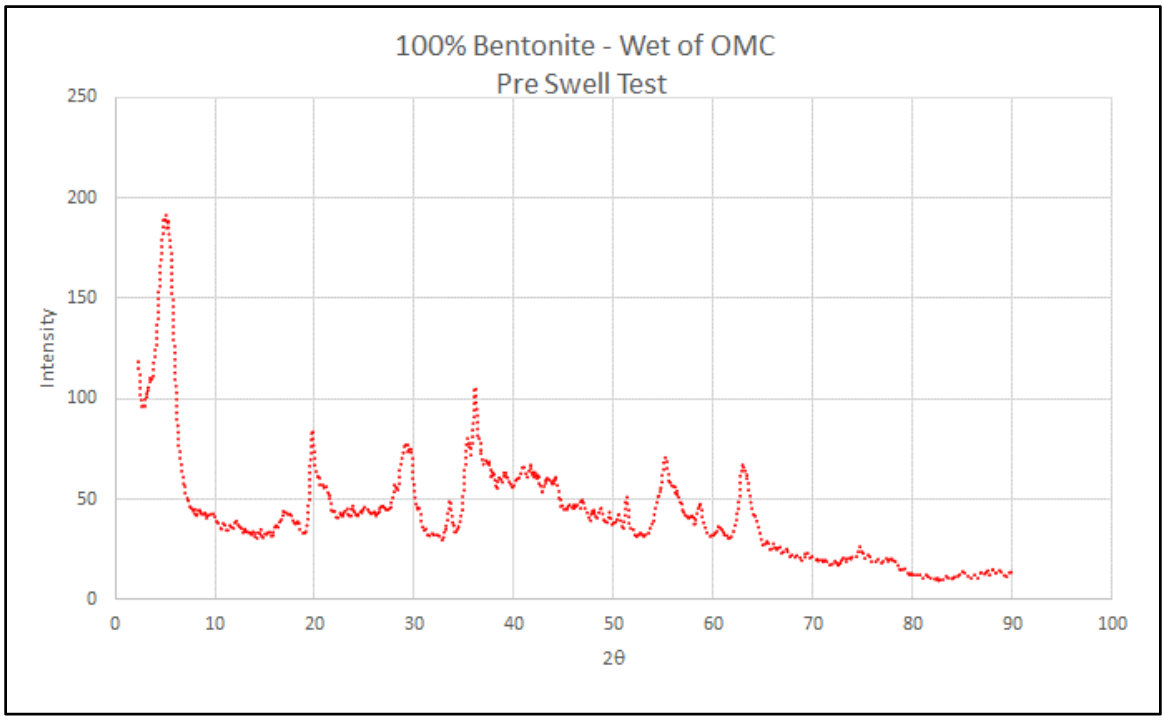

Figure A-8 XRD Results of 100 % bentonite compacted on wet of OMC – pre swell conditions

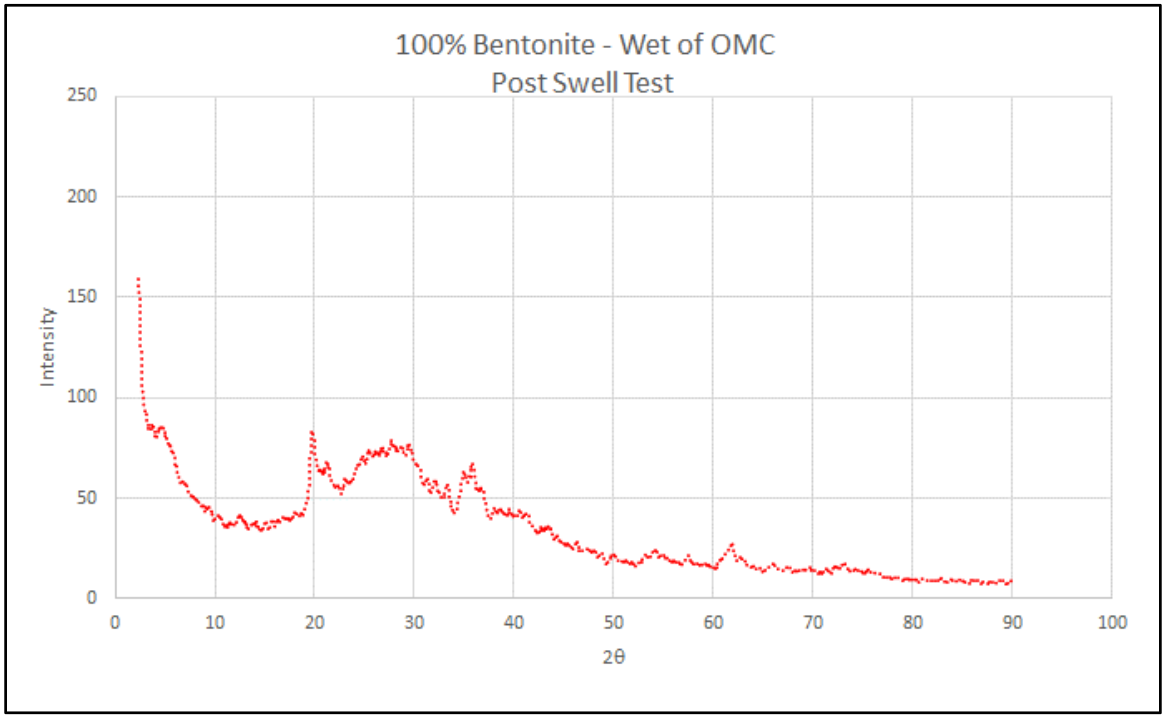

Figure A-9 XRD Results of 100 % bentonite compacted on dry of OMC – pre swell conditions

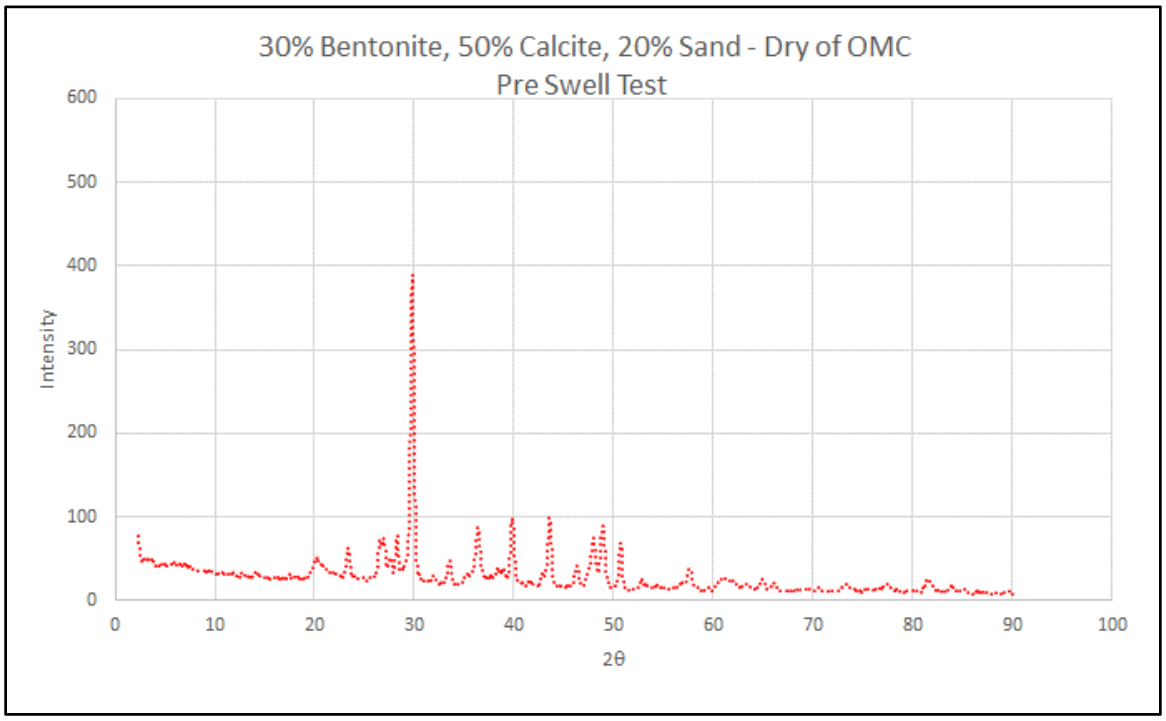

Figure A-10 XRD Results of 30% bentonite, 50% Calcite, and 20% Sand compacted on dry of OMC – pre swell conditions

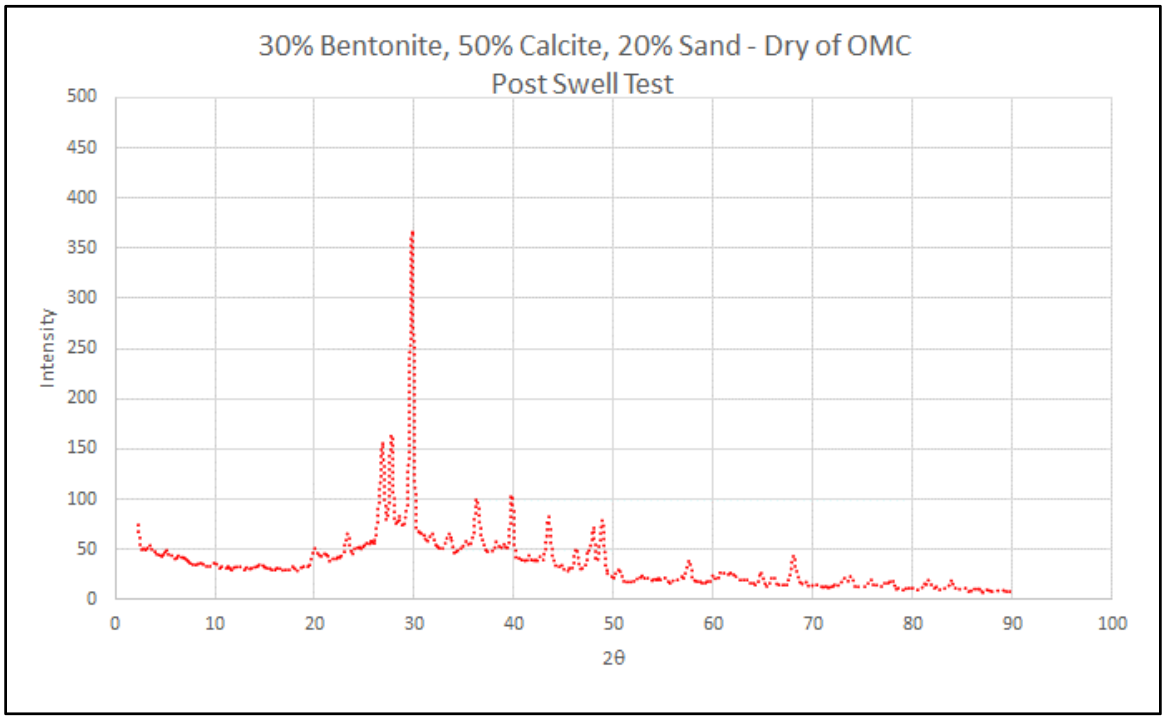

Figure A-11 XRD Results of 30% bentonite, 50% Calcite, and 20% Sand compacted on dry of OMC – post swell conditions

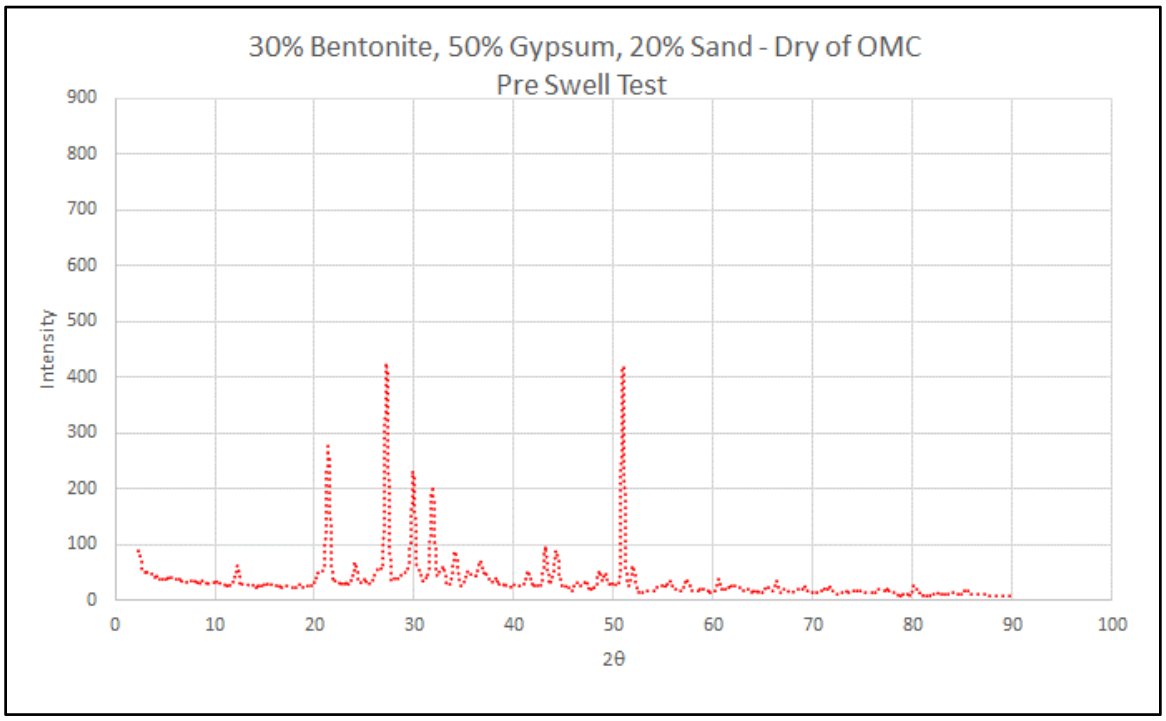

Figure A-12 XRD Results of 30% bentonite, 50% Gypsum, and 20% Sand compacted on dry of OMC – pre swell conditions

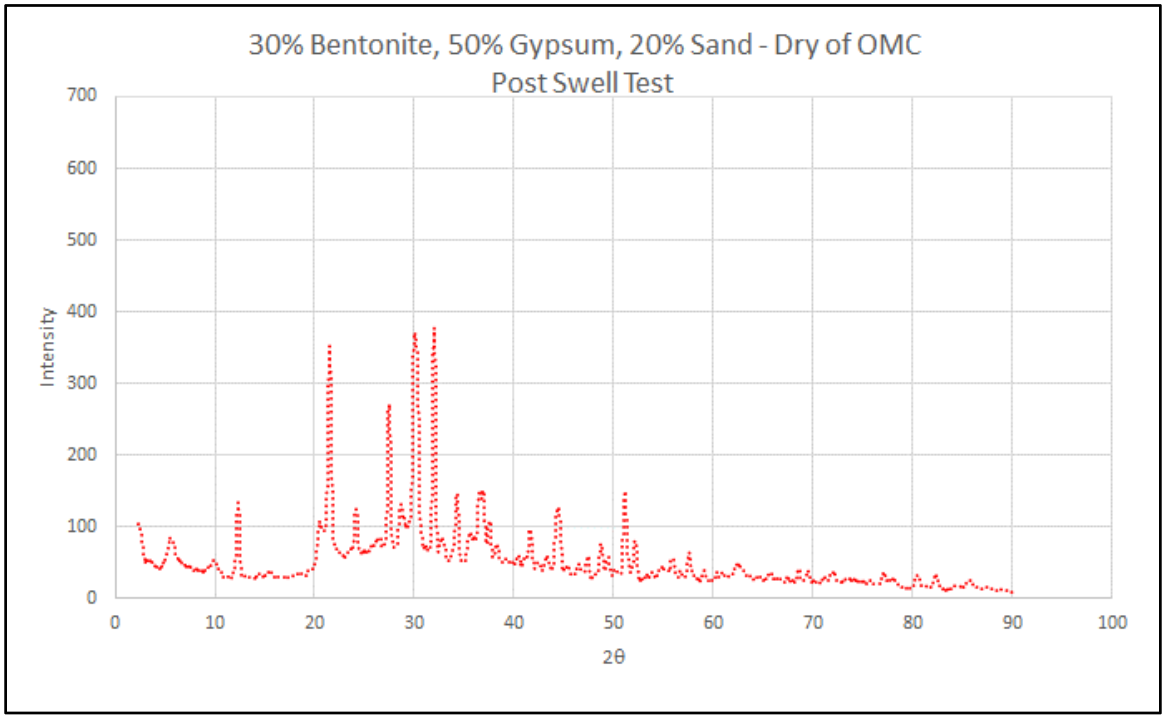

Figure A-13 XRD Results of 30 % bentonite, 50 % gypsum, and 20 % sand compacted on dry of OMC – post swell conditions

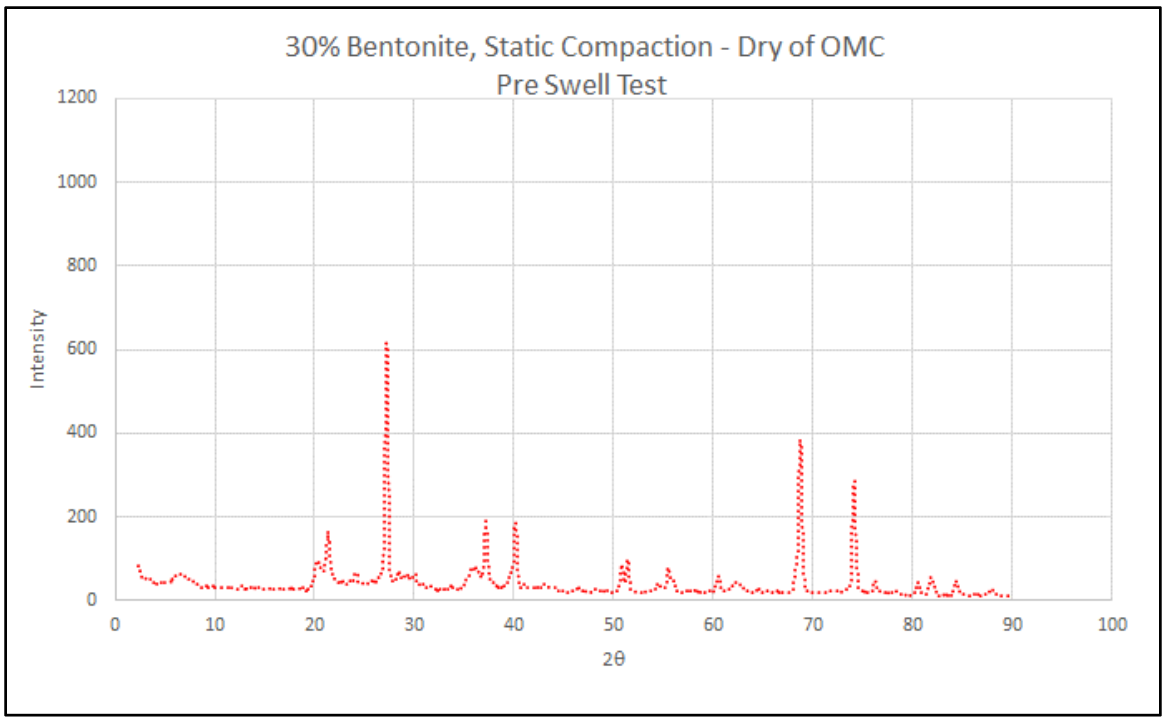

Figure A-14 XRD Results of 30 % bentonite, static compaction on dry of OMC – pre swell conditions

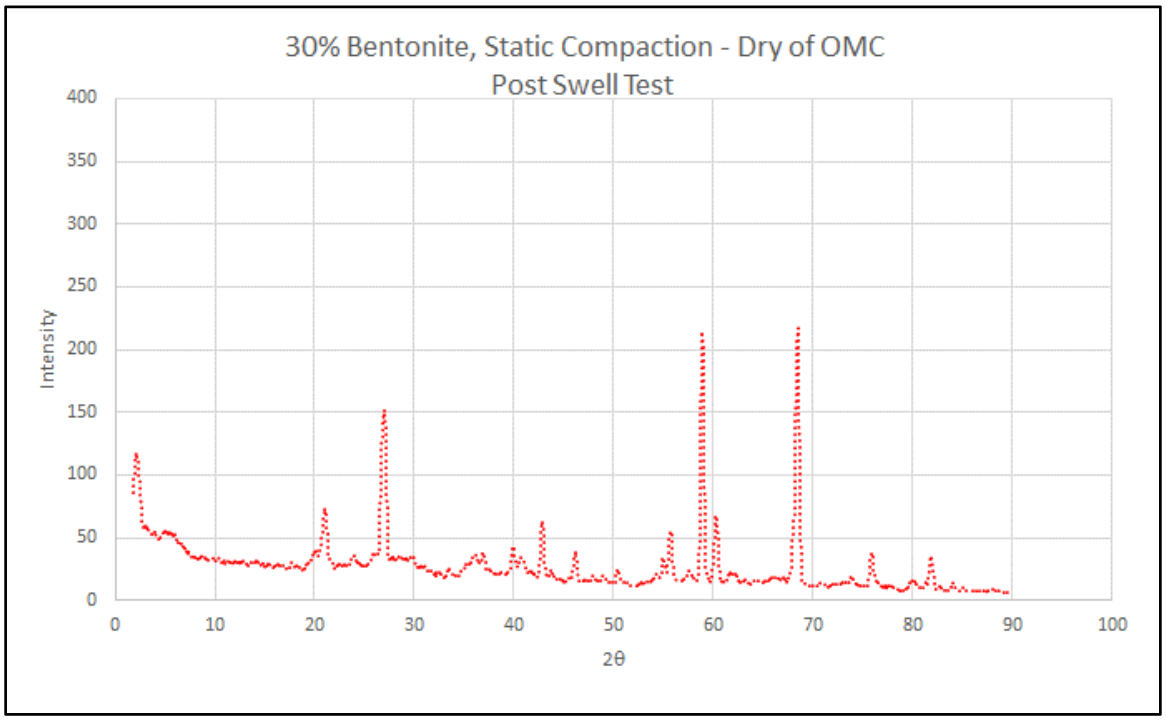

Figure A-15 XRD Results of 30 % bentonite, static compaction on dry of OMC – post swell conditions

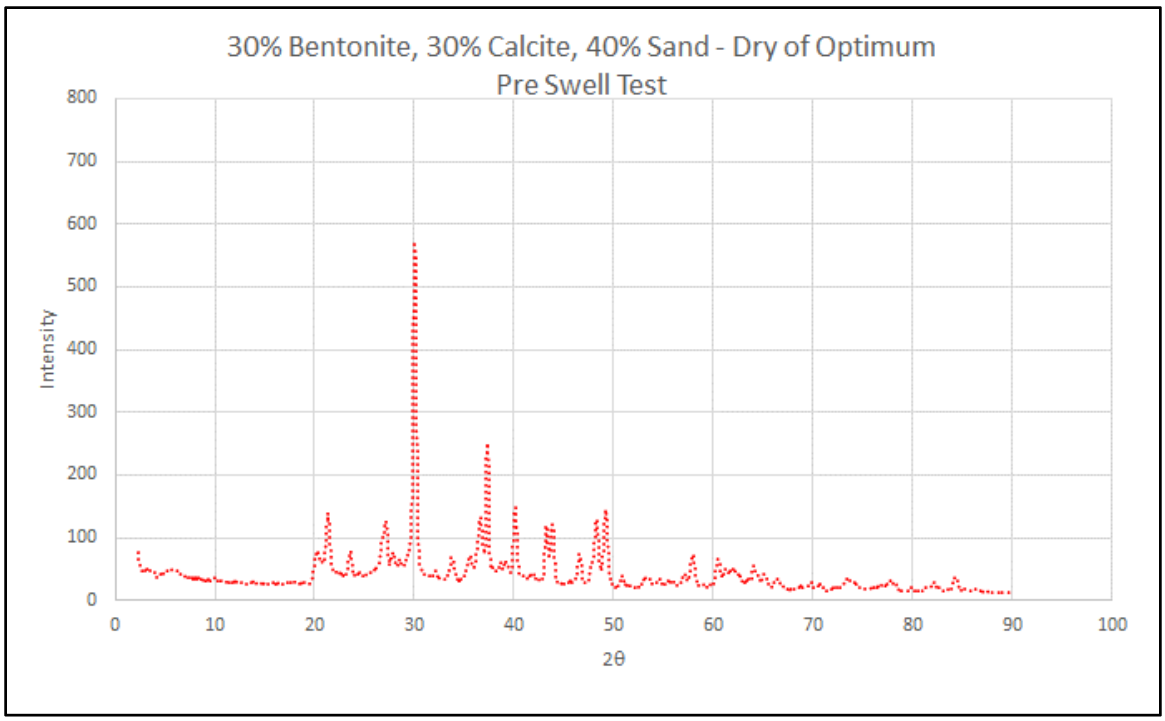

Figure A-16 XRD Results of 30 % bentonite, 30 % calcite, and 40 % sand compacted on dry of OMC – pre swell conditions

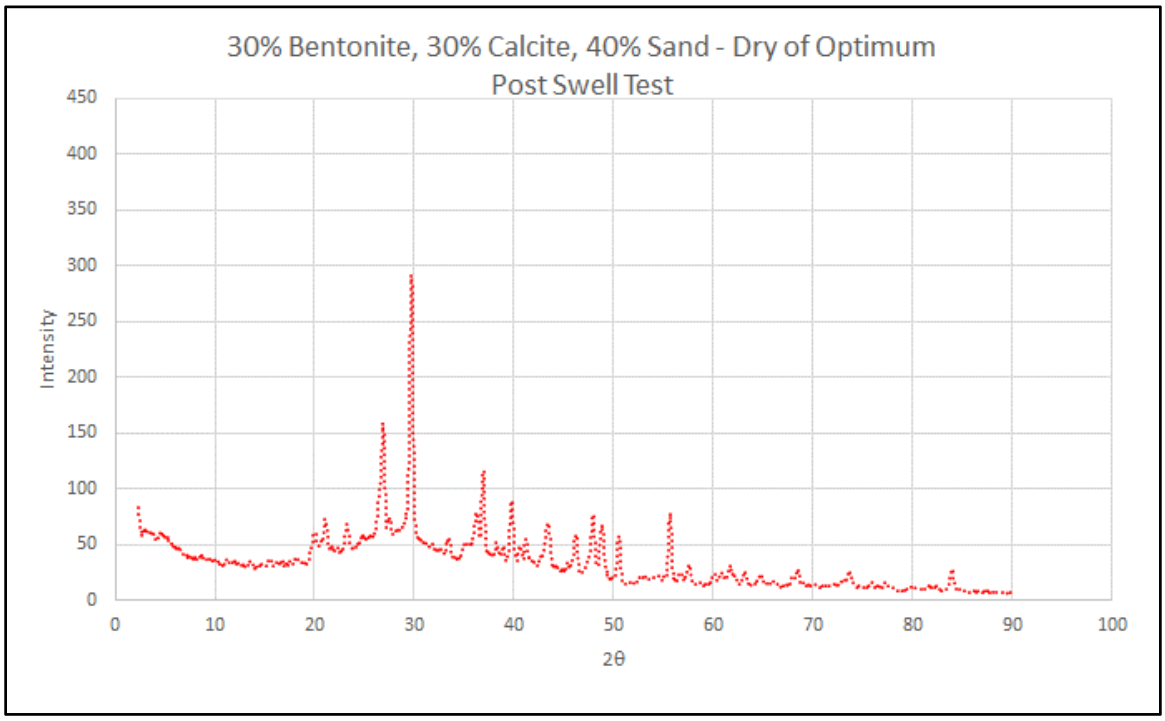

Figure A-17 XRD Results of 30 % bentonite, 30 % calcite, and 40 % sand compacted on dry of OMC – post swell conditions

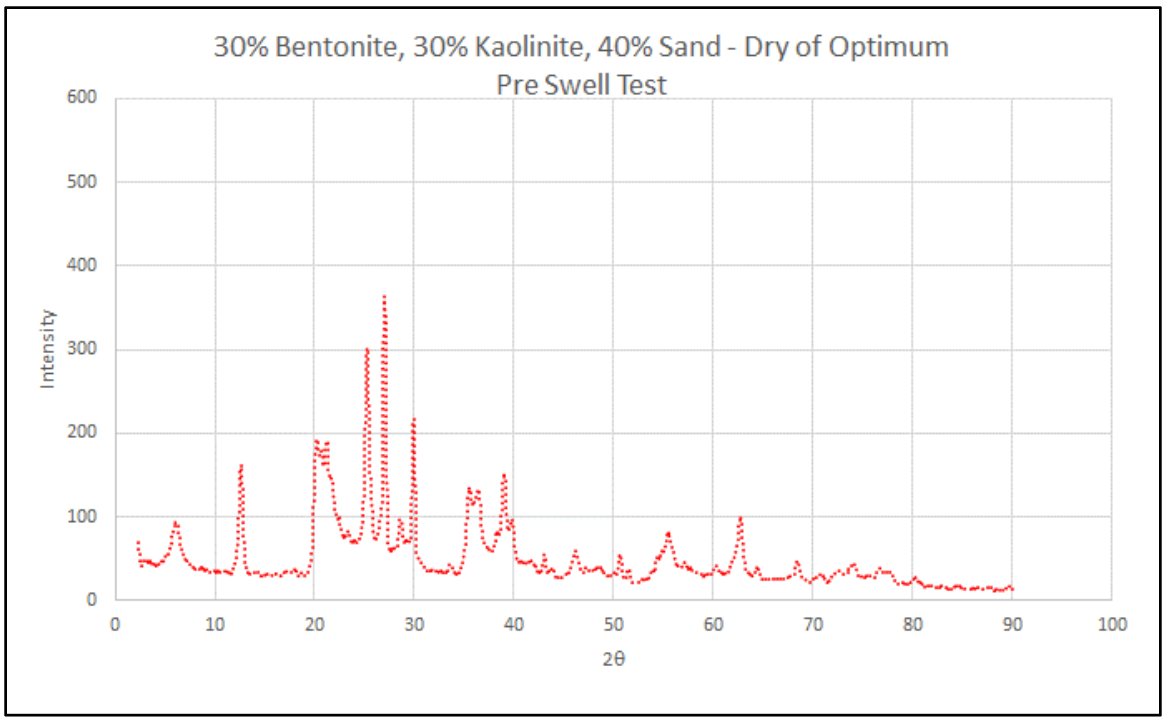

Figure A-18 XRD Results of 30 % bentonite, 30 % kaolinite, and 40 % sand compacted on dry of OMC – pre swell conditions

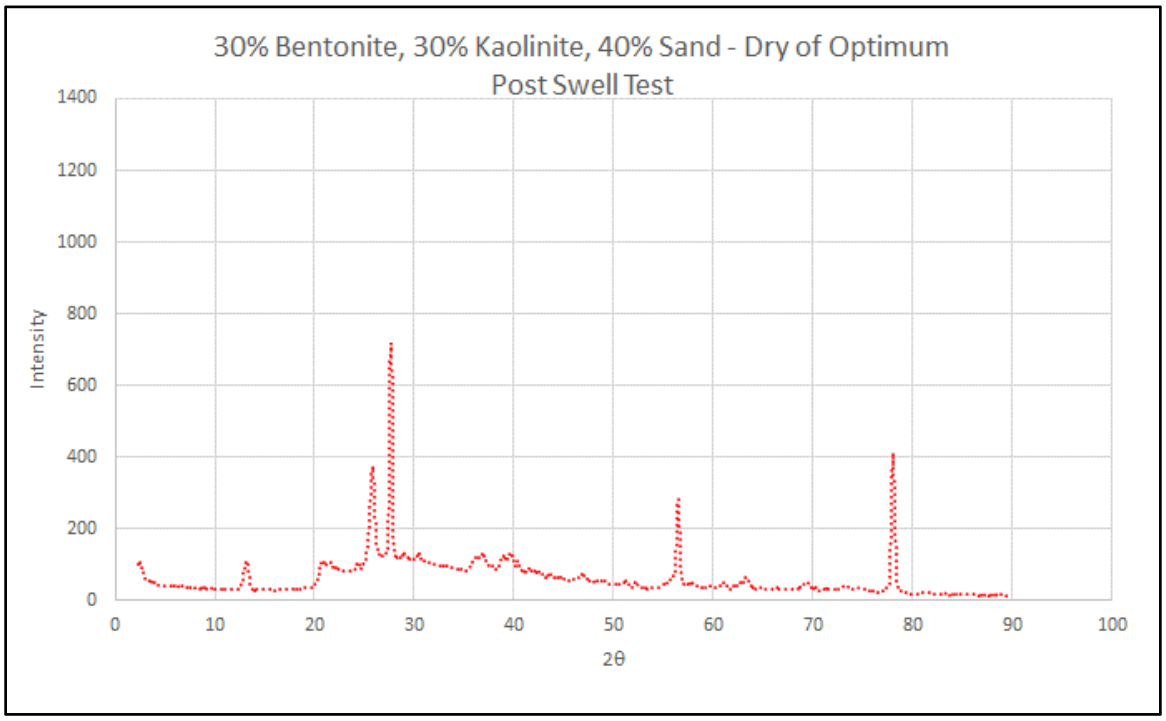

Figure A-19 XRD Results of 30 % bentonite, 30 % kaolinite, and 40 % sand compacted on dry of OMC – post swell conditions

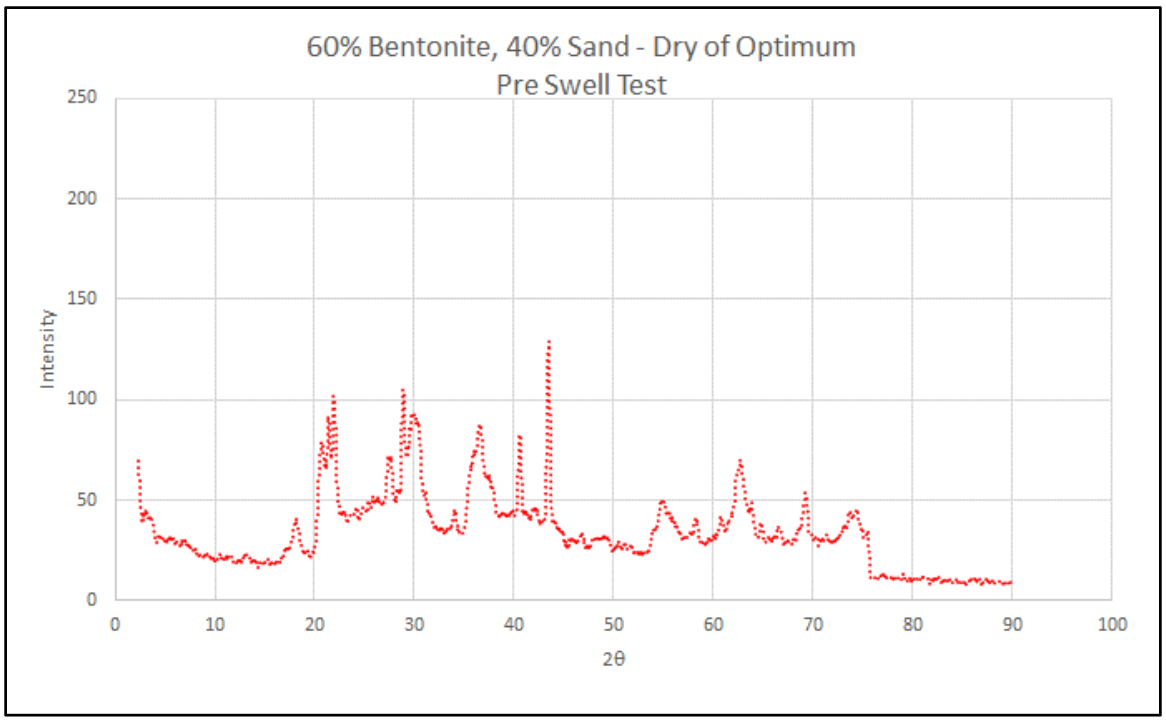

Figure A-20 XRD Results of 60 % bentonite and 40 % sand compacted on dry of OMC – pre swell conditions

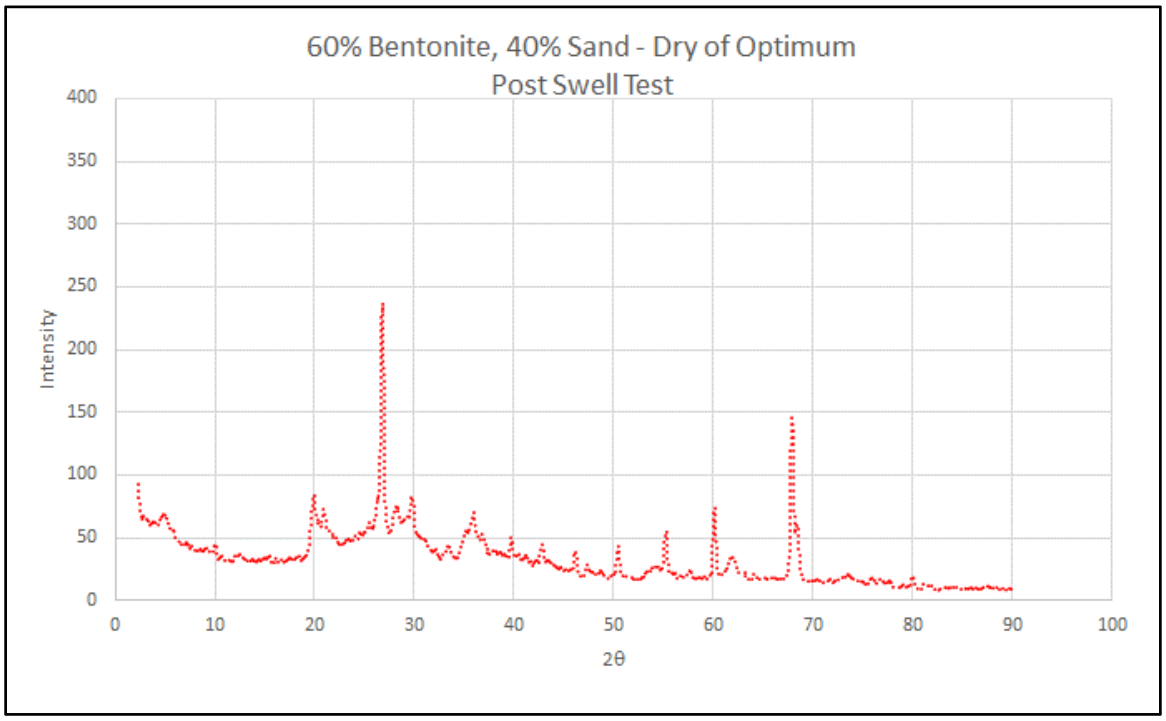

Figure A-21 XRD Results of 60 % bentonite and 20 % sand compacted on dry of OMC – post swell conditions

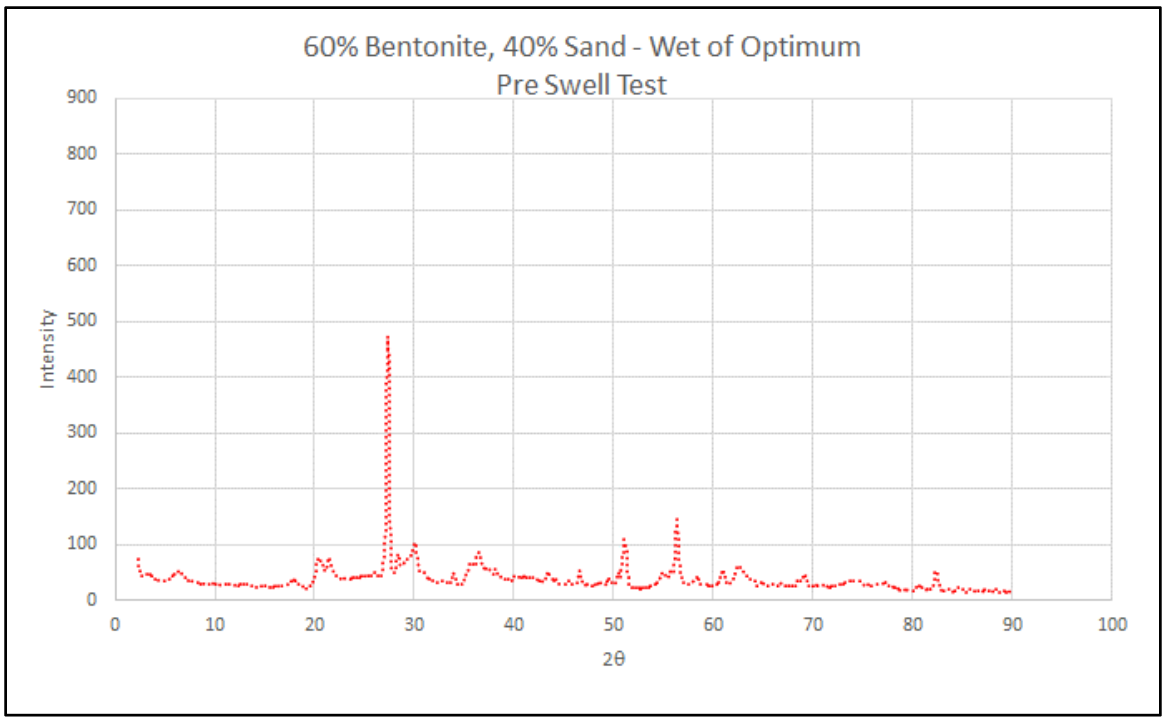

Figure A-22 XRD Results of 60 % bentonite, and 40 % sand compacted on wet of OMC – pre swell conditions

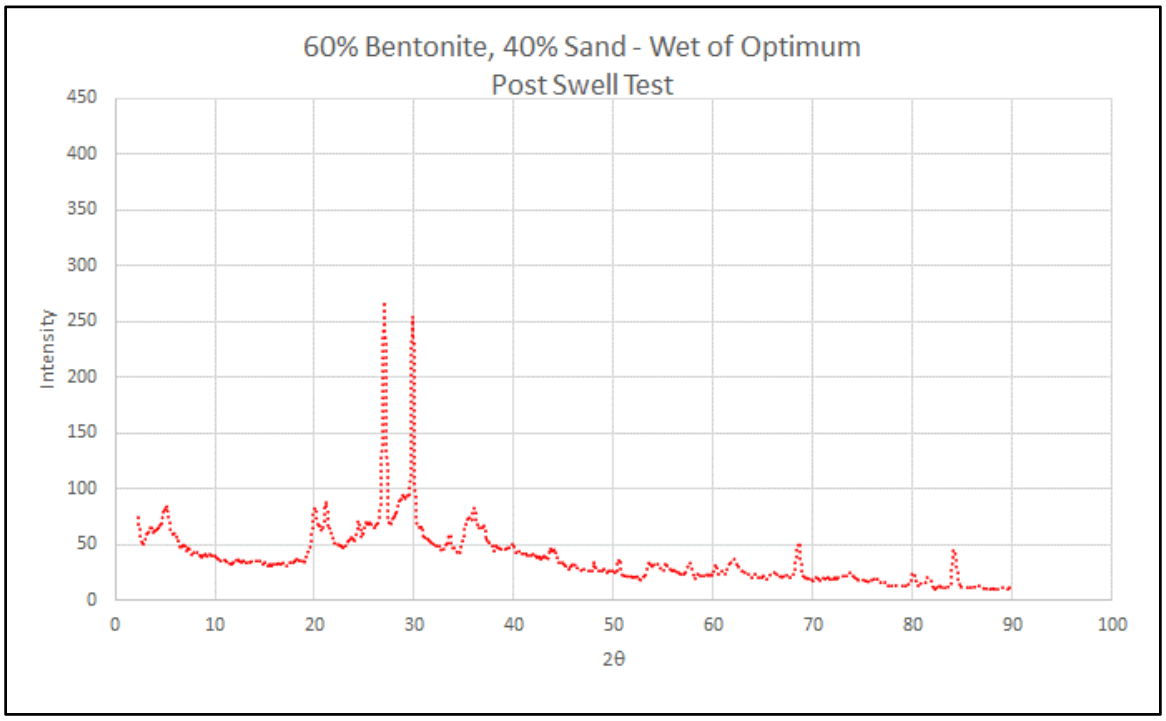

Figure A-23 XRD Results of 60 % Bentonite and 40 % Sand compacted on wet of OMC – post swell conditions

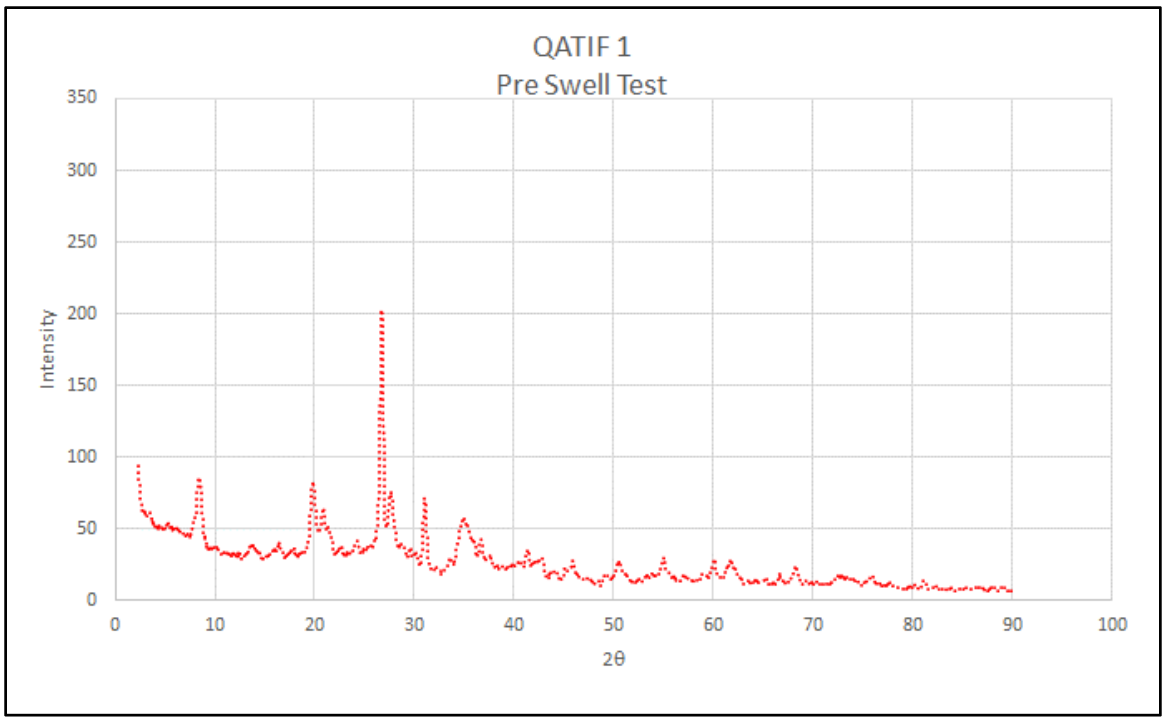

Figure A-24 XRD Results of Qatif-1 sample at NMC – pre swell conditions

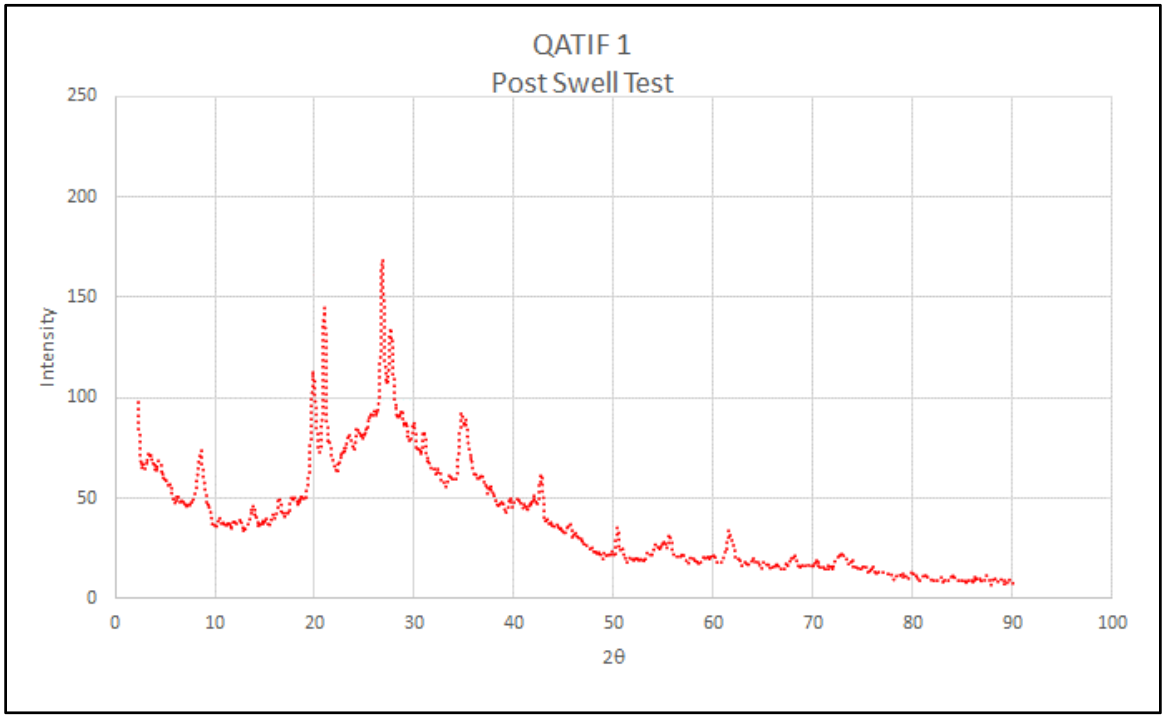

Figure A-25 XRD Results of Qatif-1 sample at NMC – post swell conditions

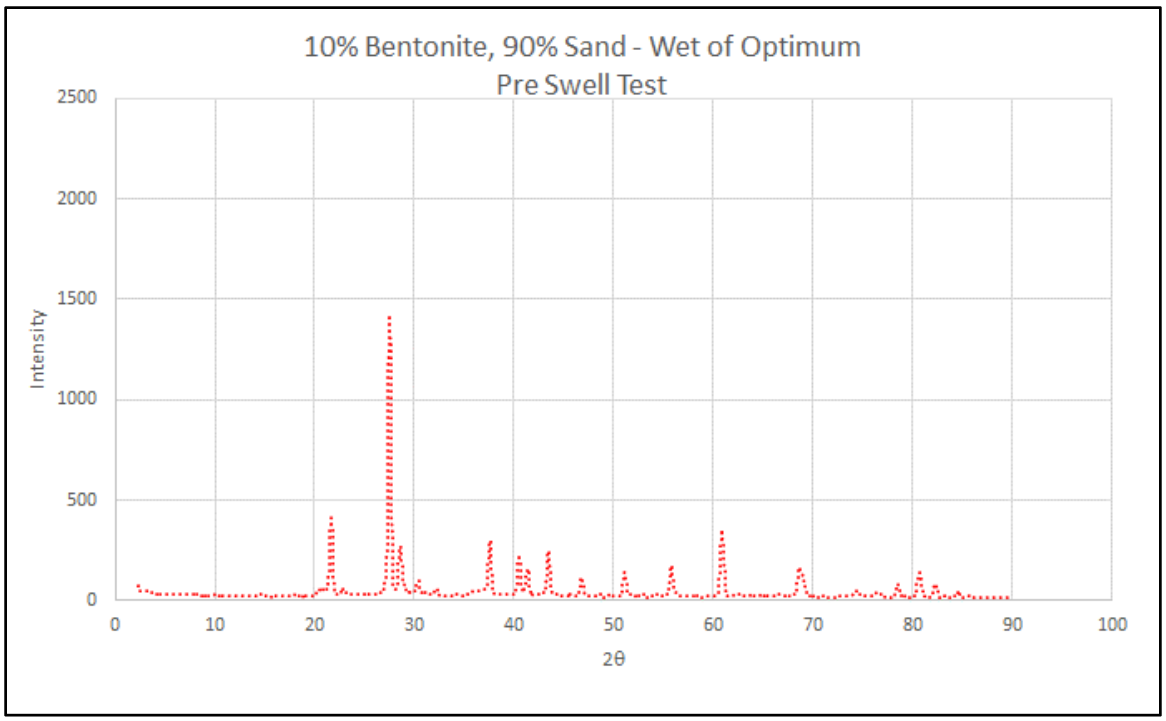

Figure A-26 XRD Results of 10 % Bentonite and 90 % Sand compacted on wet of OMC – pre swell conditions

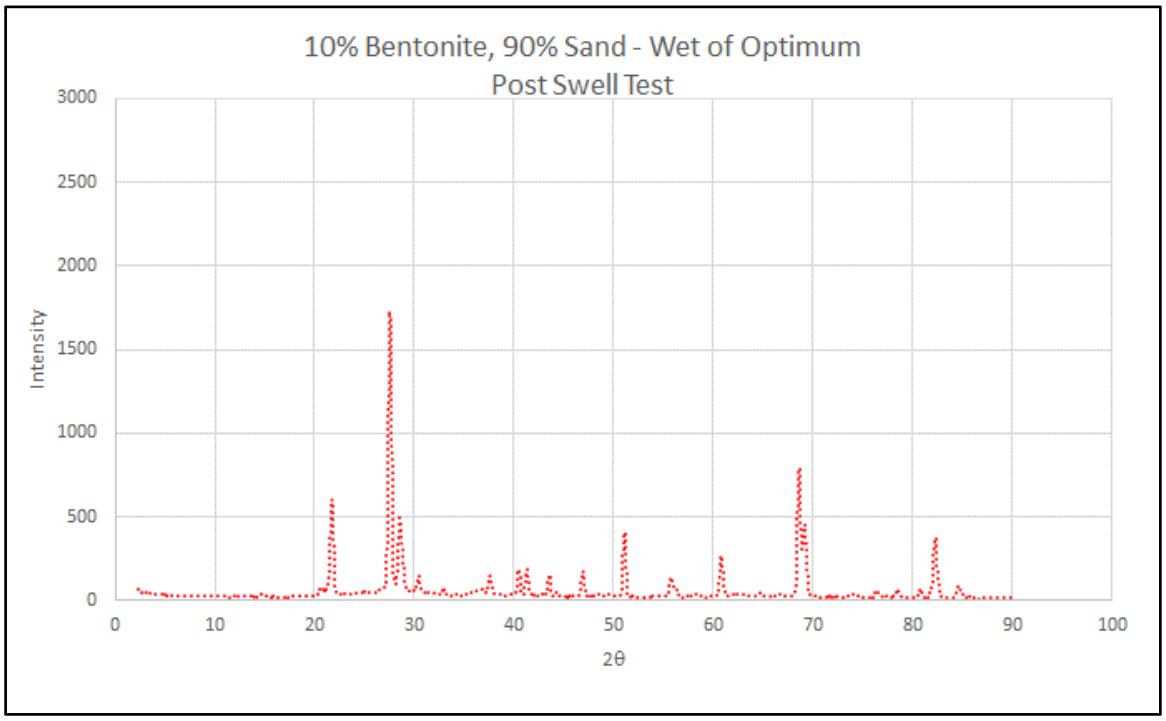

Figure A-27 XRD Results of 10 % Bentonite and 90 % Sand compacted on wet of OMC – post swell conditions

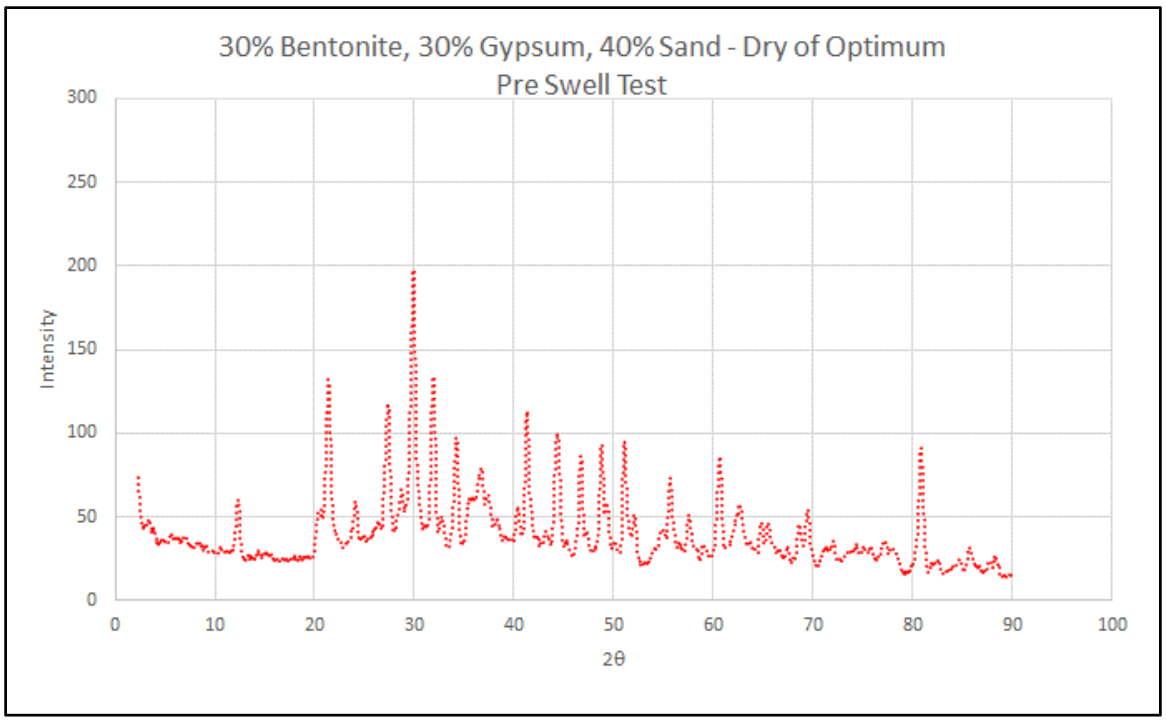

Figure A-28 XRD Results of 30 % Bentonite, 30 % Gypsum, and 40% Sand compacted on dry of OMC – pre swell conditions

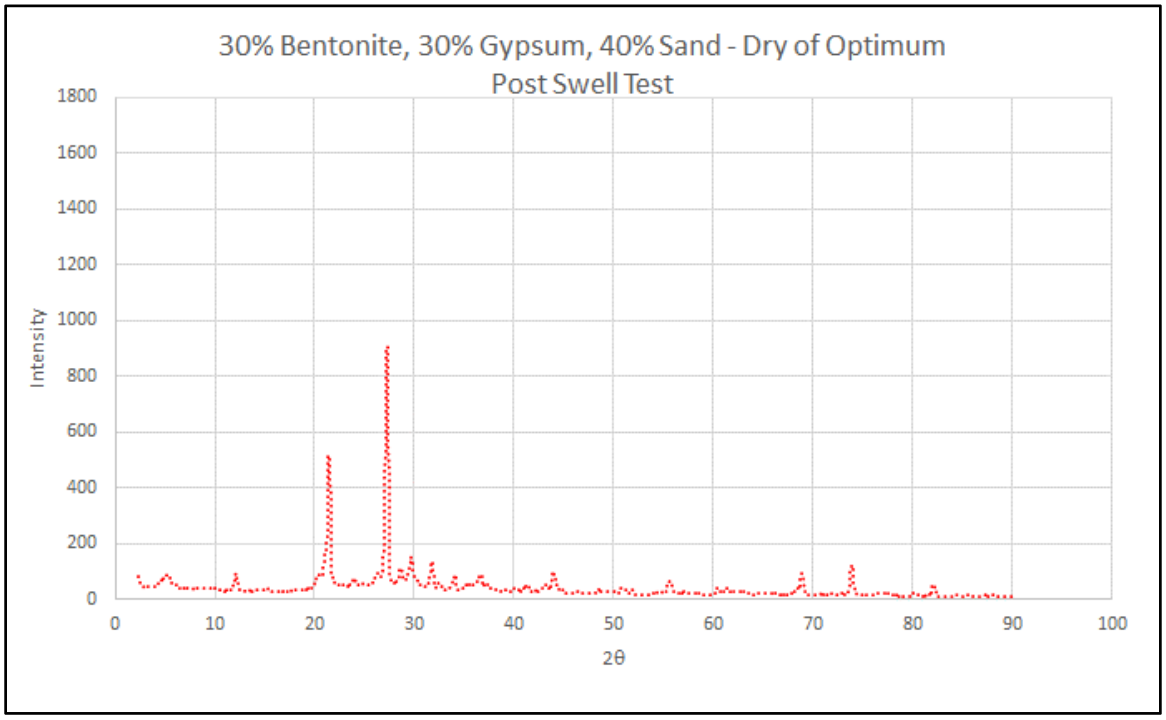

Figure A-29 XRD Results of 30% Bentonite, 30 % Gypsum, and 40 % Sand compacted on dry of OMC – post swell conditions

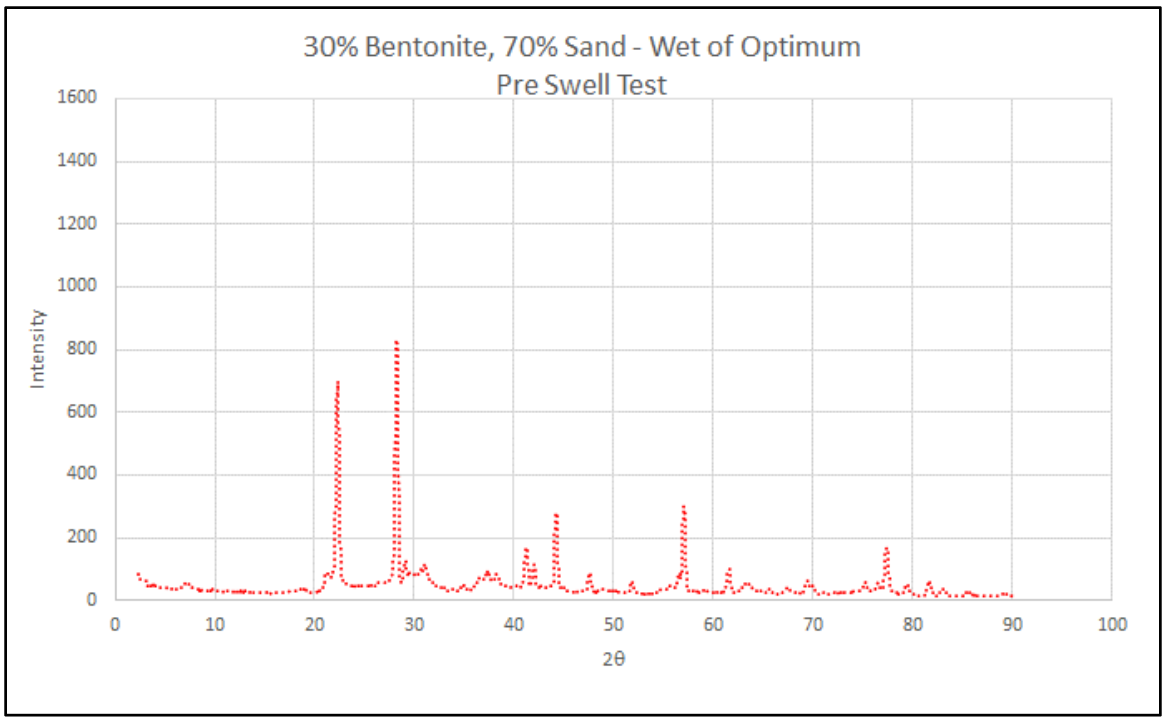

Figure A-30 XRD Results of 30 % Bentonite and 70 % Sand compacted on wet of OMC – pre swell conditions

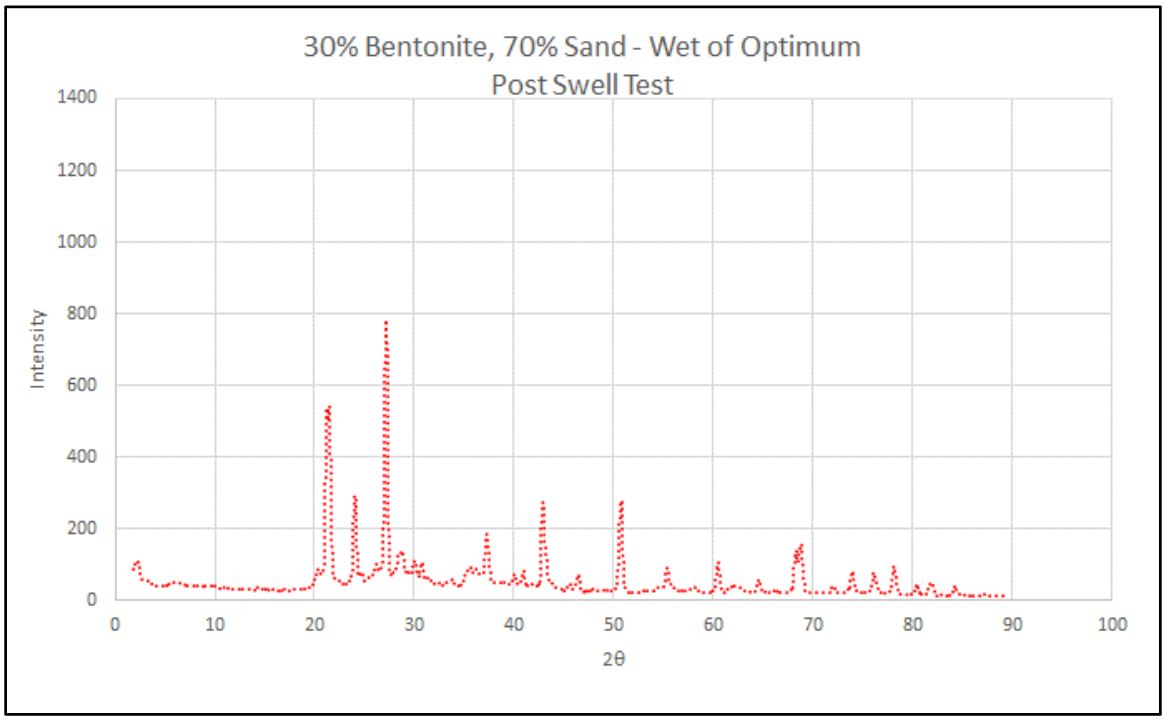

Figure A-31 XRD Results of 30 % Bentonite and 70 % Sand compacted on wet of OMC – post swell conditions

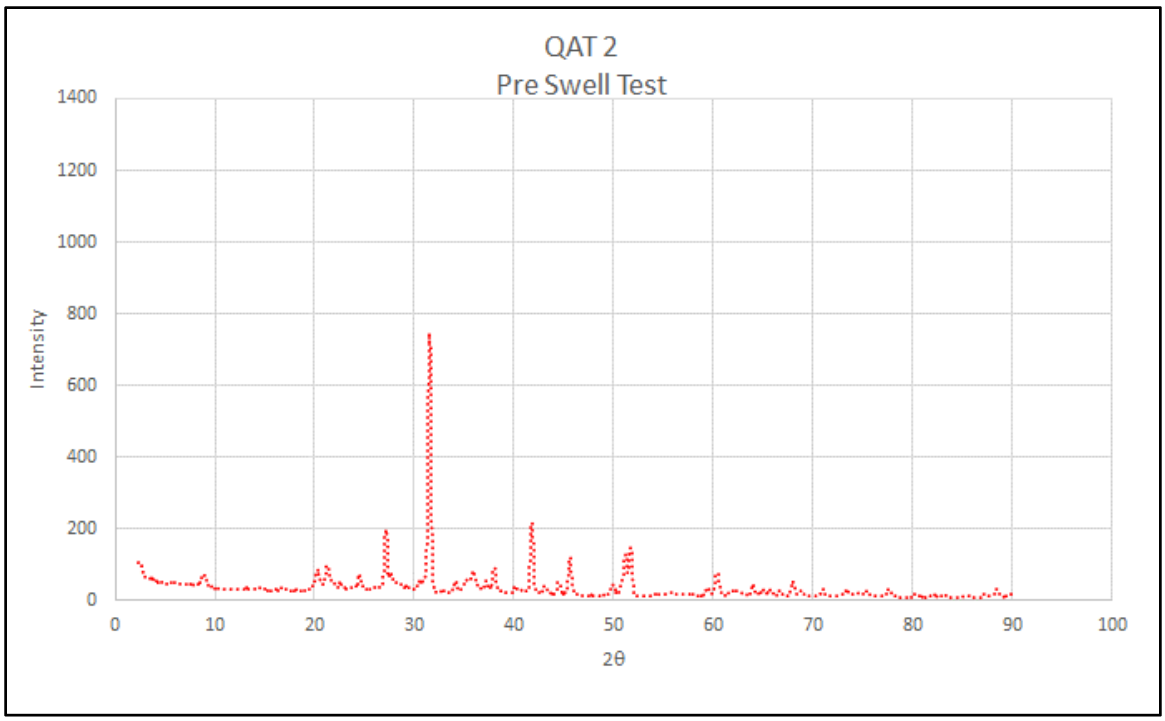

Figure A-32 XRD Results Qatif-2 sample at NMC – pre swell conditions

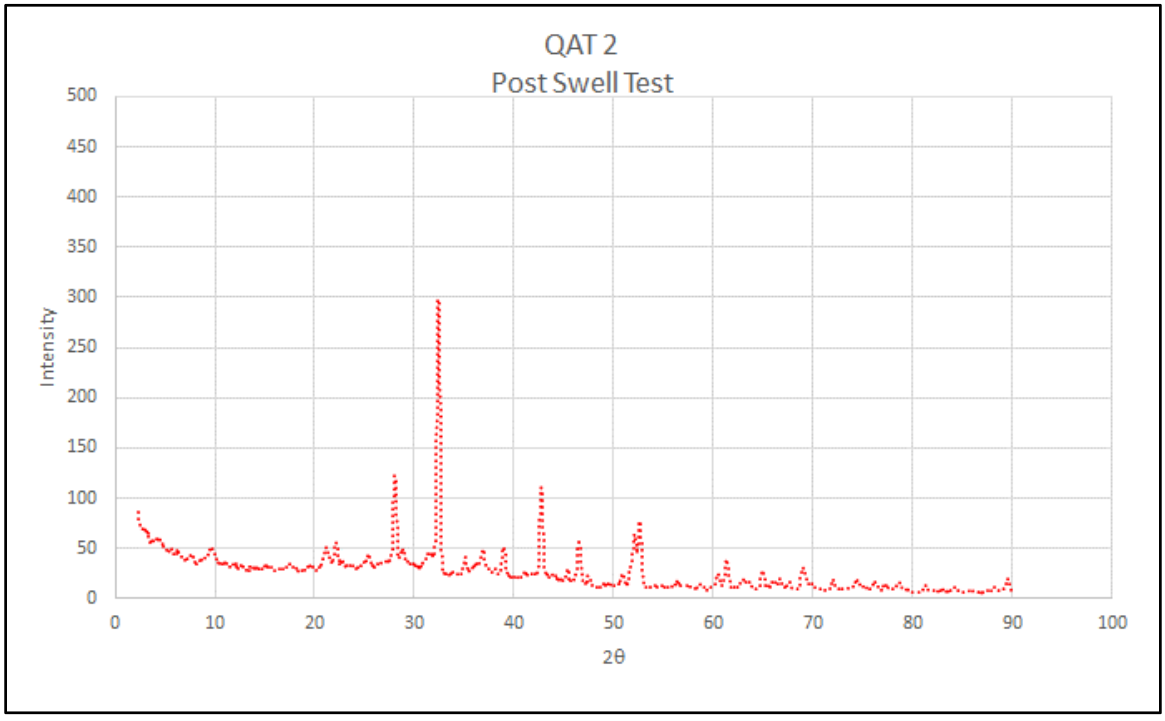

Figure A-33 XRD Results of Qatif-2 sample at NMC – post swell conditions

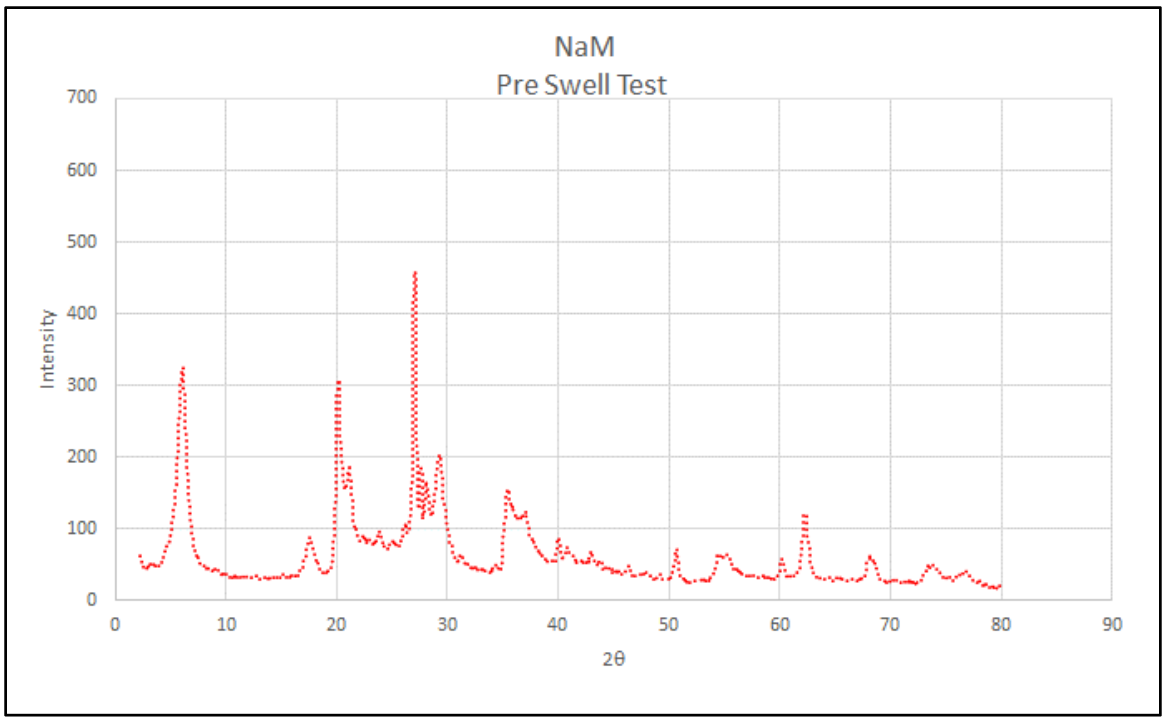

Figure A-34 XRD Results of Na-montmorillonite from The Clay Minerals Society compacted on dry of OMC – pre swell conditions

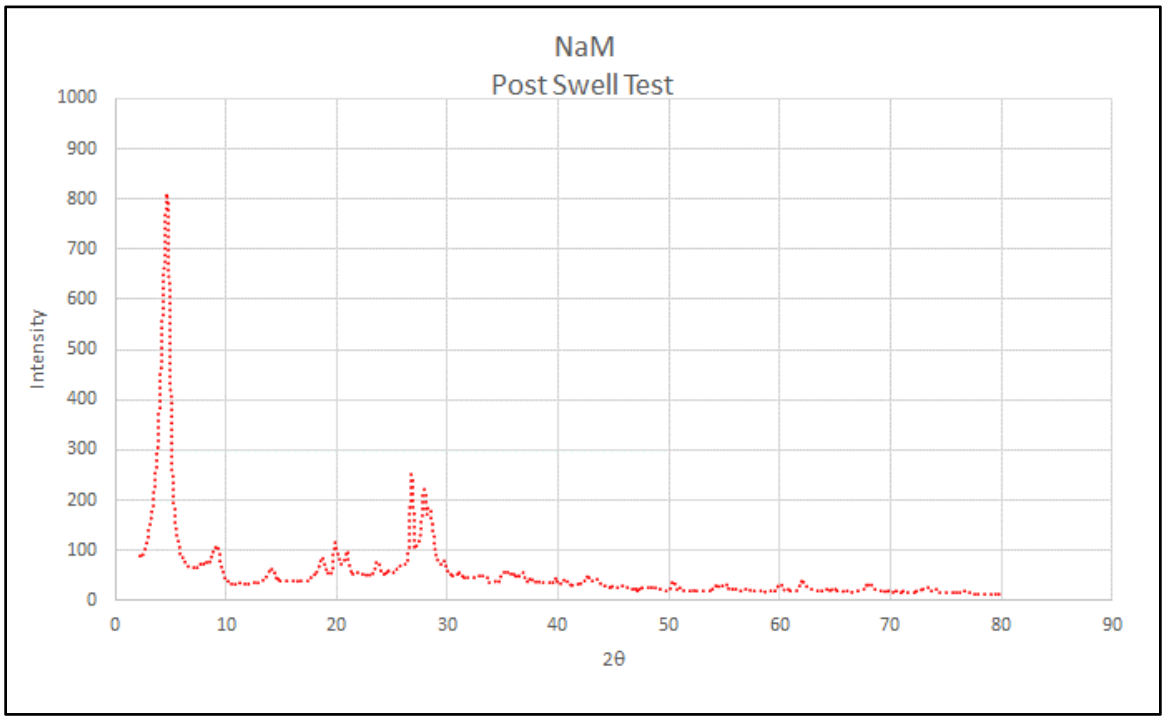

Figure A-35 XRD Results of Na-montmorillonite from The Clay Minerals Society compacted on dry of OMC – post swell conditions

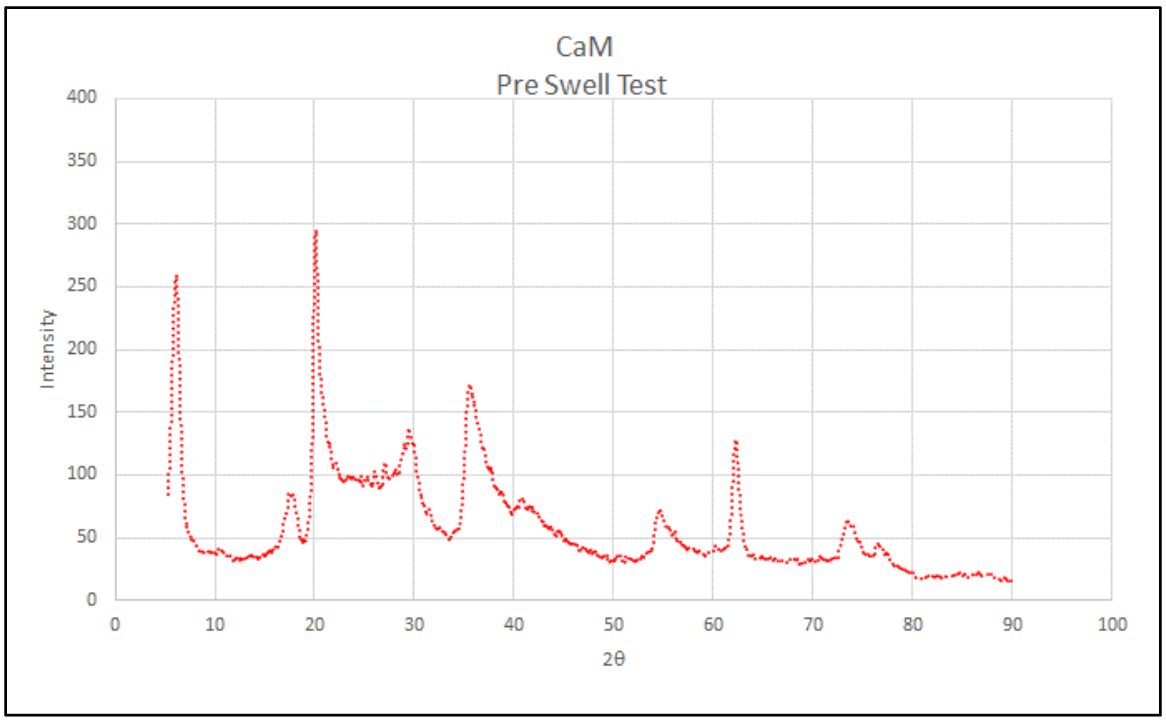

Figure A-36 XRD Results of Ca-montmorillonite from The Clay Minerals Society compacted on dry of OMC – pre swell conditions

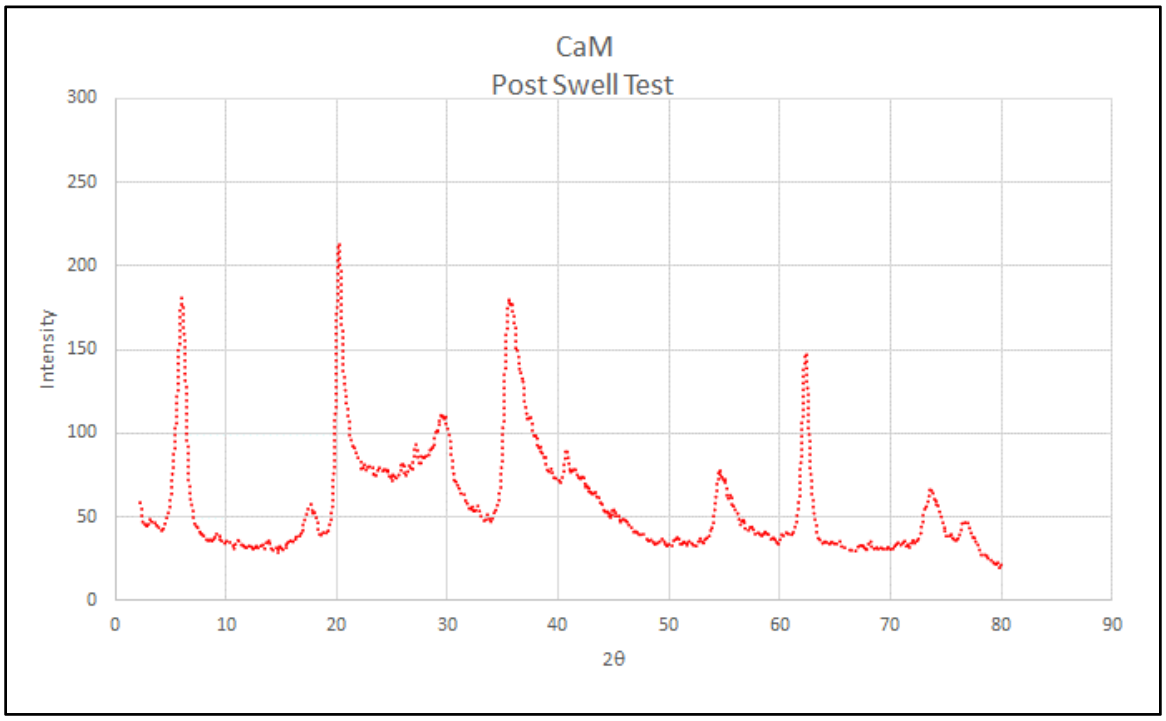

Figure A-37 XRD Results of Ca-montmorillonite from The Clay Minerals Society compacted on dry of OMC – post swell conditions

Appendix B - FTIR Results

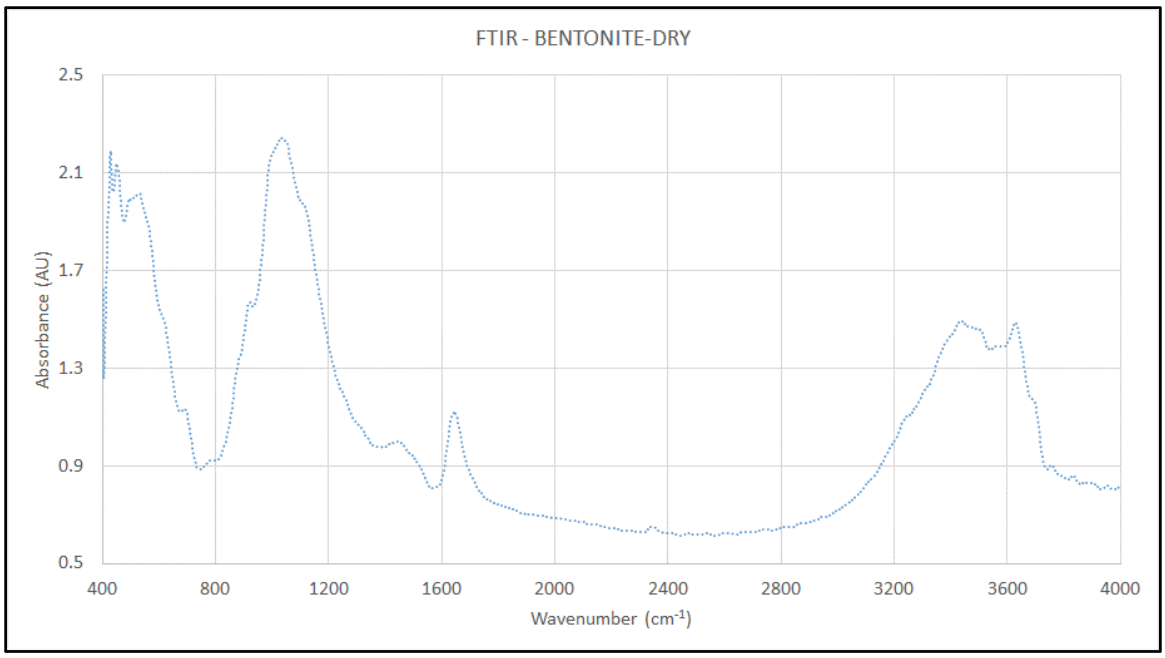

Figure B-1 FTIR results of dry Bentonite sample

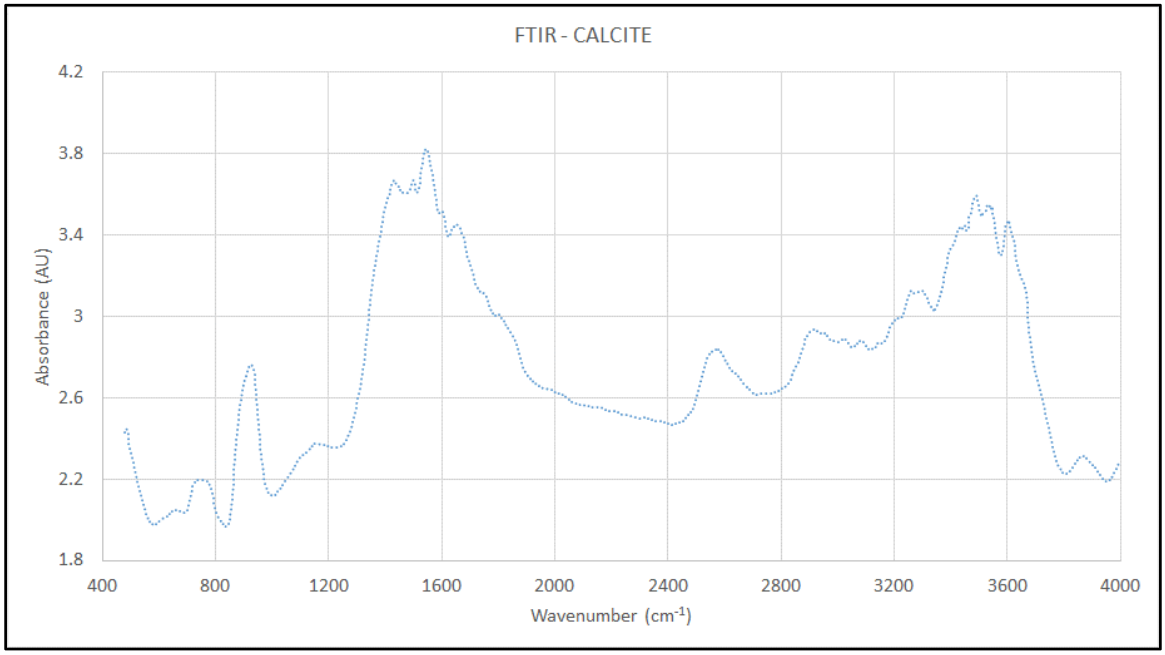

Figure B-2 FTIR results of Calcium Carbonate sample

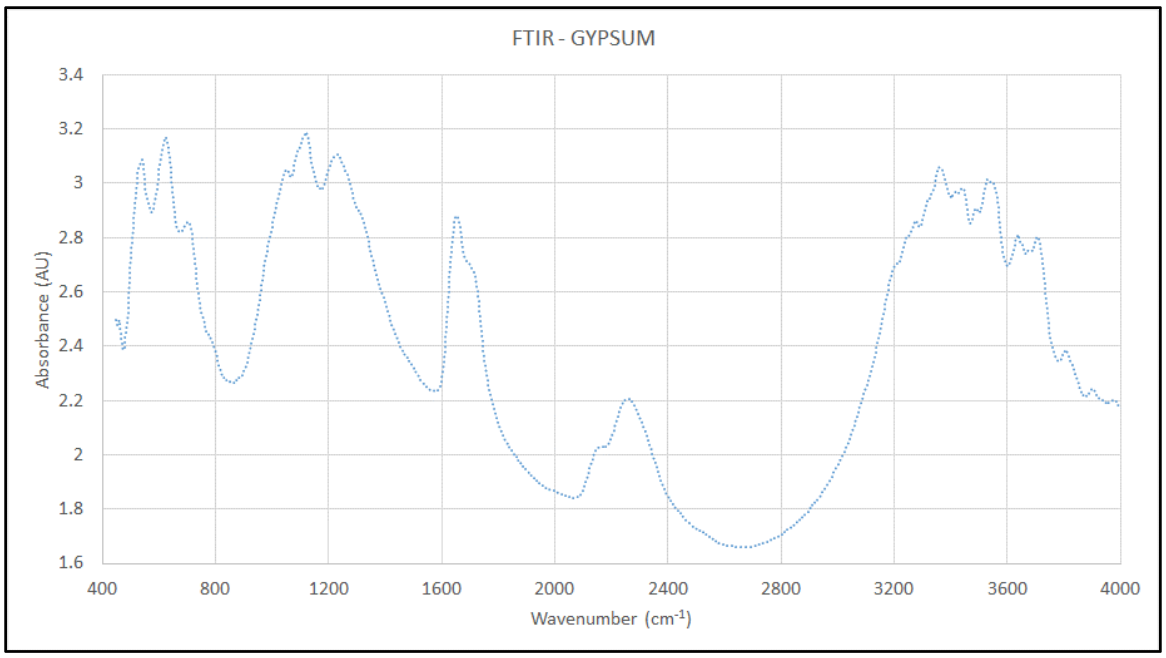

Figure B-3 FTIR results of Gypsum sample

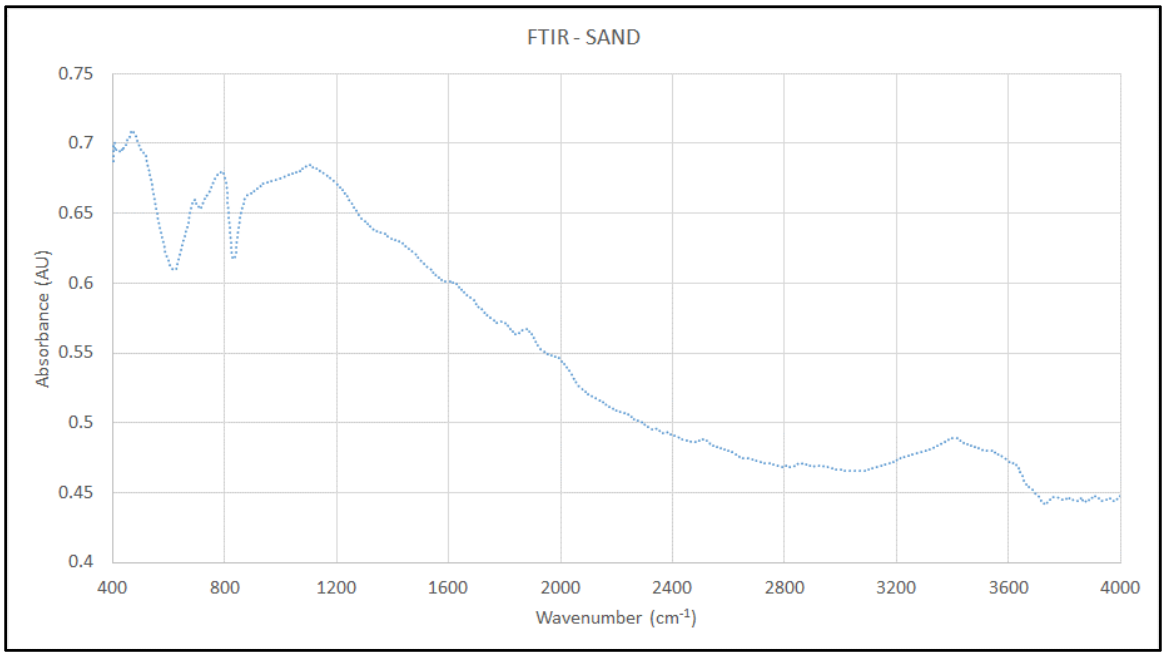

Figure B-4 FTIR results of Sand sample

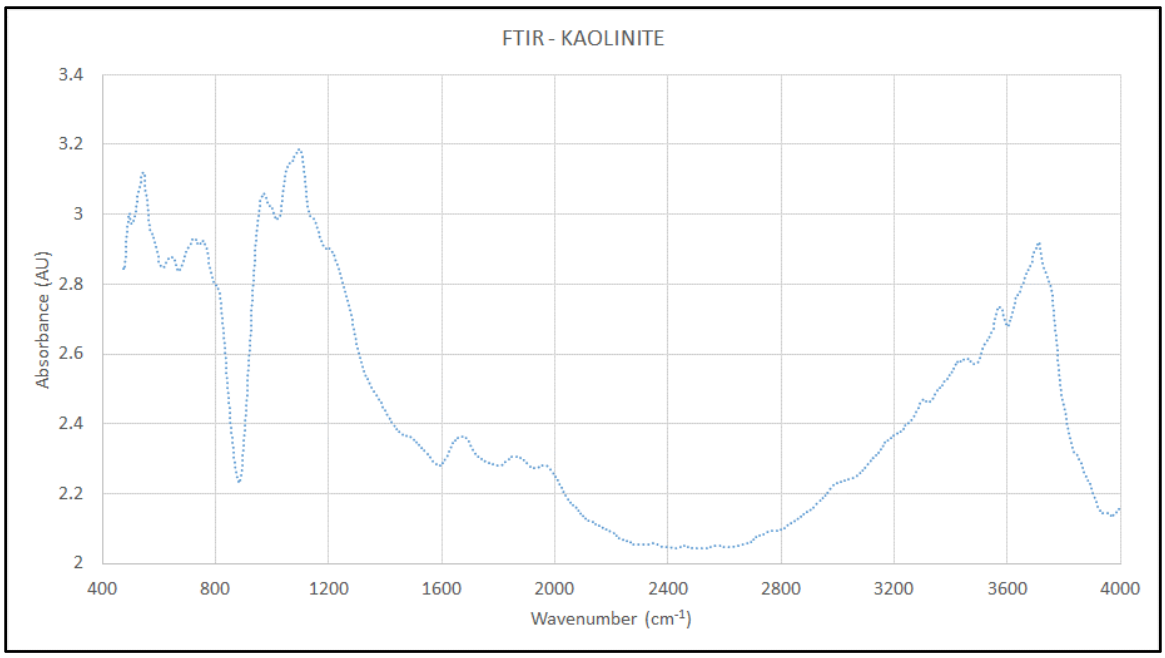

Figure B-5 FTIR results of Kaolinite sample

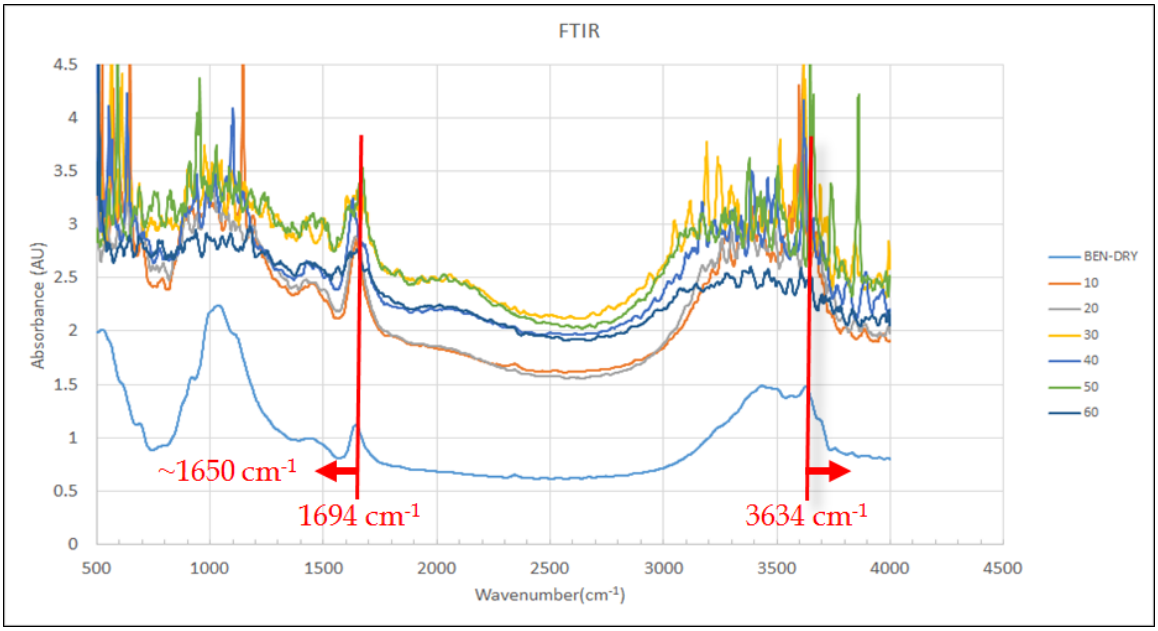

Figure B-6 Comparison of FTIR results of dry Bentonite and at various moisture contents from 10% to 60%

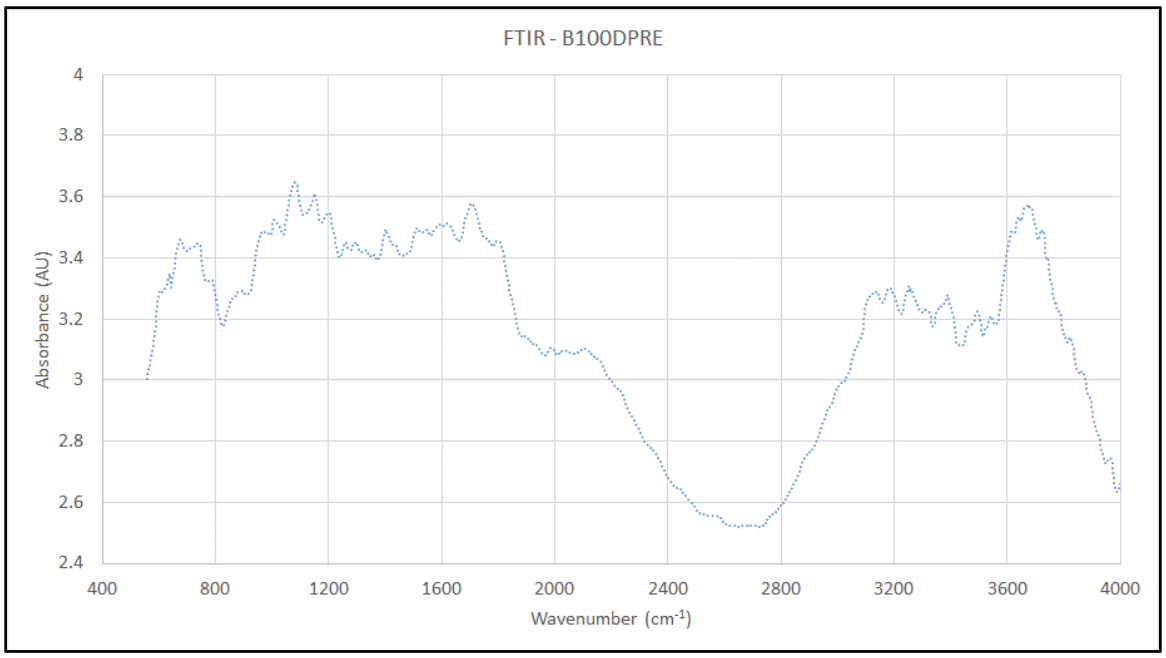

Figure B-7 FTIR results of 100% Bentonite compacted on dry of OMC – pre swell conditions

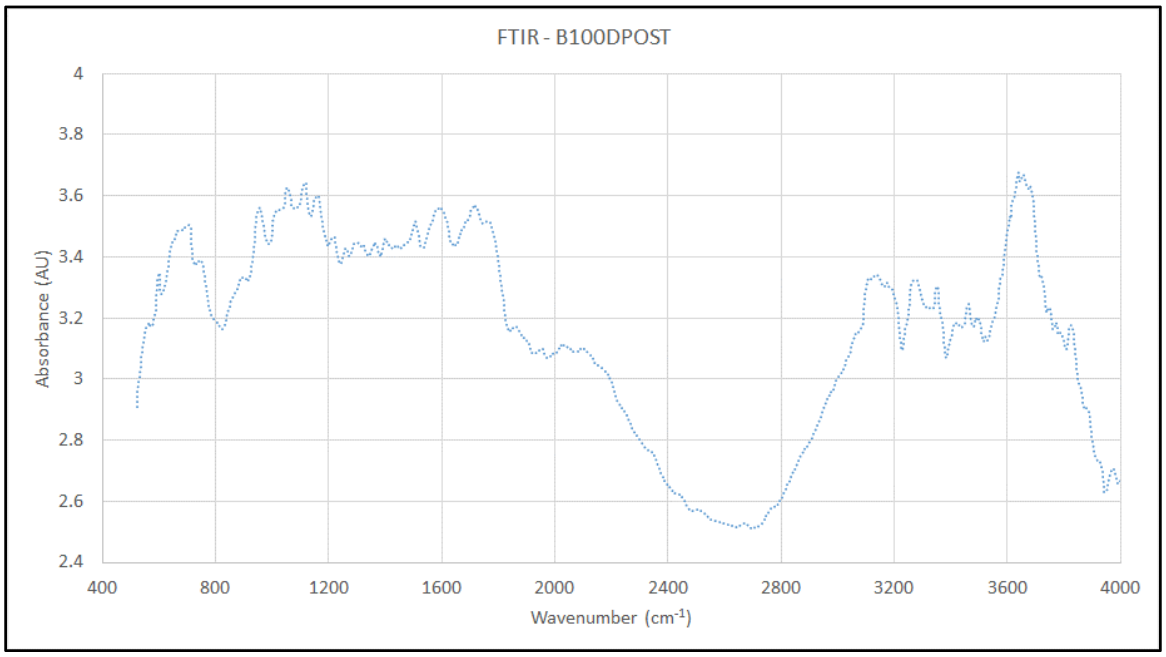

Figure B-8 FTIR results of 100% Bentonite compacted on dry of OMC – post swell conditions

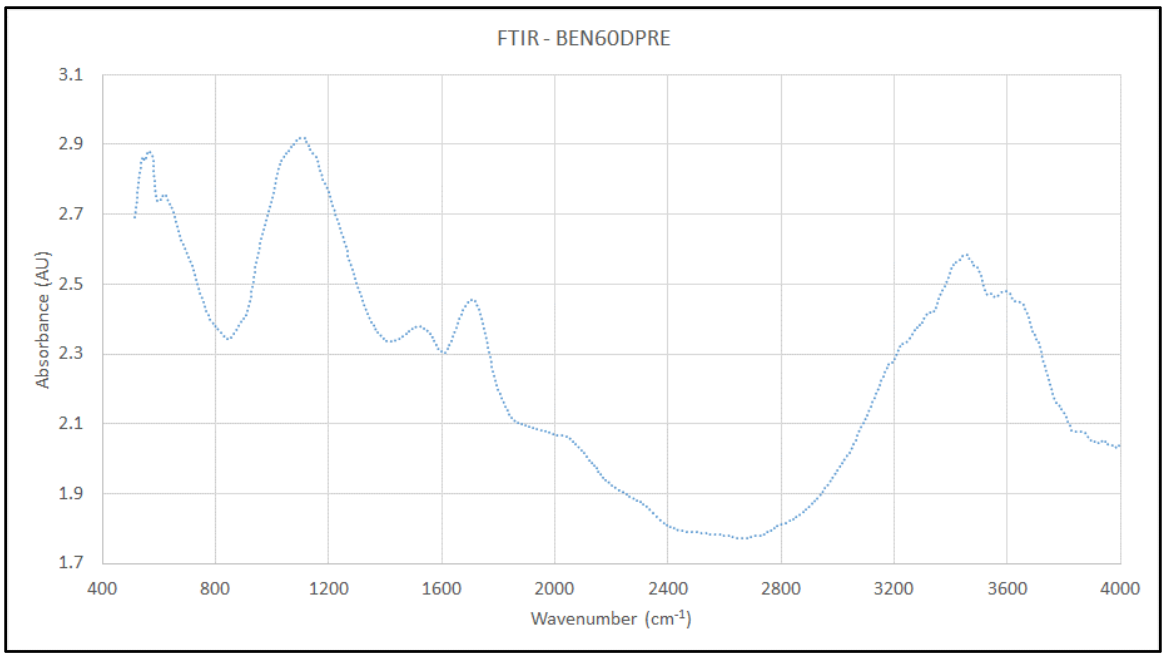

Figure B-9 FTIR results of 60 % Bentonite and 40 % Sand compacted on dry of OMC – pre swell conditions

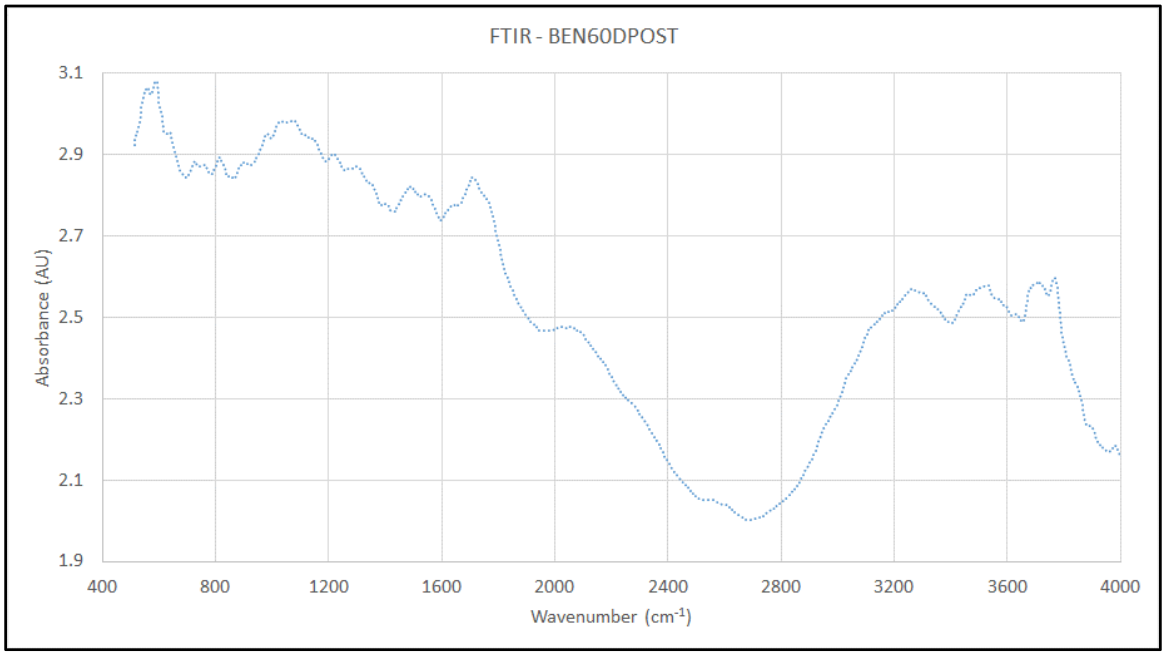

Figure B-10 FTIR results of 100 % Bentonite and 40 % Sand compacted on dry of OMC – post swell conditions

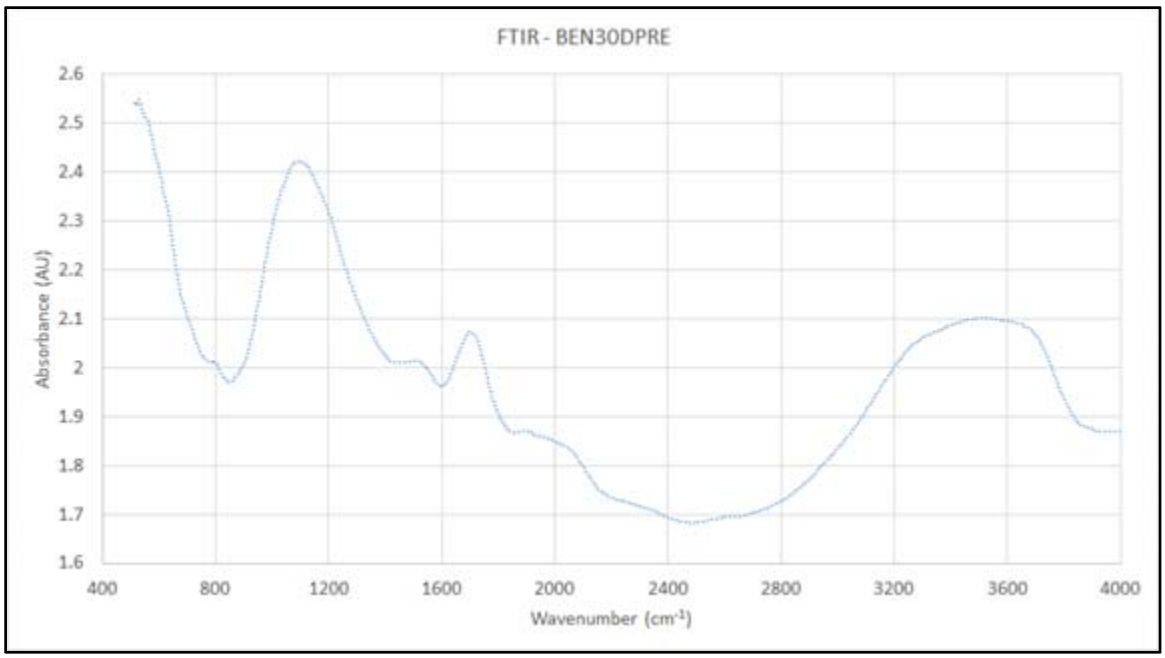

Figure B-11 FTIR results of 30 % Bentonite and 70 % Sand compacted on dry of OMC – pre swell conditions

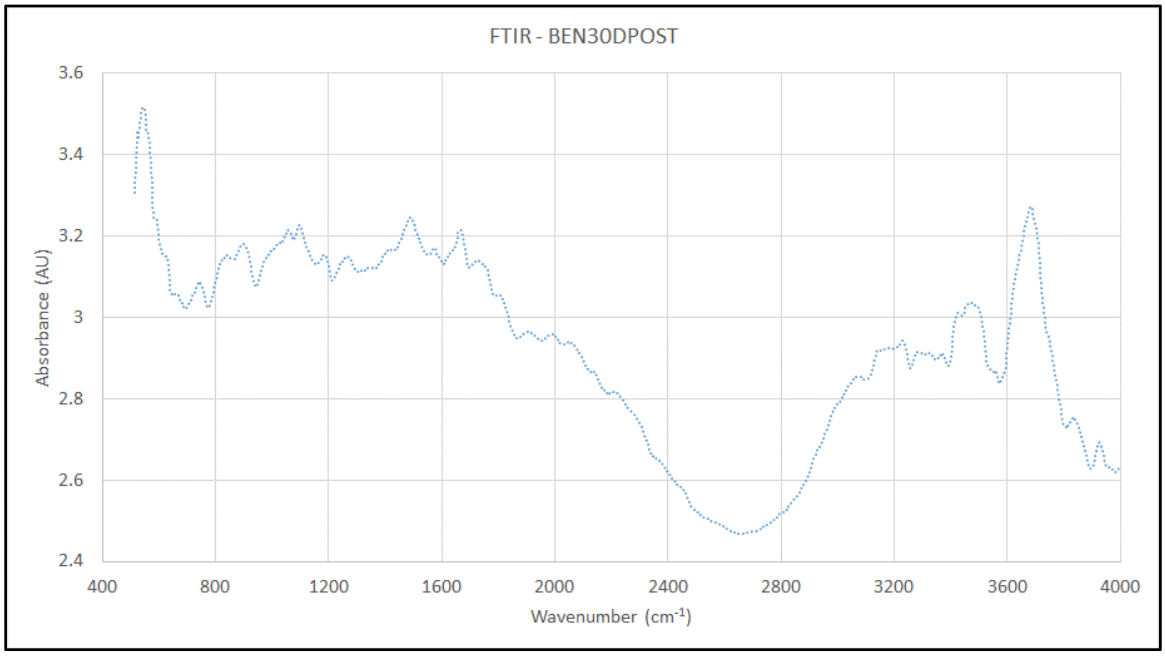

Figure B-12 FTIR results of 30 % Bentonite and 70 % Sand compacted on dry of OMC – post swell conditions

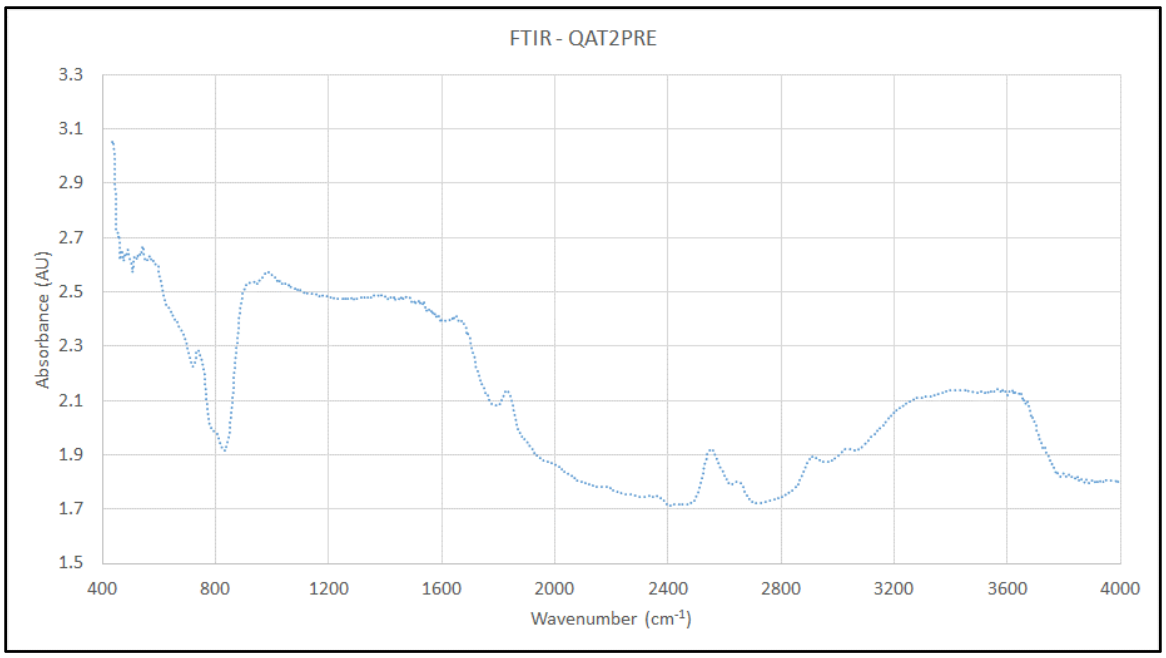

Figure B-13 FTIR results of Qatif-2 sample at NMC – pre swell conditions

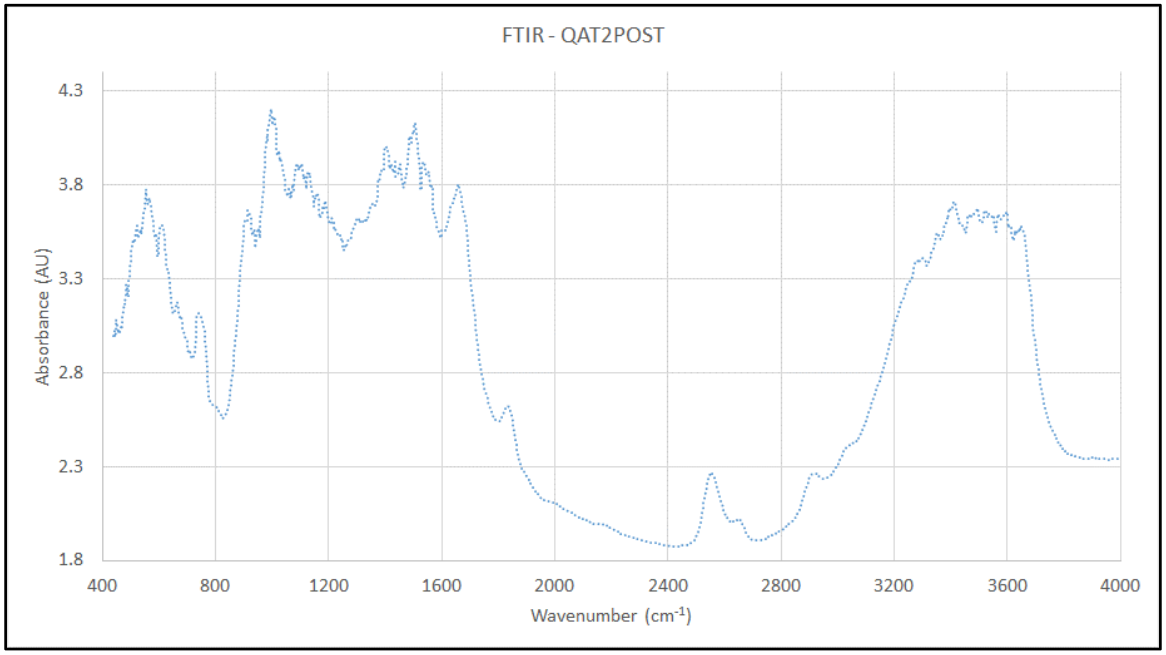

Figure B-14 FTIR results of Qatif-2 sample at NMC – post swell conditions

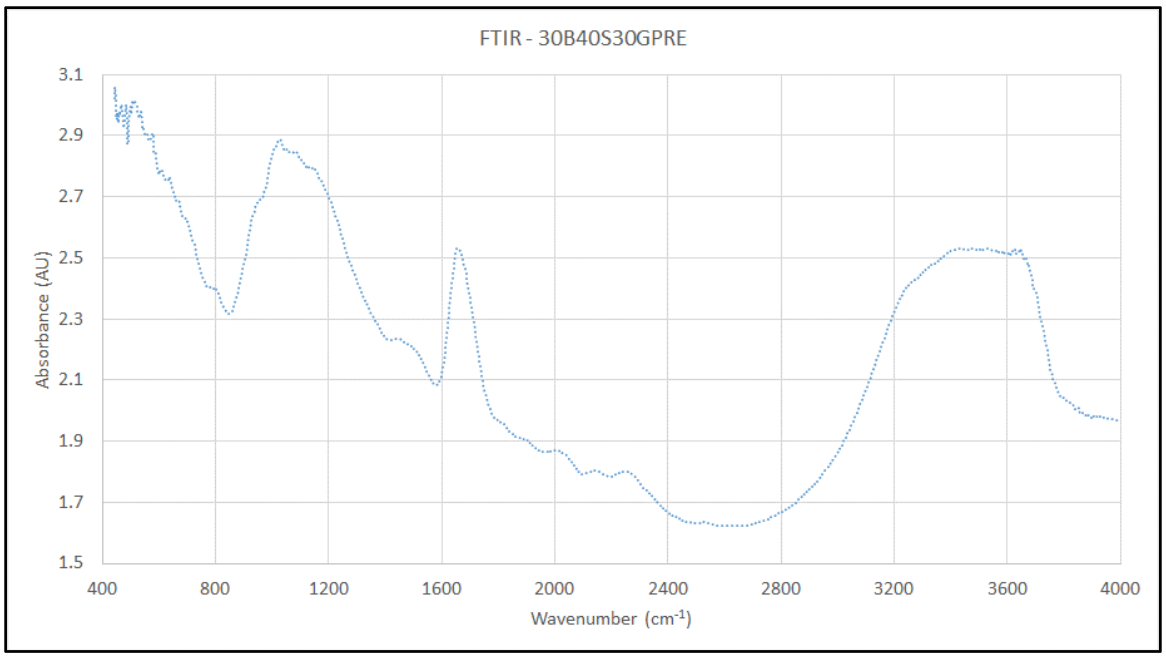

Figure B-15 FTIR results of 30 % Bentonite, 30 % Gypsum, and 40 % Sand compacted on dry of OMC – pre swell conditions

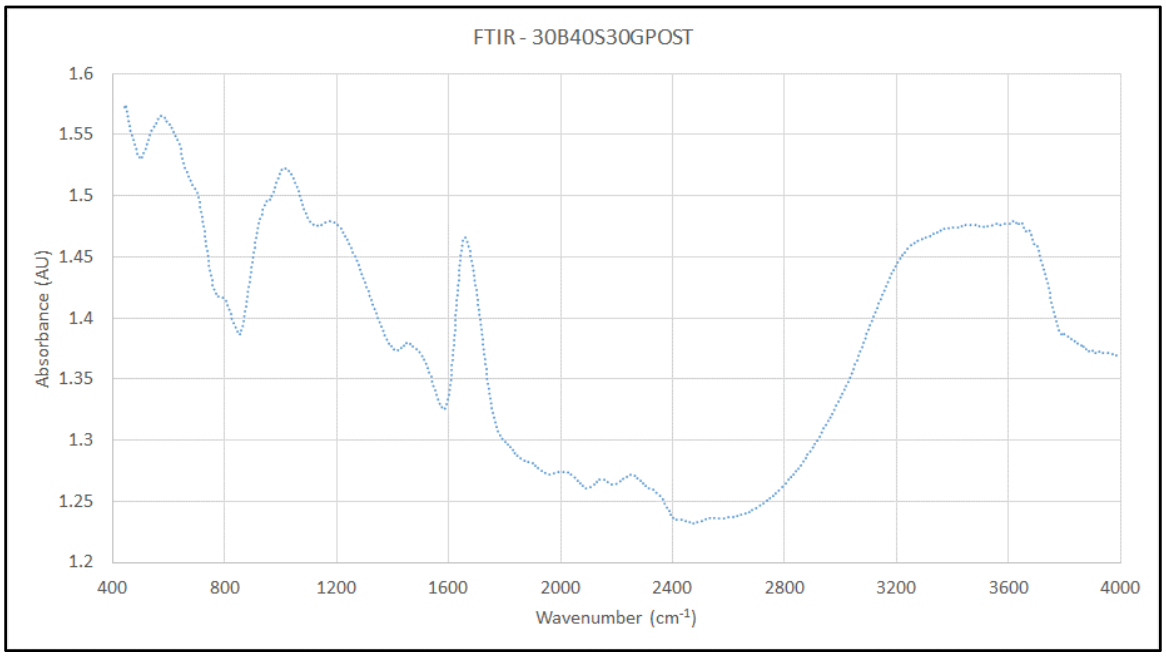

Figure B-16 FTIR results of 30 % Bentonite, 30 % Gypsum, and 40 % Sand compacted on dry of OMC – post swell conditions

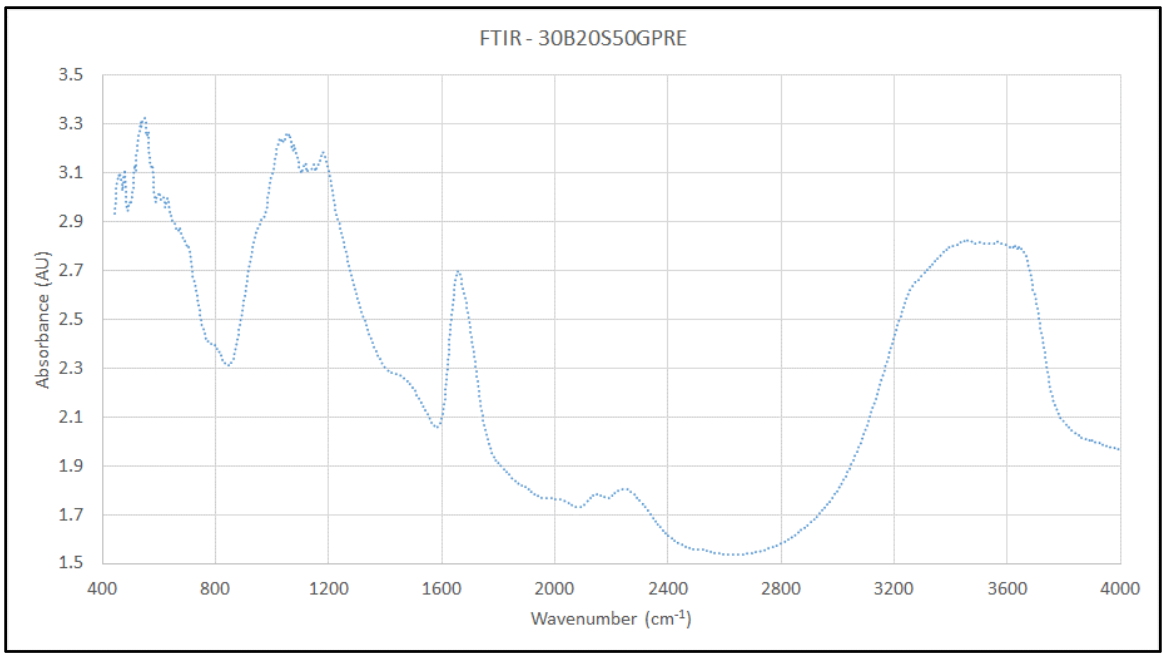

Figure B-17 FTIR results of 30 % Bentonite, 50 % Gypsum, and 20 % Sand compacted on dry of OMC – pre swell conditions

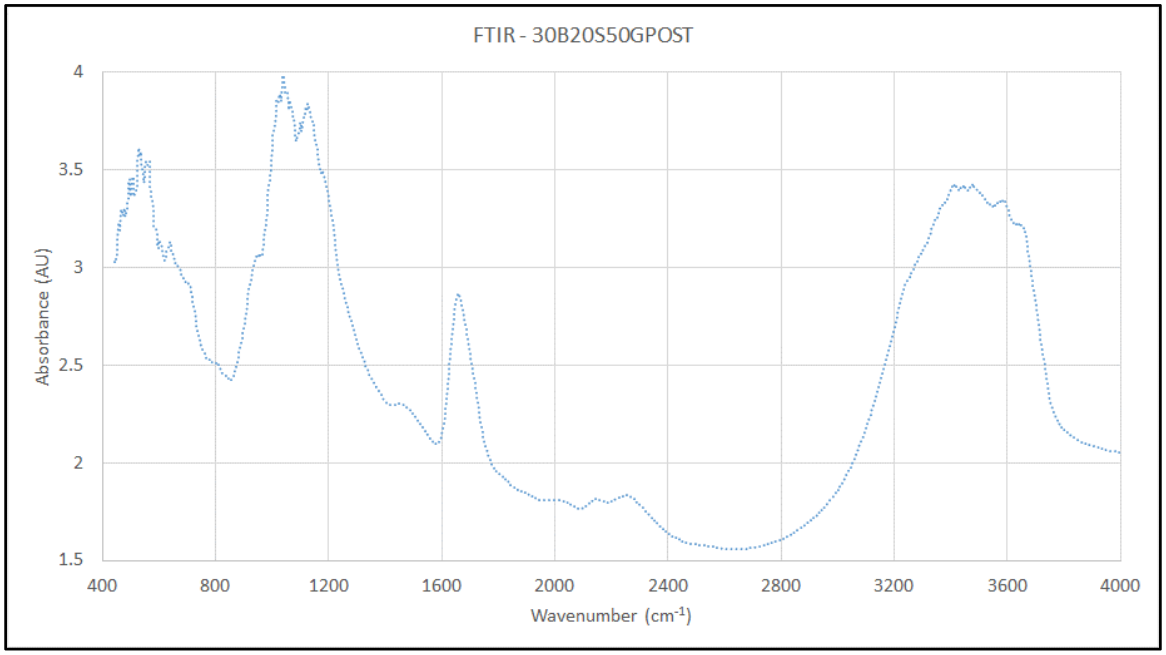

Figure B-18 FTIR results of 30 % Bentonite, 50 % Gypsum, and 20 % Sand compacted on dry of OMC – post swell conditions

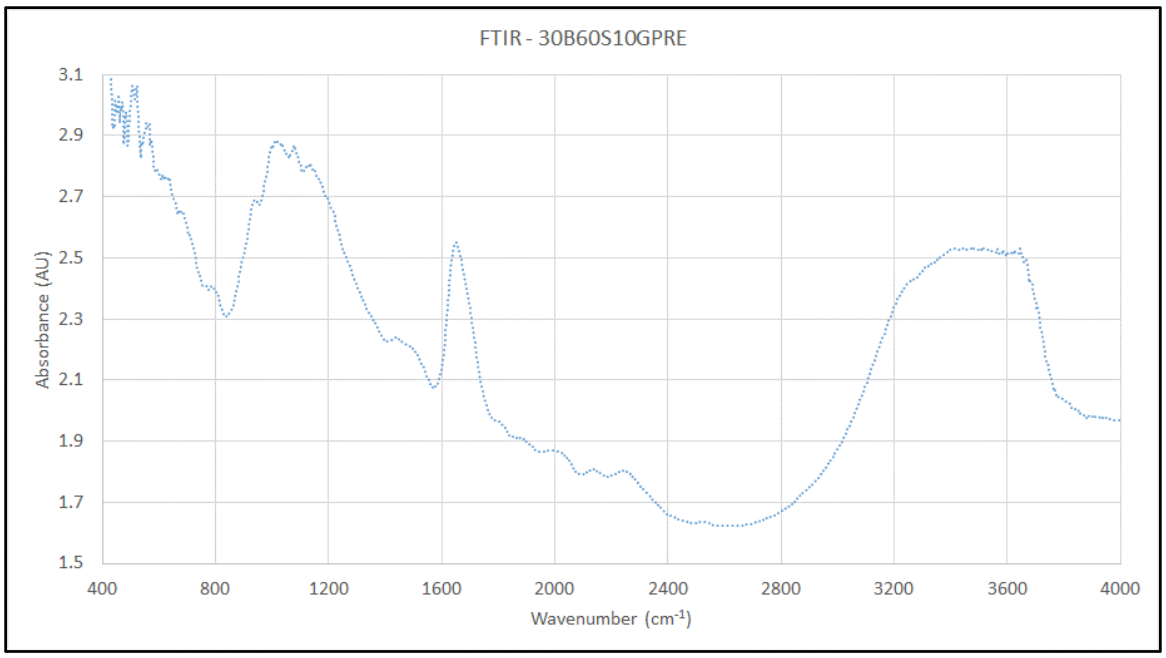

Figure B-19 FTIR results of 30 % Bentonite, 10 % Gypsum, and 60 % Sand compacted on dry of OMC – pre swell conditions

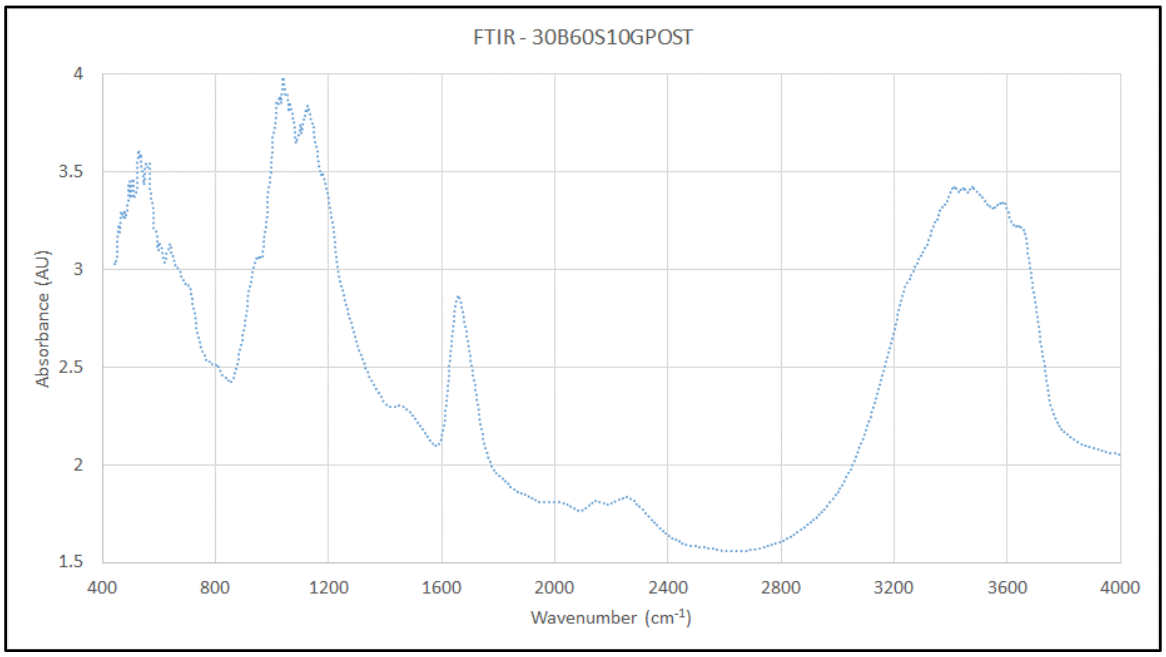

Figure B-20 FTIR results of 30 % Bentonite, 10 % Gypsum, and 60 % Sand compacted on dry of OMC – post swell conditions

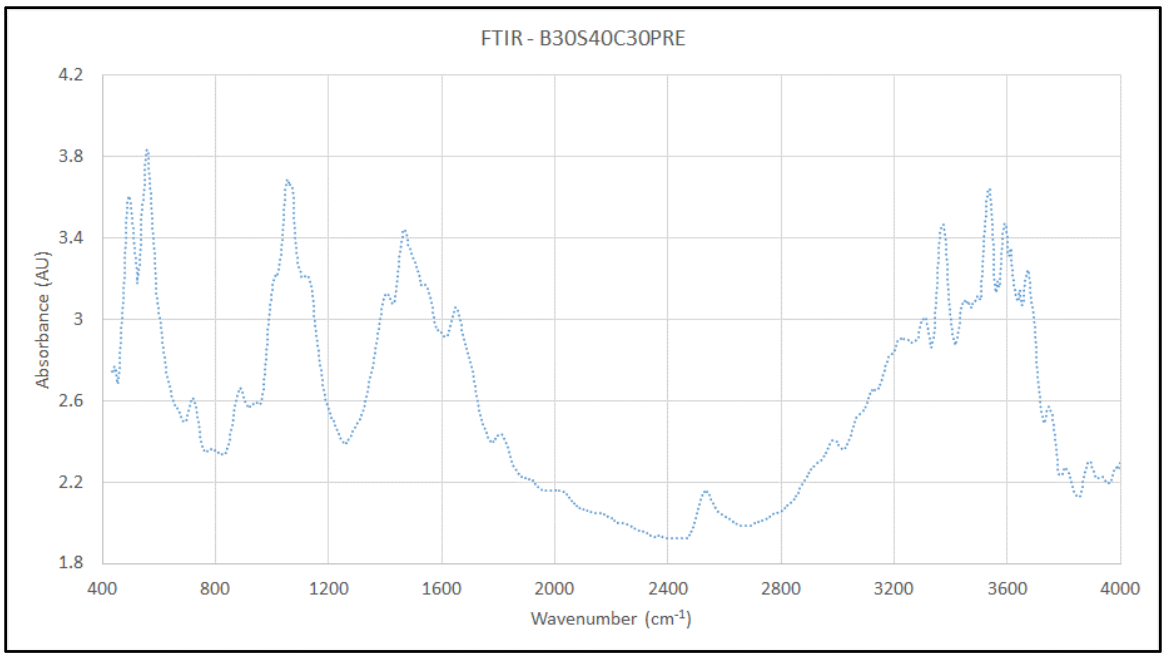

Figure B-21 FTIR results of 30 % Bentonite, 30 % Calcite, and 40 % Sand compacted on dry of OMC – pre swell conditions

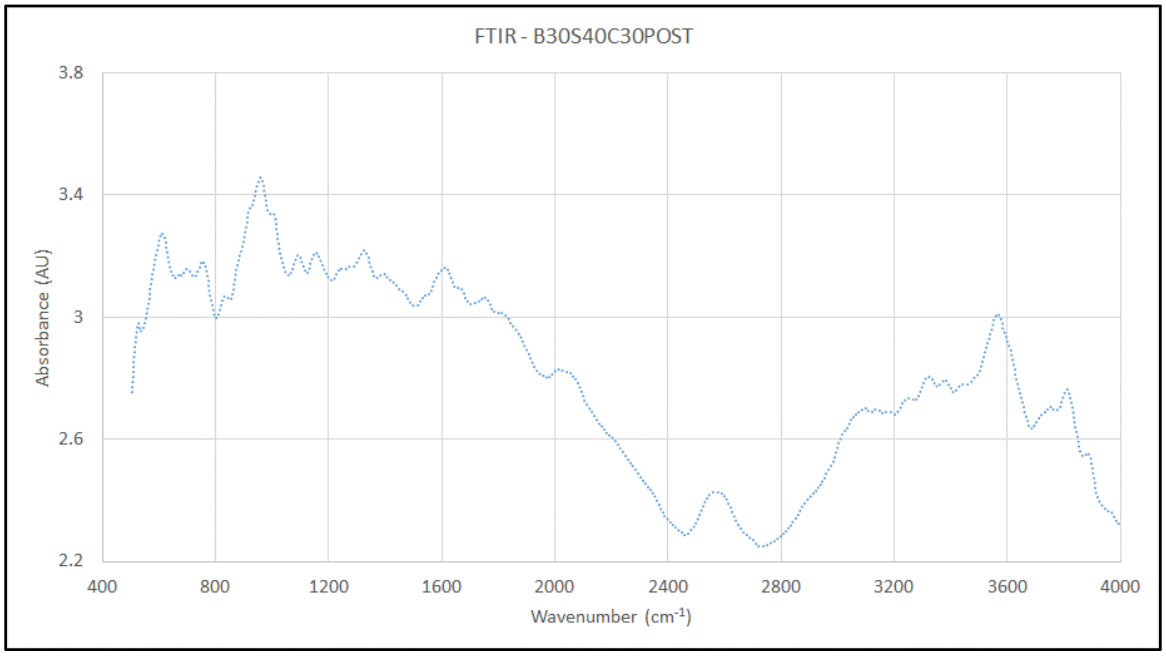

Figure B-22 FTIR results of 30 % Bentonite, 30 % Calcite, and 40 % Sand compacted on dry of OMC – post swell conditions

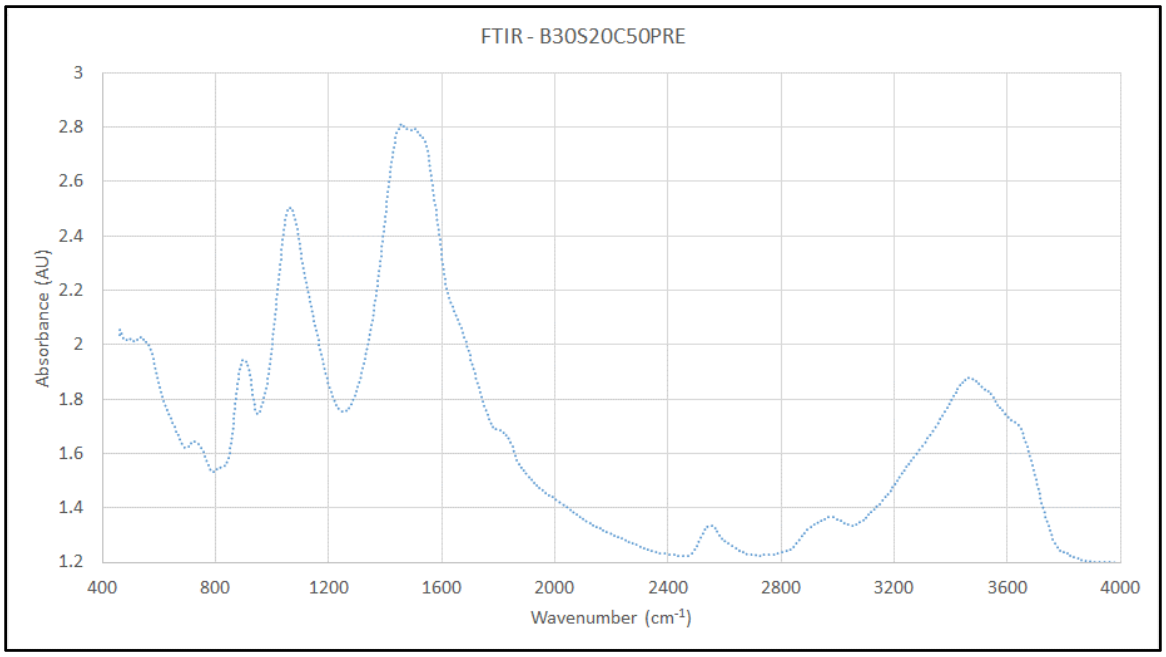

Figure B-23 FTIR results of 30 % Bentonite, 20 % Calcite, and 50 % Sand compacted on dry of OMC – pre swell conditions

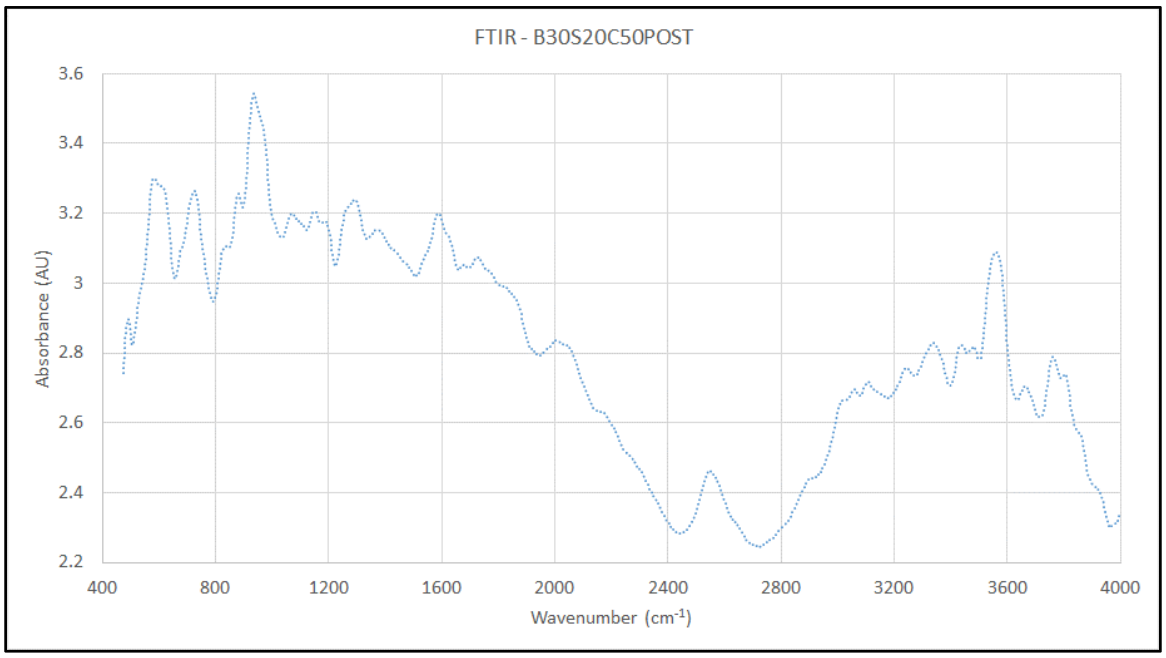

Figure B-24 FTIR results of 30 % Bentonite, 20 % Calcite, and 50 % Sand compacted on dry of OMC – post swell conditions

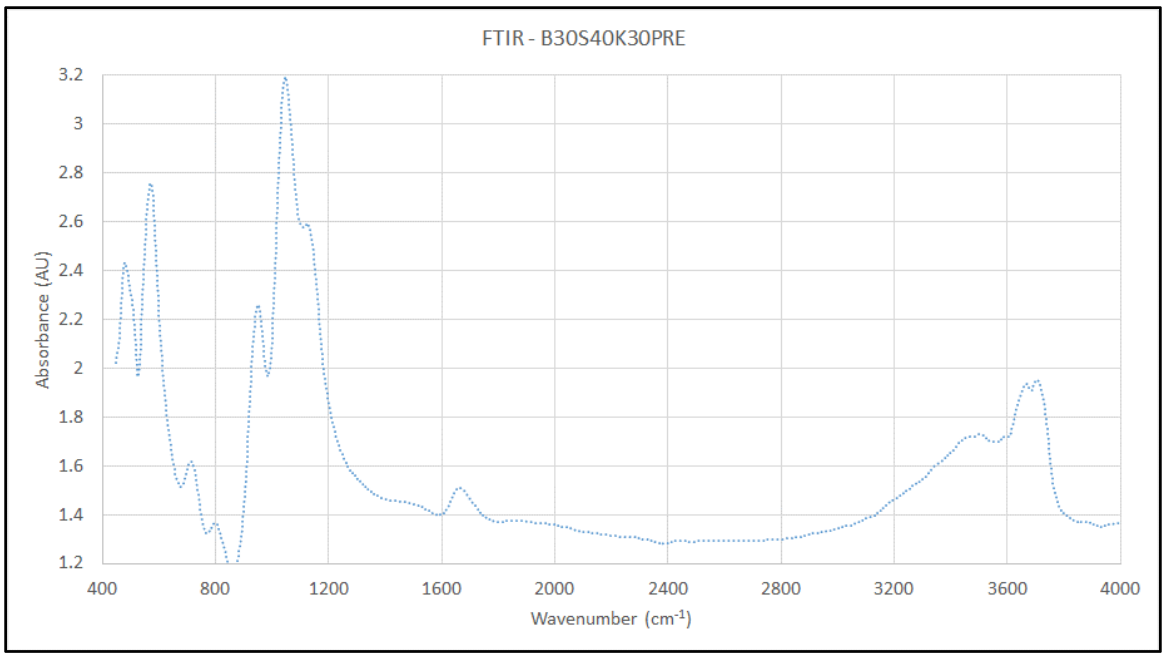

Figure B-25 FTIR results of 30 % Bentonite, 30 % Kaolinite, and 40 % Sand compacted on dry of OMC – pre swell conditions

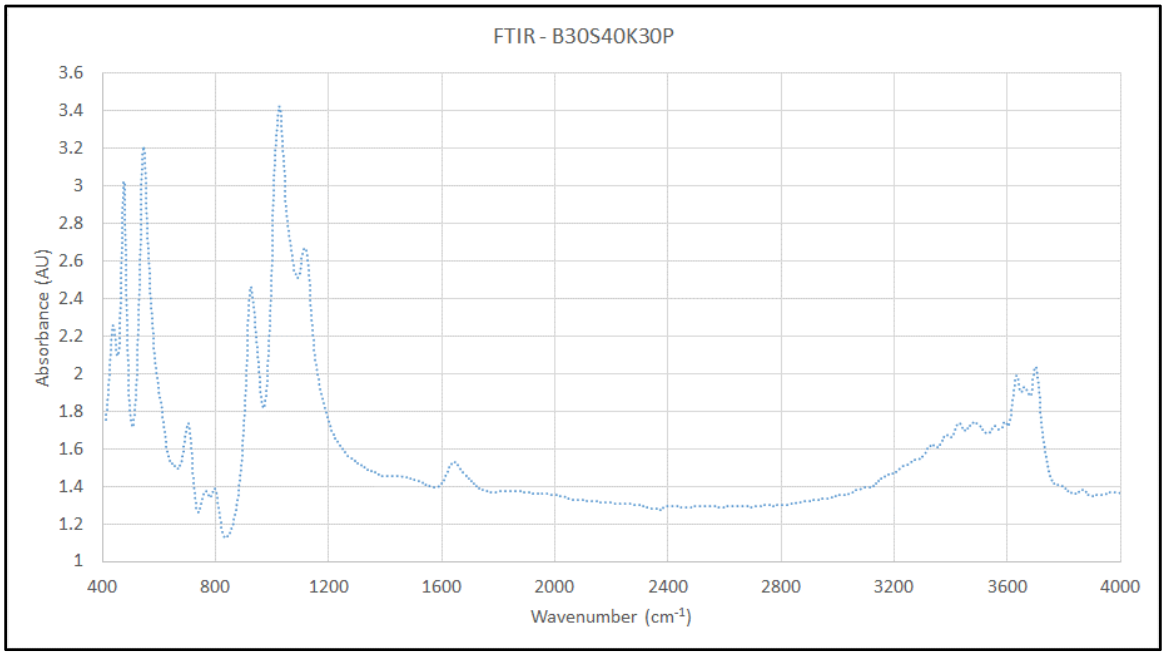

Figure B-26 FTIR results of 30 % Bentonite, 30 % Kaolinite, and 40 % Sand compacted on dry of OMC – post swell conditions

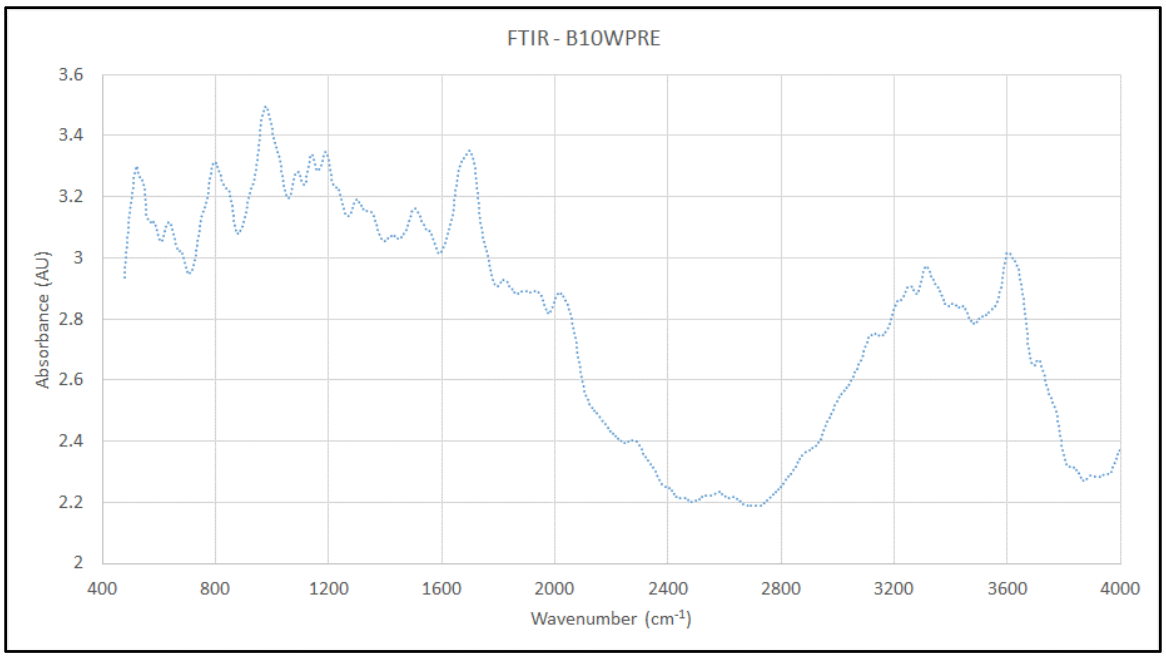

Figure B-27 FTIR results of 10 % Bentonite and 90 % Sand compacted on wet of OMC – pre swell conditions

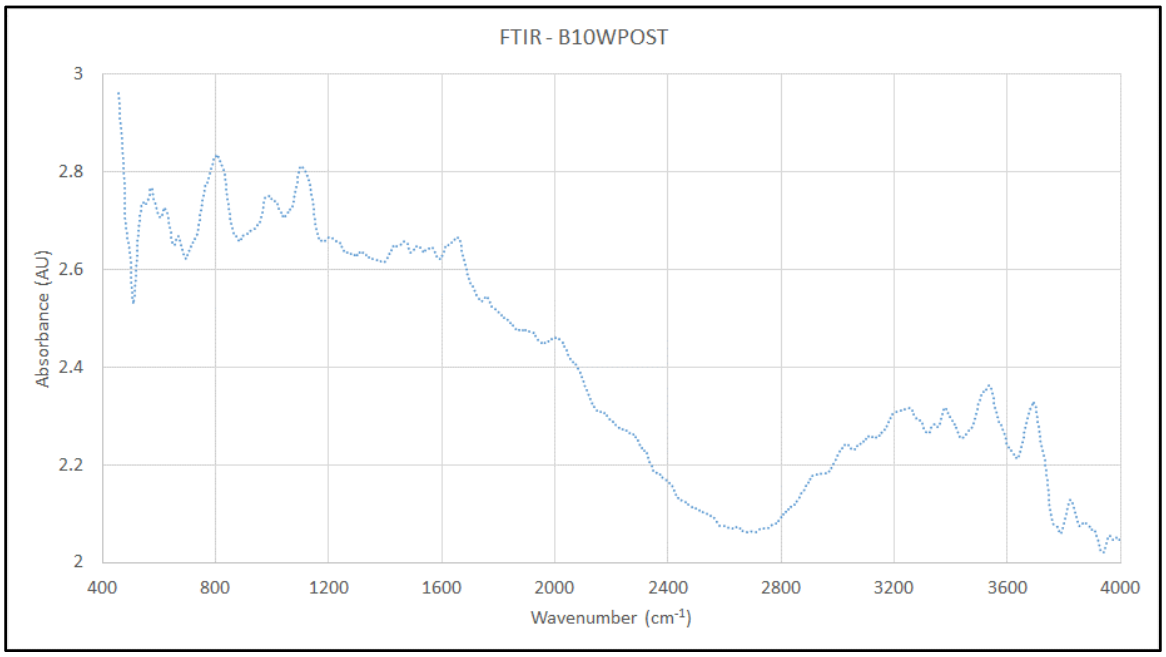

Figure B-28 FTIR results of 10 % Bentonite and 90 % Sand compacted on wet of OMC – post swell conditions

Appendix C - ESEM Results

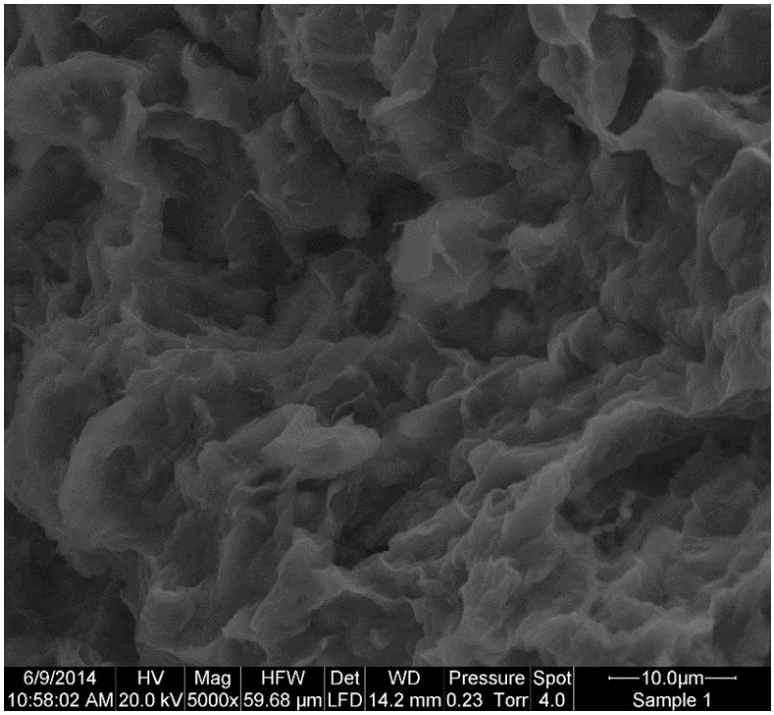

Figure C-1 ESEM of 100 % Bentonite compacted on dry of OMC – pre swell

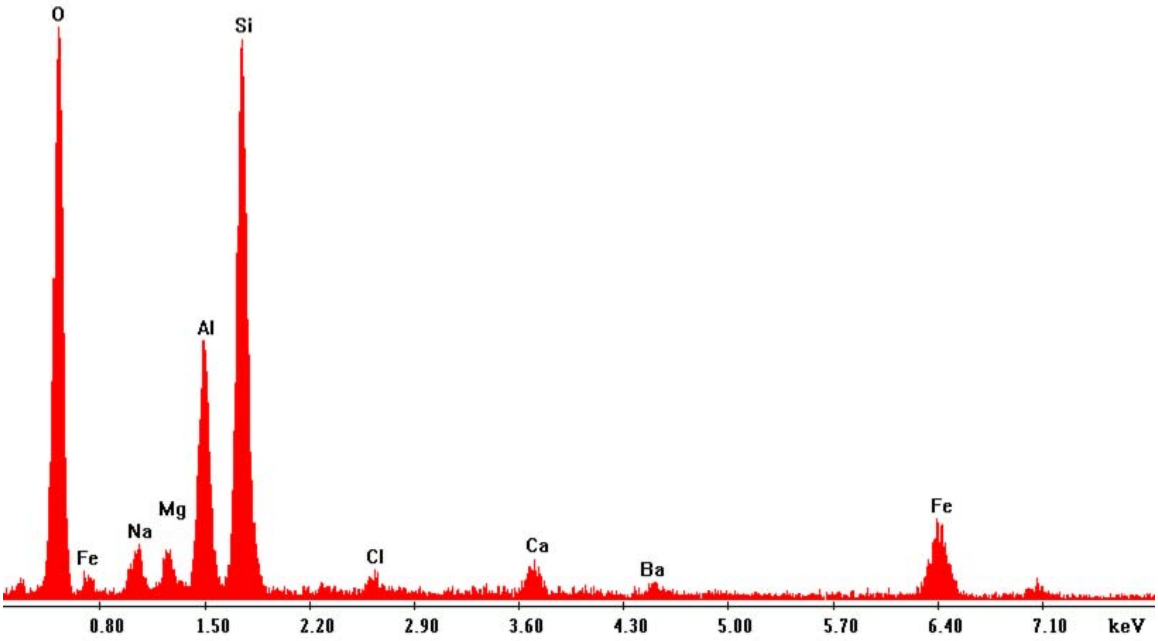

Figure C-2 EDS of general area of ESEM in Figure C-1

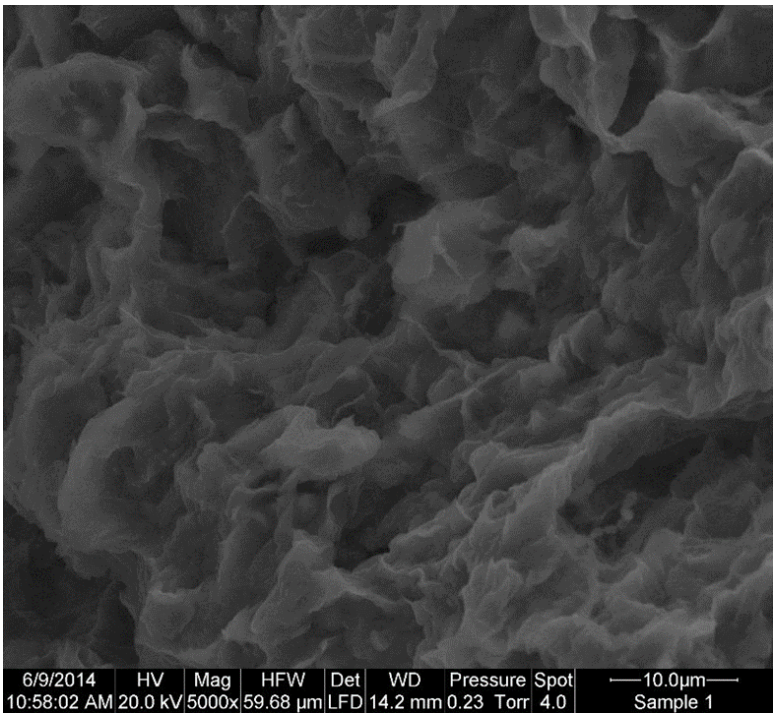

Figure C-3 ESEM of 100 % Bentonite compacted on dry of OMC – pre swell

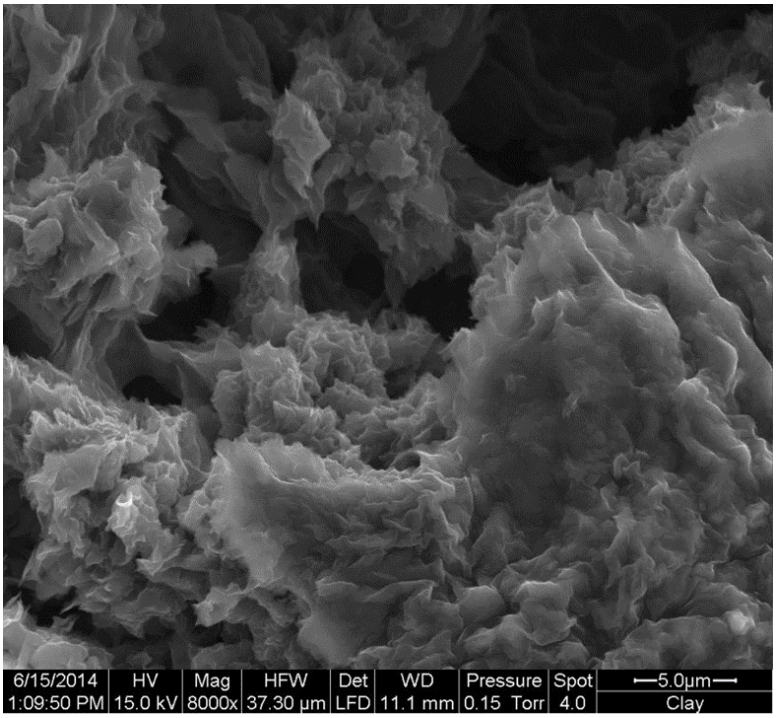

Figure C-4 ESEM of 100 % Bentonite compacted on dry of OMC – post swell

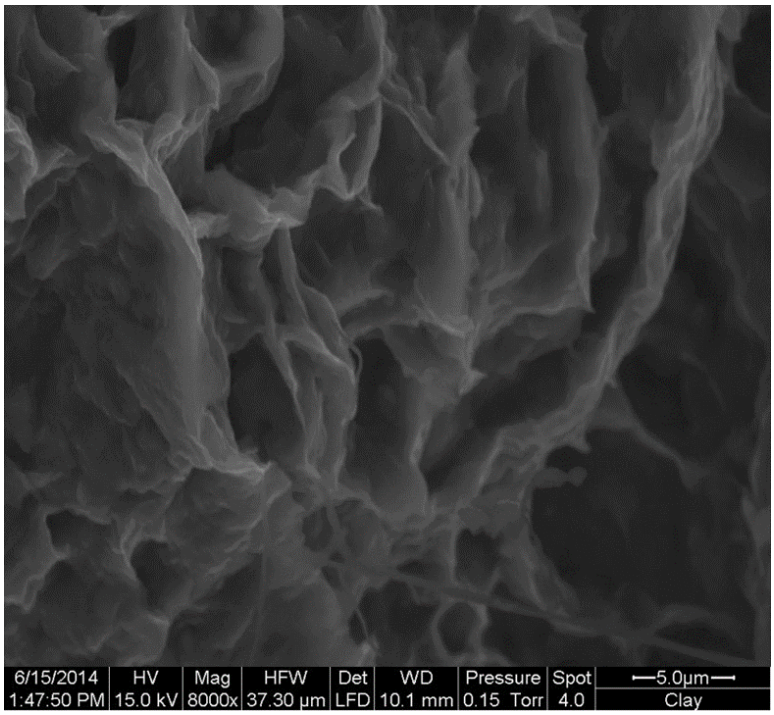

Figure C-5 ESEM of 100 % Bentonite compacted on wet of OMC – pre swell

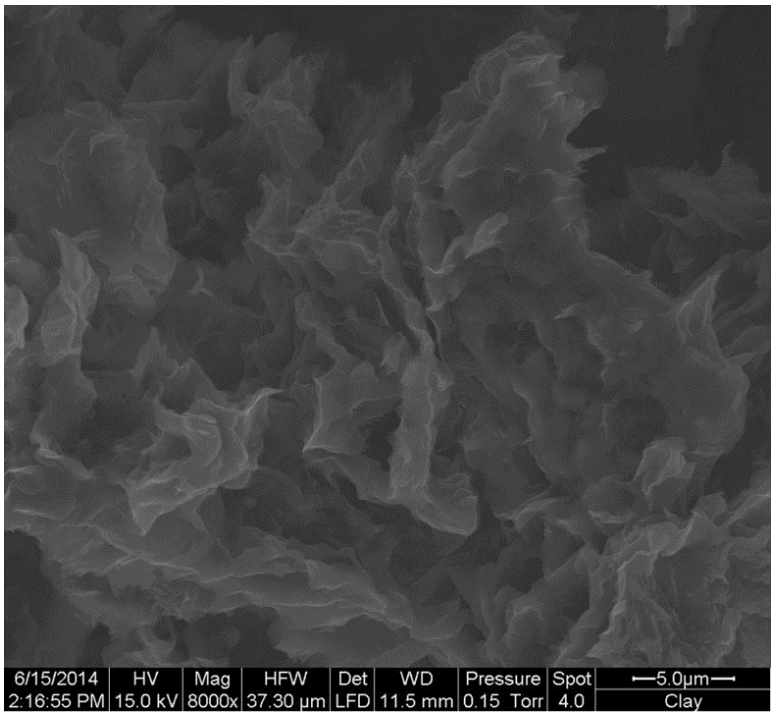

Figure C-6 ESEM of 100 % Bentonite compacted on wet of OMC – post swell

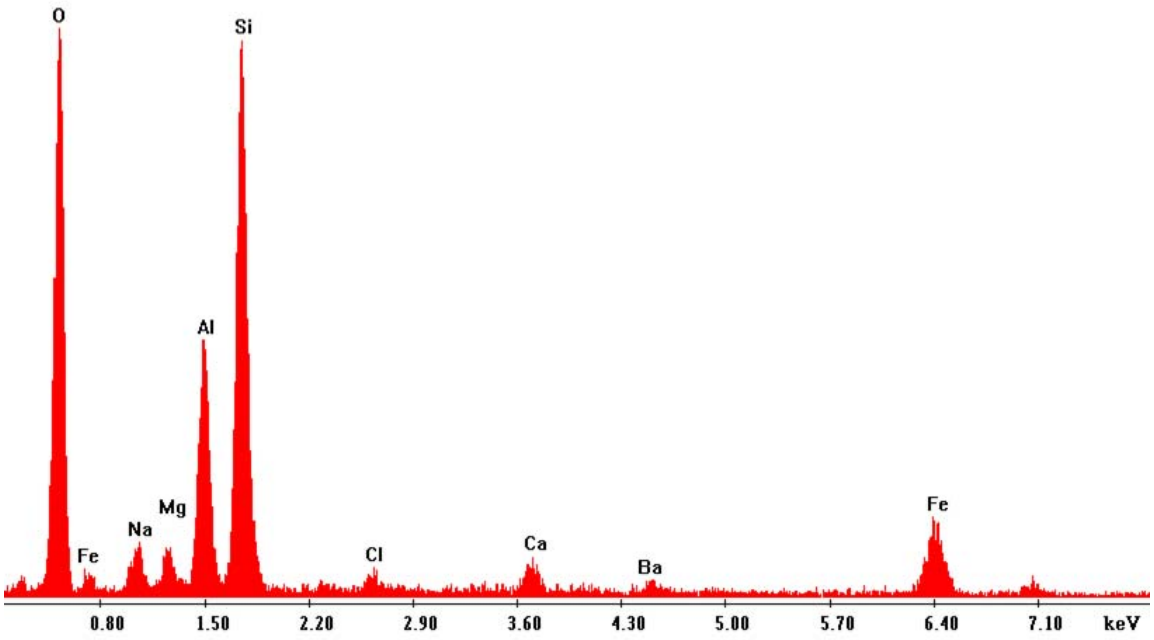

Figure C-7 EDS of 100 % Bentonite compacted on dry of OMC – pre swell

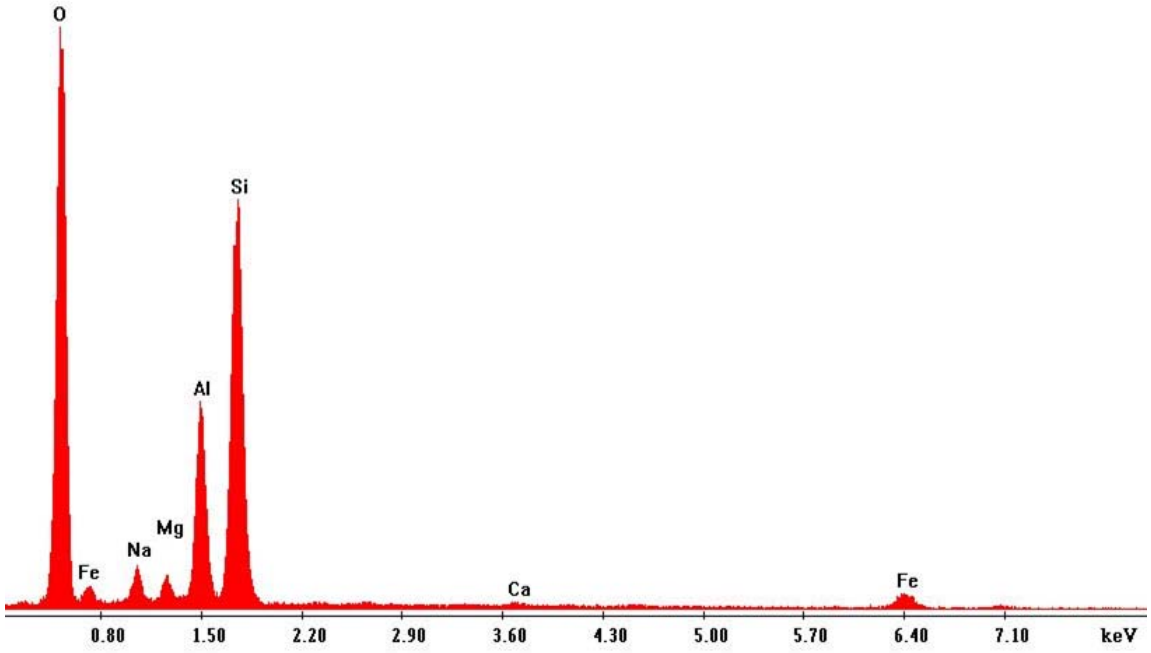

Figure C-8 EDS of 100 % Bentonite compacted on dry of OMC – post swell

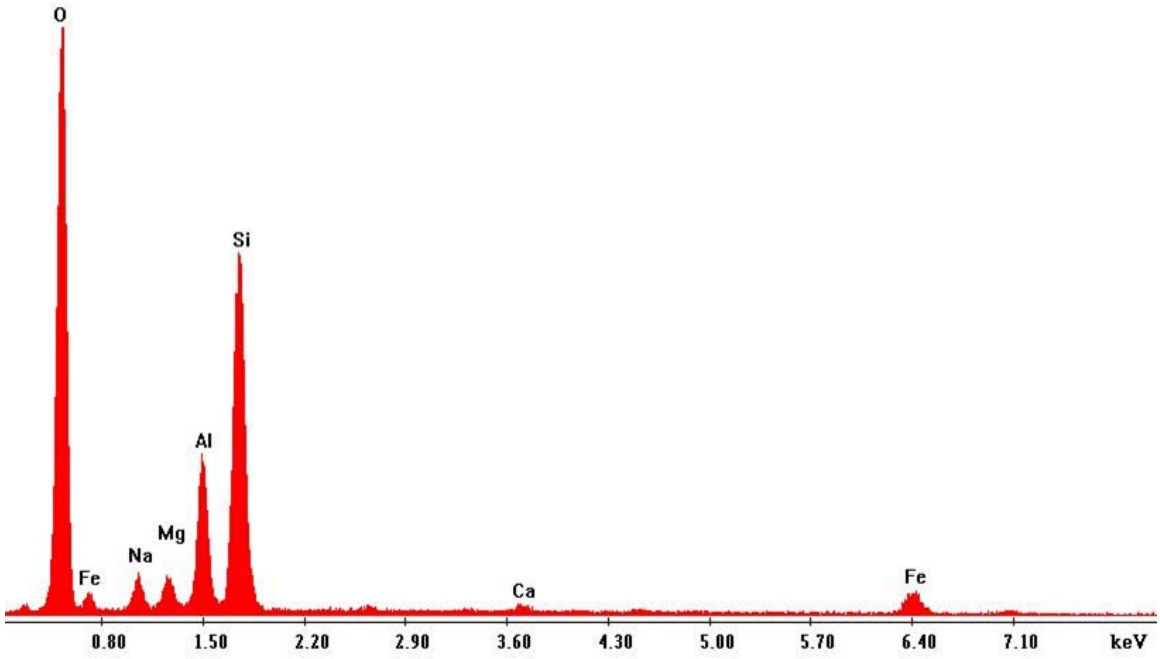

Figure C-9 EDS of 100 % Bentonite compacted on wet of OMC – pre swell

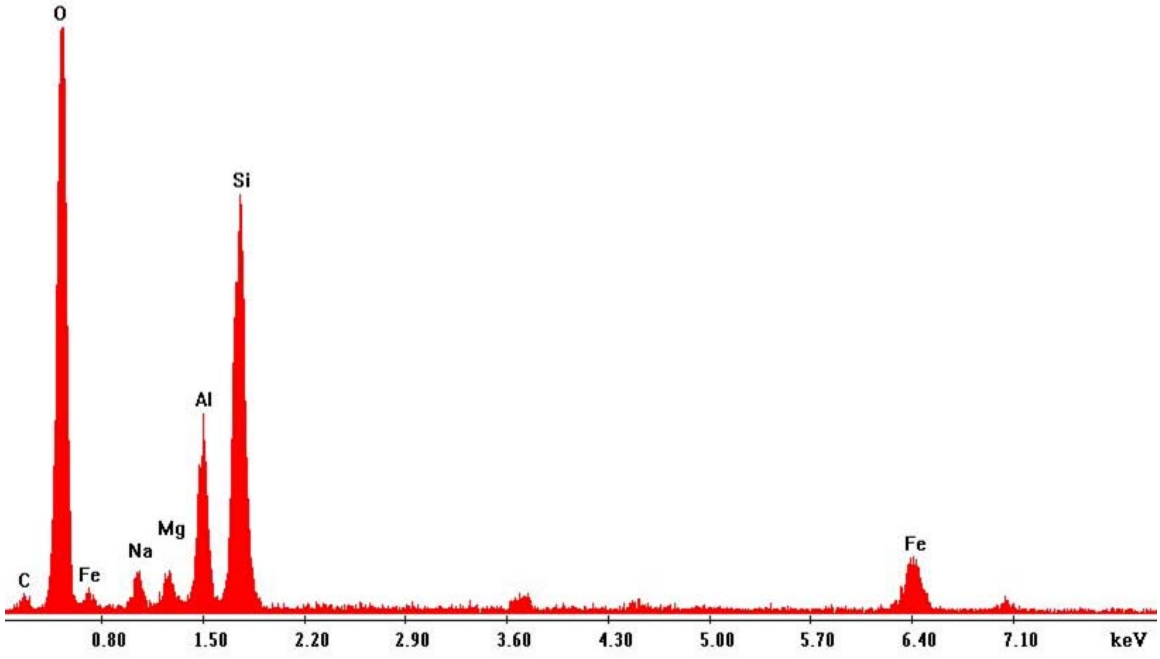

Figure C-10 EDS of 100 % Bentonite compacted on dry of OMC – post swell

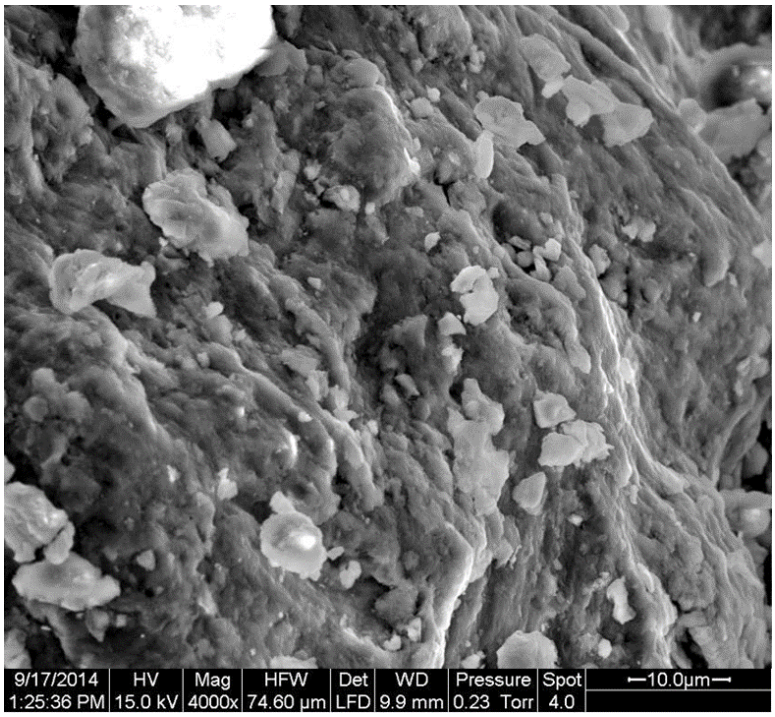

Figure C-11 ESEM of dry Bentonite sample

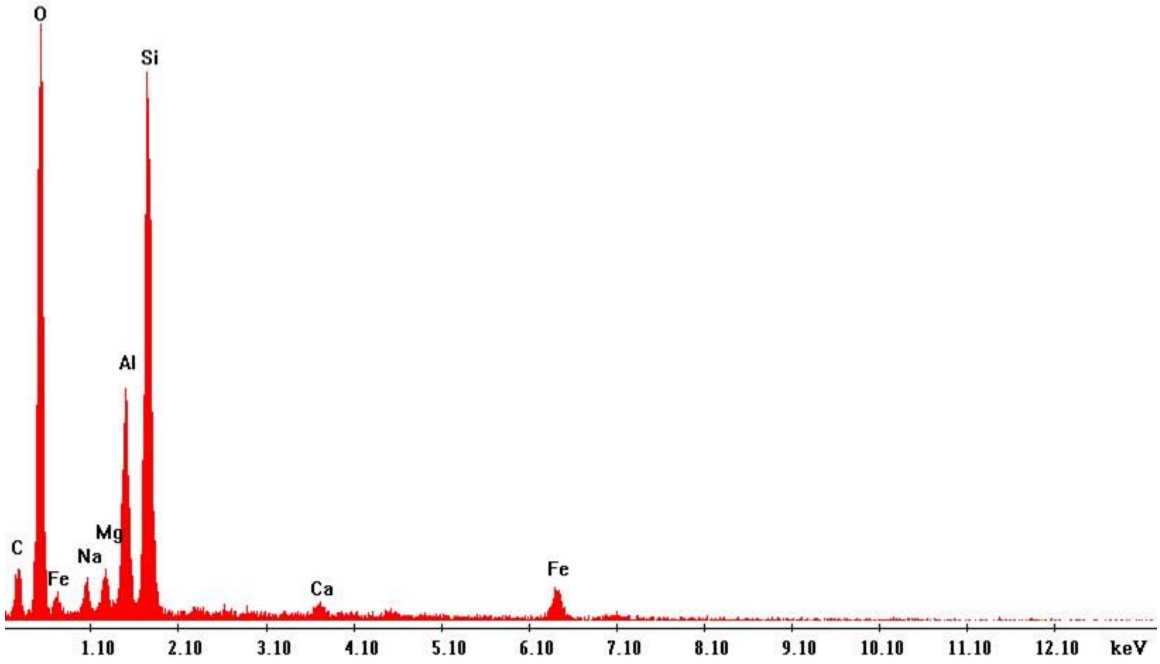

Figure C-12 EDS of dry Bentonite sample

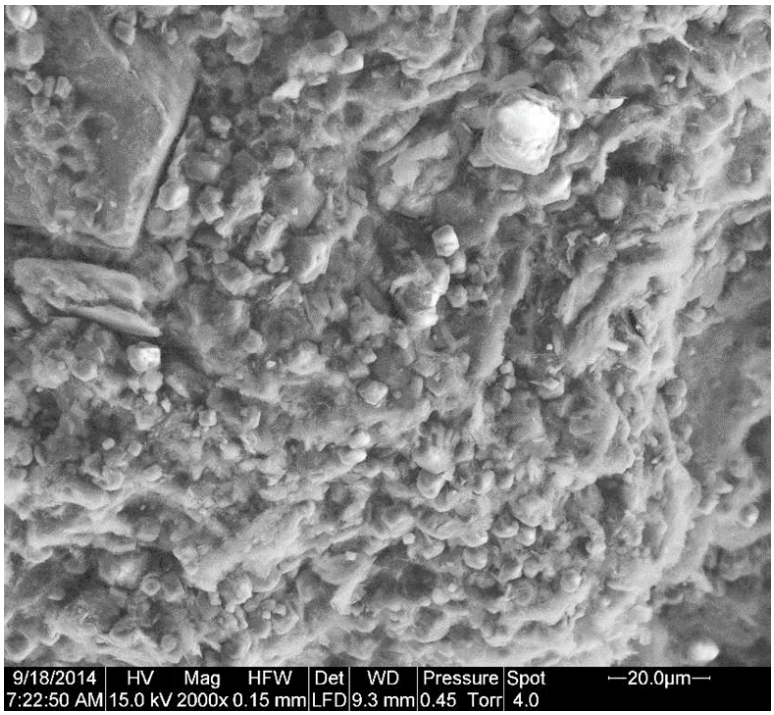

Figure C-13 ESEM of Qatif-2 sample – pre swell

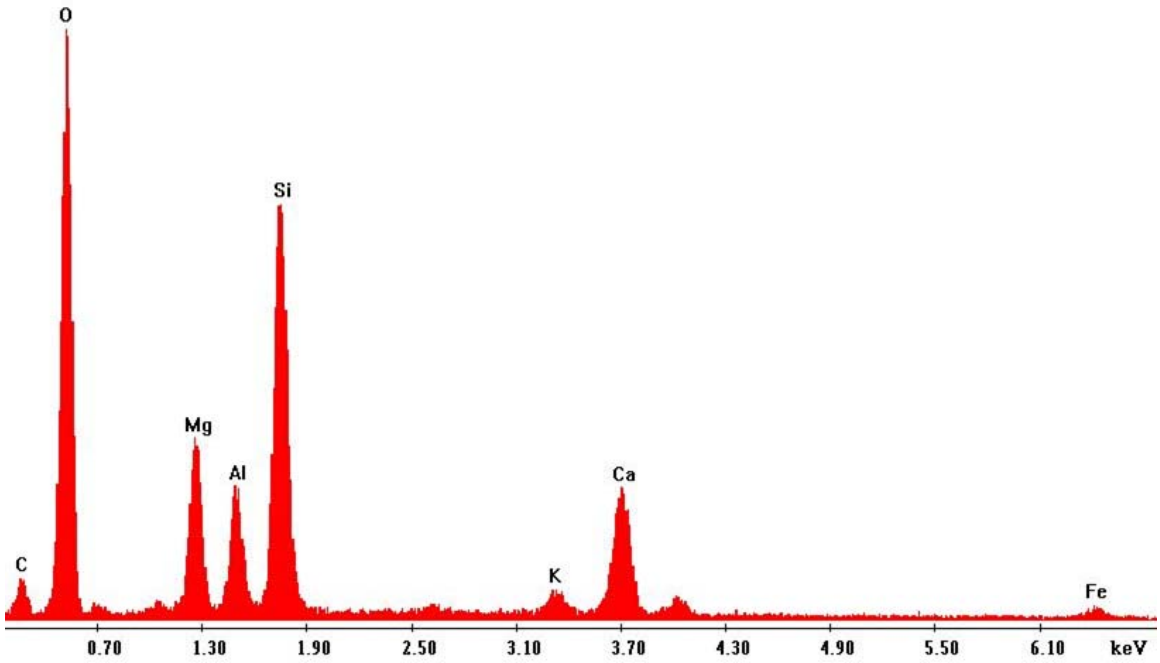

Figure C-14 EDS of Qatif-2 sample – pre swell

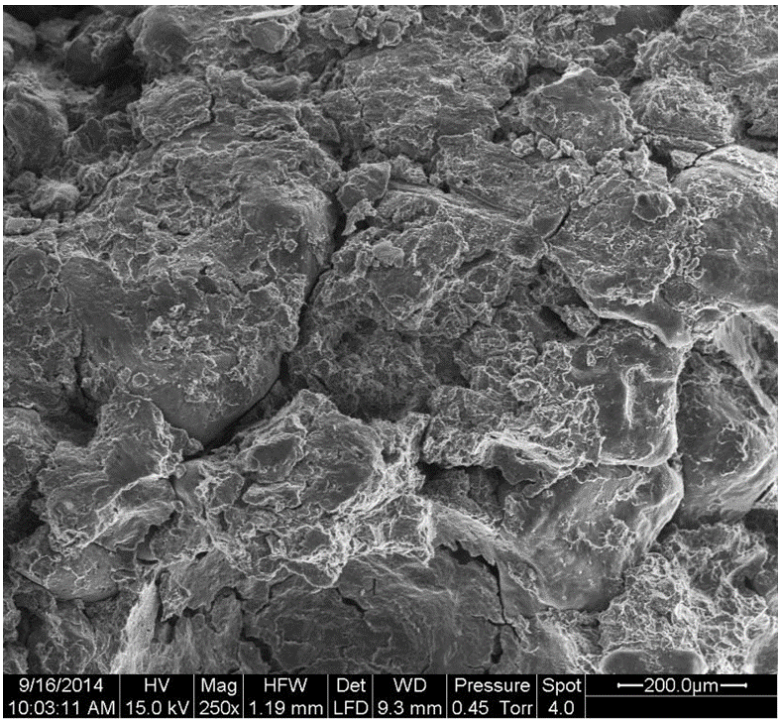

Figure C-15 ESEM of 30 % Bentonite and 70 % Sand – Dry of OMC – Pre swell

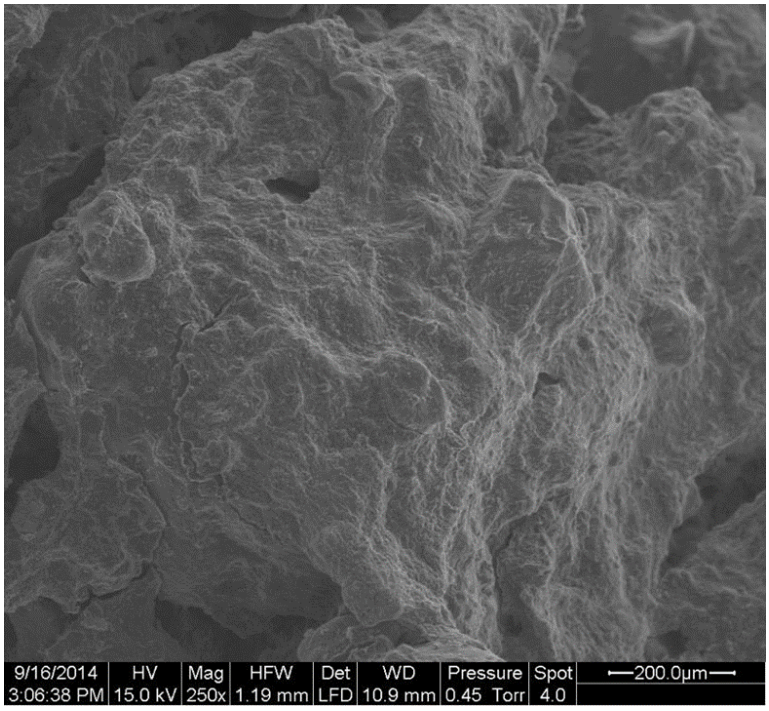

Figure C-16 ESEM of 30 % Bentonite and 70 % Sand – Dry of OMC – Post swell

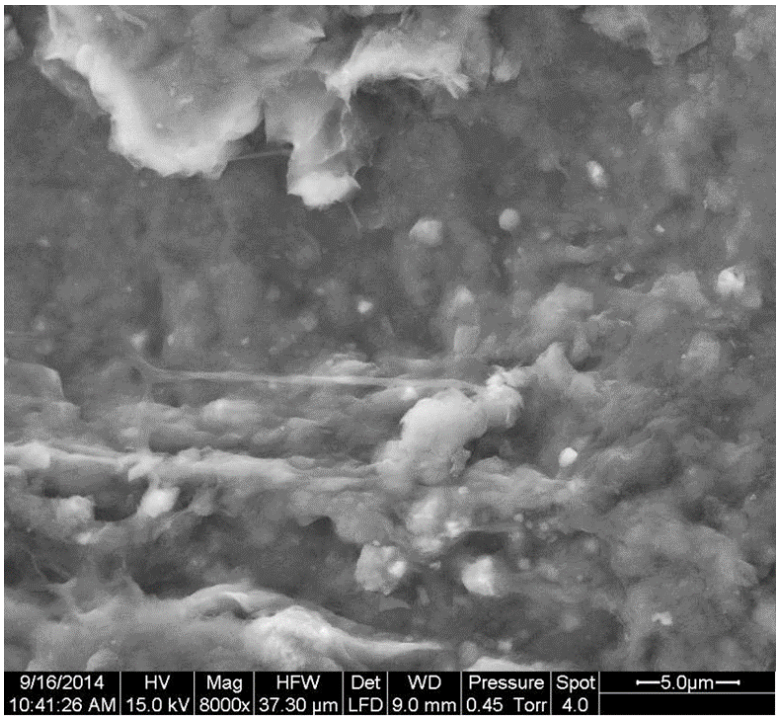

Figure C-17 ESEM of 30 % Bentonite and 70 % Sand – Dry of OMC – Pre swell

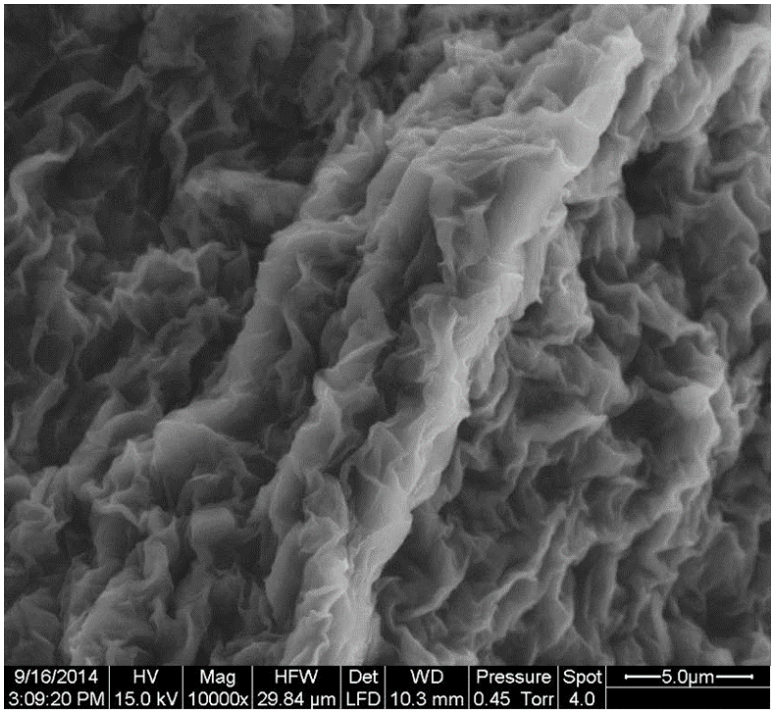

Figure C-18 ESEM of 30 % Bentonite and 70 % Sand – Dry of OMC – Post swell

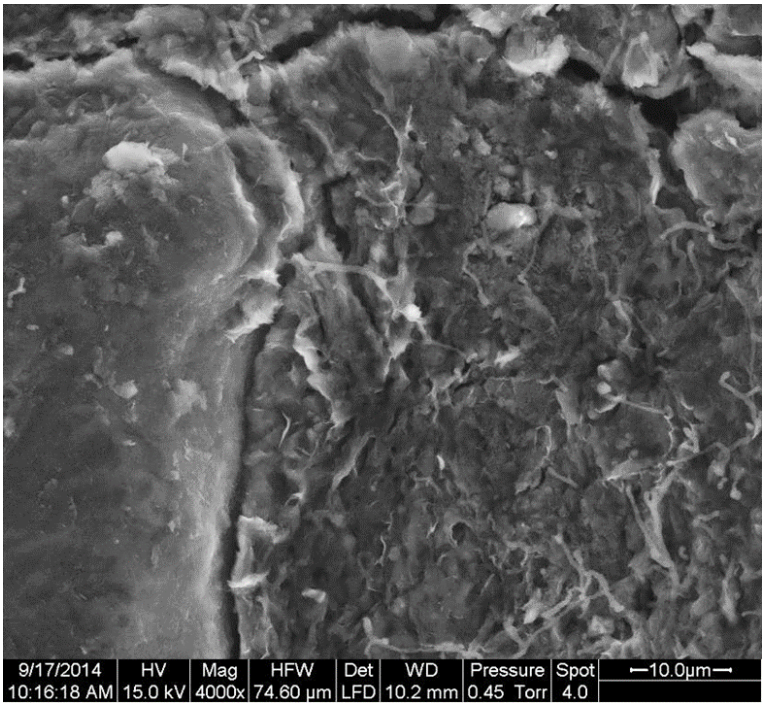

Figure C-19 ESEM of 30 % Bentonite, 70 % Sand-Static-Dry of OMC – Pre swell

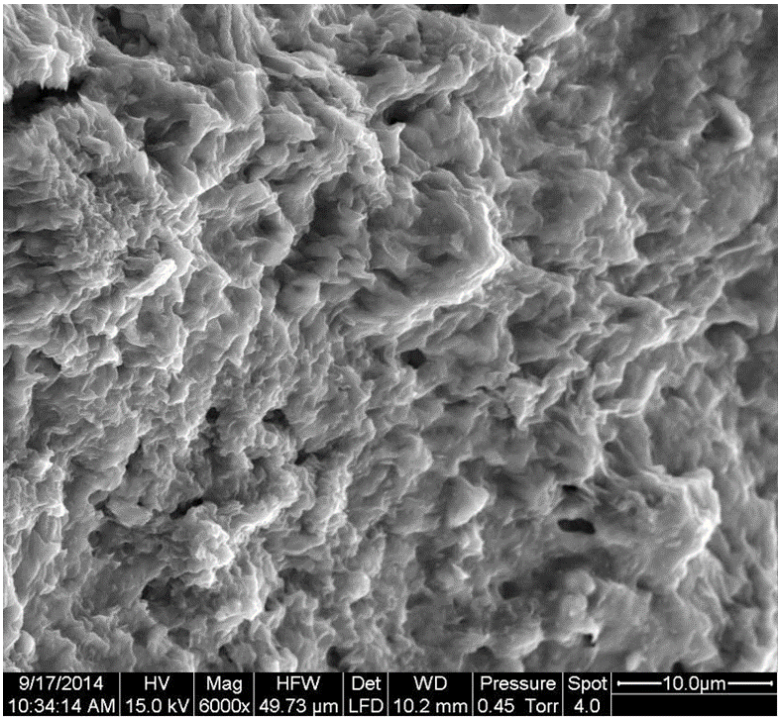

Figure C-20 ESEM of 30 % Bentonite, 70 % Sand-Static-Dry of OMC – Post swell

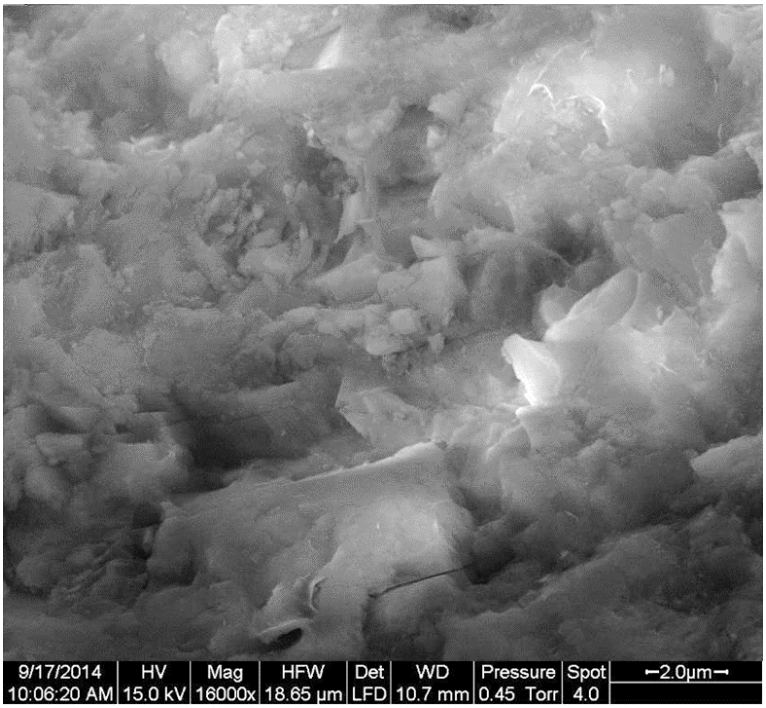

Figure C-21 ESEM of 30 % Bentonite, 70 % Sand-Static-Dry of OMC – Pre swell

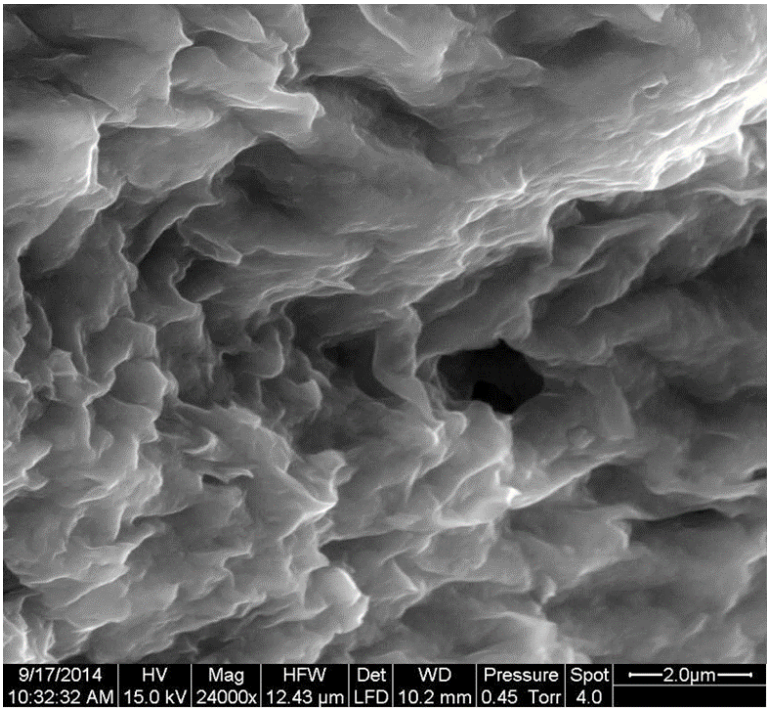

Figure C-0-22 ESEM of 30 % Bentonite, 70 % Sand-Static-Dry of OMC – Post swell

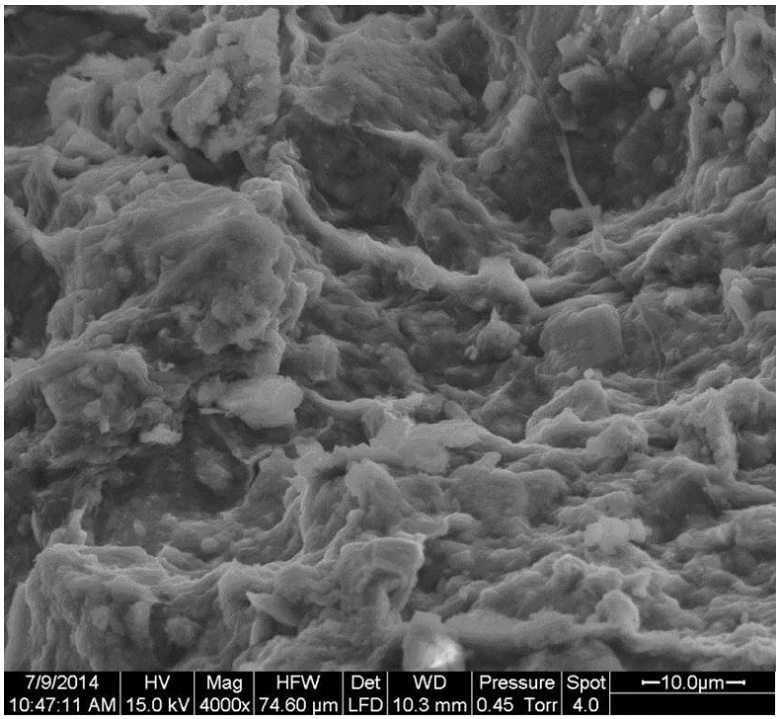

Figure C-23 ESEM of 30 % Ben, 10 % Gypsum, 70 % Sand-Dry of OMC – Pre swell

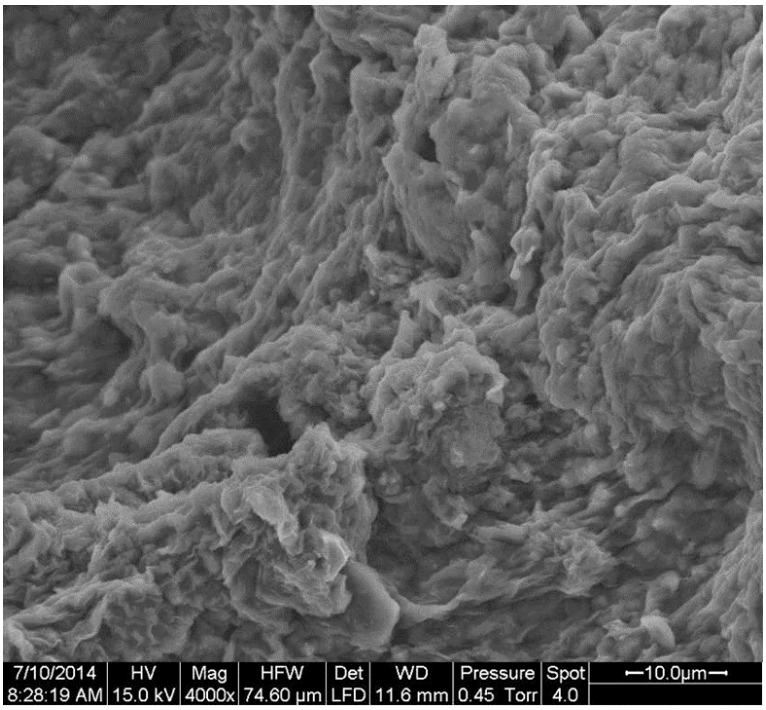

Figure C-24 ESEM of 30 % Ben, 10 % Gyps, 70 % Sand-Dry of OMC – Post swell

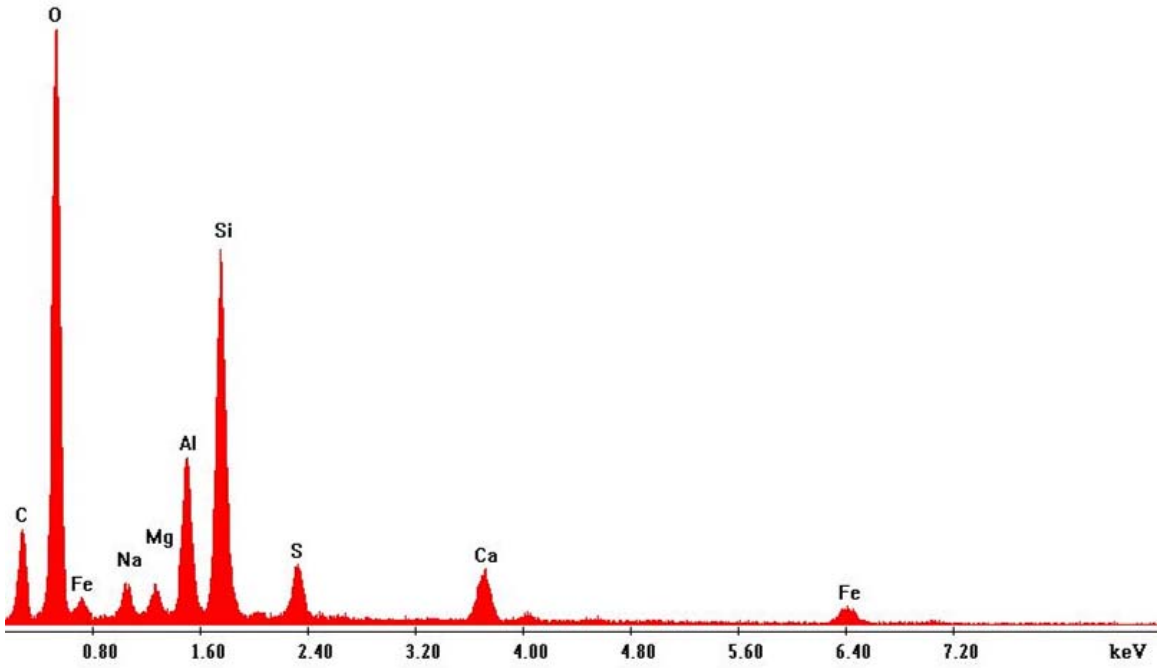

Figure C-25 ESEM of 30 % Ben, 10 % Gyps, 70 % Sand-Dry of OMC – Pre swell

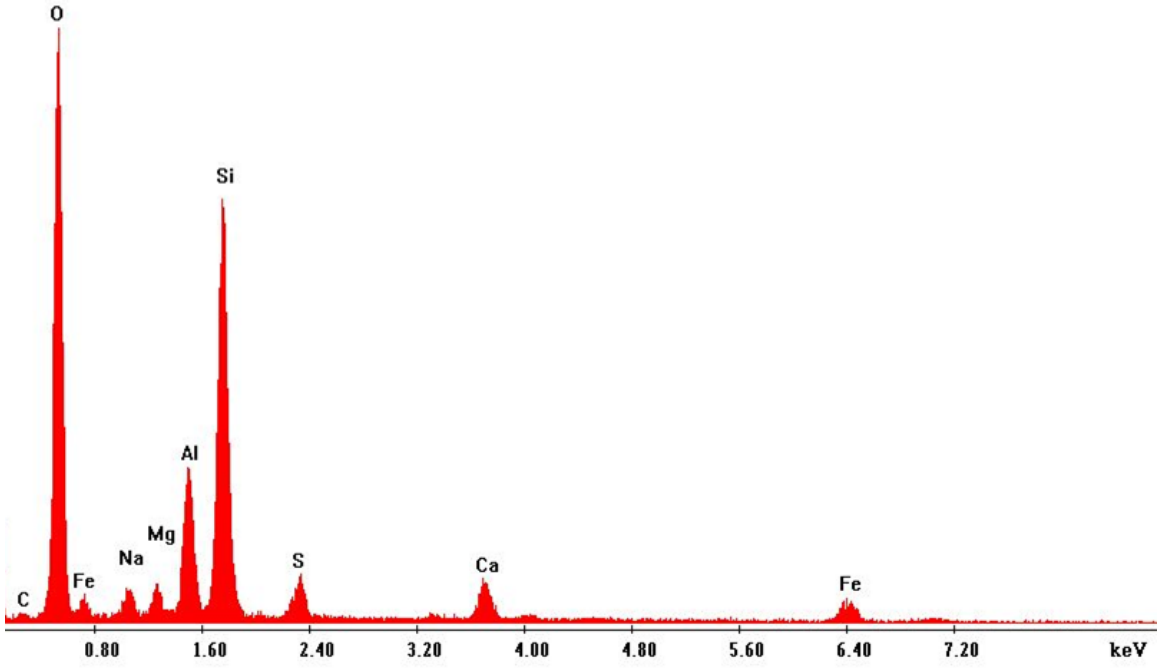

Figure C-26 ESEM of 30 % Ben, 10 % Gyps, 70 % Sand-Dry of OMC – Post swell

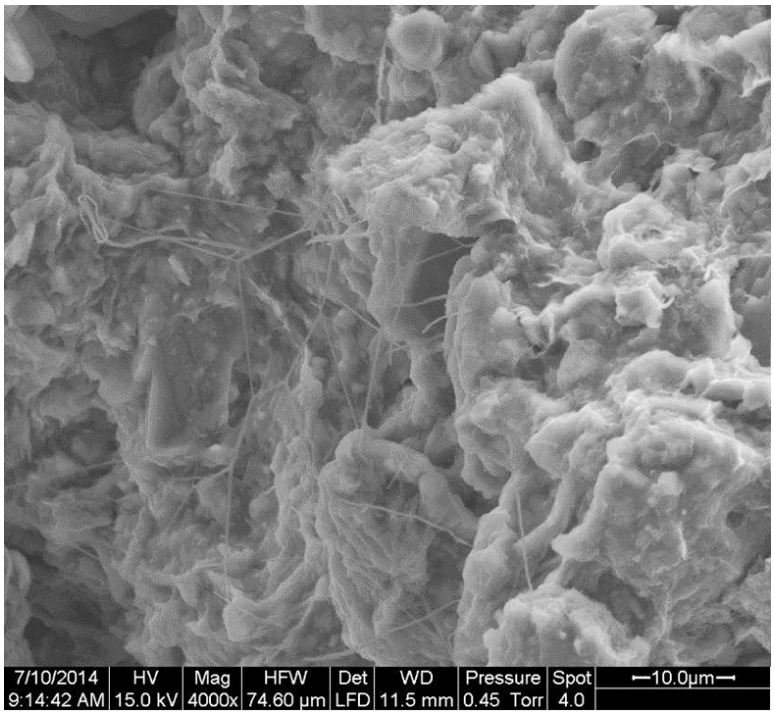

Figure C-27 ESEM of 30 % Ben, 30 % Gyps, 40 % Sand-Dry of OMC – Pre swell

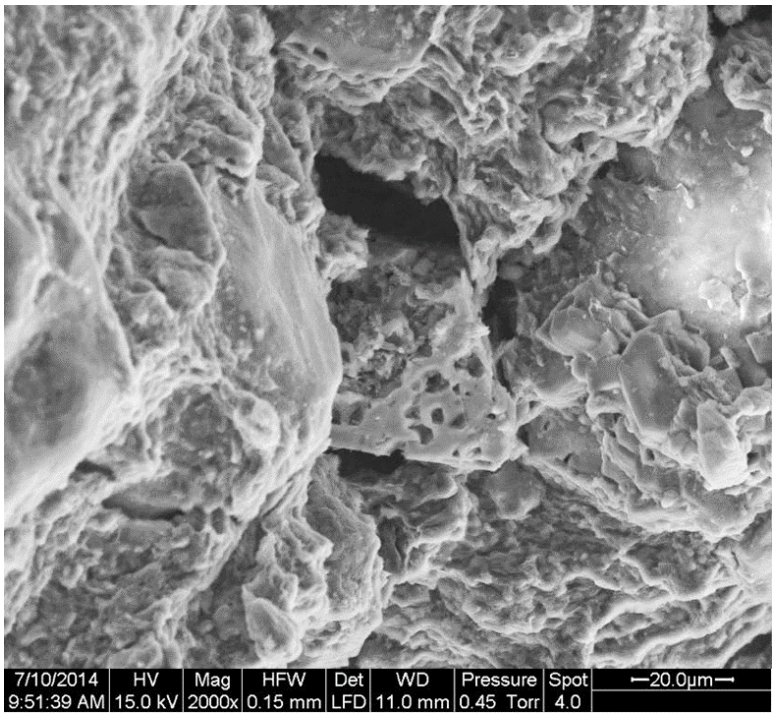

Figure C-28 ESEM of 30 % Ben, 30 % Gyps, 40 % Sand-Dry of OMC – Post swell

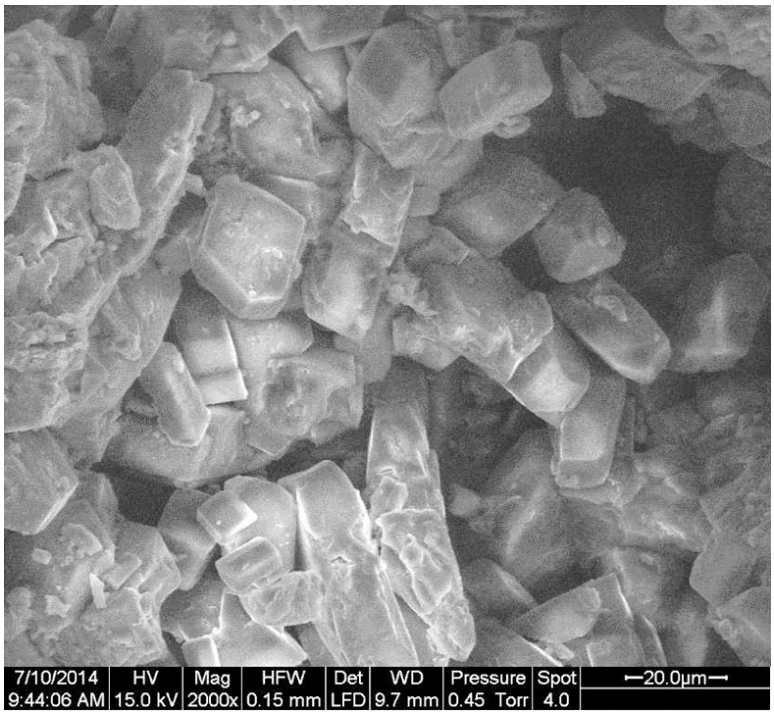

Figure C-29 ESEM of 30 % Ben, 30 % Gyps, 40 % Sand-Dry of OMC – Post swell

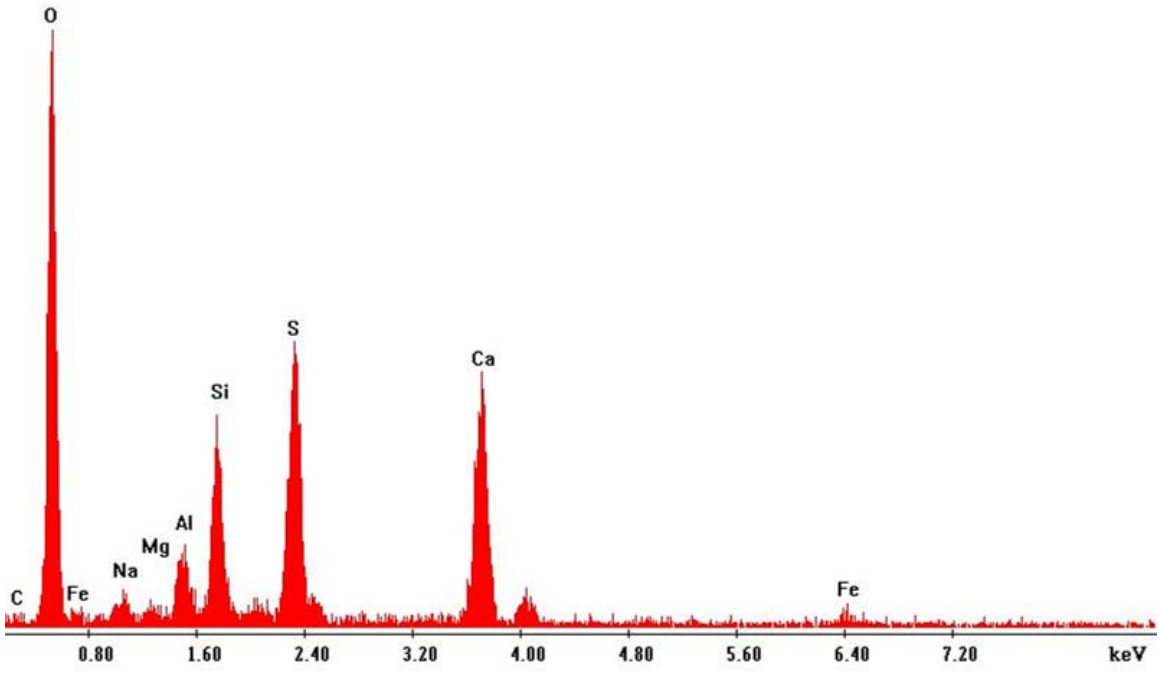

Figure C-30 EDS of 30 % Ben, 30 % Gyps, 40 % Sand-Dry of OMC – Post swell

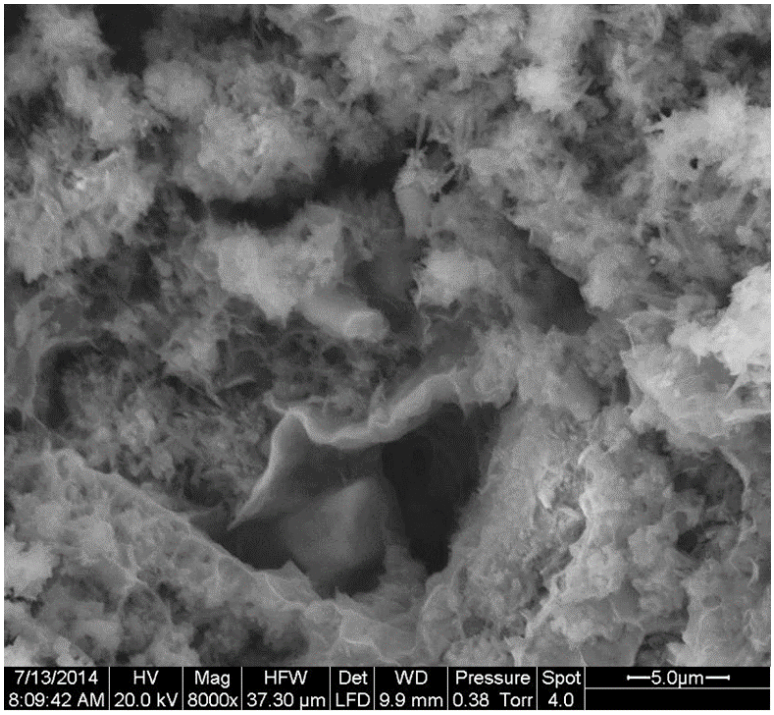

Figure C-31 ESEM of 30 % Ben, 30 % Calcite, 40 % Sand-Dry of OMC – Pre swell

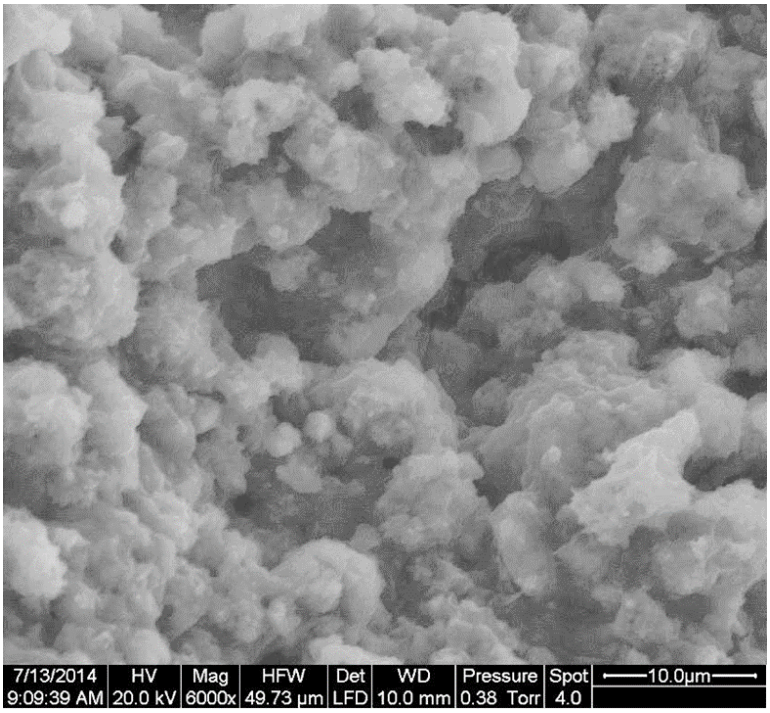

Figure C-32 ESEM of 30 % Ben, 30 % Calcite, 40 % Sand-Dry of OMC – Post swell

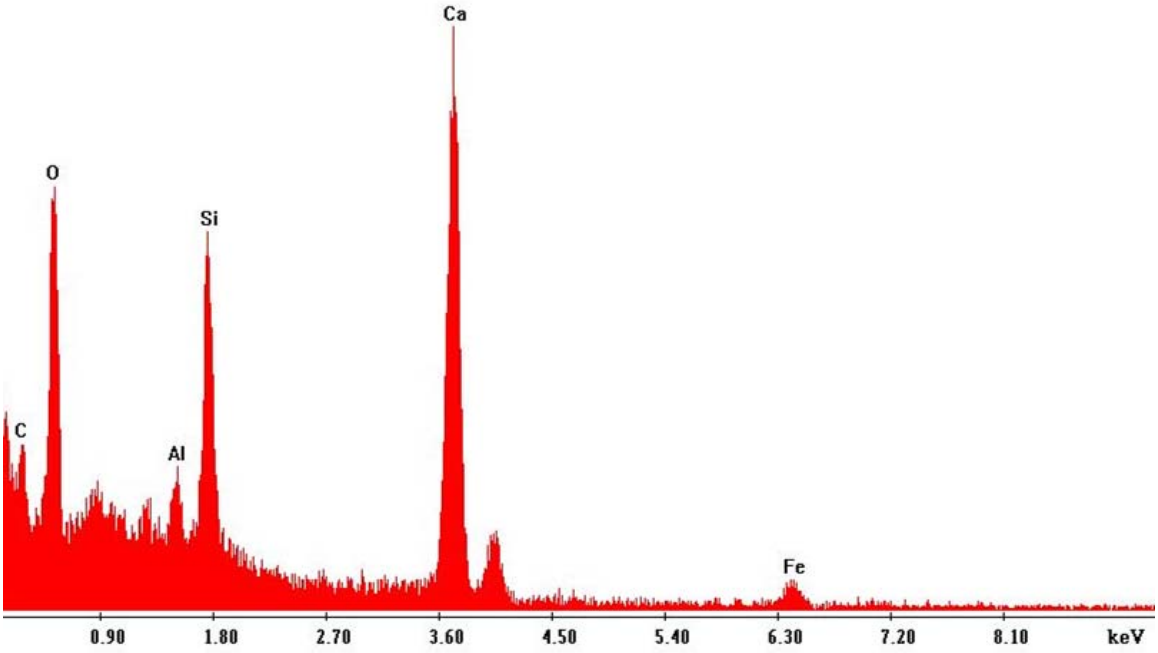

Figure C-33 EDS of 30 % Ben, 30 % Calcite, 40 % Sand-Dry of OMC – Pre swell

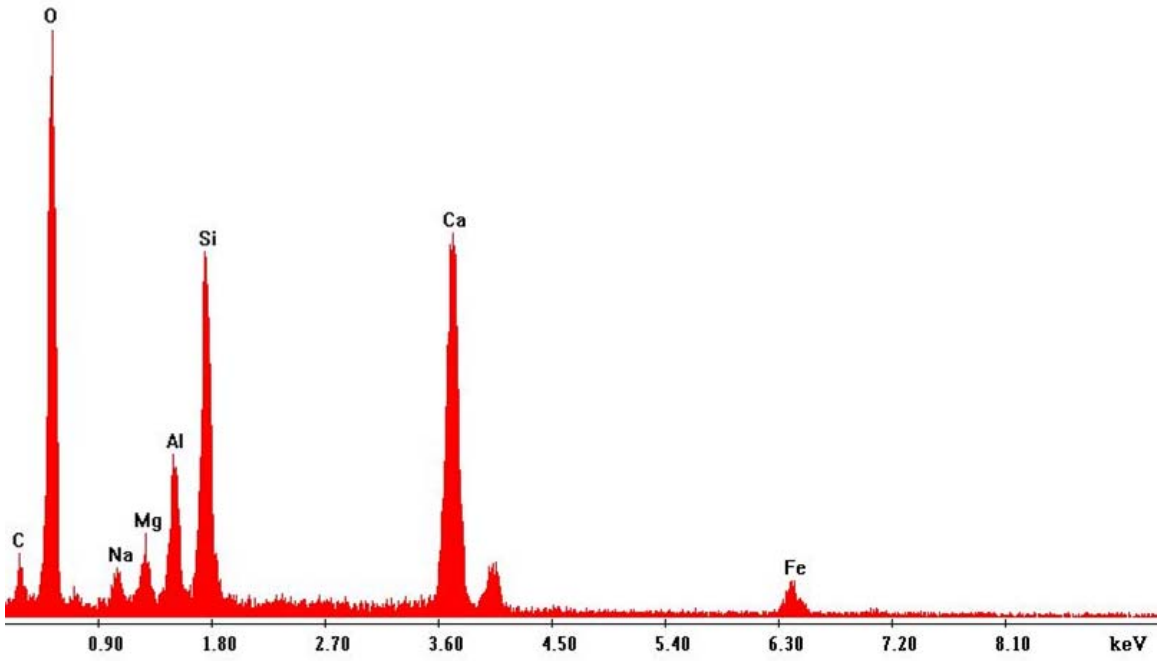

Figure C-34 EDS of 30 % Ben, 30 % Calcite, 40 % Sand-Dry of OMC – Post swell

Appendix D – Micro CT Scan Results

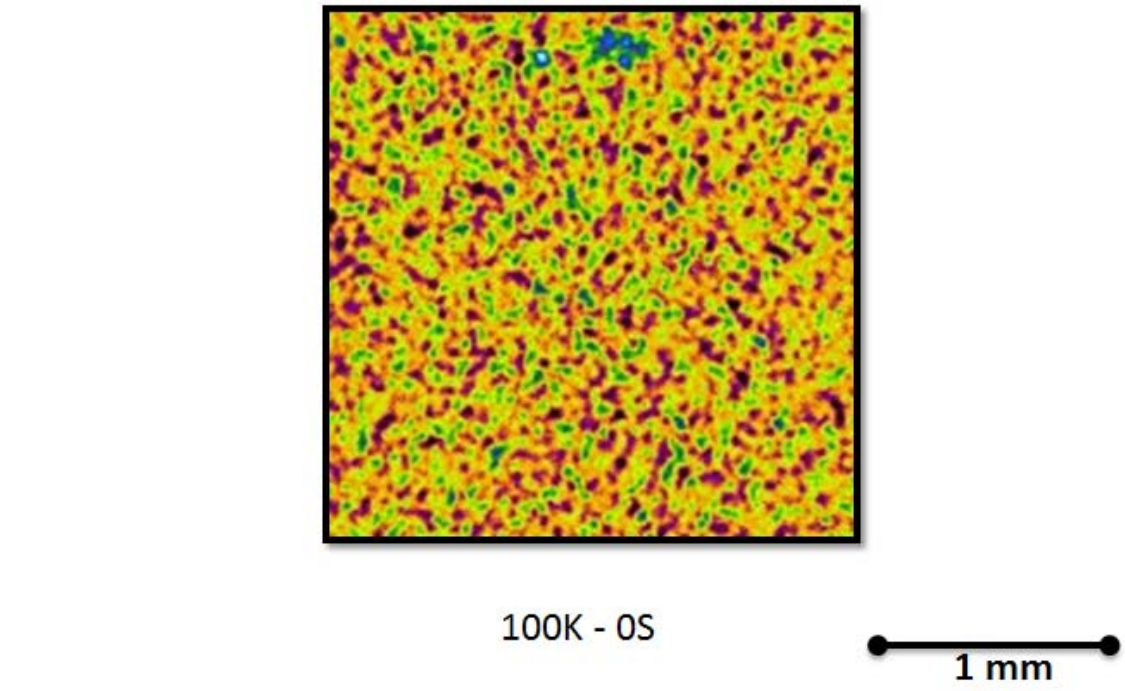

Figure D-1 Micro CT Scans of Kaolinite-Sand Compacted Specimens (Pre Swelling)

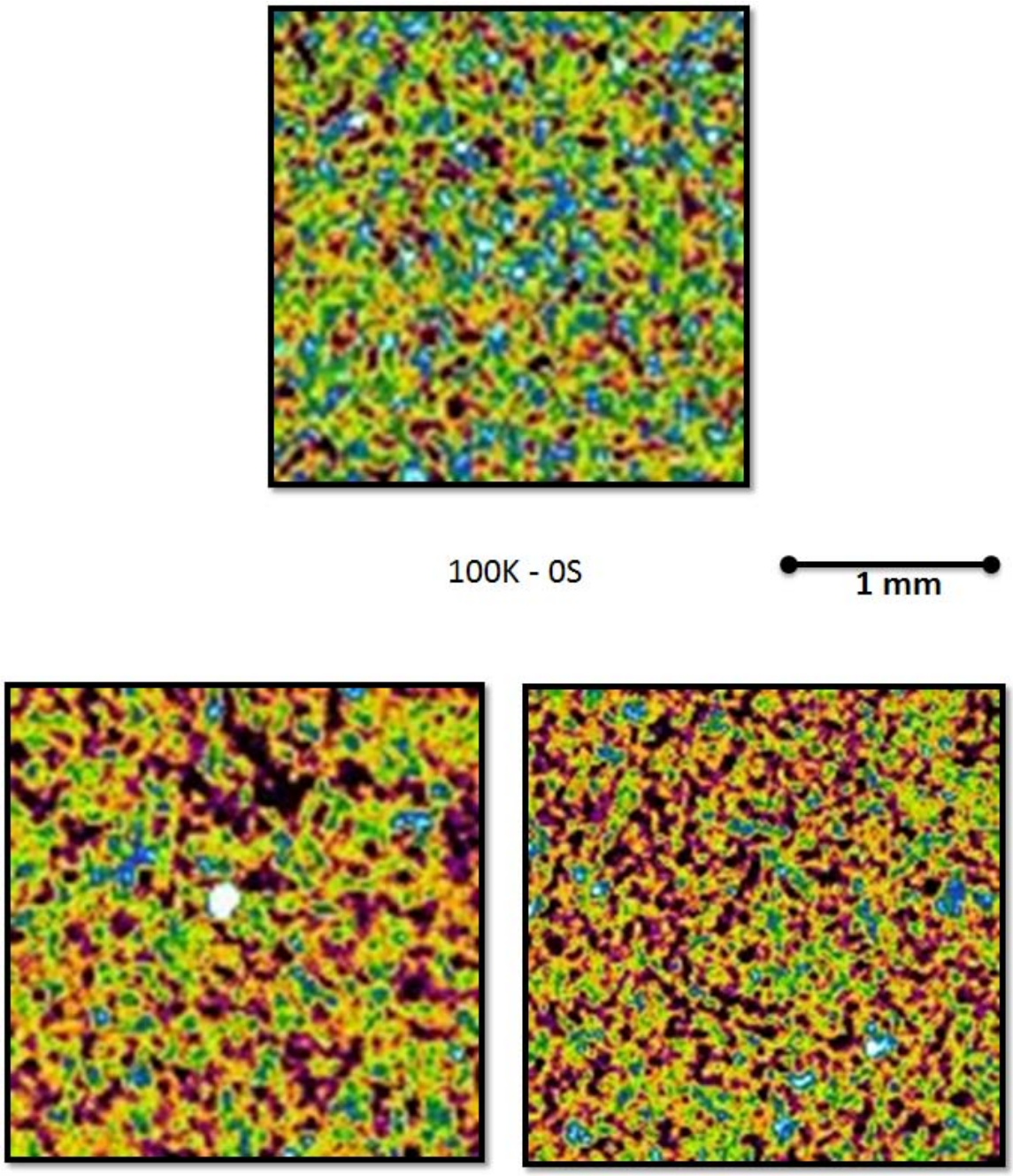

Figure D-2 Micro CT Scans of Kaolinite-Sand Compacted Specimens (Post Swelling)

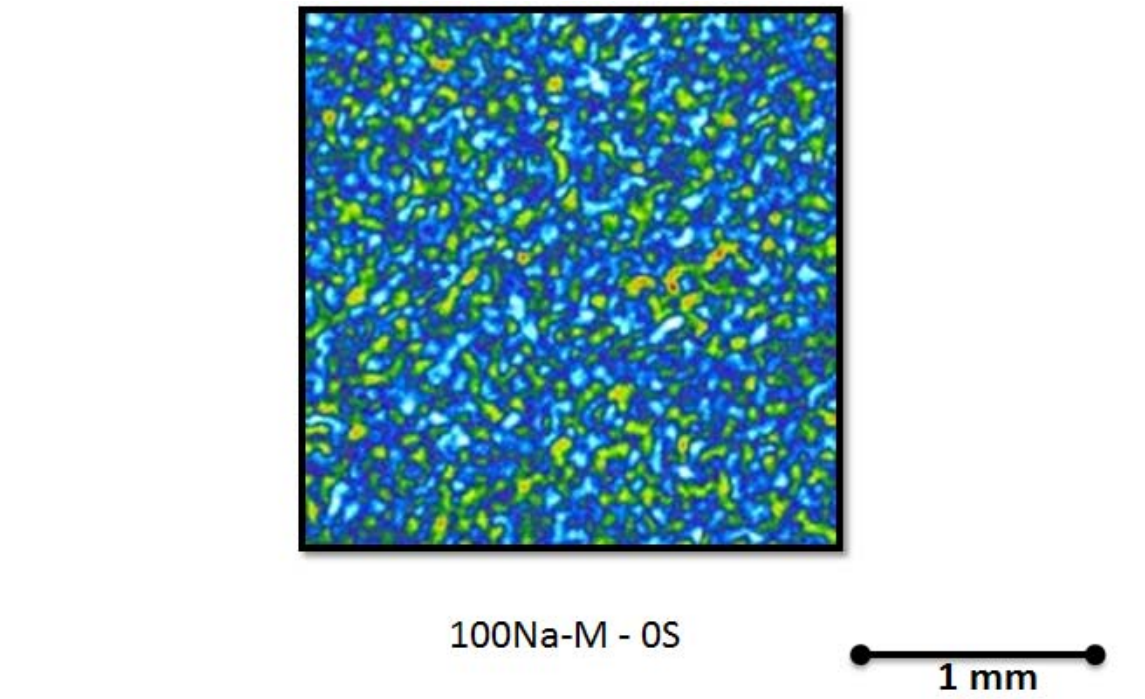

Figure D-3 Micro CT Scans of Na-Montmorillonite-Sand Compacted Specimens (Pre Swelling)

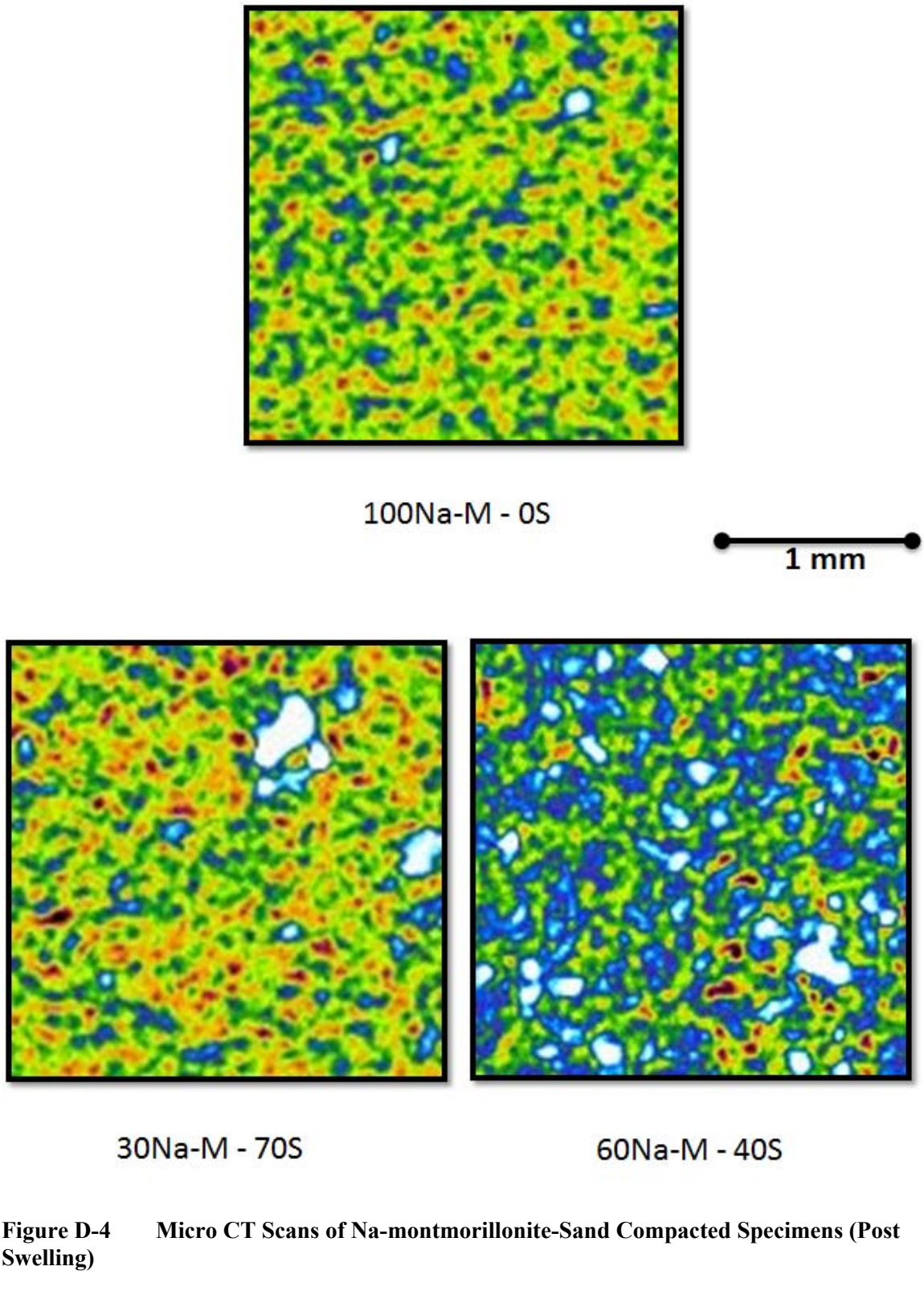

Figure D-4 Micro CT Scans of Na-montmorillonite-Sand Compacted Specimens (Post Swelling)

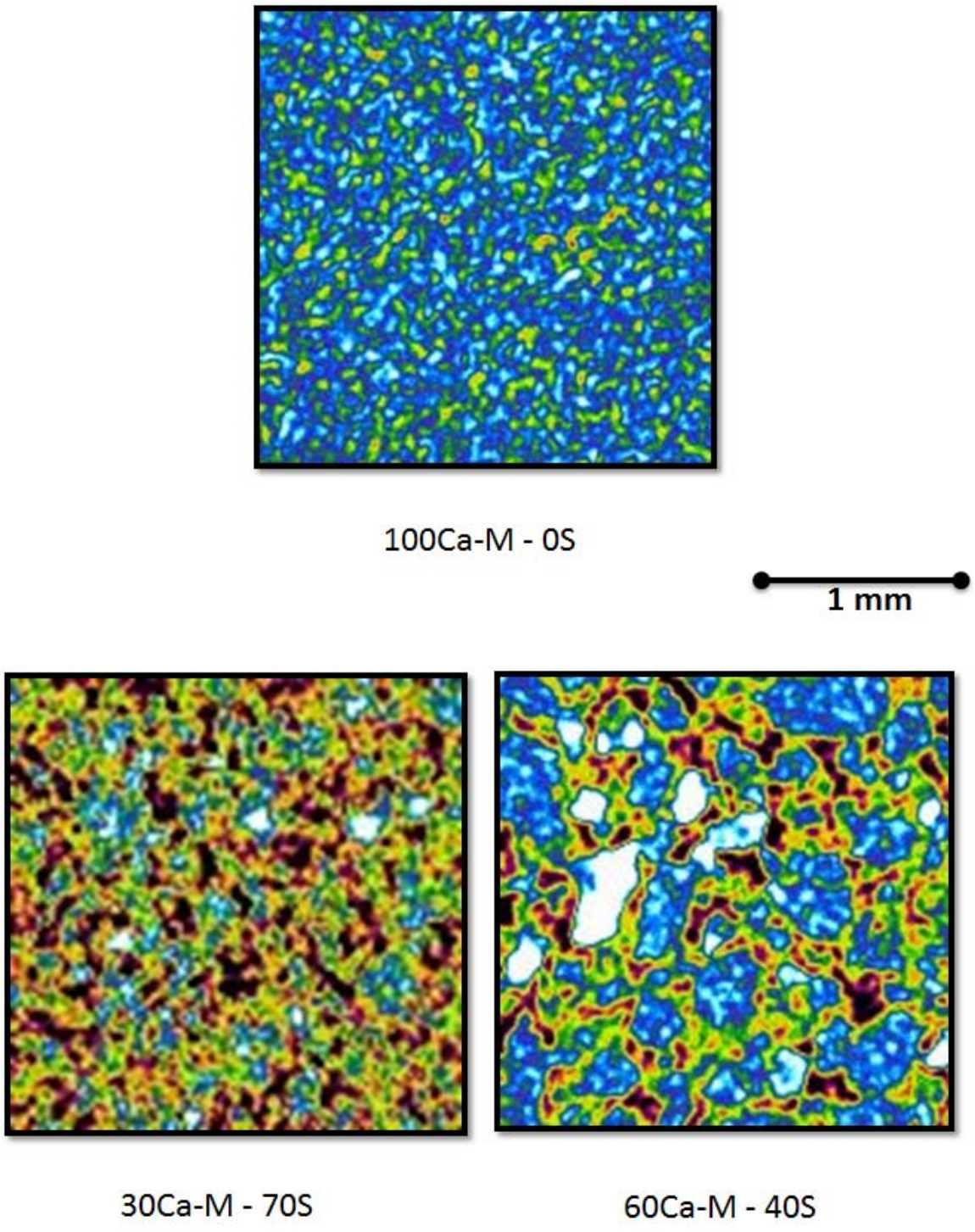

Figure D-5 Micro CT Scans of Ca-montmorillonite-Sand Compacted Specimens (Pre Swelling)

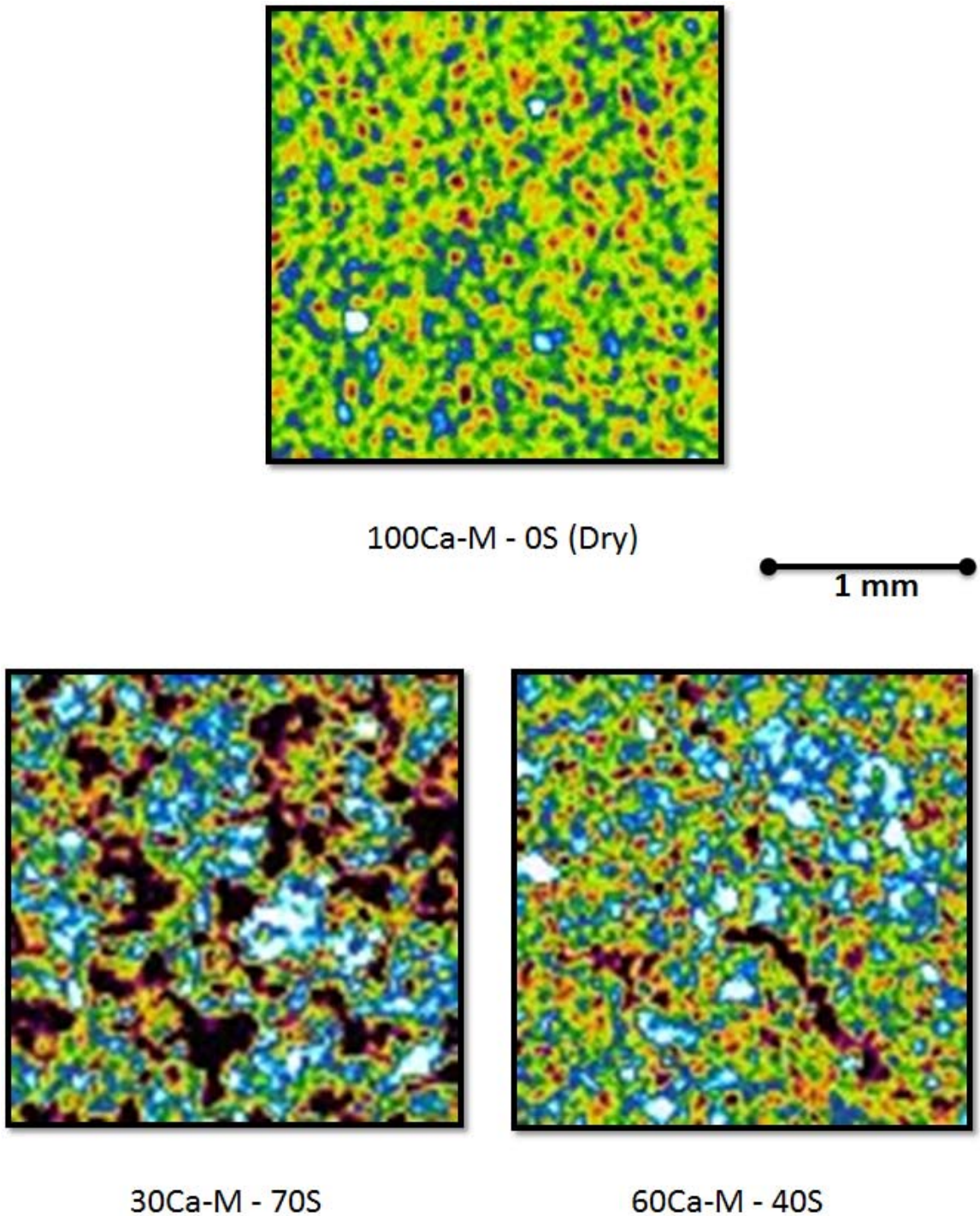

Figure D-6 Micro CT Scans of Ca-montmorillonite-Sand Compacted Specimens (Post Swelling)

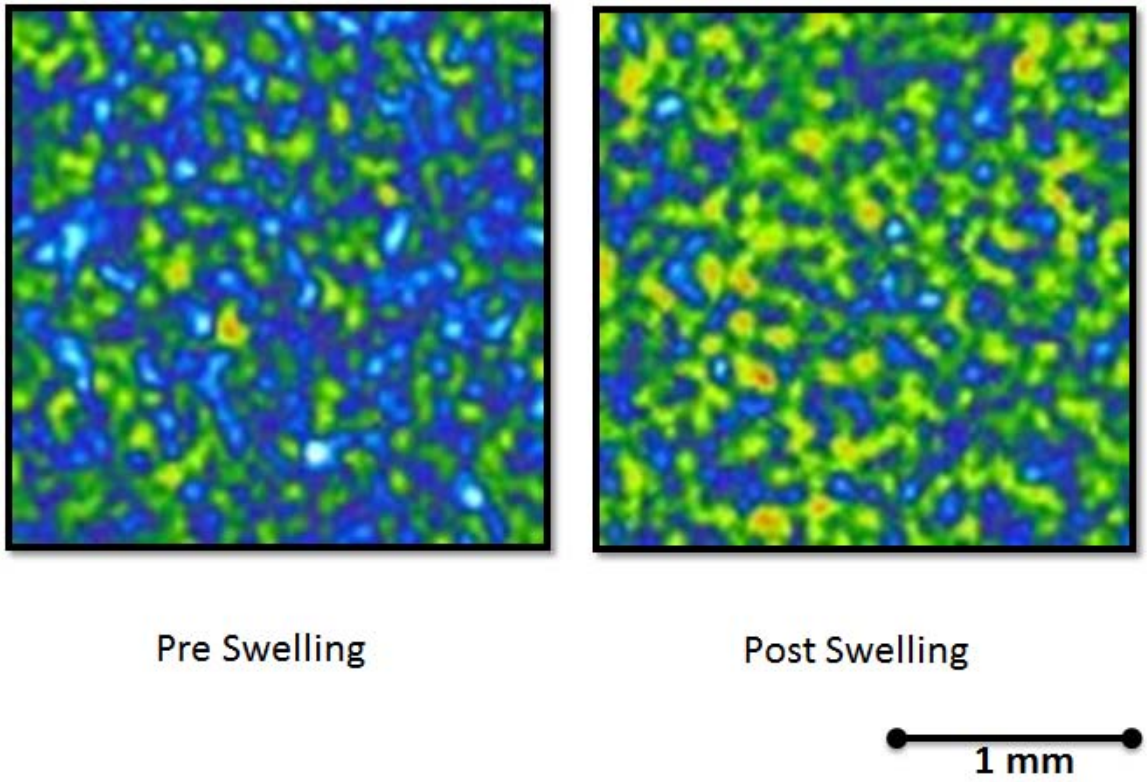

Figure D-7 Micro CT Scans of Qatif-1 Specimens (Pre and Post Swelling)

Appendix E – Molecular Simulations Results

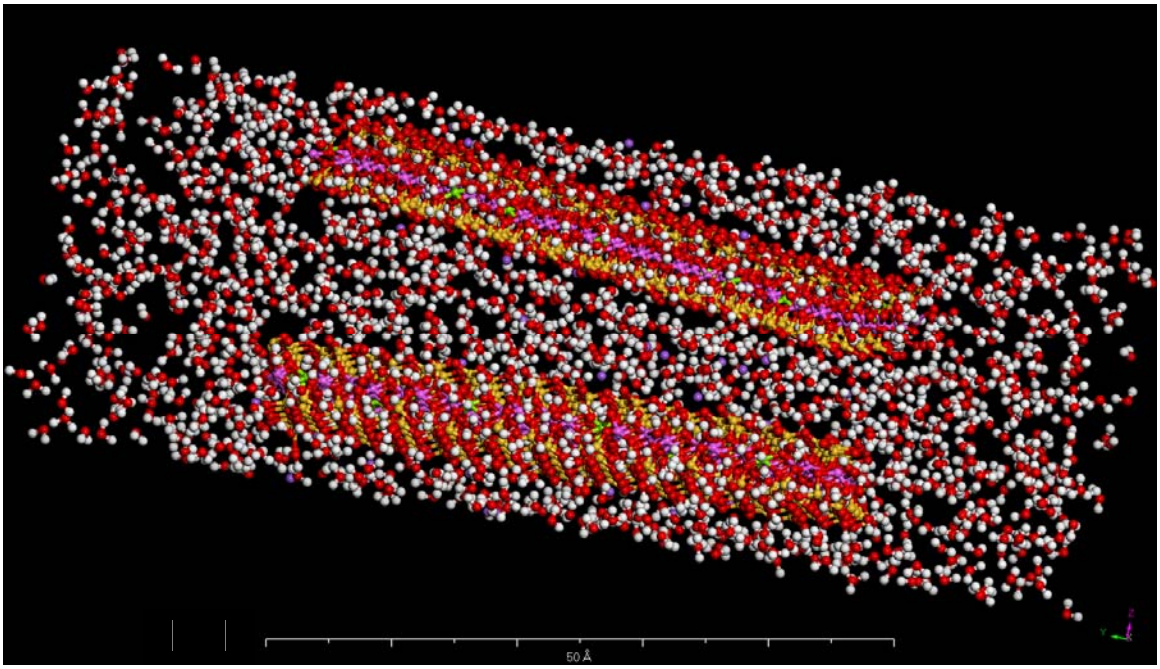

Figure E-1 Water sorbed single crystallite of Na-montmorillonite MCEC at initial water content=40%

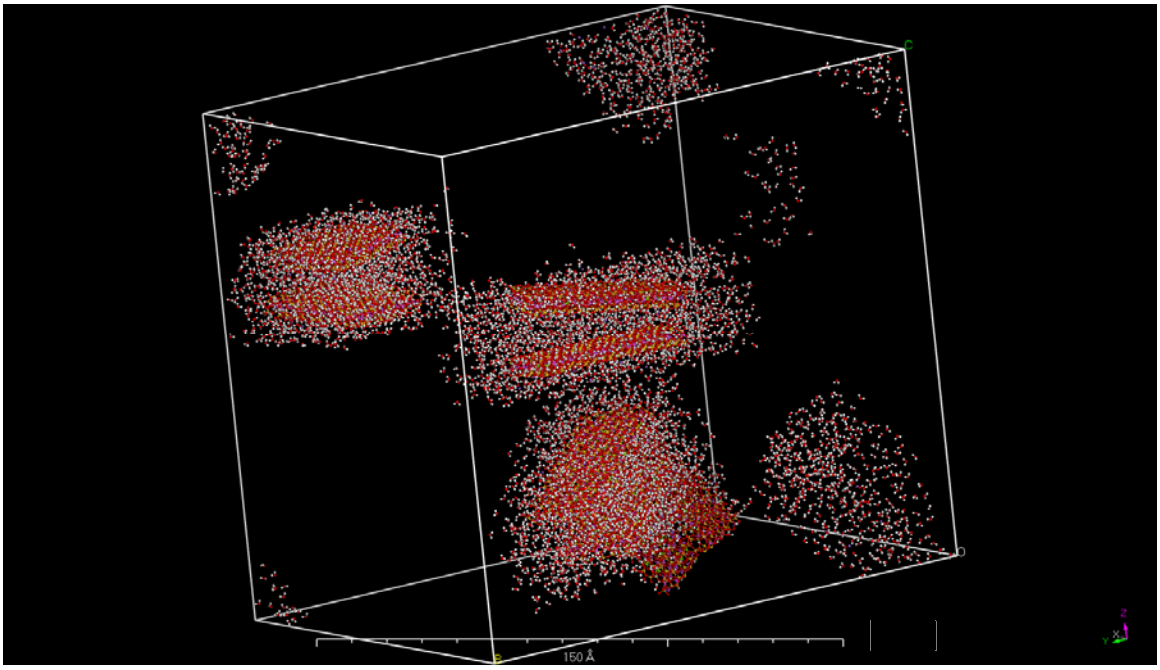

Figure E-2 Loose mix simulation of Na-montmorillonite MCEC at initial water content=40 %

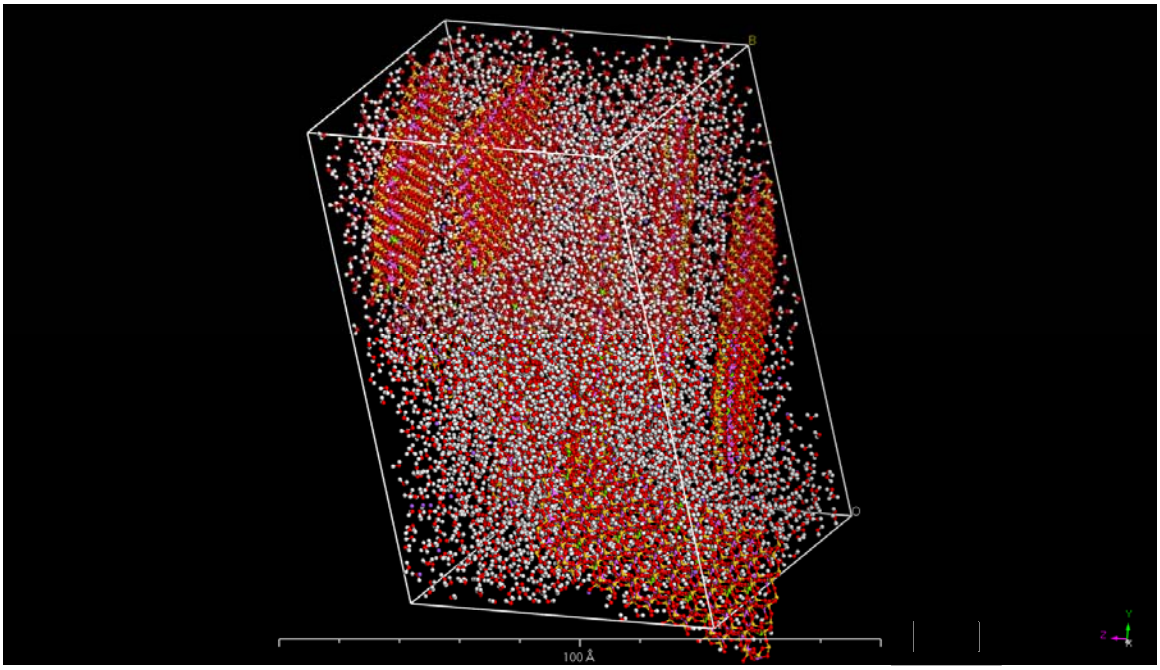

Figure E-3 Compacted unit cell of Na-montmorillonite MCEC at initial water content = 40 %

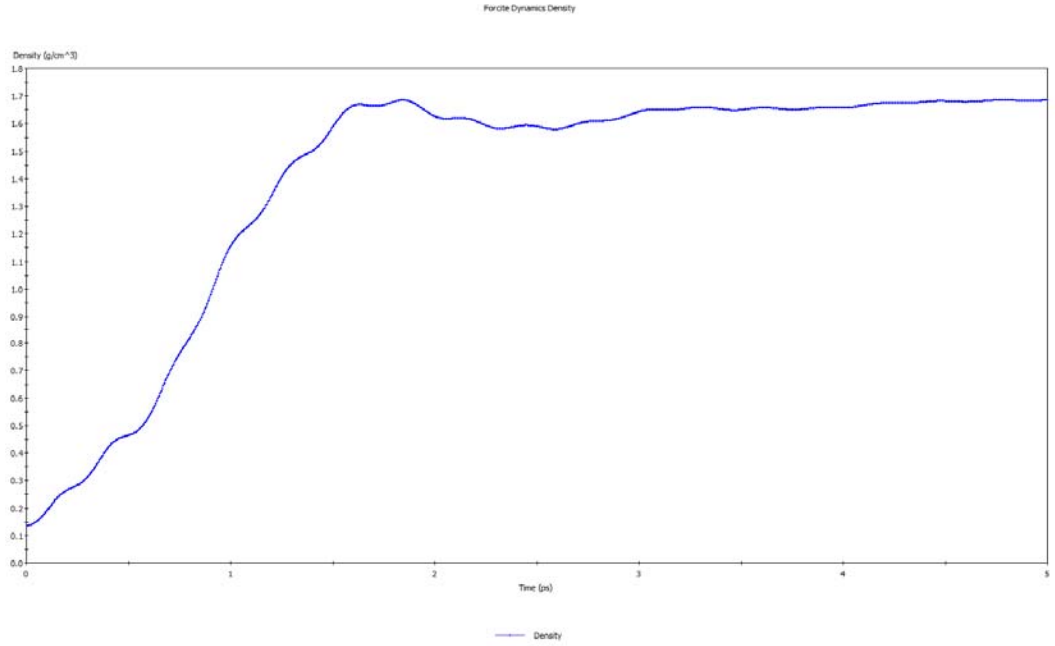

Figure E-4 Compaction plot of unit cell of Na-montmorillonite MCEC at initial water content = 40 %

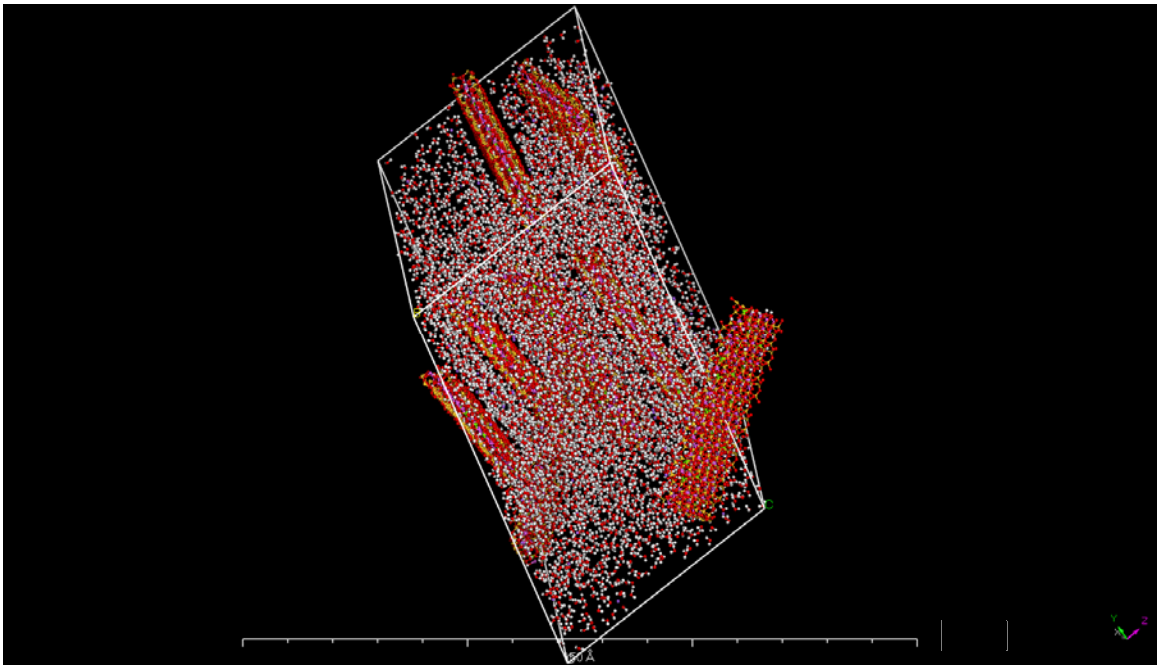

Figure E-5 Stress relaxation of the unit cell of Na-montmorillonite MCEC at initial water content=40 %

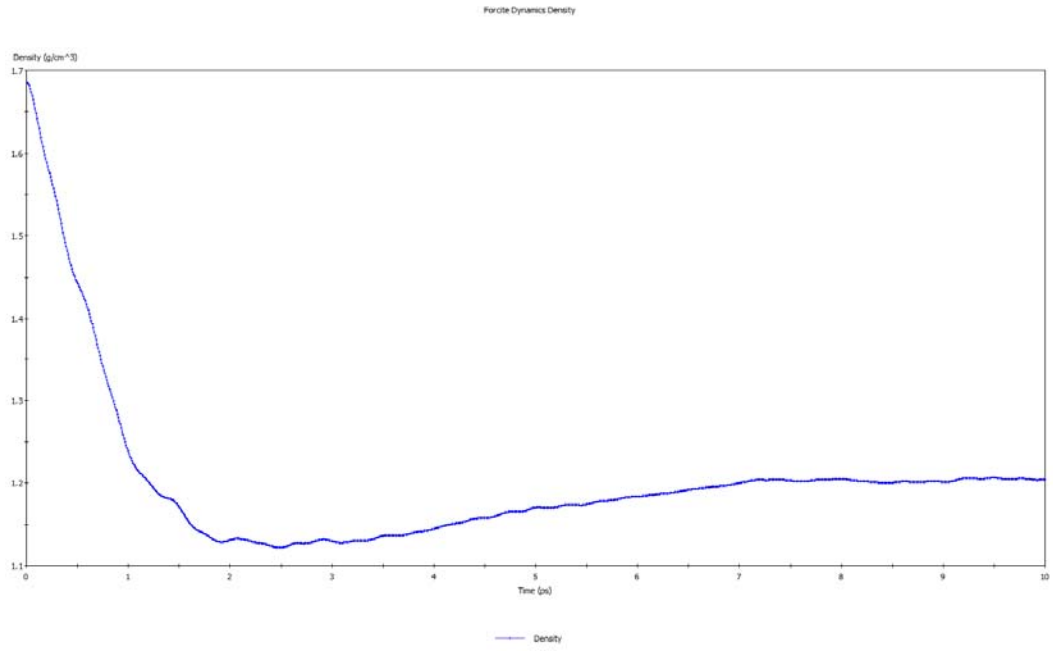

Figure E-6 Stress relaxation plot of the unit cell of Na-montmorillonite MCEC at 40 % water content

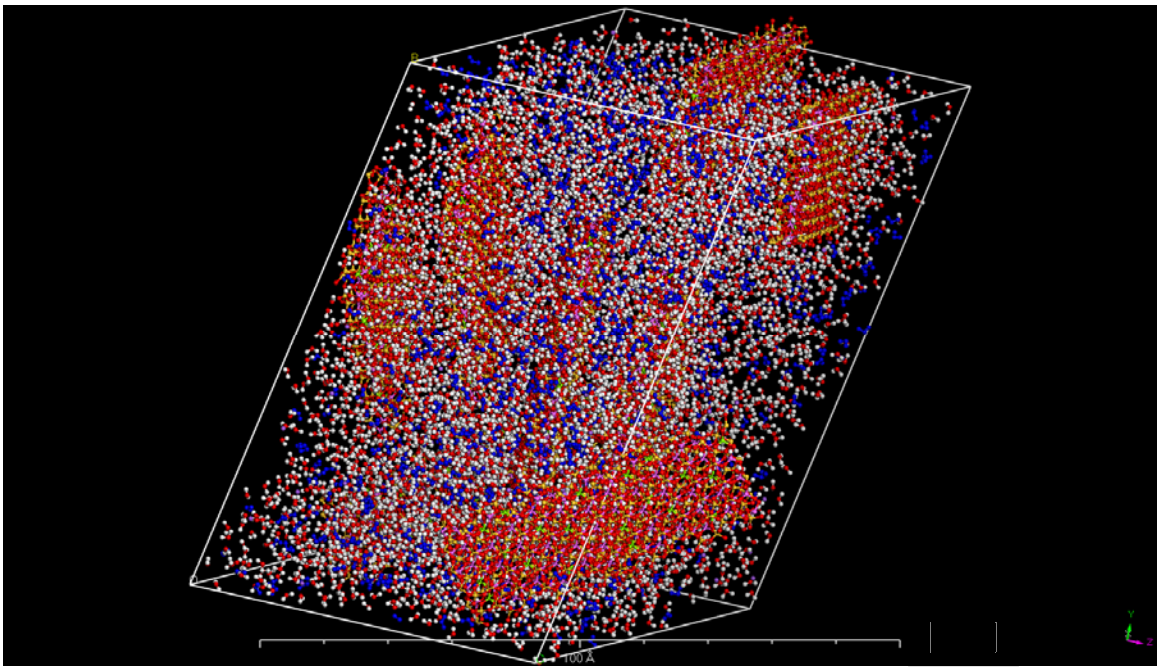

Figure E-7 10% water sorption in Na-montmorillonite MCEC crystallites unit cell (initial water content = 40 %)

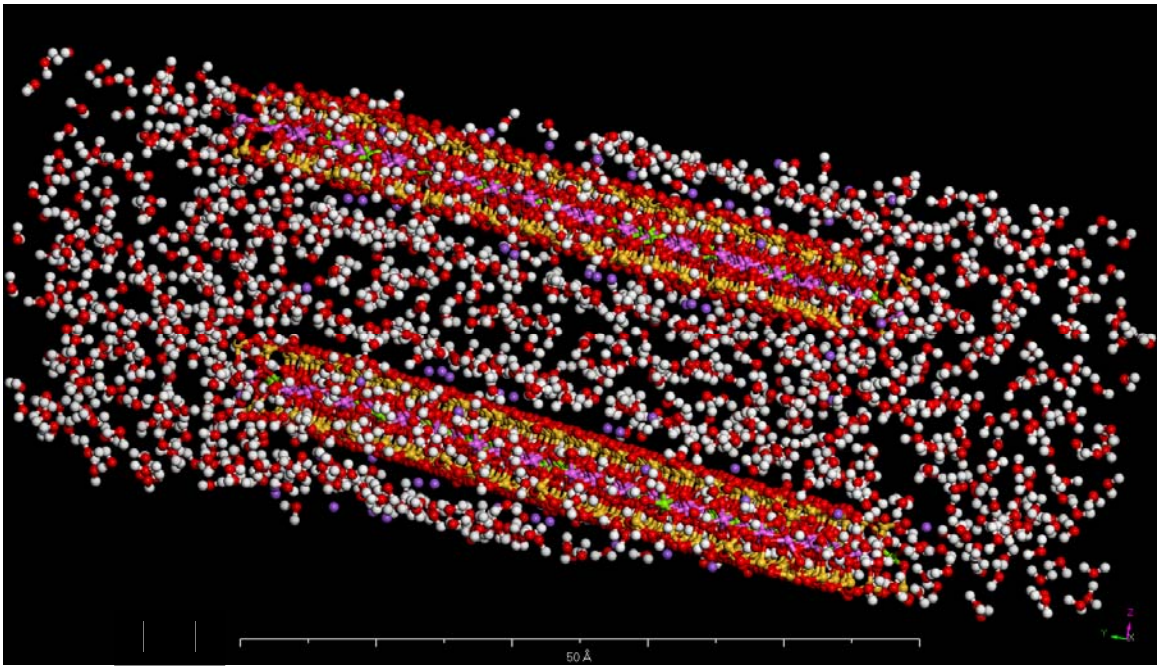

Figure E-8 Single crystallite of Na-montmorillonite HCEC at initial water content = 30 %

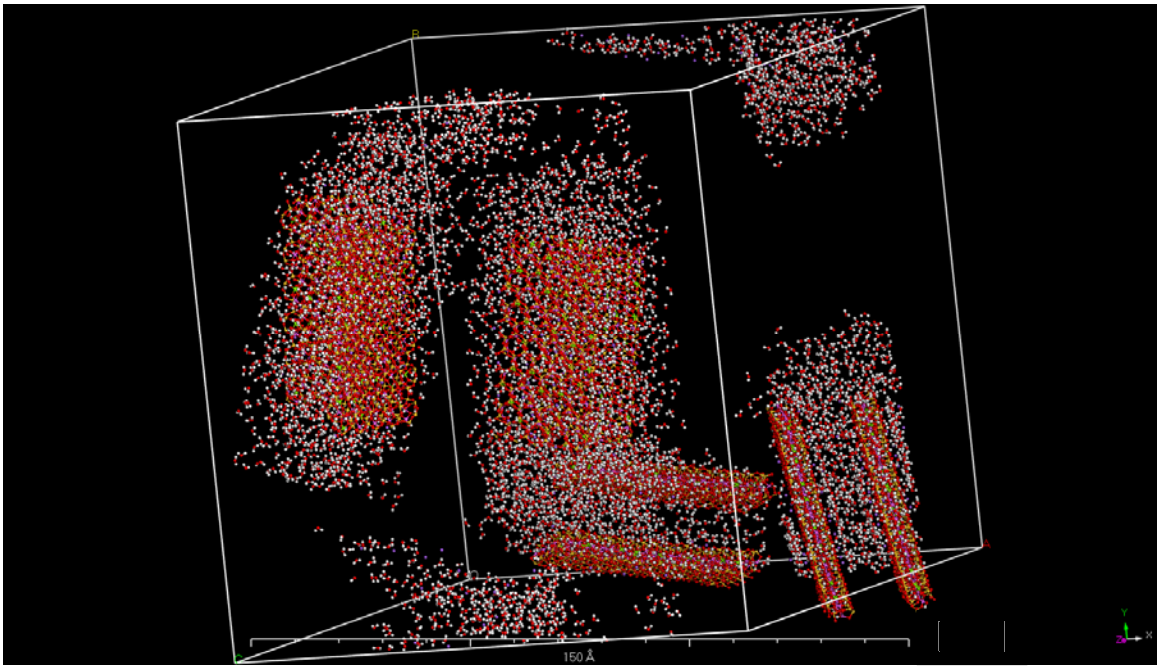

Figure E-9 Loose arrangement of crystallites of Na-montmorillonite HCEC at initial moisture content = 30 %

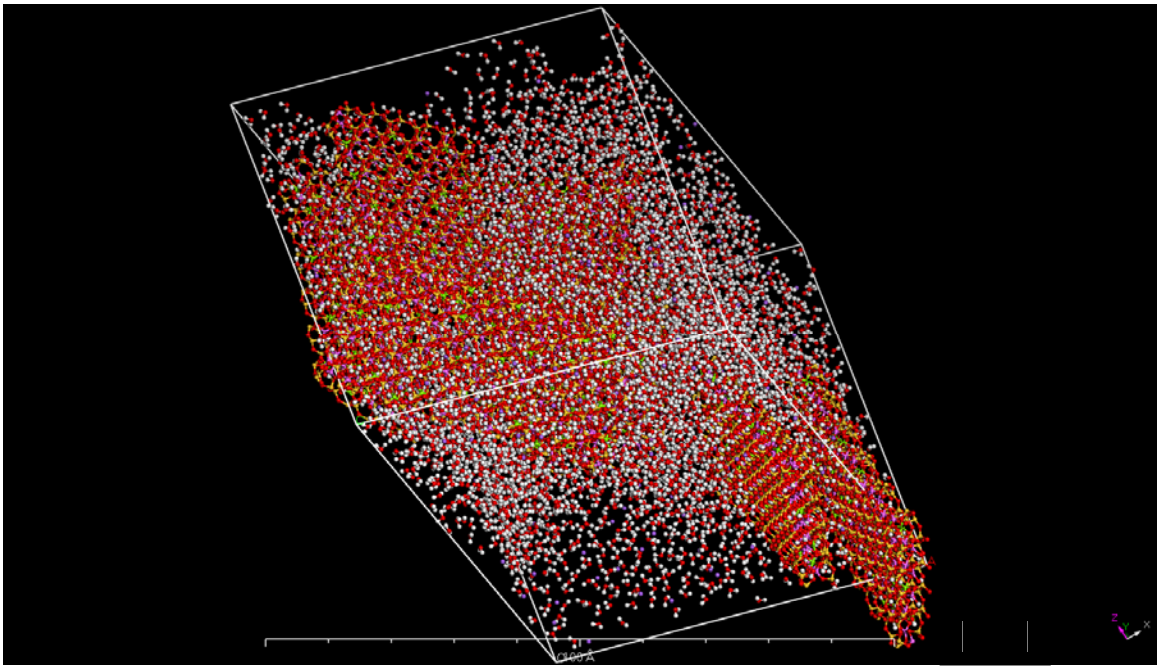

Figure E-10 Compacted unit cell of Na-montmorillonite HCEC at initial water content = 30 %

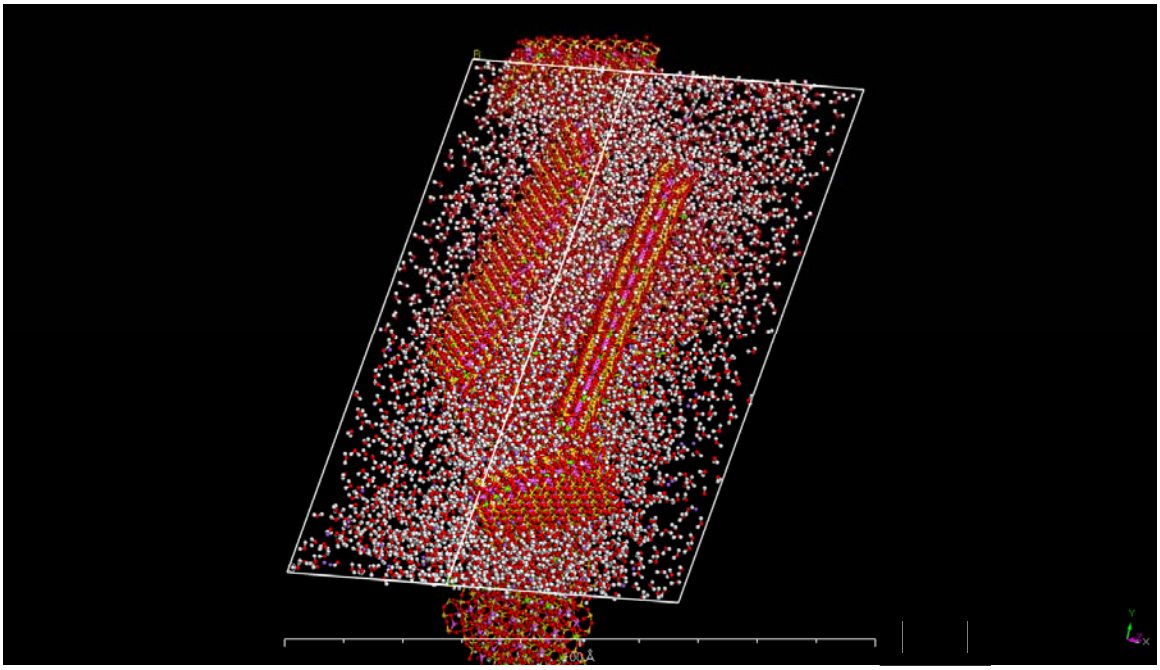

Figure E-11 Stress relaxed unit cell of Na-montmorillonite HCEC at initial water content = 30 %

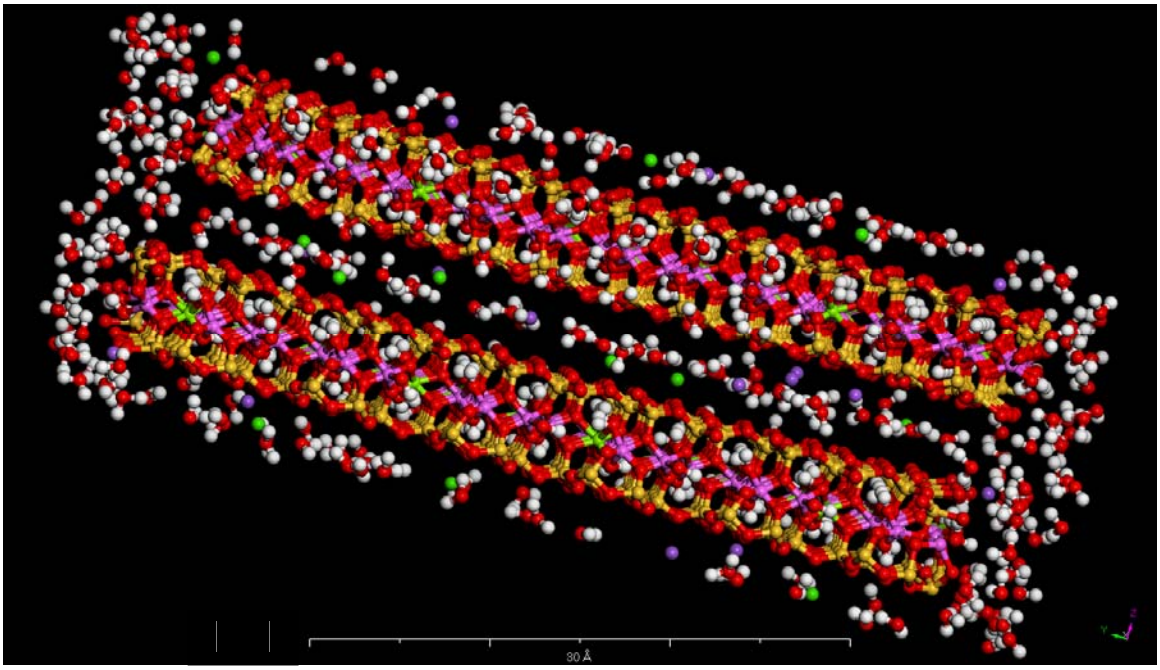

Figure E-12 Single crystallite of montmorillonite (60%Ca+40%Na) initial water content = 10 %

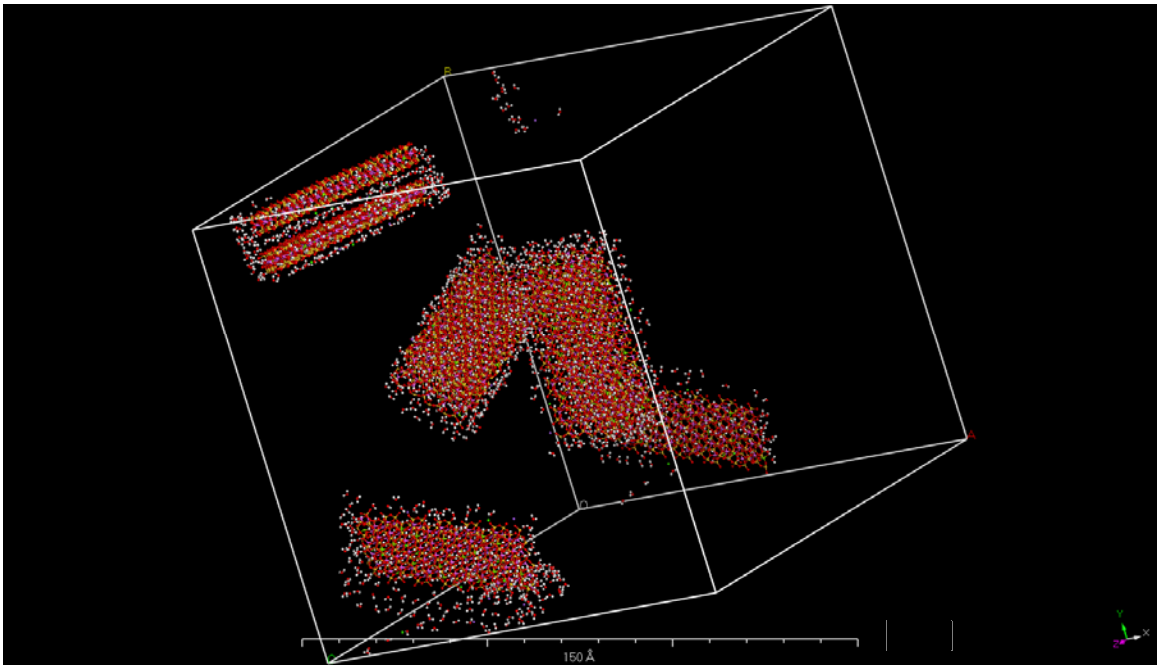

Figure E-13 Loose mix of four montmorillonite crystallites (60%Ca+40%Na) at initial moisture content = 10 %

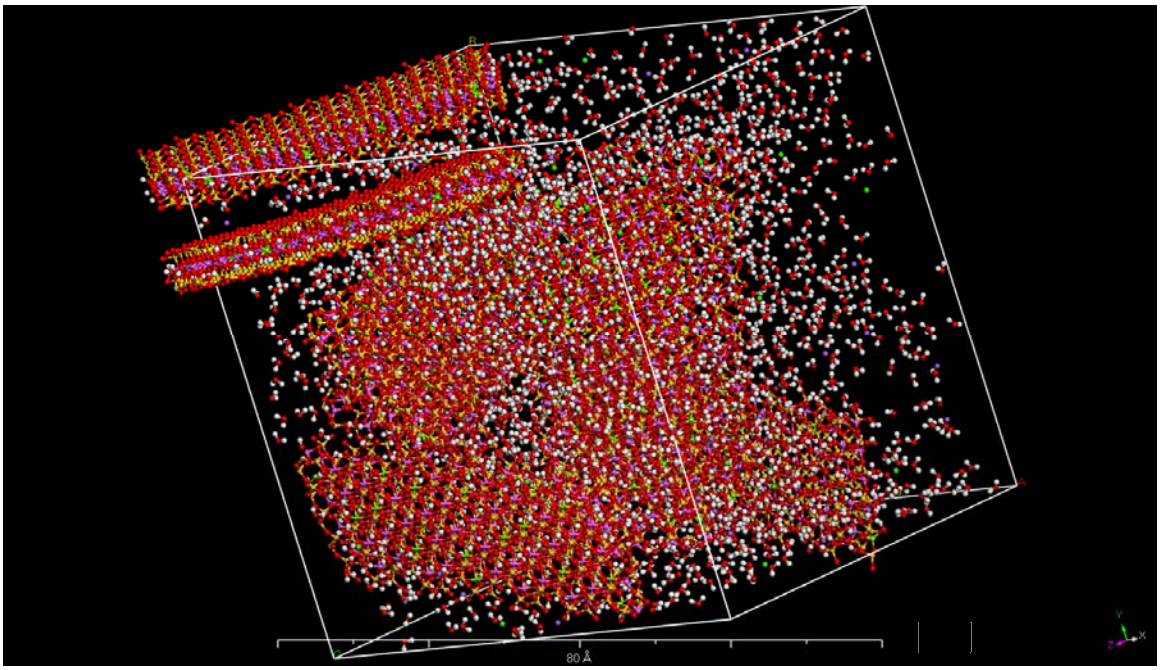

Figure E-14 Compacted four montmorillonite crystallites (60 % Ca+40 % Na) at initial moisture content = 10 %

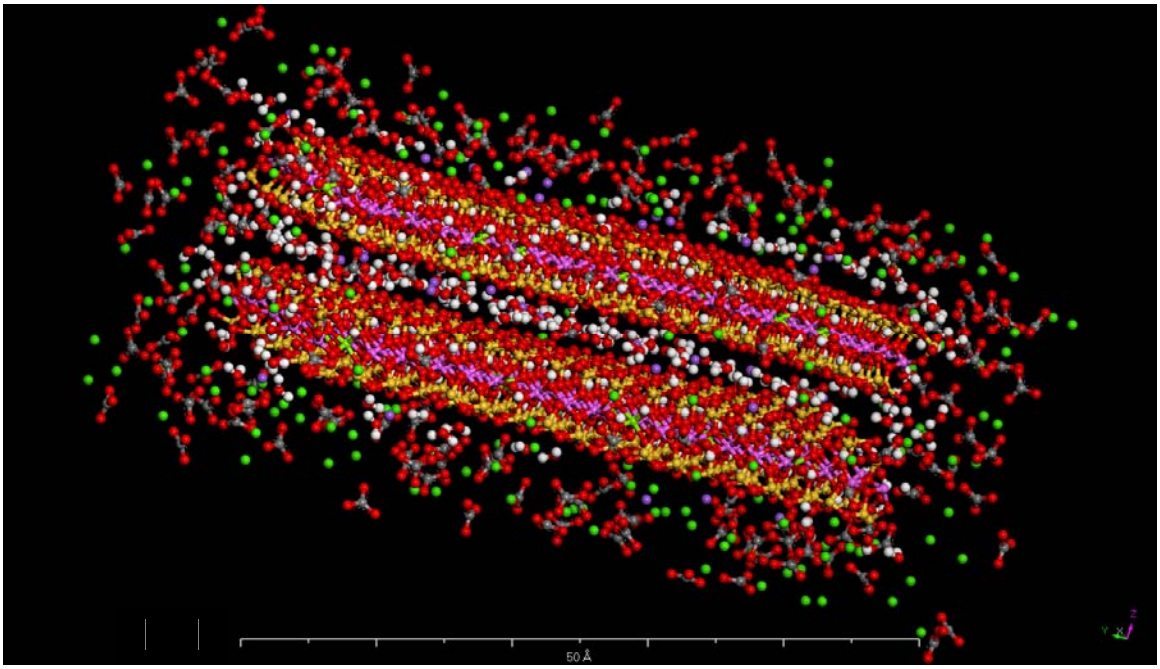

Figure E-15 Single Na-montmorillonite crystallite MCEC at initial moisture content = 10 %

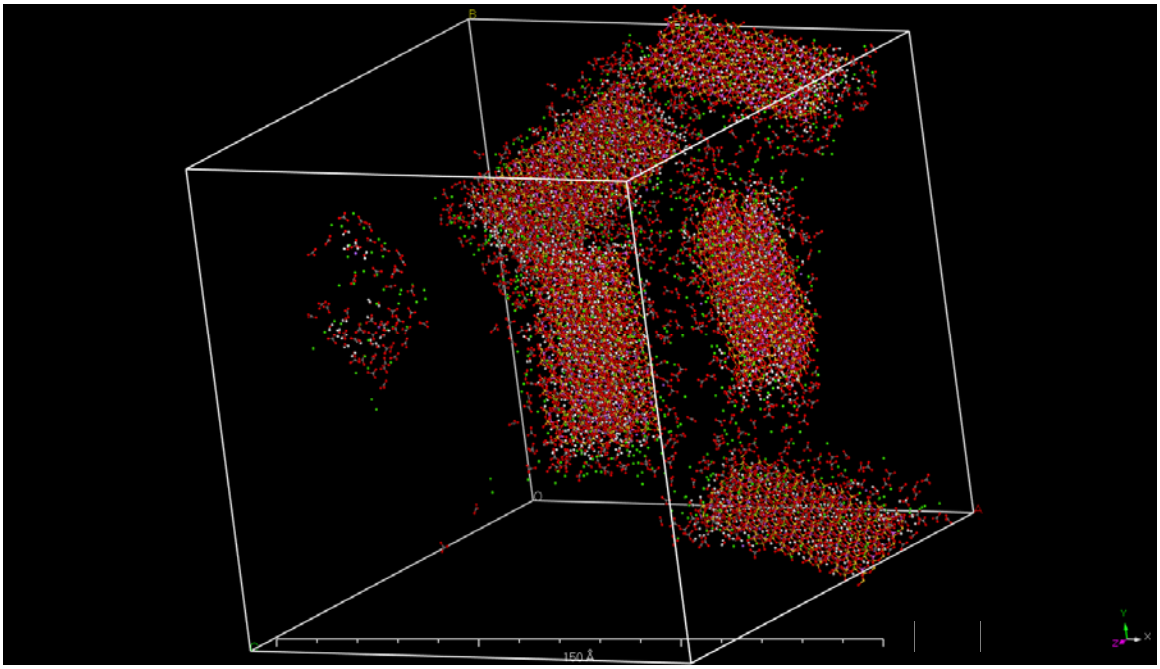

Figure E-16 Four Na-montmorillonite crystallites MCEC at initial moisture content = 10 %

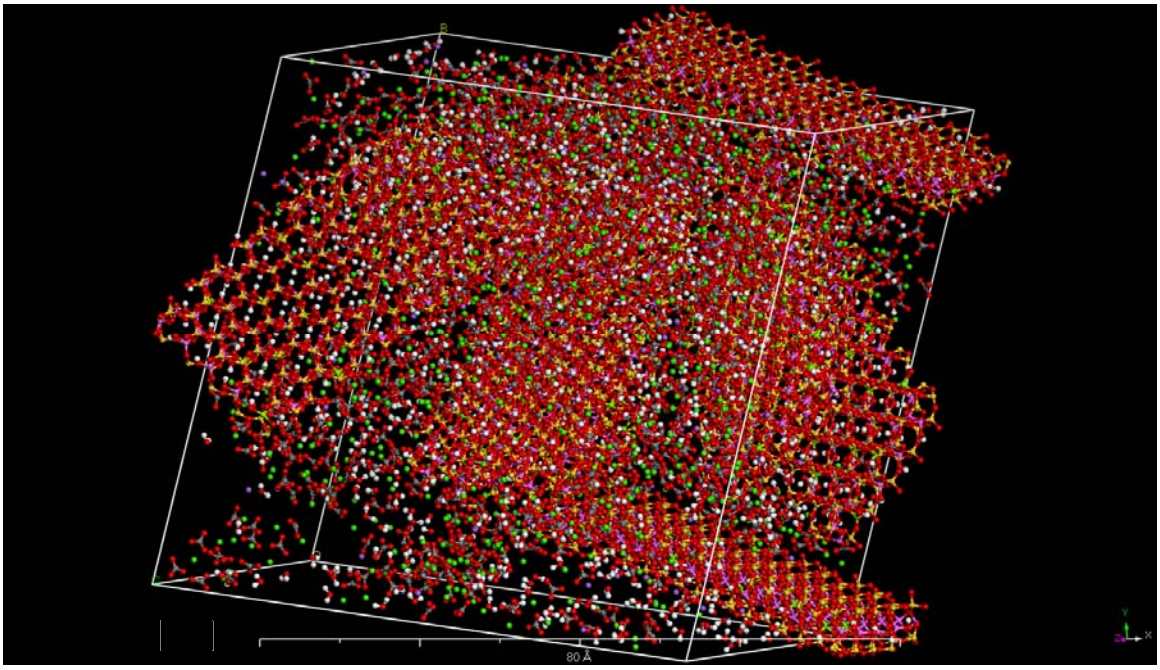

Figure E-17 Four compacted Na-montmorillonite crystallites MCEC at initial moisture content = 10 %

Appendix F – Modified Universal Forcefield (UFF)

Original Universal Forcefield

Atom Types

```
Na       Na    22.99000  0   0   0   0! sodium
Mg3+2    Mg    24.31000  0   3   0   0! magnesium, tetrahedral, +2 oxidation state
Al3      Al    26.98150  0   3   0   0! aluminium, tetrahedral
Si3      Si    28.08600  0   3   0   0    ! silicon, tetrahedral
K_       K     39.94800  0   0   0   0! potassium
Ca6+2    Ca    40.08000  0   6   0   0 ! calcium, octahedral, +2 oxidation state
```

Diagonal vdw

```
Na       LJ_6_12      2.9830  0.3000E-01
Mg3+2    LJ_6_12      3.0210  0.1110E+00
Al3      LJ_6_12      4.4990  0.5050E+00
Si3      LJ_6_12      4.2950  0.4020E+00
K_       LJ_6_12      3.8120  0.3500E-01
Ca6+2    LJ_6_12      3.3990  0.2380E+00
```

Atom typing rules

```
Mg3+2        Mg        0        0        0        1
Al3          Al        3        0        0        1
Si3          Si        3        0        0        1
```

Generators

```
Na       1.5390  180.0000   1.0809   0.0000   0.0000   0.0000      3      -1   0.0000   2.84300
Mg3+2    1.4210  109.4712   1.7866   0.0000   0.0000   0.0000      3      -1   0.0000   3.95100
Al3      1.2440  109.4712   1.7924   0.0000   0.0000   0.0000      3      -1   0.0000   3.04100
Si3      1.1170  109.4712   2.3232   0.0000   0.0000   0.0000      3      -1   1.2250   4.16800
```

Modified Universal Forcefield

Atom Types

Na	Na	22.99000	0.0000	0	0	0	! sodium
Mg6+2	Mg	24.31000	0.0000	6	0	0	! magnesium, octahedral, +2 oxidation state
Al6	Al	26.98150	0.0000	6	0	0	! aluminium, octahedral
Si3	Si	28.08600	0.0000	3	0	0	! silicon, tetrahedral
K_	K	39.94800	0.0000	0	0	0	! potassium
Ca6+2	Ca	40.08000	0.0000	6	0	0	! calcium, octahedral, +2 oxidation state

Diagonal vdw

Na	LJ_6_12	2.6378	0.1301E+00
Mg6+2	LJ_6_12	5.9090	0.9029E-06
Al6	LJ_6_12	4.7943	0.1329E-05
Si3	LJ_6_12	3.7064	0.1841E-05
K_	LJ_6_12	3.7423	0.1000E+00
Ca6+2	LJ_6_12	3.3990	0.2380E+00

Atom typing rules

Mg6+2	Mg	0	0	0	1
Al6	Al	3	0	0	1
Si3	Si	3	0	0	1

Generators

Na	1.5390	180.0000	1.0809	0.0000	0.0000	0.0000	3	-1	0.0000	2.84300
Mg6+2	1.4210	109.4712	1.7866	0.0000	0.0000	0.0000	3	-1	0.0000	3.95100
Al6	1.2440	109.4712	1.7924	0.0000	0.0000	0.0000	3	-1	0.0000	3.04100
Si3	1.1170	109.4712	2.3232	0.0000	0.0000	0.0000	3	-1	1.2250	4.16800

Vitae

Name :Habib-ur-Rehman Ahmed

Nationality :Pakistani

Date of Birth :11/4/1967

Email :habib.hurehman@gmail.com

Address :33-C, Satellite Town, Sargodha , Pakistan

Academic Background :B.Sc. Civil Engineering from UET Lahore Pakistan

M.S. Civil Engineering, KFUPM, Dhahran, Saudi Arabia

- More than 20 Years of Multinational (Saudi Arabia and Pakistan) Experience in the fields of Geotechnical engineering, design, and construction.

- Aug 2008 to date: Acting as Regional Manager / Chief Geotechnical Engineer, Eastern Province Riyadh Geotechnique and Foundations, Al-Khobar, Saudi Arabia.

- July 2002 to Aug 2008: Owned GeoMaterialSystems (GMS), Pakistan as sole owner / Director. GMS was a Geotechnical, Piling and Materials Consultancy and have accomplished more than 500 geotechnical investigations, shoring and piling designs and check engineering projects. Owned latest and state-of-the-art analysis and design software and geophysical testing equipment. Review and check engineering of geotechnical investigation reports including the assessment of the adequacy of the scope of work, authenticity of the field and laboratory

investigations, and the accuracy of the geotechnical data analysis and design. Design and review of the geotechnical designs including shallow and deep foundations, shoring, dewatering, and soil-structure interaction problems.

- August 2007 to Aug 2008: As Assistant Professor at Department of Transportation Engineering and Management (DTEM), University of Engineering and Technology (UET), Lahore, Pakistan.

- Five (5) Years Teaching and Research Experience at National Institute of Transportation (NIT), Risalpur Cantt.; a constituent Graduate Civil Engineering institute of National University of Sciences and Technology (NUST), Rawalpindi, Pakistan.

- Six (6) Years experience as Senior Geotechnical Engineer and took care of scores of Geotechnical investigations and design projects while working with Rashid Geotechnical and Materials Engineers (RGME), Saudi Arabia.

- Three (3) Years experience as Research Assistant in King Fahd University, Saudi Arabia on a funded project involving Characterization and Stabilization of Indigenous Soils / Aggregates for Road Construction purposes and also performed some specialized testing such as Resilient Modulus on Bound and Unbound Material.

- Well-versed with state-of-the-art Analysis, Design and Evaluation Software such as Plaxis 3D Foundations, Allpile, LPile, APile, CAPWAP, GRLWEAP, GEO Studio (Slope/W, Sigma/W, Seep/W, Quake/W), Settle 3D, Pdisp, gINT, GGU, RES2DINV, GEO-5, DEEP EXCAVATION CONTRACTOR and others.

- Have Fourteen (14) International and National Level Publications (Including Three (3) International Journals Publications with a minimum of Six (6) in process.

- Have taught Geotechnical Site Investigations, Slope Stability, Advanced Soil Mechanics, Pavement Materials Engineering, Pavement Rehabilitation, Geometric Design of Highways and Streets, Concrete Materials Technology courses to MS and PhD level students of Geotechnical and Pavement Engineering.

- Acted as Co-PI / key Research team member on several funded Practical Research Projects such as Landslide Hazard and Risk Mapping of Murree and Galiat, Geophysical Testing, and Pavement Materials Studies. Used innovative geotechnical investigation techniques such as 2-D Electrical Resistivity Mapping.

- Acted as Research Associate on USAID-HEC funded project "Development of Guidelines for Asphalt Pavement Recycling in Pakistan" – a joint research project NIT-Michigan State University (MSU), USA.

- Worked as Research Assistant in King Fahd University, Saudi Arabia on a funded project involving Characterization and Stabilization of Indigenous Soils / Aggregates for Road Construction purposes and also performed some specialized testing such as Resilient Modulus on Bound and Unbound Material.